

User's Guide
COMPREHENSIVE AIR QUALITY MODEL
WITH EXTENSIONS
Version 6.40

Ramboll Environ
773 San Marin Drive, Suite 2115
Novato, California, 94998
www.ramboll-environ.com
www.camx.com

P-415-899-0700
F-415-899-0707

Copyright: Ramboll Environ

1997 – 2016

This publication may be reproduced for
non-commercial purposes with appropriate attribution.

ACKNOWLEDGMENTS

Ramboll Environ acknowledges the following groups for their contributions to the development of CAMx:

- The Texas Commission on Environmental Quality (TCEQ), for sponsoring the development, testing, and review of numerous components of the model;
- The Lake Michigan Air Directors Consortium (LADCo), for sponsoring the development, testing and review of numerous components of the model;
- The U.S. Environmental Protection Agency (EPA), for sponsoring the development, testing, and review of numerous components of the model, and for co-sponsoring the development and testing of the MPI parallel processing capability. Special thanks to Dr. Jon Pleim for assistance with implementation of ACM2;
- The Coordinating Research Council (CRC), for sponsoring the development, testing, and review of numerous components of the model;
- The Texas Air Quality Research Program (AQRP), for sponsoring the development, testing, and review of numerous components of the model;
- Dr. Sasha Madronich (NCAR) for development of the TUV radiative transfer model and assistance with incorporating the in-line TUV treatment into CAMx;
- The Carnegie-Mellon University, Department of Chemical Engineering, for providing full-science PM algorithms, assistance in incorporating them into CAMx, and testing the implementation;
- The Electric Power Research Institute (EPRI), for sponsoring the development and testing of the Volatility Basis Set (VBS) organic aerosol algorithm.
- The American Petroleum Institute (API), for sponsoring the development and testing of improvements to the vertical advection algorithm;
- The Utah Department of Environmental Quality (UDEQ), for sponsoring updates to the CB6 chemistry mechanism, snow-cover treatment, and surface chemistry model;
- The University of Texas, Center for Energy and Environmental Resources, for assistance in developing and testing the Open-MP multi-processor capability;
- Atmospheric, Meteorological, and Environmental Technologies (ATMET), for providing libraries and implementation support for the MPI parallel processing capability;
- The Midwest Ozone Group (MOG), for co-sponsoring the development and testing of the MPI parallel processing capability;
- Atmospheric and Environmental Research (AER), for developing the mercury chemistry algorithm;
- The San Francisco Bay Area Air Quality Management District (BAAQMD), for supporting and testing the coupling of SAPRC gas-phase chemistry to the PM chemistry algorithm.

CONTENTS

ACKNOWLEDGMENTS.....	1
1. OVERVIEW	1
1.1 CAMX FEATURES.....	2
1.2 CAMX EXTENSIONS AND PROBING TOOLS	4
1.3 NEW FEATURES AND MAJOR UPDATES IN CAMX VERSION 6.40	5
2. THE CAMX MODELING SYSTEM.....	6
2.1 CAMX PROGRAM STRUCTURE	7
2.1.1 Memory Management	8
2.1.2 Parallel Processing.....	9
2.2 COMPILING CAMX	10
2.2.1 A Note on Fortran Binary Input/Output Files.....	11
2.3 RUNNING CAMX	12
2.3.1 Control File Namelist Input.....	12
2.3.2 Using Scripts to Run CAMx	20
2.4 BENCHMARKING MODEL RUN TIMES.....	24
2.5 CAMX PRE- AND POST-PROCESSORS.....	24
2.5.1 Emissions	24
2.5.2 Meteorology	25
2.5.3 Photolysis Rates.....	26
2.5.4 Initial and Boundary Conditions	27
2.5.5 Landuse.....	28
2.5.6 Post-processors	28
3. CORE MODEL INPUT/OUTPUT STRUCTURES.....	30
3.1 CAMX CHEMISTRY PARAMETERS FILE	31
3.2 PHOTOLYSIS RATES FILE.....	39
3.3 OZONE COLUMN FILE.....	41
3.4 FORTRAN BINARY INPUT/OUTPUT FILES.....	44
3.4.1 What is a Fortran Binary File?	44
3.4.2 CAMx Binary File Headers	44
3.4.3 Input Files	46
3.4.4 Output Files	59
4. CORE MODEL FORMULATION	64
4.1 NUMERICAL APPROACH.....	64
4.2 CAMX GRID CONFIGURATION	66
4.2.1 Grid Cell Arrangement.....	66
4.2.2 Grid Nesting.....	67
4.2.3 Flexi-Nesting.....	69
4.3 TREATMENT OF EMISSIONS	69
4.3.1 Gridded Emissions	70
4.3.2 Elevated Point Emissions	70
4.4 THREE-DIMENSIONAL TRANSPORT	73
4.4.1 Resolved Transport: Advection	73
4.4.2 Sub-Grid Turbulent Transport: Diffusion.....	75

4.5 WET DEPOSITION	77
4.5.1 Precipitation Parameters.....	79
4.5.2 Aerosol Scavenging.....	80
4.5.3 Gas Scavenging.....	81
4.6 DRY DEPOSITION	83
4.6.1 The Wesely/Slinn Model	84
4.6.2 The Zhang Model.....	87
4.7 SNOW COVER AND SURFACE ALBEDO	90
4.8 SURFACE MODEL FOR CHEMISTRY AND RE-EMISSION	92
4.8.1 Surface Model Algorithms.....	93
4.8.2 Running CAMx With the Surface Model.....	97
5. CHEMISTRY MECHANISMS	100
5.1 GAS-PHASE CHEMISTRY	101
5.1.1 Carbon Bond	101
5.1.2 SAPRC 2007.....	109
5.1.3 Implicit Gas-Phase Species	109
5.1.4 Photolysis Rates.....	110
5.1.5 Gas-Phase Chemistry Solvers	113
5.2 AEROSOL CHEMISTRY	114
5.2.1 Additional Gas-Phase Species.....	115
5.2.2 Aerosol Processes.....	115
5.2.3 Aerosol Sectional Approach	123
5.3 MERCURY CHEMISTRY	124
5.3.1 Gas-Phase Chemistry.....	125
5.3.2 Adsorption of Hg(II) on PM.....	126
5.3.3 Aqueous-Phase Chemistry.....	127
5.3.4 Implementation Approach	128
5.3.5 Chemistry Parameters for Mercury.....	129
5.4 SIMPLE CHEMISTRY VIA MECHANISM 10	130
6. PLUME-IN-GRID SUBMODEL	131
6.1 CAMX PIG FORMULATION	131
6.1.1 Basic Puff Structure and Diffusive Growth.....	131
6.1.2 Puff Transport.....	135
6.2 GREASD PIG	137
6.3 PARTICULATE MATTER IN PIG	139
6.4 IRON PIG	139
6.5 PIG FEATURES	140
6.5.1 Puff Layer Spanning (IRON and GREASD).....	140
6.5.2 Puff Overlap and the Idea of Virtual Dumping (IRON only)	140
6.5.3 Multiple Puff Reactors (IRON only)	141
6.5.4 Puff Dumping (IRON and GREASD).....	142
6.5.5 PiG Rendering (IRON and GREASD)	142
6.5.6 High Resolution Puff Sampling (IRON and GREASD)	143
6.6 DEPOSITION	143
6.6.1 Dry Deposition	143
6.6.2 Wet Deposition.....	145
6.7 PIG CONFIGURATION	145
6.7.1 Guidance on the Use of CAMx PiG	146
7. SOURCE APPORTIONMENT	150

7.1 OZONE SOURCE APPORTIONMENT	151
7.1.1 OSAT Formulation.....	152
7.1.2 OSAT2 Formulation	153
7.1.3 OSAT3 Formulation	154
7.1.4 Alternative Ozone Apportionment Using APCA.....	156
7.2 PARTICULATE SOURCE APPORTIONMENT	157
7.3 RUNNING CAMX WITH SA.....	161
7.3.1 CAMx Control File.....	161
7.3.2 Specifying Emission Groups.....	163
7.3.3 Source Area Mapping	167
7.3.4 Receptor Definition	171
7.3.5 Output File Formats.....	171
7.3.6 Postprocessing.....	173
7.4 STEPS IN DEVELOPING INPUTS AND RUNNING SA.....	173
8. DECOUPLED DIRECT METHOD FOR SENSITIVITY ANALYSIS	177
8.1 IMPLEMENTATION.....	178
8.1.1 Tracking Sensitivity Coefficients Within CAMx.....	180
8.1.2 Flexi-DDM	181
8.2 RUNNING CAMX WITH DDM AND HDDM	181
8.3 DDM OUTPUT FILES	186
8.4 DDM SENSITIVITY COEFFICIENT NAMES.....	186
8.4.1 Initial Condition Sensitivity Names.....	187
8.5 STEPS IN DEVELOPING INPUTS AND RUNNING DDM.....	190
9. PROCESS ANALYSIS	192
9.1 PROCESS ANALYSIS IN CAMX	192
9.1.1 Integrated Process Rate Analysis	193
9.1.2 Integrated Reaction Rate Analysis.....	194
9.1.3 Chemical Process Analysis.....	194
9.2 RUNNING PROCESS ANALYSIS.....	197
9.2.1 Setting CAMx Parameters.....	199
9.2.2 Output File Formats.....	200
9.3 POSTPROCESSING	200
9.3.1 IPR Output Files	200
9.3.2 IRR Output Files	201
9.3.3 CPA Output Files.....	202
10. REACTIVE TRACERS	203
10.1 DESCRIPTION OF RTRAC.....	203
10.1.1 RTRAC Gas-Phase Chemistry	205
10.2 DESCRIPTION OF RTCMC.....	207
10.2.1 RTCMC Gas-Phase Chemistry	207
10.3 REACTIVE TRACERS IN IRON PIG.....	215
10.4 RUNNING CAMX WITH REACTIVE TRACERS.....	216
10.4.1 CAMx Control File.....	216
10.4.2 User Adjustable Parameters.....	219
11. REFERENCES.....	221

APPENDIX A	236
CAMX MECHANISM 2: CB6R2 GAS-PHASE CHEMISTRY	236
APPENDIX B	245
CAMX MECHANISM 3: CB6R2 WITH HALOGEN CHEMISTRY	245
APPENDIX C	249
CAMX MECHANISM 4: CB6R4 GAS-PHASE CHEMISTRY	249
APPENDIX D	261
CAMX MECHANISM 5: SAPRC07TC GAS-PHASE CHEMISTRY	261

TABLES

Table 2-1. Parameters and their defaults in <code>Includes/camx.prm</code> used to statically dimension local arrays in low-level subroutines.	8
Table 2-2. CAMx output file suffixes and their corresponding file types.	20
Table 2-3. CAMx v6.20 speed performance with MPI and OMP parallelization from the LADCo tests described above.	24
Table 3-1. Data requirements of CAMx.	30
Table 3-2. Description of the CAMx chemistry parameters file. The record labels exist in columns 1-20, and where given, the input data for that record start in column 21. The format denoted "list" indicates a free-format list of numbers (comma or space-delimited).	32
Table 3-3a. Rate constant expression types supported in CAMx and order of expression parameters for the chemistry parameters file.....	40
Table 3-3b. List of parameters that must be provided in the CAMx chemistry parameter file for each of the seven types of rate constant expressions. Use ppm/minute units for A and Kelvin for E_a and T_R . The variable O is the order of the reaction (1 to 3).....	41
Table 3-4. The 11 WESELY89 landuse categories, their default UV surface albedos, and their surface roughness values (m) by season. Winter is defined for conditions where there is snow present; winter months with no snow are assigned to the Fall category. Roughness for water is calculated from the function $z_0 = 2 \times 10^{-6} w^{2.5}$, where w is surface wind speed (m/s).	47
Table 3-5. The 26 ZHANG03 landuse categories, their UV albedos, default annual minimum and maximum LAI and surface roughness (m) ranges, and mapping to the Wesely scheme (Table 3-4). Roughness for water is calculated from the function $z_0 = 2 \times 10^{-6} w^{2.5}$, where w is surface wind speed (m/s).	48

Table 4-1. Summary of the CAMx models and methods for key physical processes.	64
Table 4-2. Relationships between season and month/latitude used in the CAMx Wesely/Slinn dry deposition model. Exception: seasons for the area within 50N-75N and 15W-15E are internally set to those of latitude band 35-50 to account for regions of Europe in which the climate is influenced by the Gulf Stream.	87
Table 4-3. Description of CAMx surface model variables shown in Figure 4-7.	94
Table 4-4(a). Wesely landuse categories and associated annual-averaged soil/vegetation split factors, UV albedo, and SWE W_c	95
Table 4-4(b). Zhang landuse categories and associated annual-averaged soil/vegetation split factors, UV albedo, and SWE W_c	95
Table 5-1. Gas-phase chemical mechanisms currently implemented in CAMx v6.4.	100
Table 5-2. Species names and descriptions common to all Carbon Bond Mechanisms in CAMx.	102
Table 5-3. Default dry extinction efficiency and single-scattering albedo at 350 nm (Takemura et al., 2002) in the distributed CAMx chemistry parameters file.	112
Table 5-4. List of inorganic PM species for the CAMx CF aerosol option.	117
Table 5-5. SOA parameters for SOAP.	118
Table 5-6. SOA parameters for SOAP2.	119
Table 5-7. Molecular properties of the 1.5-D VBS species.	122
Table 5-8. Input species for 1.5-D VBS scheme.	123
Table 5-9. Volatility distribution factors used to allocate POA emissions from five different source types to the five PAP, PCP, and PFP volatility bins.	123
Table 7-1. Numbers of emission file sets (i.e., gridded files and point source file) needed for different model configurations. APCA requires at least two emission groups, and the first group must be biogenic emissions.	163
Table 7-2. Format for the receptor definition file.	172
Table 8-1. DDM output file suffix names.	186
Table 9-1. Process information reported by the IPR option.	194
Table 9-2. Chemical Process Analysis (CPA) variables calculated in CAMx for the CB05 and CB6r2 mechanisms. Concentrations are ppb; production and destruction are ppb/hr; photolysis rates are hr^{-1} , ratios are unitless.	195

Table 9-3. Process analysis keywords and associated CAMx output files.	197
Table 10-1. Keywords, options and default values for the Control section of the IMC file.	209
Table 10-2a. Recommended SCICHEM rate constant expression types for use in CAMx.	214
Table 10-2b. Parameters required by SCICHEM rate constant expression types.	215
Table 10-3. Determining the reaction order and consequent unit dimensions for rate constants.	215
Table 10-4. RTCMC parameters default settings in the <code>includes/rtcmcchm.inc</code> include file.	220
Table A-1. Reactions and rate constant expressions for the CB6r2 mechanism. k_{298} is the rate constant at 298 K and 1 atmosphere using units in molecules/cm ³ and 1/s. For photolysis reactions k_{298} shows the photolysis rate at a solar zenith angle of 60° and height of 600 m MSL/AGL. See Table 5-2 for species names. See Section 3.1 on temperature and pressure dependencies.	236
Table B-1. Listing of the CB6r2 halogen mechanism (see Table A-1 for a complete listing of CB6r2). k_{298} is the rate constant at 298 K and 1 atmosphere using units in molecules/cm ³ and 1/s. For photolysis reactions k_{298} shows the photolysis rate at a solar zenith angle of 60° and height of 600 m MSL/AGL. See Table B-2 for species names. See Section 3.1 on temperature and pressure dependencies.	245
Table B-2. Chemical species included in CB6r2h.	248
Table C-1. Reactions and rate constant expressions for the CB6r4 mechanism. k_{298} is the rate constant at 298 K and 1 atmosphere using units in molecules/cm ³ and 1/s. See Table C-2 for species names. See Section 3.1 on temperature and pressure dependencies. For photolysis reactions k_{298} shows the photolysis rate at a solar zenith angle of 60° and height of 600 m MSL/AGL. See Table C-3 for a listing of photolysis rates by zenith angle.	249
Table C-2. CB6r4 species names and descriptions.	258
Table C-3. CB6r4 primary (unshaded) and secondary (shaded) photolysis rates (1/s) by solar zenith angle at 600 m MSL/AGL.	260
Table D-1. Reactions and rate constants for the SAPRC07TC mechanism. k_{300} is the rate constant at 300 K and 1 atmosphere using units in molecules/cm ⁻³ and 1/s. See Table D-2 for species names. See Section 3.1 on temperature and pressure dependencies.	261
Table D-2. Explicit species in the SAPRC07TC mechanism.	280

FIGURES

Figure 2-1. Schematic diagram of the CAMx modeling system. See Table 3-1 for a detailed list of specific model input requirements for the five major data classes shown at the top of the figure. Certain pre- and post-processor programs shown in the figure are described in this section. Third-party models, processors, and visualization software are not described in this User's Guide and are not distributed with CAMx.	6
Figure 2-2. A sample CAMx job script that generates a "CAMx.in" file and runs the model with OMP parallelization.....	21
Figure 2-3. An example of global ozone column from the Ozone Monitoring Instrument (OMI) platform. White areas denote missing data. From ftp://toms.gsfc.nasa.gov/pub/omi/data/	27
Figure 3-1a. Example CAMx chemistry parameters file for Mechanism 6 (CB05) with CF PM scheme that includes the mercury species HG0, HG2, and HGP.	34
Figure 3-1b. Example inert chemistry parameters file (requires chemistry flag to be set false – see the description of the CAMx control file).	38
Figure 3-2. Example of the first several panels of lookup data in the photolysis rates input file.....	42
Figure 3-3. Example structure of a single-grid ozone column input file showing a single panel for the time-varying ozone column field.	44
Figure 4-1. A horizontal representation of the Arakawa C variable configuration used in CAMx.	67
Figure 4-2. An example of horizontal grid nesting, showing two telescoping nested grids within a 10×10 cell master grid. The outer nest contains 10×12 cells (including buffer cells to hold internal lateral boundary conditions), and the inner nest contains 6×10 cells (including buffer cells).	68
Figure 4-3. Schematic representation of the turbulent exchange among layers within a vertical grid column during convective adjustment in the ACM2 (taken from Pleim [2007])......	77
Figure 4-4. Comparison of monthly LAI data embedded in the Zhang dry deposition scheme against episode-specific LAI for June 2005.	89
Figure 4-5. Comparison of particle dry deposition velocities as a function of size and wind speeds (m/s) for three models: black – Zhang et al. (2001); blue – Slinn and Slinn (1980); orange – AERMOD (EPA, 1998). Results are shown for a forest landuse category during daytime neutral stability. Particle density was set at 1.5 g/cm ³	91
Figure 4-6. Example of grid-cell albedo evolution for a hypothetical 20-day springtime snow event (assuming ablation conditions) for low and tall vegetation grid cells with a terrestrial (non-snow) albedo of 0.05.	92

Figure 4-7. Schematic of the CAMx surface model.....	93
Figure 4-8. The portions of the CAMx chemistry parameters file (highlighted) to support the surface model. In this example, 3 gases are treated, where nitric acid (HNO ₃) and peroxyxynitric acid (PNA) react to form nitrous acid (HONO). All three are subject to decay by soil leaching, plant penetration, and snow melt loss. The values shown here are for illustrative purposes only and do not represent any known surface chemistry mechanism.....	99
Figure 5-1. Relative humidity adjustment factor applied to the dry extinction efficiency for hygroscopic aerosols (FLAG, 2000).	113
Figure 5-2. Schematic diagram of the CAMx VBS module. The model VBS species name consists of 4 characters that indicate the phase (P – particle; V – vapor), the source (A – anthropogenic; B – biogenic; C – cooking; F – fire), the formation (P – primary; S – secondary), and the volatility bin number. The solid and dashed arrows represent gas-aerosol partitioning and chemical aging, respectively. The thick colored arrows represent POA emissions or oxidation of SOA precursors.	121
Figure 6-1. Schematic representation of CAMx PiG puff shape in the horizontal plane. Directional orientation of the puff is arbitrary, and evolves according to wind direction, shears and diffusive growth along its trajectory.	132
Figure 6-2. Plan-view schematic representation of a chain of PiG puffs emitted from a point source into an evolving gridded wind field. The red line connected by dots represents puff centerlines, with dots representing leading and trailing points of each puff. The CAMx computational grid is denoted by the blue lines.....	136
Figure 6-3. Example of a single point source PiG plume as depicted by a sampling grid with 200 m resolution (shown by the extent of the plot; 40 km by 32 km total extent). This sampling grid was set within a CAMx computational grid with 4-km resolution. The source location is arbitrary and is emitting an inert tracer.	144
Figure 7-1. Example of the sub-division of a CAMx domain into separate areas for geographic source apportionment.	151
Figure 7-2. The original OSAT scheme for ozone apportionment. Information flows along arrows. Changes in core model species are shown in blue, OSAT tracers are in black, the diamond represents the OSAT algorithm that determines ozone tracer changes. $\Delta\text{H}_2\text{O}_2/\Delta\text{HNO}_3$ is the indicator ratio used to determine NO _x - or VOC-limited ozone production.	152
Figure 7-3. Daytime reactions of ozone with HO _x (OH and HO ₂) showing potential for reformation of ozone or ozone destruction via peroxide formation.	154
Figure 7-4. The OSAT2 scheme for ozone apportionment. Information flows along arrows. Changes in core model species are shown in blue, OSAT tracers are in black, the diamond represents the OSAT algorithm that determines ozone tracer	

producton. $\Delta\text{H}_2\text{O}_2/\Delta\text{HNO}_3$ is the indicator ratio used to determine NO _x - or VOC-limited ozone production.	154
Figure 7-5. Correspondence between NO _y species in CB6 and tracer families in OSAT3 with conversions between species/tracers shown by arrows.	155
Figure 7-6. The OSAT3 scheme for ozone apportionment. Information flows along arrows. Changes in core model species are shown in blue, OSAT tracers are in black, the diamond represent the OSAT algorithms that determine ozone tracer production. $\Delta\text{H}_2\text{O}_2/\Delta\text{HNO}_3$ is the indicator ratio used to determine NO _x - or VOC-limited ozone production. RGN apportions the nitrogen in NO ₂ whereas OON and OOV apportion the odd-oxygen in NO ₂	157
Figure 7-7a. An example of SA input records in the CAMx run control file. The options for this OSAT run are as follows: this is a two-grid run, master and nested grid surface concentrations are written to file, a single tracer type is to be used for all boundaries, 19 source regions, and one emission group (i.e., zero additional emission files and no leftover group). This is the first day of the simulation (i.e., restart is false), so no OSAT restart files are supplied.	164
Figure 7-7b. As in Figure 7-7a, but in this case the run is a continuation day of a run with three emission groups. The three emission groups are defined by supplying extra emission files for point and area sources for each grid (emission groups 1 and 2), and setting the "Use_Leftover_Group" flag to TRUE so that the model calculates the third group internally. The point source group 1 filename is blank because group 1 is a category with no point source emissions (e.g., biogenics).	165
Figure 7-7c. This figure follows from Figure 7-7b: it is a continuation day of a 2-grid run with three emission groups, and all three emission groups are defined explicitly by supplying extra emission files; therefore, the "Use_Leftover_Group" flag is set to FALSE. The point source group 1 filename is blank because group 1 is a category with no point source emissions (e.g., biogenics). APCA is used to attribute ozone sources, so biogenic emissions MUST be present as group 1. PSAT will trace PM sulfate and nitrate species.	166
Figure 7-8. Example of the original source area map file for the domain and source areas shown in Figure 7-1.	168
Figure 7-9. Example fractional area map file for a small (10x10) grid. This file is for source category/group #3 and includes 2 map panels. The grid covers source region #5 and #6 and these regions overlap in the middle of the domain. Panel 2 shows just the remaining overlap information for region #6.	170
Figure 7-10. Example receptor concentration file. Lines ending with "..." are truncated to fit the page, and the file would continue with data for additional receptors and hours in the same format.	174

Figure 8-1. Example of DDM inputs in the CAMx control file. CAMx is run with two grids, and DDM is configured to track emissions from four source regions and two source groups. Sensitivity to ozone initial and boundary conditions are tracked, while sensitivities to NO _x and VOC emissions are tracked. Sensitivity for a single rate constant group will be calculated involving mechanism reaction numbers 120, 121, and 122. Three groups of second-order sensitivities to anthropogenic NO _x and VOC emissions (from emissions group 2, source region 1) will be computed (d^2/dNO_x^2 , $d^2/dVOC^2$ and d^2/dNO_xdVOC). No source region map is provided for the nested grid (the region assignments on the nest are defined by the master grid). Only the group 2 point sources are tracked (no biogenic point sources are available).	185
Figure 8-2. Example concordance of long and short sensitivity coefficient names from the CAMx diagnostic output file.....	187
Figure 9-1. Example section of a CAMx control file specifying options for Process Analysis.....	199
Figure 9-2. Example IPR time series analysis for PSO ₄ ; lateral boundary and chemistry terms are not aggregated.....	201
Figure 10-1. Example RTRAC chemistry input file for modeling specific toxic species.....	204
Figure 10-2. Example RTRAC receptor input file identifying the grid cells with locations where hourly decay rates will be output for subgrid-scale point source modeling (see format for SA receptor file in Table 7-2).	207
Figure 10-3. Example free-format RTCMC IMC chemistry input file.	208
Figure 10-4. Example input of RTRAC options and filenames within the CAMx control file.	218

1. OVERVIEW

The **C**omprehensive **A**ir quality **M**odel with **e**xtensions (CAMx) is an Eulerian regional photochemical dispersion model that allows for integrated “one-atmosphere” assessments of tropospheric air pollution (ozone, particulates, air toxics) over spatial scales ranging from neighborhoods to continents. It is a “state-of-the-science” open-source system that is computationally efficient, flexible, and publicly available. The model’s Fortran source code is modular and well-documented. The Fortran binary input/output file formats are based on the Urban Airshed Model (UAM) convention and are compatible with many existing pre- and post-processing tools. Meteorological fields are supplied to CAMx from separate weather prediction models. All emission inputs are supplied from external pre-processing systems.

CAMx simulates the emission, dispersion, chemical reaction, and removal of pollutants by marching the Eulerian continuity equation forward in time (t) for each chemical species (I) on a system of nested three-dimensional grids. The continuity equation specifically describes the time dependency of volume-average species concentration within each grid cell as a sum of all physical and chemical processes operating on that volume. This equation is expressed mathematically in terrain-following height (z) coordinates as follows:

$$\frac{\partial c_I}{\partial t} = -\nabla_H \cdot V_H c_I + \left[\frac{\partial(c_I \eta)}{\partial z} - c_I \frac{\partial^2 h}{\partial z \partial t} \right] + \nabla \cdot \rho K \nabla(c_I / \rho) \\ + \left. \frac{\partial c_I}{\partial t} \right|_{Emission} + \left. \frac{\partial c_I}{\partial t} \right|_{Chemistry} + \left. \frac{\partial c_I}{\partial t} \right|_{Removal}$$

where c_I is species concentration (mass/volume), V_H is the horizontal wind vector, η is the net vertical transport rate, h is the layer interface height, ρ is atmospheric density, and K is the turbulent exchange (diffusion) coefficient. The first term on the right-hand side represents horizontal advection, the second term represents net resolved vertical transport across an arbitrary space- and time-varying height grid, and the third term represents sub-grid scale turbulent diffusion. Chemistry is treated by simultaneously solving a set of reaction equations defined by specific chemical mechanisms. Pollutant removal to the surface (deposition) includes both dry surface uptake and wet scavenging by precipitation.

CAMx can perform simulations on four types of Cartesian map projections: Lambert Conic Conformal, Polar Stereographic, Mercator, and Universal Transverse Mercator. CAMx also offers the option of operating on a geodetic latitude/longitude grid system. The vertical grid structure is defined externally, so layer interface heights may be specified as any arbitrary function of space and/or time. This flexibility in defining the horizontal and vertical grid structures allows CAMx to be configured to match the grid of any meteorological model that is used to provide environmental input fields.

1.1 CAMx Features

Two-Way Nested Grid Structure: CAMx can be run with variable grid spacing. Use a coarse grid for regional domains where high spatial resolution is not particularly needed, while in the same run, nest finer grids in specific areas of interest. Two-way nesting propagates information both up- and down-scale across all grids. Nests may possess different meshing factors from their parent grids, as long as they are common denominators of parent resolution. A "Flexi-Nesting" feature allows you to introduce and/or remove nested grids at any point during a simulation. You can supply complete information for new grids (emissions, meteorology, surface characteristics) or allow CAMx to interpolate any or all of these inputs from parent grids.

Parallel Processing: CAMx supports two types of parallelization: (1) OpenMP (OMP), which allows parallel processing on shared-memory (e.g., multi-core) computers; and (2) Message Passing Interface (MPI), which allows parallel processing across distributed memory (networked) computer cluster environments. Both OMP and MPI can be used in combination to maximize speed performance. To use OMP, your Fortran compiler must include libraries to enable in-code directives. To use MPI, you must have external MPI libraries installed on your system.

Multiple Photochemical Gas Phase Chemistry Mechanisms: CAMx offers several versions of Carbon Bond chemistry (CB05 and CB6 variants) and the 2007 version of Statewide Air Pollution Research Center chemistry (SAPRC07TC). These mechanisms are solved using the Euler-Backward Iterative (EBI) method, which is fast and accurate. CAMx also includes the fully explicit Gear-type Livermore Solver for Ordinary Differential Equations (LSODE), which we use to "benchmark" new mechanisms and evaluate the performance of EBI. We do not recommend LSODE for typical applications as the model will run *much* more slowly.

Advanced Photolysis Model: The TUV radiative transfer and photolysis model, developed and distributed by the National Center of Atmospheric Research (NCAR, 2011), is used as a CAMx preprocessor to provide the air quality model with a multi-dimensional lookup table of clear-sky photolysis rates. CAMx internally adjusts clear-sky rates for the presence of clouds and aerosols using a fast in-line version of TUV.

Particulate Matter (PM) Chemistry: CAMx includes updated algorithms for inorganic aqueous chemistry (RADM-AQ), inorganic gas-aerosol partitioning (ISORROPIA), and two approaches for organic gas-aerosol partitioning and oxidation (VBS or SOAP). These algorithms use products from the gas-phase mechanisms for the production of sulfate, nitrate, and condensable organic gases. CAMx provides two options to represent the particle size distribution: a static two-mode coarse/fine (CF) scheme, and an evolving multi-section (CMU) scheme. The efficient and easy-to-use Secondary Organic Aerosol Partitioning (SOAP) treatment has been recently updated for the latest information on SOA yields, saturation concentrations, and water solubility. SOAP is compatible with CF and CMU aerosol options and works with all Probing Tools. The hybrid 1.5-dimensional (1.5-D) Volatility Basis Set (VBS) describes the evolution of organics according to oxidation state and volatility, and is implemented to provide a unified full-science framework for gas-aerosol partitioning and chemical aging of both primary and secondary atmospheric organic aerosols. VBS is compatible with all gas-phase mechanisms and the 2-mode CF aerosol

option; it is not currently enabled for Source Apportionment or Decoupled Direct Method Probing Tools.

Mercury Chemistry: CAMx optionally treats the chemistry of five mercury species (two gases and three particulates) via gas-phase and aqueous pathways, including Hg(II) adsorption to PM. The mercury chemistry module requires PM concentrations, so mercury must be modeled with the “CF” two-mode PM mechanism by including mercury species among the list of modeled species. All of the rate and equilibrium constants for the mercury mechanism are hard-coded within the chemistry module.

User-Defined Chemistry Mechanism: “Mechanism 10” provides a simple way to define your own chemistry mechanism. This option is intended to define simple chemical decay or transformations between gas and/or aerosol species. You must develop your own Mechanism 10 subroutine and chemistry parameters file.

Plume-in-Grid (PiG) Module: PiG treats the chemistry and dispersion of point source emission plumes at sub-grid scales using a Lagrangian puff model, until such time as the pollutant mass can be adequately represented within the grid model framework. Both gas-phase and PM chemistry can be treated. PiG includes a “sampling grid” capability to passively sample plume concentrations at any resolution, which is particularly useful to visualize near-source sub-grid scale impacts.

Vertical Diffusion (Mixing) Options: CAMx offers a standard “K-theory” approach for vertical diffusion or alternatively version 2 of the Asymmetric Convective Model (ACM2; Pleim, 2007). ACM2 is a hybrid of local K-theory diffusion and non-local convective transport between the surface and layers aloft. ACM2 does not work with the Integrated Process Rate (IPR) component of the Process Analysis (PA) tool.

Dry Deposition Options: CAMx offers two dry deposition options: an older approach based on the models of Wesely (1989) and Slinn and Slinn (1980); and an updated approach based on the algorithms of Zhang et al. (2001; 2003). The Wesely/Slinn model is formulated for 11 landuse categories, while the Zhang model uses 26 landuse categories.

Horizontal Advection Solver Options: CAMx offers the Piecewise Parabolic Method (PPM) of Colella and Woodward (1984), and the area-preserving advection solver of Bott (1989). Both possess high-order accuracy, little numerical diffusion, and are sufficiently quick for applications on very large grids.

Surface Chemistry/Re-emission Model: CAMx includes a simple surface sub-model that treats sorption and penetration of deposited pollutant mass into soils and vegetation, chemical degradation and transformation, and volatilization back into the air (re-emission). The surface model treats any subset of species listed in the core model's chemical mechanism. The surface model can only be used with the Wesely (1989) dry deposition option; it cannot be used with the Plume-in-Grid treatment.

Lateral and Top Boundary Conditions: Time- and space-variable boundary conditions for the master grid may be developed from down-scaling three-dimensional output from global chemistry models like GEOS-Chem and MOZART. Top boundary conditions improve the characterization of chemicals entering vertically across the model top, which is particularly important for common stratospheric constituents such as ozone and nitrogen oxides. A simpler top boundary treatment remains available, which is not reliant on an input file and internally assumes a “zero gradient” volume mixing ratio condition between the top model layer and the environment above the model.

1.2 CAMx Extensions and Probing Tools

Ozone and Particulate Source Apportionment Technology (OSAT/PSAT): Source apportionment technology tracks emission contributions to predicted ozone and/or PM species concentrations by source region and/or category. OSAT also reports information to determine whether each ozone component formed in NO_x or VOC sensitive conditions. OSAT/PSAT provides ozone/PM attribution to source regions and categories for a given emissions matrix, but does not provide quantitative information as to how ozone/PM contributions would change as emissions are altered because chemical interactions are non-linear. Source apportionment is available only for all CB chemical mechanisms, the CF aerosol scheme and the SOAP organic partitioning algorithm.

Decoupled Direct Method (DDM) and High-Order DDM (HDDM) Source Sensitivity: This tool calculates first-order (DDM) and second-order (HDDM) gas concentration sensitivity to changes in emissions, initial conditions and boundary conditions. PM concentration sensitivity is limited to first-order DDM. (H)DDM estimates how pollutant concentrations respond to region- and category-specific emission changes, but does not provide information on source attribution. (H)DDM can be run with any CB or SAPRC chemical mechanism, the CF aerosol scheme and the SOAP organic partitioning algorithm. (H)DDM does not account for in-line oceanic iodine emissions.

Process Analysis (PA): This probing tool provides in-depth information on the physical and chemical processes occurring during a CAMx run. Through PA, one can more fully understand the complex interactions of the different processes, explain simulation results within the context of model formulation, and improve the design of control strategies. The integrated process rates (IPR) option can be run with any CB or SAPRC chemical mechanism and any PM aerosol treatment; it is not available for the ACM2 vertical diffusion option. Chemical process analysis (IRR and CPA) is fully available only for CB05; a limited set of chemical process rates are available for CB6r2. PM rates are not tracked by PA.

Reactive Tracers (RTRAC): RTRAC provides a flexible add-on to simulate the emission, dispersion, chemistry, and deposition of multiple gas and particle tracers (such as specific toxics) that are not included in the model's core gas/PM chemistry mechanisms. Gas-phase chemistry may involve user-defined linear decay (photolysis and/or oxidation) by species, or complex non-linear systems solved with the RTRAC Chemical Mechanism Compiler (RTCMC). RTRAC can be run in combination with any CB or SAPRC chemical mechanism and is independent from all aerosol treatments.

1.3 New Features and Major Updates In CAMx Version 6.40

Updated CB6 Chemistry Mechanism: CB6 “revision 4” (CB6r4) is now available as chemistry mechanism 4. CB6r4 combines a condensed set of reactions involving ocean-borne inorganic iodine from the CB6r2h full halogen mechanism (mechanism 3) with the temperature- and pressure-dependent organic nitrate branching ratio introduced in CB6r3 (replaced by CB6r4). Source apportionment (OSAT/APCA) has been updated to account for ozone destruction by iodine and for iodine chemistry impacts on nitrate and isoprene nitrate

New In-line Oceanic Halogen Emissions: CB6r4 is supported by a new optional in-line iodine emissions parameterization that computes inorganic iodine emissions caused by ozone deposition to seawater. Emission fluxes of I_2 and HOI are added as new fields to the CAMx deposition output files so that they can be plotted and analyzed. Be sure the CAMx input landuse file correctly differentiates water bodies as ocean and fresh water.

Updated PM Chemistry: Several modifications have been implemented for the particulate matter (PM) chemistry algorithms, including: (1) a major revision to the SOAP algorithm, including updated aerosol yield, saturation and water solubility parameters, a condensed list of biogenic SOA species, and a new aqueous pathway for biogenic SOA formation from glyoxal, methyl glyoxal, and glycolaldehyde; (2) updated rates for metal-catalyzed sulfate reactions in the Regional Acid Deposition Model aqueous chemistry algorithm (RADM-AQ); and (3) a new heterogeneous SO_2 reaction pathway on crustal aerosols. Source apportionment (PSAT) has been updated for the revised SOAP and heterogeneous chemistry algorithms.

NOTE: These updates have not been extended to DDM yet, so DDM is disengaged for all chemistry mechanisms that include PM in this version of CAMx. You may continue to use H/DDM with gas-only chemistry mechanisms.

Updated Wet Deposition Scheme: The wet deposition algorithm was reviewed in detail to identify assumptions or processes that were unintentionally or otherwise unreasonably limiting gas and PM uptake into precipitation. The wet deposition algorithm was simplified and improved in several ways, resulting in increased scavenging of gases and PM.

Faster ACM2 Vertical Diffusion Solver: The faster ACM solver technique recently implemented in CMAQ v5.1 was incorporated into the CAMx ACM2 option to improve model runtime, which is now similar to the default K-theory option.

2. THE CAMX MODELING SYSTEM

CAMx comprises the core component of an overall air quality modeling system, as illustrated in Figure 2-1. CAMx inputs are developed using independent third-party models and processing tools that characterize meteorology, emissions, and various other environmental conditions (land cover, radiative/photolysis properties, and initial/boundary conditions). Interface programs are needed to translate the products of each of these models/processors into the specific input fields and formats required by CAMx. After the air quality simulation is completed, additional programs are used to post-process the concentration fields, develop model performance statistics and measures, manipulate Probing Tool output into various reportable formats, and further translate raw results into forms necessary for regulatory purposes. Commonly available graphical software can be used to view CAMx output files; some like PAVE and VERDI can read CAMx files directly, others require reformatting CAMx files to common data formats like NetCDF. While third-party visualization software, meteorological models, and emission processors are not distributed with CAMx, Ramboll Environ does distribute many of the necessary interface programs and post-processors on the CAMx web site (www.camx.com). A brief description of each of these is provided at the end of this section.

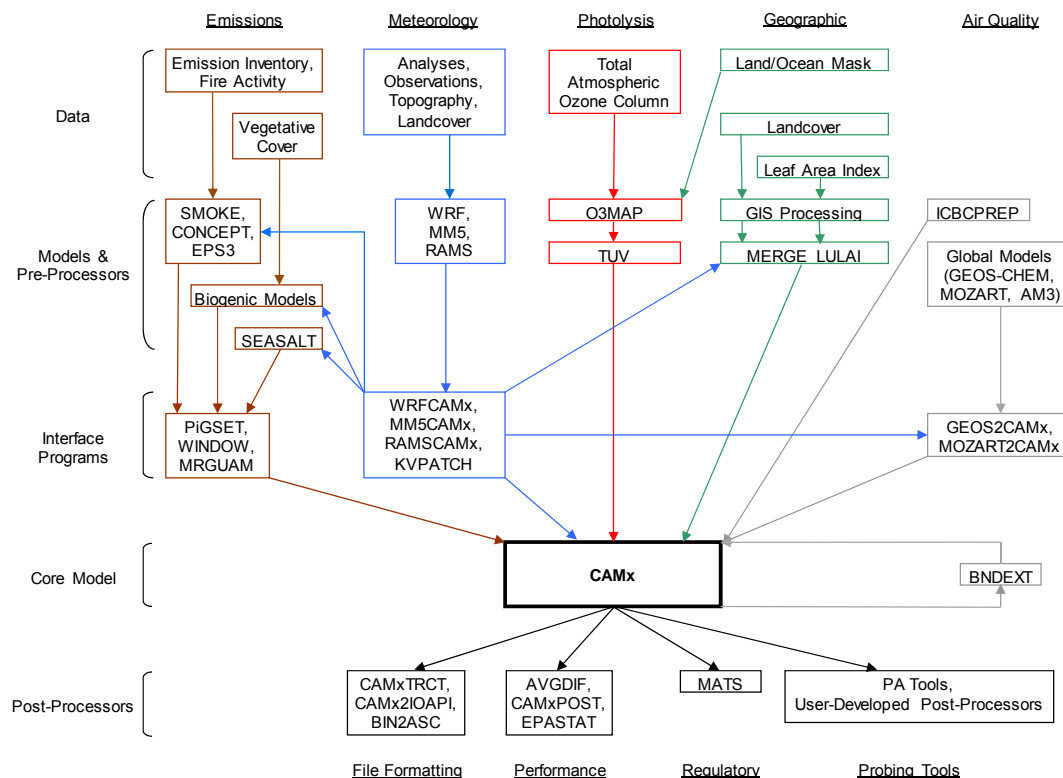


Figure 2-1. Schematic diagram of the CAMx modeling system. See Table 3-1 for a detailed list of specific model input requirements for the five major data classes shown at the top of the figure. Certain pre- and post-processor programs shown in the figure are described in this section. Third-party models, processors, and visualization software are not described in this User's Guide and are not distributed with CAMx.

2.1 CAMx Program Structure

The core CAMx model is written in Fortran, but includes some utilities written in C to interface with MPI. The program is highly modular and well documented to ease code review, modifications and substitution of alternate routines. The source code is arranged in several directories, grouped according to function. The main source directory contains version release notes, the GNU user license, the "Makefile" compile utility, and a control file namelist template. Sub-directories contain source code for the core model and ancillary routines according to the following:

CAMx/	Source code for the main driver routine <code>CAMx.f</code> and core model routines.
CF_AERO/	Source code for inorganic aerosol chemistry (aqueous and thermodynamic partitioning) for the 2-mode CF scheme.
CMC/	Source code for the gas-phase chemical mechanism routines.
CMU_AERO/	Source code for inorganic aerosol chemistry (aqueous and thermodynamic partitioning) for the multi-section CMU scheme.
DDM/	Source code for the (H)DDM Probing Tool, consisting of I/O and core routines that are unique to (H)DDM.
HG/	Source code for the mercury chemistry routines.
Includes/	Fortran "include" files, consisting of program parameters and memory management code.
IO_bin/	Source code for Fortran binary (unformatted) I/O.
Mod_src/	Source code for F90 memory management modules.
MPI/	Source code for routines specific to MPI parallelization.
OSAT/	Source code for the OSAT/PSAT Probing Tools, consisting of I/O and core routines that are unique to OSAT/PSAT.
PA/	Source code for the Process Analysis Probing Tool, consisting of I/O and core routines that are unique to PA.
PiG/	Source code for the Plume-in-Grid sub-model, consisting of I/O and core routines that are unique to PiG.
RTRAC/	Source code for the Reactive Tracer Probing Tool, consisting of I/O and core routines that are unique to RTRAC/RTCMC.
SOAP/	Source code for secondary organic aerosol thermodynamic partitioning.

2.1.1 Memory Management

All of the model's global data structures are dynamically allocated when the model starts. The data necessary to allocate memory space for a given model run are read from the CAMx control file developed by the user (see Section 2.3). However, to alleviate compiler dependency on speed performance, CAMx utilizes some hard-coded Fortran parameters to statically allocate local arrays in low-level subroutines. All of these parameters are defined in the `Includes/camx.prm` file. The distribution version of this "include" file sets key array parameters to default values that should be sufficiently large to accommodate most applications: see Table 2-1 for a description of parameters and their default values. However, you may want to customize these values to ensure that they are large enough to accommodate all of your model configurations, or to exactly match your specific application, thus preventing wasted memory.

If any parameter is set to a value that is too small to support your application the model will stop, displaying an informative error message. To conserve memory, default values of 1 are set for Probing Tool tracers, PiG sampling grids, and sampling grid dimensions. These must be increased accordingly if Probing Tools or sampling grids are to be used.

Table 2-1. Parameters and their defaults in `Includes/camx.prm` used to statically dimension local arrays in low-level subroutines.

Parameter Name	Description	Default Value
MXCELLS	Number of cells in X/Y direction for any grid	200
MXLAYER	Number of layers	30
MXSPEC	Number of species (could be number of radicals, number of input species, or total number of model species)	155
MXREACT	Number of reactions (depends on the mechanism; see the user's guide for the value for each mechanism)	565
MXGRID	Number of grids	10
MXPTSRC	Number of point sources	100000
MXTRSP	Number of Probing Tool tracer species	1
MXPIG	Number of PiG puffs	50000
MXSAMPLE	Number of PiG sampling grids	1
MXCOLSMP	Number of PiG sampling grid columns	1
MXROWSMP	Number of PiG sampling grid rows	1

All of the parameters in the table above can be determined before starting a simulation except for MXPIG. A value of 50,000 is usually sufficient for most applications in which PiG is used; set this parameter to 1 if PiG is not used to conserve memory. If this parameter is exceeded during a simulation, the model will stop with an informative error message. If this happens, simply increase MXPIG, recompile the model executable, and restart the simulation. The other parameters in `camx.prm` beyond those listed in Table 2-1 will not normally need to be changed and are not discussed further.

2.1.2 Parallel Processing

Parallel processing refers to distributing a model application to multiple processors (CPUs) that share the computational load. CAMx supports two types of parallelization: (1) OpenMP (OMP), which allows parallel processing on shared-memory (e.g., multi-core) computers; and (2) Message Passing Interface (MPI), which allows parallel processing across distributed memory (networked) computer cluster environments. Both OMP and MPI can be used in combination to maximize speed performance.

To use OMP, your Fortran compiler must include libraries to enable the in-code parallelization directives. OMP distributes calculations for individual processes, such as chemistry within a single grid cell or advection/diffusion along a single row of cells, to a number of CPUs defined by the user. Once each CPU has completed its calculations, it works on the next individual process until all processes over the entire grid are completed.

To use MPI, you must have an external MPI library installed on your system. MPICH is a specific open source MPI library widely used in the numerical modeling community; CAMx has been specifically developed and tested using MPICH. With MPI, each CAMx grid is divided into sub-domains ("slices") and each slice is assigned to a CPU on the user-defined network. Each CPU operates the entire model on its assigned slice and passes common information needed by other CPUs via data "messages".

MPI in CAMx is designed using a "master/slave" parallel processing approach. The CPU on which the program is launched serves as the master node and will not conduct any model computations on any part of the modeling domain. This process will perform all of the model setup, the vast majority of I/O, and manage the communication between the slave or compute nodes, which integrate the model forward for each grid slice. Since the master node handles the important I/O it is the only CPU that needs access to the disk volume containing the input files and the location of the output directory. This approach allows for a minimal amount of network traffic to/among the compute nodes by eliminating the need for them to manage NFS mounts. The master node may need access to the LAN for data access, but the compute nodes only need access to the internal cluster network. However, the compute nodes will need access to a copy of the executable program. This can be accomplished in a number of ways: (1) have an NFS mount on the master node accessible to the internal cluster network and launch the model from that location; or (2) port a copy of the executable program, using `rsh` or `scp`, to the user's home directory on each compute node and launch the model from the user's home directory on the master node.

During each model time step, when grid slice computations are performed by the compute nodes, some information is written to the diagnostic and message output files. Rather than just eliminate this information altogether, we decided to create node-specific versions of each of these two files and have each compute node write the information to its own version. However, in order to prevent the need to have the output directory available to the compute node across the network, we have designed the model so that the node-specific files are created in the current working directory. This means that if the model is launched from an NFS-mounted directory, all of the node-specific files will all be created in that location. On the other

hand, if the model is launched from a user's home directory on the compute nodes, you will have to log in to the specific compute node to view the files.

When using a hybrid MPI/OMP approach, the grids will be divided into slices in the usual way as part of MPI, but when operating on a particular slice, the host will spawn multiple OMP threads to parallelize the portions of the code where OMP directives have been included.

2.2 Compiling CAMx

A "Makefile" script is provided in the main source directory. The Makefile will compile all CAMx source code, link with necessary libraries, and build an executable program. It supports platforms running Linux (Portland Group and Intel compilers) and Macintosh OSX (Absoft compiler); it does not currently support compilers on platforms running Windows.

The choice for OMP and MPI parallelization, and the memory configuration for probing tools, are set during model compilation. All other CAMx choices for chemical mechanism, model algorithms, Probing Tools, and other options are selected at run time.

CAMx is compiled by issuing the following command at a shell prompt within the main source directory:

```
make COMPILER=my_compiler <CONFIG=my_app> <MPI=mpi_option> <IEEE=true>
```

where the text within the brackets "<>" is optional. To display an interactive help message, you may type

```
make help
```

The mandatory COMPILER argument should be set to one of the following:

```
pgf or pgfomp (Portland Group compiler for Linux)
ifort or ifortomp (Intel compiler for Linux)
gfortran or gfortranomp (Gnu compiler for Linux)
absoft or absoftomp (Absoft compiler for Macintosh OSX)
```

These keywords inform the Makefile of the compiler being used to compile and run the model, so that the Makefile can invoke the proper compiler-specific commands and flags. If OMP is not specified as part of the keyword then CAMx will not be able to run with OMP parallelization.

The optional CONFIG argument allows the CAMx executable program to be labeled for a specific memory configuration as defined within the CAMx parameters file (`Includes/camx.prm`) described above. You may want to customize some applications, for example to configure the Probing Tool extensions, and it is convenient to be able to distinguish between these executables. The Makefile will search for a CAMx parameters file called:

```
Includes/camx.prm.my_app
```

If `CONFIG` is not set on the make command line, the Makefile will compile CAMx using the default parameters file, `Includes/camx.prm.v6.40`.

The optional `MPI` argument will enable MPI parallel processing. This requires that third-party MPI libraries have been built and installed on the machine that is running this Makefile script and compiling CAMx. If `MPI` is not set on the command line, the Makefile script will ignore the MPI libraries and CAMx will not be able to run with MPI parallelization. The optional `MPI` argument should be set to one of the following:

```
mpich (MPICH versions 1 or 2)
mpich3 (MPICH version 3)
mvapch
openmpi (PGF and IFORT compilers only)
```

You should check that the variable “MPI_INST” in the CAMx Makefile, and in the MPI utilities Makefile (located in the MPI/ut11 sub-directory), are correctly set to your system's MPI installation path.

CAMx supports the use of both OMP and MPI parallelization in a single run using PGF and IFORT compilers. To utilize OMP in your MPI application, be sure to specify the appropriate OMP compiler keyword.

The IEEE flag will invoke IEEE-standard math, which will maximize consistency in model results across platforms and compilers. The IEEE flag may cause CAMx to run somewhat slower. The IEEE option is available only for PGF and IFORT compilers.

The Makefile will generate a CAMx executable program named

```
CAMx.my_app.MPI_option.my_compiler.ieee
```

which will reside in the main source directory. For example, a default compilation using the Portland Group compiler will result in an executable named

```
CAMx.v6.40.noMPI.pgf.
```

If you need to rebuild CAMx using different Makefile arguments we recommend typing “make clean” between builds. Make clean will delete all existing object files and force a complete re-build.

2.2.1 A Note on Fortran Binary Input/Output Files

Large CAMx input and output data fields are contained within Fortran “unformatted” (binary) files. This means that the data are read and written as represented in memory, without translation between binary and ASCII character sets as is performed for “text” files. Binary files reduce file volume and improve program read/write speed, but the user cannot directly view or manually edit them. There are two ways to represent binary information in memory: “big endian” and “little endian.” The difference between these is essentially the order of bits in a

word, and which order is used depends on the computer chipset. Historically, big endian has been used in many Unix workstations (Sun, SGI, HP, and IBM). The x86 processors on personal computer platforms (e.g., Intel and AMD) use little endian, while PowerPC chips are big endian.

CAMx can be compiled and run on machines that use either big or little endian binary representations, as long as the model and all of its pre- and post-processors are consistently compiled and run on the same type of platform. If any component of the modeling system is compiled on a different platform using the opposite binary representation, I/O files will not be properly read and will likely lead to a program crash.

A typical run-time error message from trying to read the wrong binary format is "input record too long," so if you get this error message, check for big endian / little endian consistency between your binary files and Fortran compiler options.

Compilers for little endian machines (e.g., x86 PC chipsets) provide compile-time switches that allow binary files to be read and written as big endian. The Portland Group compiler option is `"-byteswapio"`, whereas the Intel compiler option is `"-convert big_endian."` The CAMx Makefile sets compiler flags to consistently use big endian to maximize platform portability. Therefore, use of the CAMx Makefile will by default result in the model reading and writing big endian binary files. In practice, users should use the default binary format that is built into the CAMx Makefile and that is used for the CAMx distribution test case.

2.3 Running CAMx

2.3.1 Control File Namelist Input

CAMx reads a text run control file named `"CAMx.in"` that must exist locally in the directory from which the model is run. This file must be in the Fortran "namelist" format, and contains all user-specified control parameters for a given simulation, including model configuration, option-specific inputs, and I/O filenames. The run control file must contain the primary namelist module labeled `"&CAMx_Control"`, which provides all of the information to configure the core model. Additional namelist modules may be provided in the run control file to configure the various CAMx Probing Tool extensions. These optional namelist modules are ignored if no Probing Tools are selected in the primary namelist.

Each record in the CAMx control file contains a variable name that is explicitly set to a numerical, logical, or character value. The variable names are used by the program directly, and therefore cannot be changed without source code modifications. Character strings must be enclosed by single quotes, and all variable assignments must be delimited with commas. The order of the records may be arranged in any fashion that the user prefers. Any number of comment statements may be included anywhere within the namelists, provided that they do not interrupt variable assignments (`variable_name = value,`). The `"!"` character is the Fortran namelist comment delimiter.

Certain variables are multi-dimension arrays; the user may provide a comma-delimited list of values to fill the array or assign values to specific array elements. Certain other variables are

optional or associated with option flags; these do not need to appear in the namelist if their associated options are not invoked, and they will be ignored if they remain in the file.

If the user does not provide necessary inputs, the model will stop with a descriptive error message.

2.3.1.1 Common Errors When Creating a Namelist

Fortran programs ingest the entire contents of namelist modules using a single READ statement. If the program experiences an error reading the namelist, it echoes a simple error message like "error reading namelist" and the program stops. It is therefore difficult to determine the cause of the read error, especially if the namelist is lengthy and contains a variety of data types. When experiencing an error reading the CAMx control file namelist, you must carefully inspect the file for any syntax errors. These errors can be subtle and difficult to spot. Here are a few of the common reasons an error occurs when reading a namelist:

- *Mistyped variable name:*
All variables to be assigned within a namelist must be recognized as a declared namelist variable within the reading program. If a variable is misspelled or an unknown variable is assigned a value, a read error will occur.
- *Incorrect data type for the assigned variable:*
If the data type of the value assigned to a namelist variable does not match the variable's declared data type within the reading program, an error will occur. Some compilers will allow real type variables to be assigned to integer values, but not the converse.
- *Missing period around a logical value:*
The logical values `.true.` and `.false.` must be surrounded by a period.
- *Missing quotes around a character variable:*
Any character data type must be surrounded by quotes.
- *Overflow when assigning values to an array:*
The values in an array can be assigned using array index notation. If the index used to assign an array value exceeds the declared dimension of the array, a read error occurs. Check the "MXNAM" parameter in the `Includes/namelist.inc` include file to see if this value needs to be increased. Alternatively, check your namelist file to be sure all of your array indices are correct.
- *Wrong number of dimensions when assigning values to a multi-dimensional array:*
When assigning values to an array using array index notation, the number of subscripts in the assignment must match the declared dimensions of the array (e.g., assignments to an array dimensioned `var(i, j)` must be referenced using two indices).
- *Missing comma following a variable definition:*
A comma must be the last character in a variable assignment (`variable = value,`). A comment may be placed after the comma (delimited using the "!" symbol, see below)

on the same file record. This restriction on the use of commas is ignored on some compilers.

- *Too many commas following a scalar variable definition:*
More than one comma following a scalar variable assignment will result in a read error.
- *Too many commas following the variable assignment list for an array:*
The entire contents of an array can be assigned using a single statement by listing the values of each element separated by commas. The read will fail if there are more commas than the dimension of the array.
- *Comment does not begin with !:*
The character that delimits a comment in a namelist is the exclamation point. Comments can appear anywhere within the namelist. However, all text in the namelist must either be part of a namelist variable assignment or part of an identified comment.

We suggest that new CAMx users start with the “CAMx.namelist.template” that is provided with the source code.

2.3.1.2 The Primary Namelist Module

This section describes the primary namelist module; detailed descriptions of each of the Probing Tool modules are provided in their respective sections (Sections 7 through 10). A listing of all namelist variables necessary to run the core model is presented on the following pages.

Description of CAMx Run Control File Variables

&CAMx_Control	Label for the primary namelist module that configures the core model; it must begin in column 2
&	Flag ending a namelist module; it must be in column 2
Run_Message	60-character simulation message, written to output files to label the run

The short simulation “run message” is written to all output files to describe and label the run.

Model Clock Control

Time_Zone	Integer time zone (0=UTC, 5=EST, 6=CST, 7=MST, 8=PST)
Restart	Logical model restart flag (TRUE=read restart file, FALSE=read initial conditions file)
Start_Date_Hour	Integer array start time (YYYY, MM, DD, HHmm)
End_Date_Hour	Integer array end time (YYYY, MM, DD, HHmm)
Maximum_Timestep	Real maximum allowable timestep (minutes)
Met_Input_Frequency	Real input frequency of environmental fields (minutes)
Ems_Input_Frequency	Real input frequency of emissions (minutes)
Output_Frequency	Real output frequency (minutes)

The user specifies the simulation start/end year, month, day, and hour; the model uses Julian dates internally. All times must be given in military format (e.g., 1:30 PM must be given as 1330). The simulation time zone must match the time zone in which the emission and environmental inputs are developed.

Map Projection Parameters

Map_Projection	Character map projection keyword (LAMBERT, POLAR, RPOLAR, MERCATOR, UTM, LATLON)
UTM_Zone	Integer UTM zone
Longitude_Pole	Real longitude of projection pole or origin (degrees, west<0)
Latitude_Pole	Real latitude of projection pole or origin (degrees, south<0)
True_Latitude1	Real first true latitude of projection (degrees, south<0)
True_Latitude2	Real second true latitude of projection (degrees, south<0)

The grid projection may be selected as Cartesian (fixed physical distance coordinates on a flat plane) or curvi-linear geodetic (following the curved surface of the Earth). The Cartesian options include Lambert Conic Conformal (LAMBERT), Polar Stereographic (POLAR), Rotated Polar Stereographic (RPOLAR), Mercator (MERCATOR), and Universal Transverse Mercator (UTM). The geodetic option performs the simulation on a latitude/longitude grid (LATLON). All gridded input files must be defined on the grid projection specified for the CAMx simulation.

The LAMBERT, POLAR, and MERCATOR projections are all equivalent to the definitions used in the WRF meteorological model, which assumes a spherical Earth with radius of 6370 km. The RPOLAR projection is equivalent to the definition used in the RAMS meteorological model. While the POLAR projection of WRF is defined to be tangent at (or secant around) the North and South Poles, the RPOLAR projection of RAMS is defined to be only tangent to the Earth's surface at any user-defined latitude/longitude.

If the LAMBERT projection is specified, the Longitude_Pole and Latitude_Pole must be specified to define the projection origin (where LAMBERT coordinates are defined to be 0,0 km), and True_Latitude1 and True_Latitude2 must be specified to define the projection true latitudes (they may be equal, which is a projection tangent at that latitude).

If the MERCATOR projection is specified, the Longitude_Pole and Latitude_Pole must be specified to define the projection origin (where MERCATOR coordinates are defined to be 0,0 km), and True_Latitude1 must be specified to define the projection true latitude (it may be zero, which is a projection tangent at the Equator).

If the POLAR projection is specified, the Longitude_Pole and Latitude_Pole must be specified to define the projection origin (where coordinates are defined to be 0,0 km), and True_Latitude1 must be specified to define the projection true latitude or secant (it may be ± 90 degrees, which is a projection tangent at the North or South Poles).

If the RPOLAR projection is specified, the `Longitude_Pole` and `Latitude_Pole` must be specified to define the projection pole (where coordinates are defined to be 0,0 km). True latitudes are not specified as RPOLAR is always tangent at the pole point.

If the UTM projection is specified, a UTM zone must be specified (1 through 60). Pole and true latitude values are ignored for UTM and LATLON projections.

Parameters For The Master (First) Grid

<code>Number_of_Grids</code>	Integer number of grids in simulation
<code>Master_SW_XCoord</code>	Real x-coordinate of domain southwest corner (km, or degrees for LATLON)
<code>Master_SW_YCoord</code>	Real y-coordinate of domain southwest corner (km, or degrees for LATLON)
<code>Master_Cell_XSize</code>	Real cell size in x (km, or degrees for LATLON)
<code>Master_Cell_Ysize</code>	Real cell size in y (km, or degrees for LATLON)
<code>Master_Grid_Columns</code>	Integer number of master grid columns (E-W grid cells)
<code>Master_Grid_Rows</code>	Integer number of master grid rows (N-S grid cells)
<code>Number_of_Layers</code>	Integer number of grid layers (applies to all grids)

The master grid is defined by its location (southwest corner of cell [1,1] in the coordinates of the chosen projection space), number of grid cells (east-west, north-south, vertically), and horizontal resolution. Vertical resolution is defined by the layer structure specified in the input 3D meteorological file.

Parameters For The Nested Grids

<code>Nest_Meshing_Factor</code>	Integer array (by grid) nested grid cell size relative to master grid
<code>Nest_Beg_I_Index</code>	Integer array (by grid) master grid column containing western edge of nest
<code>Nest_End_I_Index</code>	Integer array (by grid) master grid column containing eastern edge of nest
<code>Nest_Beg_J_Index</code>	Integer array (by grid) master grid row containing southern edge of nest
<code>Nest_End_J_Index</code>	Integer array (by grid) master grid row containing northern edge of nest

The definition of nested grids is specified in the `CAMx.in` file in terms of the range of master grid cells that each nested grid spans (see Section 4). The "meshing factor" sets the resolution or cell size of the nested grids relative to the master grid. The CAMx diagnostic output file provides information on the location and size of each nested grid to help ensure proper setup.

Model Options

<code>Diagnostic_Error_Check</code>	Logical model startup diagnostic flag (TRUE=stops before first timestep indicating successful model initialization, FALSE=continues with simulation after model initialization)
-------------------------------------	---

Flexi_Nest	Logical flexi-nesting flag (TRUE=allow some/all nested input fields to be interpolated from the parent grid, FALSE=all data must be provided for all nests)
Advection_Solver	Character horizontal advection solver keyword (PPM, BOTT)
Chemistry_Solver	Character chemistry solver keyword (EBI, LSODE)
PiG_Submodel	Character PiG submodel keyword (NONE, GREASD, IRON)
Probing_Tool	Character Probing Tool keyword (NONE, SA, DDM, HDDM, PA, IPR, IRR, RTRAC, RTCMC)
Chemistry	Logical chemistry flag (TRUE=chemistry on, FALSE=chemistry off)
Drydep_Model	Character dry deposition model keyword (NONE, WESELY89, ZHANG03)
Wet_Deposition	Logical wet deposition flag (TRUE=deposition on, FALSE=deposition off)
ACM2_Diffusion	Logical ACM2 vertical diffusion flag (TRUE=ACM2 on, FALSE=standard K-theory diffusion)
Surface_Model	Logical surface model flag (TRUE=surface model on, FALSE=surface model off)
Inline_Ix_Emissions	Logical in-line oceanic inorganic iodine emissions flag (TRUE=in-line emission on, FALSE=in-line emissions off)
Super_Stepping	Logical super-stepping flag (TRUE=use super-stepping for horizontal advection to maximize model speed, FALSE=do not use super-stepping).
Gridded_Emissions	Logical gridded emissions flag (TRUE=gridded emissions will be used, FALSE=gridded emissions will be ignored)
Point_Emissions	Logical elevated point source flag (TRUE=point emissions will be used, FALSE=point emissions will be ignored)
Ignore_Emission_Dates	Logical date-insensitive emission flag (TRUE=dates on emission files will be ignored, FALSE=dates on emission files will be checked against simulation date)

Probing Tools are selected by specifying one of the allowed keywords; no Probing Tool will be run if this keyword is set to "None". The description of the PiG submodel is provided in Section 6.

Super stepping maximizes the model's speed performance by setting the largest grid-specific driving time steps possible. This results in the need for potentially many sub-steps to be applied in horizontal advection on a layer-by-layer basis to maintain a stable solution. While super stepping has little impact on surface concentrations in non-MPI mode, larger differences are seen using MPI. A "super-stepping" flag was added to the control namelist that allows users to specifically turn off super stepping when they wish to compare concentrations between MPI and non-MPI runs in the most consistent manner possible. Super stepping can reduce the accuracy of the vertical transport solution, especially in high wind conditions over complex terrain. Turning super stepping off will cause the model to run much more slowly.

Output Specifications

Root_Output_Name	Character root output path/filename (see Table 2-2 for description of file suffixes)
Average_Output_3D	Logical 3-D average output file flag (TRUE=output full 3-D concentration fields, FALSE=output surface layer concentration fields)
Output_3D_Grid	Logical array (by grid) 3-D average output file flag (TRUE=output full 3-D concentration fields for specified grid, FALSE=output surface layer concentration fields)
Output_Species_Names	Character array (by output species) species names to be written to average and deposition output files, or the single name "ALL" to output all state gas and PM species (excluding radicals), or the single name "ALLR" to include radicals
PiG_Sampling_Grid	Logical sampling grid flag for IRON PiG output (TRUE=sampling grids are specified, FALSE=sampling grids will not be generated)
Sample_Background	Logical flag to include background concentrations (TRUE=background concentrations from the host computational grid will be added to puff increments, FALSE=only puff increments will be shown)
Number_of_Sampling_Grids	Integer number of sampling grids
SG_Beg_I_Index	Integer array (by sampling grid) master grid column containing western edge of sampling grid
SG_End_I_Index	Integer array (by sampling grid) master grid column containing eastern edge of sampling grid
SG_Beg_J_Index	Integer array (by sampling grid) master grid row containing southern edge of sampling grid
SG_End_J_Index	Integer array (by sampling grid) master grid row containing northern edge of sampling grid
SG_Mesh_Factor	Integer array (by sampling grid) cell size relative to master grid

The user specifies a "root" path and filename that will be used for all standard CAMx core model output files. The model appends suffixes to these root names according to the file type generated.

The types of CAMx output files are listed in Table 2-2. A subset of state (gas or PM) and radical species may be output to the average concentration output files; see the description of output file formats in Section 3. By specifying a single output name "ALL", the model will automatically output fields for all state gas and PM species listed in the input chemistry parameters file, excluding radicals (use "ALLR" to include radicals). If "ALL" or "ALLR" are specified, it must be the only name listed; no species names may be listed before or after "ALL". There are two flags that control whether 3-D average output files are generated. The first (original) flag will toggle 3-D output for all grids in the run. The second is the "Output_3D_Grid" flag array, which allows 3-D average output to be set for specific grids. The original flag supersedes the grid-specific flag.

PiG sampling grids are set identically to the way nested grids are specified for the host model, with one exception: there are no vertical levels to define (sampling grids are currently only 2-D layer 1 fields). The same rules that apply for the specification of nested grids holds for the specification of all sampling grids (see Section 4).

Input Files

Chemistry_Parameters	Character input chemistry parameters path/filename
Photolysis_Rates	Character input photolysis rates path/filename (optional according to Chemistry flag and Chemistry_Parameters file)
Ozone_Column	Character input ozone column path/filename (ignored if Chemistry=FALSE)
Initial_Conditions	Character input master grid initial conditions path/filename (ignored if Restart=TRUE)
Boundary_Conditions	Character input master grid lateral boundary conditions path/filename
Top_Concentrations	Character input master grid top boundary conditions path/filename
Point_Sources	Character input elevated point source emissions path/filename (ignored if Point_Emissions=FALSE)
Master_Grid_Restart	Character input master grid restart path/filename (ignored if Restart=FALSE)
Nested_Grid_Restart	Character input nested grid restart path/filename (ignored if Restart=FALSE or Number_of_Grids=1)
PiG_Restart	Character input PiG restart path/filename (ignored if Restart=FALSE or PiG_Submodel=FALSE)
Srfmod_Grid	Character array (by grid) input surface model restart path/filename (ignored if Restart=FALSE or Surface_Model=FALSE)
Surface_Grid	Character array (by grid) input static 2D surface path/filename (optional for nested grids)
Met2D_Grid	Character array (by grid) input time-variant 2D surface meteorology path/filename (optional for nested grids)
Met3D_Grid	Character array (by grid) input time-variant 3D meteorology path/filename (optional for nested grids)
Vdiff_Grid	Character array (by grid) input time-variant 3D vertical diffusivity path/filename (optional for nested grids)
Cloud_Grid	Character array (by grid) input time-variant 3D cloud/rain path/filename (optional but required if Wet_Deposition=TRUE, optional for nested grids)
Emiss_Grid	Character array (by grid) input gridded emissions path/filename (ignored if Gridded_Emissions=FALSE, optional for nested grids)

If CAMx cannot find or open a non-blank input filename provided in the run control file, the model will stop with an error. CAMx will accept blank input filenames for only those files that are optional.

Table 2-2. CAMx output file suffixes and their corresponding file types.

Suffix	CAMx File Type
.out	Text simulation tracking file (CPU, input files read, error/warning messages)
.diag	Text simulation diagnostic file (repeat of run control inputs, PiG diagnostics, miscellaneous diagnostic output)
.mass	Text mass budget file for subsequent postprocessing
.inst	Fortran binary master grid 3-D instantaneous concentration file at the end of the simulation (used for restarts)
.finst	Fortran binary nested grid 3-D instantaneous concentration file at the end of the simulation (used for restarts)
.pig	Fortran binary PiG sub-model file (used for restarts)
Standard CAMx Output Option	
.avrg.grdnn	Fortran binary average concentration file for grid <i>nn</i> ; optionally contains 2-D layer 1 concentration field or full 3-D concentration field
.depn.grdnn	Fortran binary 2-D surface deposition file for grid <i>nn</i>
.srf.grdnn	Fortran binary 2-D surface model mass file for grid <i>nn</i> (optional)
.smpnn	Fortran binary 2-D layer 1 average concentration file for PiG sampling grid <i>nn</i> (optional)

2.3.2 Using Scripts to Run CAMx

The generation of the run control file is most easily accomplished in the job script that actually runs the model; Figure 2-2 shows an example of a CAMx job script that builds a "CAMx.in" file and runs the model for each day to be simulated. Alternatively, the run control file could be written separately with a name specific to a given simulation, then linked or copied to the standard "CAMx.in" filename before the model is executed at a command line or in a job script.

```

#!/bin/csh
#
# CAMx v6.40
#
setenv OMP_NUM_THREADS 4
setenv MPSTKZ 128M
limit stacksize unlimited
#
set EXEC      = "../src/CAMx.v6.40.noMPI.pg_linuxomp"
#
set RUN       = "v6.40.midwest.36.12.noMPI"
set INPUT    = "../inputs"
set MET       = "../inputs/met"
set EMIS     = "../emiss"
set PTRSCE   = "../ptrsce"
set OUTPUT   = "../outputs"
#
mkdir -p $OUTPUT
#
# --- set the dates and times ----
#
set RESTART = "NO"
foreach today (03.154 04.155)
set JUL = $today:e
set CAL = $today:r
set YESTERDAY = `echo ${CAL} | awk '{printf("%2.2d", $1-1)}'`
#
if( ${RESTART} == "NO" ) then
    set RESTART = "false"
else
    set RESTART = "true"
endif
#
# --- Create the input file (always called CAMx.in)
#
cat << ieof > CAMx.in

&CAMx_Control

Run_Message      = 'CAMx 6.30 Test Problem -- Mech6 CF CB05 $RUN',

!--- Model clock control ---

Time_Zone        = 0,                ! (0=UTC, 5=EST, 6=CST, 7=MST, 8=PST)
Restart          = .${RESTART}.,
Start_Date_Hour  = 2002,06,${CAL},0000, ! (YYYY,MM,DD,HHmm)
End_Date_Hour    = 2002,06,${CAL},2400, ! (YYYY,MM,DD,HHmm)

Maximum_Timestep = 15.,              ! minutes
Met_Input_Frequency = 60.,          ! minutes
Ems_Input_Frequency = 60.,          ! minutes
Output_Frequency = 60.,             ! minutes

```

Figure 2-2. A sample CAMx job script that generates a “CAMx.in” file and runs the model with OMP parallelization.

```

!--- Map projection parameters ---

Map_Projection           = 'LAMBERT', ! (LAMBERT,POLAR,UTM,LATLON)
Longitude_Pole           = -97.,      ! deg (west<0,south<0)
Latitude_Pole            = 40.,       ! deg (west<0,south<0)
True_Latitude1           = 45.,       ! deg (west<0,south<0)
True_Latitude2           = 33.,       ! deg (west<0,south<0)

!--- Parameters for the master (first) grid ---

Number_of_Grids          = 2,
Master_SW_XCoord         = -792.,      ! km or deg, SW corner of cell(1,1)
Master_SW_YCoord         = -1656.,     ! km or deg, SW corner of cell (1,1)
Master_Cell_XSize        = 36.,        ! km or deg
Master_Cell_YSize        = 36.,        ! km or deg
Master_Grid_Columns      = 68,
Master_Grid_Rows         = 68,
Number_of_Layers         = 16,

!--- Parameters for the second grid ---

Nest_Meshing_Factor(2)  = 3,          ! Cell size relative to master grid
Nest_Beg_I_Index(2)     = 22,         ! Relative to master grid
Nest_End_I_Index(2)     = 51,         ! Relative to master grid
Nest_Beg_J_Index(2)     = 22,         ! Relative to master grid
Nest_End_J_Index(2)     = 58,         ! Relative to master grid

!--- Model options ---

Diagnostic_Error_Check   = .false.,    ! True = will stop after 1st timestep
Advection_Solver         = 'PPM',      ! (PPM,BOTT)
Chemistry_Solver         = 'EBI',      ! (EBI,LSODE)
PiG_Submodel             = 'None',     ! (None,GREASD,IRON)
Probing_Tool             = 'None',     ! (None,SA,DDM,HDDM,PA,IPR,IRR,RTRAC,RTCMC)
Chemistry                 = .true.,
Drydep_Model             = 'WESELY89', ! (None, WESELY89, ZHANG03)
Wet_Deposition           = .true.,
ACM2_Diffusion           = .false.,
Surface_Model            = .false.,
Super_Stepping           = .true.,
Gridded_Emissions       = .true.,
Point_Emissions          = .true.,
Ignore_Emission_Dates   = .true.,

!--- Output specifications ---

Root_Output_Name         = '$OUTPUT/CAMx.$RUN.200206${CAL}',
Average_Output_3D        = .false.,
Output_Species_Names(1)  = 'NO',
Output_Species_Names(2)  = 'NO2',
Output_Species_Names(3)  = 'O3',
Output_Species_Names(4)  = 'SO2',
Output_Species_Names(5)  = 'H2O2',
Output_Species_Names(6)  = 'HNO3',
Output_Species_Names(7)  = 'NH3',
Output_Species_Names(8)  = 'PNO3',
Output_Species_Names(9)  = 'PSO4',
Output_Species_Names(10) = 'PNH4',
Output_Species_Names(11) = 'POA',

```

Figure 2-2 (continued).

```

Output_Species_Names(12) = 'PEC',
Output_Species_Names(13) = 'FPRM',
Output_Species_Names(14) = 'CPRM',
Output_Species_Names(15) = 'CCRS',
Output_Species_Names(16) = 'FCRS',
Output_Species_Names(17) = 'SOA1',
Output_Species_Names(18) = 'SOA2',
Output_Species_Names(19) = 'SOA3',
Output_Species_Names(20) = 'SOA4',
Output_Species_Names(21) = 'SOA5',

!--- Input files ---

Chemistry_Parameters = '$INPUT/CAMx6.3.chemparam.6_CF',
Photolysis_Rates    = '$INPUT/tuv.200206.STL.txt',
Ozone_Column        = '$INPUT/o3col.200206.STL_36_68X68_12_92X113.txt',
Initial_Conditions  = '$INPUT/IC.vistas_2002gt2a_STL_36_68X68_16L.2002081',
Boundary_Conditions = '$INPUT/BC.vistas_2002gt2a_STL_36_68X68_16L.2002${JUL}',
Top_Concentrations = ' ',
Point_Sources       = '$PTSRC/ptsrce.stl.36km.2002${JUL}.a0.bin',
Master_Grid_Restart = '$OUTPUT/CAMx.$RUN.200206${YESTERDAY}.inst',
Nested_Grid_Restart = '$OUTPUT/CAMx.$RUN.200206${YESTERDAY}.finst',
PiG_Restart         = ' ',
Srfmod_Grid(1)     = ' ',
Srfmod_Grid(2)     = ' ',

Flexi_Nest          = .false.
Emiss_Grid(1)      = '$EMIS/emiss.stl.36km.200206${CAL}.al.bin',
Surface_Grid(1)    = '$INPUT/met/camx.lu.36k.bin',
Met2D_Grid(1)      = '$INPUT/met/camx.2d.200206${CAL}.36k.bin',
Met3D_Grid(1)      = '$INPUT/met/camx.3d.200206${CAL}.36k.bin',
Vdiff_Grid(1)      = '$INPUT/met/camx.kv.200206${CAL}.36k.bin',
Cloud_Grid(1)      = '$INPUT/met/camx.cr.200206${CAL}.36k.bin',
Emiss_Grid(2)      = '$EMIS/emiss.stl.12ksmall.200206${CAL}.al.bin',
Surface_Grid(2)    = '$INPUT/met/camx.lu.12ksmall.bin',
Met2D_Grid(2)      = '$INPUT/met/camx.2d.200206${CAL}.12ksmall.bin',
Met3D_Grid(2)      = '$INPUT/met/camx.3d.200206${CAL}.12ksmall.bin',
Vdiff_Grid(2)      = '$INPUT/met/camx.kv.200206${CAL}.12ksmall.bin',
Cloud_Grid(2)      = '$INPUT/met/camx.cr.200206${CAL}.12ksmall.bin',

/
!-----

ieof
#
# --- Execute the model ---
#
if( ! { $EXEC } ) then
    exit
endif

end

```

Figure 2-2 (concluded).

2.4 Benchmarking Model Run Times

Overall model speed and OMP/MPI scalability depends on several factors, including the number and sizes of grids; the choice of chemistry mechanism; the number of point sources to be treated with PiG and total PiG puffs that accumulate during a run; and the use of Probing Tools. Parallelization is most advantageous for larger applications in which overhead processes (e.g., model setup, I/O, etc.) are a much smaller fraction of total model run time. In other words, CAMx applications on multiple expansive grids, employing PiG, and/or including Probing Tools would scale most effectively and thus benefit most from parallelization.

A set of systematic run time tests were recently conducted by the Lake Michigan Air Directors Consortium (LADCo) using CAMx v6.20 with various combinations of OMP and MPI parallelization. Note that model speed has been improved somewhat since v6.20; however, results from LADCo's test are informative. LADCo's CAMx configuration was relatively simple, employing a single large grid covering the entire US with 12 km grid spacing (396×246, 25 layers), and using CB6r2 photochemistry with the CF PM treatment. PiG and Probing Tools were not active. CAMx was compiled using Portland Group v15.7-0 with OMP and MPICH v3.1.4. CAMx was run on a 2.60 Ghz Intel Xeon chipsets with 12 physical cores (24 cores hyper-threaded). Run time results are shown in Table 2-3.

Table 2-3. CAMx v6.20 speed performance with MPI and OMP parallelization from the LADCo tests described above.

OMP Threads	MPI Slices	Total Cores	Hours/Sim Day
12	0	12	4:05:12
12	2	24	3:30:47
8	3	24	2:59:08
6	4	24	2:36:10
4	6	24	2:35:17
3	8	24	2:27:34
2	12	24	2:25:25
1	24	24	3:06:57

2.5 CAMx Pre- And Post-Processors

This section describes several important CAMx pre- and post-processors that we make available to the user community. Like CAMx itself, these programs are written in Fortran and distributed as free software under the terms of the GNU General Public License. Each come with README files, makefiles, and sample job scripts that document their purpose and usage. Ramboll Environ occasionally posts updates for certain widely-used programs when necessary, but does not actively support or maintain every one. Users can e-mail questions, comments, suggestions or improvements to ask-camx@environ.org.

2.5.1 Emissions

Certain emission models (those shown in Figure 2-1) can provide speciated, temporally-allocated, gridded and point source emission input files in the CAMx-ready format. Further

processing may be required, however, to select point sources for the PiG treatment, translate the point source files from a common text format to CAMx-ready binary files, or to refine the domain size/resolution for gridded emissions.

PIGSET: This program allows the user to select and set certain point sources for the Plume-in-Grid (PiG) treatment in a CAMx simulation. It also converts text point source files commonly generated by emission models such as SMOKE, CONCEPT, and EPS3 to CAMx-ready binary format. See the source code for more information, and the sample job for usage. Also see Section 6 for guidance in selecting PiG point sources and manipulating day-specific point source files.

WINDOW: This program is used to “window” out a sub-section of the surface emissions grid for use on a smaller CAMx grid. It can also be used to aggregate or distribute surface emissions to coarser or finer resolution, respectively. See the sample job for usage.

SEASALT: This program generates aerosol emissions of sodium and chloride (for PM chemistry), and gaseous emissions of chlorine and halo-methane compounds (for the CB6r2h full-science halogen mechanism), using CAMx-ready meteorological and landuse files. A separate merging program is included that allows sea salt emissions to be merged in with pre-existing CAMx-ready gridded emission files.

PREPVBS: This program converts the organic compound emissions (VOC precursors and POA) prepared for the CAMx CF aerosol scheme to those compatible with the VBS scheme so that the user can employ the VBS scheme without having to develop emission inputs for the scheme from scratch. However, this approach should be used with caution because significant uncertainties exist in the VBS emissions estimated by this. See the sample job for usage.

REGNMAP: This program supports the development of source apportionment fractional (partial) region maps with which to allocate gridded emissions to source regions. It reads SMOKE spatial allocation reports for a specific modeling grid and source category (or group of categories), extracts emissions data by grid cell and state/county FIPS code, and generates a new CAMx input file that defines a fractional region map for that grid and source category/group.

2.5.2 Meteorology

The recommended approach to develop meteorological inputs for CAMx is through the use of prognostic meteorological models. Ramboll Environ distributes interface programs for three specific models: WRF, MM5, and RAMS; This does not necessarily preclude other meteorological models to be used, but users will need to develop interface programs on their own.

WRF-CAMx: This program generates CAMx v6 meteorological input files from WRF (ARW core) v3 output files. See the README in the archive for a description of the program and how it is applied. You will need NetCDF libraries to compile and run this program.

MM5CAMx: This program generates CAMx v6 meteorological input files from MM5 v3 output files. See the README in the archive for a description of the program and how it is applied.

RAMSCAMx: This program generates CAMx v6 meteorological input files from RAMS v4/5/6 output files. See the README in the archive for a description of the program and how it is applied. You will need HDF5 libraries to compile and run this program.

METCONVERT: This program converts older meteorological files from CAMx v4 and v5 to the CAMx format introduced with CAMx v6.

KVPATCH: This program applies minimum limits on vertical diffusivity (Kv) within a user-defined surface layer depth based on an input landuse grid. It optionally allows Kv profiles to be extended into daytime boundary-layer capping convection as defined by input cloud/rain files. See the source code for more information. Use of this program to adjust Kv inputs is entirely optional.

2.5.3 Photolysis Rates

The development of photolysis rate inputs for CAMx is crucial for the photochemical mechanisms, but is not needed for inert or simple chemistry (e.g., Mechanism 10) applications. Two programs are available to assist the user in developing photolysis and ozone column input files.

O3MAP: This program prepares ozone column input files for CAMx, and must be run prior to running the TUV model as it defines the atmospheric ozone column intervals based on input data. Ozone column data files (<http://ozoneaq.gsfc.nasa.gov/data/ozone> or <ftp://toms.gsfc.nasa.gov/pub/omi/data/>) in latitude/longitude text format must be supplied as input. O3MAP attempts to fill data gaps in day-specific ozone column files (Figure 2-3) from valid data processed for the extraction domain. Alternatively, you may use monthly-average ozone column files (no data gaps). See the Readme file and job script in the archive for usage.

TUV: This is a radiative transfer model that develops clear-sky photolysis rate inputs for all CAMx photochemical mechanisms. TUV is developed and distributed by NCAR (2011). The program specifies default intervals for 5 surface UV albedos, 3 terrain heights, 11 altitudes above ground, 10 solar zenith angles, and 5 atmospheric ozone column intervals (from O3MAP). See the sample job in the archive for usage.

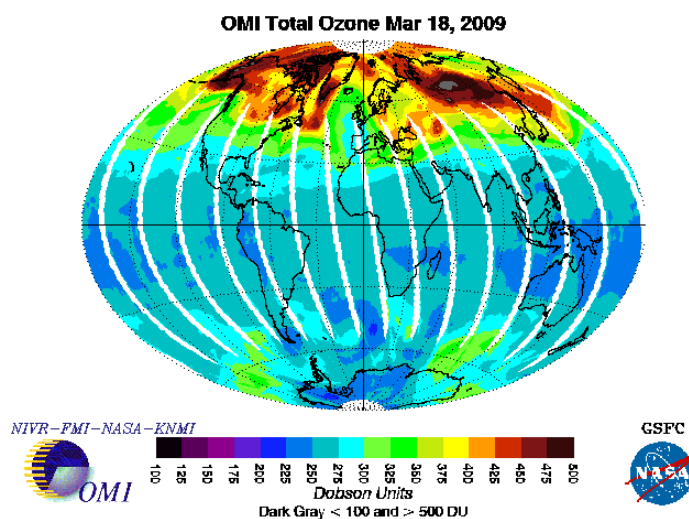


Figure 2-3. An example of global ozone column from the Ozone Monitoring Instrument (OMI) platform. White areas denote missing data. From <ftp://toms.gsfc.nasa.gov/pub/omi/data/>.

2.5.4 Initial and Boundary Conditions

Ramboll Environ provides a few programs to develop initial and boundary conditions, but there are many ways to generate these important inputs. The most common approach involves “down-scaling” (or extracting) the output from larger-scale (e.g., global) models to the CAMx domain. Users will need to develop their own programs if they choose an alternative methodology or source of data to generate initial/boundary conditions.

ICBCPREP: This program prepares simple CAMx initial and lateral boundary condition files.

Values are constant in space and time, but unique values may be specified for each chemical species to be modeled; they are defined in a text file. See the sample job in the archive for usage.

GEOS2CAMx: This program generates CAMx initial, lateral boundary, and (optionally) top boundary condition input files from GEOS-Chem global model output. See the Release Notes and job scripts in the archive for a description of the program and how it is applied.

MOZART2CAMx: This program generates CAMx and CMAQ initial and lateral boundary condition input files from MOZART4 output. This program will also process AM3 datasets if output is first translated to a geodetic (latitude/longitude) grid, concentrations are provided as volume mixing ratio, and all needed state variables are available. See the README in the archive for a description of the program and how it is applied. You will need I/O-API and NetCDF libraries to compile and run this program.

2.5.5 Landuse

Approaches for developing landuse/landcover inputs for CAMx include: (1) translating gridded spatial allocation surrogates developed during emissions processing into the CAMx categories described in Section 3; (2) translating the gridded landuse/landcover fields from the meteorological model; or (3) separately developing landuse input fields from raw data (such as from USGS, MODIS or NLCD) using GIS or other programs. Ramboll Environ distributes meteorological interface programs (described above) that translate the meteorological model landuse/landcover fields to the CAMx definitions and grid configuration.

MERGE_LULAI: This program merges independently-developed landuse and/or LAI fields (for example via GIS processing of common terrestrial datasets) with an existing CAMx 2D surface file generated by the meteorological interface programs. See the sample job and source code for a description of the program and how it is applied.

WATERMASK: This program converts existing CAMx landuse files to distinguish between ocean/salt water and fresh water coverages. The CAMx input landuse file lists the fractional coverage of "WATER" (index = 1) and "LAKE" (index=3), but since none of the land cover datasets employed by meteorological models (WRF, MM5, RAMS) differentiate between fresh and ocean water bodies, the respective CAMx meteorological interface programs populate only the "WATER" classification for any water type. The in-line iodine emissions algorithm and mercury chemistry need to differentiate between ocean and fresh water bodies. The WATERMASK program is run twice: (1) read an existing landuse file and develop a text-based water map that shows all grid cells containing some fraction of water in each grid cell, which must then be edited to remove fresh water cells; and (2) read the edited water map and convert the existing landuse file to populate the "WATER" category with ocean fractions and the "LAKE" category with fresh water fractions. This change is compatible with the Zhang and Wesely dry deposition options within CAMx.

2.5.6 Post-processors

Most of the CAMx post-processors distributed by Ramboll Environ provide some manner of concentration file manipulation, either to extract certain information from the raw output files, to re-format for use in other programs and applications, to concatenate files, etc. A few others are distributed to assist in evaluating Probing Tool output. Ramboll Environ does not advocate or support any particular visualization or graphics software.

AVGDIF: This program is used to compare two CAMx format output average files and print a table of differences. This is useful for checking differences between CAMx runs on different machines or different compile options for the test case. See the sample job in the archive for usage.

BNDEXTR: Use this program to extract boundary conditions for a nested grid when you apply CAMx in one-way nesting mode. One-way nesting means that CAMx is run successively for each grid, with BNDEXTR as the interface between each run. This program is not needed when CAMx is run in the more standard two-way nesting mode, where all grids are run in a single simulation. See the example job for usage.

CAMxPOST: This is a suite of post-processing utilities designed to facilitate the evaluation of model performance. It is used to combine observations and predictions, calculate statistics, and plot time series. See the README file in the archive for usage.

CAMxTRCT: This program extracts a single chemical species for specified grids from the output average concentration and deposition files, and from input emission files. Output from this program can be written in the standard CAMx format, or alternatively to a text format in Surfer® "GRD" format for subsequent plotting. It also has the capability to convert units and combine species to yield certain hard-coded bulk compounds like NOx and VOC. See the sample job in the archive for usage.

CAMx2IOAPI: This program converts CAMx output average concentration and deposition files to I/O-API format. You will need I/O-API and NetCDF libraries to compile and run this program. This program allows you to use various third-party manipulation and visualization software that handle I/O-API and NetCDF formats.

PA_Tools: This is a suite of post-processing utilities designed to extract IPR, IRR, and CPA data from CAMx Process Analysis output files and reformat the data suitable for subsequent analysis (e.g. using spreadsheets).

XSPCMAP: Similar to CAMxTRCT yet more flexible, this program extracts any number of specific chemical species or user-defined combinations of species for specified grids from the output average concentration and deposition files, and writes results to a new file in CAMx format. See the sample job and species mapping table in the archive for usage.

3. CORE MODEL INPUT/OUTPUT STRUCTURES

Most CAMx input/output (I/O) files are Fortran binary and based on the Urban Airshed Model (UAM) convention. This allows the user to employ widely available software designed specifically for these formats to develop the input files or to post-process and visualize the output files.

CAMx requires input files that define the chemical mechanism and describe the photochemical conditions, surface characteristics, initial/boundary conditions, emission rates, and various meteorological fields over the entire modeling domain. Table 3-1 summarizes the input data requirements of CAMx. Preparing this information requires several preprocessing steps to translate "raw" emissions, meteorological, air quality and other data into final input files for CAMx. Prognostic meteorological models are used to generate all of the required time varying three-dimensional meteorological fields.

Table 3-1. Data requirements of CAMx.

Data Types	Data Fields
<u>Meteorology</u> <i>Supplied by Prognostic Meteorological Models</i>	<ul style="list-style-type: none"> • 3-Dimensional Gridded Fields: <ul style="list-style-type: none"> - Vertical Grid Structure - Horizontal Wind Components - Temperature - Pressure - Water Vapor - Vertical Diffusivity - Clouds/Precipitation (optional) - Snow Cover (optional)
<u>Air Quality</u> <i>Developed from Other Models or Measurement Data</i>	<ul style="list-style-type: none"> • Gridded Initial Concentrations • Gridded Lateral Boundary Concentrations • Gridded Top Boundary Concentrations (optional)
<u>Emissions</u> <i>Supplied by Emissions Models and Processors</i>	<ul style="list-style-type: none"> • Elevated Point Sources (optional), e.g.: <ul style="list-style-type: none"> - Industrial Facilities - Prescribed, Agricultural, Wild Fires - Lightning NOx • Combined Gridded Sources (optional), e.g.: <ul style="list-style-type: none"> - Low-Level Point - On-Road and Non-Road Mobile - Area - Biogenic - Oceanic
<u>Geographic</u> <i>Developed from Terrain, Landuse/Landcover, and Vegetation Density Datasets</i>	<ul style="list-style-type: none"> • Gridded Surface Characteristics <ul style="list-style-type: none"> - Landuse/LandCover - Terrain Elevation (optional) - Leaf Area Index (LAI; optional)
<u>Photolysis</u> <i>Derived from Satellite Measurements and Radiative Transfer Models</i>	<ul style="list-style-type: none"> • Atmospheric Radiative Properties <ul style="list-style-type: none"> - Gridded Ozone Column Codes - Photolysis Rates Lookup Table

CAMx produces gridded time-averaged concentration output files; the user selects the time interval (usually hourly), the species to be output, and whether the output contains just two-dimensional surface layer fields or entire three-dimensional fields. A separate average output file is written for each grid employed in the simulation. Two-dimensional surface deposition fields for the same user-selected species are also written to output files with the same structure as the average concentration files. Gridded three-dimensional instantaneous concentrations of all species on all grids are written at the end of the simulation to allow for a model restart. The CAMx Probing Tool options provide their own information in separate output files in the same CAMx output format. Diagnostic output files include three files that track computer resources, echo input selections, provide mass budget and diagnostic summaries, and provide error/warning messages.

3.1 CAMx Chemistry Parameters File

Chemistry parameters are provided in a text file that specifies the chemical mechanism to be used and associated details on species properties and reaction types and rates. The chemistry parameters file format is defined in Table 3-2, and samples are given in Figure 3-1. Some records in this file are labeled (columns 1-20) to indicate the type of information to supply on that line (starting in column 21). For records that are not labeled, data start in column 1. Some chemistry parameter records are optional, depending upon the logical flags indicated for such records, and are shown in Table 3-2 by a check in the third column; if the indicated option is not invoked these records should not appear in the file. The first record of the chemistry parameters file must contain the string "VERSION6.4", which indicates that the file is specific to this version of CAMx.

If the chemistry flag is set "true" on the CAMx.in file, CAMx checks that certain properties of the selected mechanism are consistent with parameters supplied on the input file (e.g., number of reactions, photolysis reactions and species). If any discrepancies are found, they are reported in the output message file and the simulation is halted. The user may also specify an inert simulation by setting the chemistry flag to "false". In this case, any number of arbitrarily named species may be listed, and chemistry reaction parameters are ignored.

Gas-phase chemistry is selected by a Mechanism ID assigned to each photochemical mechanism (see Section 5). Aerosol chemistry is selected by the keywords "NONE", "INERT", "CF" or "CMU". In the "INERT" case, the user can define any number of arbitrary particulate names and sizes. The "CF" and "CMU" options invoke aerosol chemistry and treat aerosol size using either static coarse and fine modes (CF) or an evolving size section model (CMU). Both CF and CMU options require a minimum set of specific aerosol names with associated chemistry.

The chemistry parameters file controls how photolysis rates are calculated in CAMx. So-called "primary" photolysis rates are input to CAMx via the photolysis rates file. The primary photolysis reactions are identified by number in the chemistry parameters file and the photolysis rates file must match this declaration. So-called "secondary" photolysis rates are set by scaling factors to one of the primary reactions. Use of secondary rates requires at least one primary photolysis reaction.

Table 3-2. Description of the CAMx chemistry parameters file. The record labels exist in columns 1-20, and where given, the input data for that record start in column 21. The format denoted "list" indicates a free-format list of numbers (comma or space-delimited).

Record Label (columns 1-20)	Record Optional	Format	Description
CAMx version		A	Model version keyword (VERSION6.4)
Mechanism ID		list	ID number of chemical mechanism (see Table 5-1)
Aerosol Option		A	Keyword for aerosol scheme (NONE, INERT, CF, or CMU) ¹
Description		A	Message record to describe this file
No of gas species		list	Number of radical and state gas species (NGAS ≥ 1)
No of aero species		list	Number of aerosol species (NAERO ≥ 0) Aerosol chemistry timestep (min) (if NAERO > 0) Number of size bins (NBIN ≥ 1) (if NAERO > 0) ² Aerosol diameter (μm) for NBIN+1 cut points (if NAERO > 0)
No of reactions		list	Number of reactions (NREACT ≥ 0)
Prim photo rxns		list	Number of primary photolysis reactions (NPHOT1 ≥ 0) List of primary photolysis reaction ID numbers (must match the photolysis rates input file)
No of sec photo rxn		list	Number of secondary photolysis reactions (NPHOT2 ≥ 0)
ID, prim ID, scale	√	list	If NPHOT2 > 0, repeat this record for each secondary photolysis reaction ID number of the secondary photolysis reaction ID number of the primary photolysis reaction used for scaling Secondary reaction scale factor
SrfMod #spc, #rxns		list	Number of Surface Model species and reactions (see Section 4.8) Set to 0,0 if not using the Surface Model
Species Records			Heading
Gas Spec ...			Heading
		5X, A10, E10.0, E10.0, F10.0, F10.0, F10.0, F10.0	Repeat this record for each gas species (start in column 1) Gas species name (radicals first, followed by state species) Lower bound concentration (ppm) Henry's law constant (M/atm) Henry's law temperature dependence (K) Molecular weight (g/mol) Wesley's reactivity parameter Surface resistance scaling factor for strong acids (0-1)

Table 3-2 (continued). Description of the CAMx chemistry parameters file. The record labels exist in columns 1-20, and where given, the input data for that record start in column 21. The format denoted "list" indicates a free-format list of numbers (comma or space-delimited).

Record Label (columns 1-20)	Record Optional	Format	Description
Aero Spec ...	√		Heading (<i>if NAERO > 0</i>)
	√	5X, A10, E10.0, F10.0 F10.0 I10 F10.0 I10	<i>if NAERO > 0, repeat this record for each aerosol species</i> (start in column 1) Aerosol species name Lower bound concentration ($\mu\text{g}/\text{m}^3$) Species density (g/cm^3) Dry extinction efficiency ($\text{m}^2/\mu\text{m}$) Hygroscopic extinction adjustment (0 = no adjustment, 1 = RH-dependent) Single-scattering albedo Assigned size bin (INERT and CF aerosols only – references cut points in record 6)
Reaction Records	√		Heading (<i>if NREACT > 0</i>)
Rxn Typ Param ...	√		Heading (<i>if NREACT > 0</i>)
	√	list	<i>if NREACT > 0, repeat this record for each gas-phase reaction</i> (start in column 1) Reaction ID number Rate constant expression ID number (1-7, as shown in Table 3-3) Rate constant parameters (depending on expression type in Table 3-3). For reactions identified as photolysis reactions above, the rate constant is not used and is customarily set to zero.

1 NONE = gas-phase chemistry only; INERT = user-defined inert PM species; CF = Coarse/Fine aerosol chemistry scheme; CMU = multi-sectional aerosol chemistry scheme;

2 For the CF scheme, NBIN *must be set to 2*, and the user specifies the coarse/fine size ranges.

3. Core Model Input / Output Structures

```

CAMx Version      |VERSION6.4
Mechanism ID     |6
Aerosol Option   |CF
Description      |CB05 plus PM (CF) with Hg: PNA rates set to 0; molecular units
No of gas species |68
#aero, dt, bins  |25 15.0 2 0.039 2.5 10.0
No of reactions  |156
Prim photo rxns  |19 1 8 9 14 15 25 36 51 52 53 62 65 75 76 87 91 102 143 152
No of sec photo rxn|4
ID, prim ID, scale |72 65 1.0
                  |97 65 0.0
                  |106 91 1.0
                  |138 75 9.0

SrfMod #spc, #rxns |0 0

```

Species Records

	Gas Spec	lower bnd	H-law	T-fact	Molwt	Reactivty	Rscale
1	O1D	1.00E-15	1.00E+00	0.	0.0	0.0	0.
2	O	1.00E-15	1.00E+00	0.	0.0	0.0	0.
3	OH	1.00E-15	1.00E+00	0.	0.0	0.0	0.
4	HO2	1.00E-15	1.00E+00	0.	0.0	0.0	0.
5	C2O3	1.00E-15	1.00E+00	0.	0.0	0.0	0.
6	XO2	1.00E-15	1.00E+00	0.	0.0	0.0	0.
7	XO2N	1.00E-15	1.00E+00	0.	0.0	0.0	0.
8	CXO3	1.00E-15	1.00E+00	0.	0.0	0.0	0.
9	MEO2	1.00E-15	1.00E+00	0.	0.0	0.0	0.
10	TO2	1.00E-15	1.00E+00	0.	0.0	0.0	0.
11	ROR	1.00E-15	1.00E+00	0.	0.0	0.0	0.
12	HCO3	1.00E-15	1.00E+00	0.	0.0	0.0	0.
13	CRO	1.00E-15	1.00E+00	0.	0.0	0.0	0.
14	AACD	1.00E-12	5.00E+03	-4000.	60.0	1.0	1.
15	ALD2	1.00E-12	6.30E+03	-6492.	44.0	1.0	1.
16	ALDX	1.00E-12	6.30E+03	-6492.	58.1	1.0	1.
17	CO	1.00E-04	1.00E-10	0.	28.0	0.0	1.
18	CRES	1.00E-12	2.70E+03	-6492.	108.1	1.0	1.
19	ETH	1.00E-12	1.00E-02	-4000.	28.0	0.0	1.
20	ETHA	1.00E-04	1.73E-03	-4000.	30.1	0.0	1.
21	ETOH	1.00E-12	2.20E+02	-4932.	46.1	1.0	1.
22	FACD	1.00E-12	5.68E+03	-6060.	46.0	1.0	1.
23	FORM	1.00E-12	6.30E+03	-6492.	30.0	1.0	1.
24	H2O2	1.00E-12	7.40E+04	-6643.	34.0	1.0	0.
25	HNO3	1.00E-12	2.10E+05	-8707.	63.0	0.0	0.
26	HONO	1.00E-12	5.90E+01	-4781.	47.0	1.0	1.
27	IOLE	1.00E-12	5.00E-03	-4000.	56.1	0.0	1.
28	ISOP	1.00E-12	1.00E-02	-4000.	68.1	0.0	1.
29	ISPD	1.00E-12	6.30E+03	-6492.	70.1	1.0	1.
30	MEOH	1.00E-12	2.20E+02	-4932.	32.0	1.0	1.
31	MEPX	1.00E-12	3.05E+02	-5250.	48.0	0.8	0.
32	MGLY	1.00E-12	2.70E+03	-6492.	72.0	1.0	1.
33	N2O5	1.00E-12	1.00E+05	-4000.	108.0	0.1	0.
34	NO	1.00E-09	1.90E-03	-1480.	30.0	0.0	1.
35	NO2	1.00E-12	1.00E-02	-2516.	46.0	0.8	1.
36	NO3	1.00E-15	1.00E+05	-4000.	62.0	0.1	0.
37	NTR	1.00E-12	9.40E+03	-8706.	119.1	0.0	1.
38	O3	1.00E-12	1.10E-02	-2415.	48.0	1.0	1.
39	OLE	1.00E-12	5.00E-03	-4000.	42.1	0.0	1.
40	OPEN	1.00E-12	2.70E+03	-6492.	84.0	1.0	1.
41	PACD	1.00E-12	5.00E+03	-4000.	76.0	1.0	1.
42	PAN	1.00E-12	3.60E+00	-5910.	121.0	0.6	1.
43	PANX	1.00E-12	3.60E+00	-5910.	135.0	0.6	1.
44	PAR	1.00E-04	1.00E-03	-4000.	72.1	0.0	1.
45	PNA	1.00E-12	2.00E+04	-5910.	79.0	1.0	1.

Figure 3-1a. Example CAMx chemistry parameters file for Mechanism 6 (CB05) with CF PM scheme that includes the mercury species HGO, HG2, and HGP.

3. Core Model Input / Output Structures

46	ROOH	1.00E-12	1.00E+02	-4000.	90.1	0.8	0.
47	SO2	1.00E-09	1.22E+00	-3156.	64.0	0.0	1.
48	SULF	1.00E-12	1.00E+10	0.	98.0	0.0	0.
49	TERP	1.00E-12	4.90E-02	-4000.	136.2	0.0	1.
50	TOL	1.00E-12	1.20E+00	-4000.	92.1	0.0	1.
51	XYL	1.00E-12	1.40E+00	-4000.	106.2	0.0	1.
52	NH3	1.00E-09	5.76E+01	-4100.	17.0	0.0	0.
53	HCL	1.00E-12	1.00E+05	-4000.	36.5	0.0	0.
54	TOLA	1.00E-12	1.20E+00	-4000.	92.0	0.0	1.
55	XYLA	1.00E-12	1.40E+00	-4000.	106.0	0.0	1.
56	BNZA	1.00E-12	1.80E-01	-4000.	78.0	0.0	1.
57	ISP	1.00E-12	1.00E-02	-4000.	68.0	0.0	1.
58	TRP	1.00E-12	4.90E-02	-4000.	136.0	0.0	1.
59	SQT	1.00E-12	4.90E-02	-4000.	204.0	0.0	1.
60	CG1	1.00E-12	1.00E+05	-4000.	150.0	0.0	1.
61	CG2	1.00E-12	1.00E+05	-4000.	150.0	0.0	1.
62	CG3	1.00E-12	1.00E+05	-4000.	130.0	0.0	1.
63	CG4	1.00E-12	1.00E+05	-4000.	130.0	0.0	1.
64	CG5	1.00E-12	1.00E+05	-4000.	180.0	0.0	1.
65	CG6	1.00E-12	1.00E+05	-4000.	180.0	0.0	1.
66	CG7	1.00E-12	1.00E+05	-4000.	210.0	0.0	1.
67	HG0	1.00E-12	1.11E-01	-4970.	200.6	0.0	1.
68	HG2	1.00E-12	2.00E+05	-4000.	253.1	0.0	0.
	Aero Spec	lower bnd	Density	Dry Bext	RH Adjust	SSA	SizeBin
1	PNO3	1.00E-09	1.5	7.0	1	0.99	1
2	PSO4	1.00E-09	1.5	7.0	1	0.99	1
3	PNH4	1.00E-09	1.5	7.0	1	0.99	1
4	POA	1.00E-09	1.0	7.0	0	0.80	1
5	SOA1	1.00E-09	1.0	7.0	0	0.80	1
6	SOA2	1.00E-09	1.0	7.0	0	0.80	1
7	SOA3	1.00E-09	1.0	7.0	0	0.80	1
8	SOA4	1.00E-09	1.0	7.0	0	0.80	1
9	SOA5	1.00E-09	1.0	7.0	0	0.80	1
10	SOA6	1.00E-09	1.0	7.0	0	0.80	1
11	SOA7	1.00E-09	1.0	7.0	0	0.80	1
12	SOAH	1.00E-09	1.0	7.0	0	0.80	1
13	SOPA	1.00E-09	1.0	7.0	0	0.80	1
14	SOPB	1.00E-09	1.0	7.0	0	0.80	1
15	PEC	1.00E-09	2.0	18.0	0	0.25	1
16	FPRM	1.00E-09	3.0	0.4	0	0.70	1
17	FCRS	1.00E-09	3.0	0.4	0	0.70	1
18	CPRM	1.00E-09	3.0	0.4	0	0.70	2
19	CCRS	1.00E-09	3.0	0.4	0	0.70	2
20	NA	1.00E-09	2.0	1.5	1	0.99	1
21	PCL	1.00E-09	2.0	1.5	1	0.99	1
22	PH2O	1.00E-09	1.0	0.0	0	0.99	1
23	HGP	1.00E-15	8.0	0.0	0	0.99	1
24	HGIIP	1.00E-20	8.0	0.0	0	0.99	1
25	HGIIPC	1.00E-20	8.0	0.0	0	0.99	2
Reaction Records							
Rxn Typ Order Parameters (1 to 12, depending upon Typ)							
1	1	1	0.000E+00				
2	3	3	6.000E-34	0.0	-2.40	300.0	
3	3	2	3.000E-12	1500.0	0.00	300.0	
4	3	2	5.600E-12	-180.0	0.00	300.0	
5	4	2	2.500E-31	0.0	-1.80	300.0	2.200E-11 0.0 -
0.70			300.0	0.60	1.00		
6	4	2	9.000E-32	0.0	-1.50	300.0	3.000E-11 0.0 0.00
300.0			0.60	1.00			
7	3	2	1.200E-13	2450.0	0.00	300.0	
8	1	1	0.000E+00				

Figure 3-1a (continued).

3. Core Model Input / Output Structures

9	1	1	0.000E+00							
10	3	2	2.100E-11	-102.0	0.00	300.0				
11	1	2	2.200E-10							
12	3	2	1.700E-12	940.0	0.00	300.0				
13	3	2	1.000E-14	490.0	0.00	300.0				
14	1	1	0.000E+00							
15	1	1	0.000E+00							
16	3	2	1.500E-11	-170.0	0.00	300.0				
17	3	2	4.500E-14	1260.0	0.00	300.0				
18	4	2	2.000E-30	0.0	-4.40	300.0	1.400E-12	0.0	-	
0.70			300.0	0.60	1.00					
19	1	2	2.500E-22							
20	1	3	1.800E-39							
21	4	1	1.000E-03	11000.0	-3.50	300.0	9.700E+14	11080.0	0.10	
300.0			0.45	1.00						
22	3	3	3.300E-39	-530.0	0.00	300.0				
23	1	3	5.000E-40							
24	4	2	7.000E-31	0.0	-2.60	300.0	3.600E-11	0.0	-	
0.10			300.0	0.60	1.00					
25	1	1	0.000E+00							
26	3	2	1.800E-11	390.0	0.00	300.0				
27	1	2	1.000E-20							
28	4	2	2.000E-30	0.0	-3.00	300.0	2.500E-11	0.0	0.00	
300.0			0.60	1.00						
29	6	2	2.400E-14	-460.0	0.00	300.0	2.700E-17	-2199.0	0.00	
300.0			6.500E-34	-1335.0	0.00	300.0				
30	3	2	3.500E-12	-250.0	0.00	300.0				
31	1	2	0.000E+00							
32	1	1	0.000E+00							
33	1	2	0.000E+00							
34	7	2	2.300E-13	-600.0	0.00	300.0	1.700E-33	-1000.0	0.00	
300.0										
35	7	3	3.220E-34	-2800.0	0.00	300.0	2.380E-54	-3200.0	0.00	
300.0										
36	1	1	0.000E+00							
37	3	2	2.900E-12	160.0	0.00	300.0				
38	1	2	1.100E-10							
39	3	2	5.500E-12	2000.0	0.00	300.0				
40	3	2	2.200E-11	-120.0	0.00	300.0				
41	3	2	4.200E-12	240.0	0.00	300.0				
42	4	2	6.900E-31	0.0	-1.00	300.0	2.600E-11	0.0	0.00	
300.0			0.60	1.00						
43	3	2	4.800E-11	-250.0	0.00	300.0				
44	3	2	3.000E-11	-200.0	0.00	300.0				
45	3	2	1.400E-12	2000.0	0.00	300.0				
46	1	2	1.000E-11							
47	1	2	2.200E-11							
48	1	2	3.500E-12							
49	1	2	1.000E-17							
50	3	2	8.500E-13	2450.0	0.00	300.0				
51	1	1	0.000E+00							
52	1	1	0.000E+00							
53	1	1	0.000E+00							
54	3	2	2.600E-12	-365.0	0.00	300.0				
55	3	2	2.600E-12	-365.0	0.00	300.0				
56	3	2	7.500E-13	-700.0	0.00	300.0				
57	3	2	7.500E-13	-700.0	0.00	300.0				
58	1	2	6.800E-14							
59	1	2	6.800E-14							
60	1	2	6.800E-14							
61	3	2	5.900E-13	360.0	0.00	300.0				

Figure 3-1a (continued).

3. Core Model Input / Output Structures

62	1	1	0.000E+00							
63	4	2	3.000E-31	0.0	-3.30	300.0	1.500E-12	0.0	0.00	
300.0			0.60	1.00						
64	3	2	3.010E-12	-190.0	0.00	300.0				
65	1	1	0.000E+00							
66	7	2	1.440E-13	0.0	0.00	300.0	3.430E-33	0.0	0.00	
300.0										
67	3	2	2.450E-12	1775.0	0.00	300.0				
68	3	2	2.800E-12	-300.0	0.00	300.0				
69	3	2	4.100E-13	-750.0	0.00	300.0				
70	3	2	9.500E-14	-390.0	0.00	300.0				
71	3	2	3.800E-12	-200.0	0.00	300.0				
72	1	1	0.000E+00							
73	3	2	7.300E-12	620.0	0.00	300.0				
74	1	2	9.000E-12							
75	1	1	0.000E+00							
76	1	1	0.000E+00							
77	3	2	3.400E-11	1600.0	0.00	300.0				
78	1	2	5.800E-16							
79	3	2	9.700E-15	-625.0	0.00	300.0				
80	3	1	2.400E+12	7000.0	0.00	300.0				
81	1	2	5.600E-12							
82	3	2	5.600E-15	-2300.0	0.00	300.0				
83	1	2	4.000E-13							
84	3	2	1.800E-11	1100.0	0.00	300.0				
85	3	2	5.600E-12	-270.0	0.00	300.0				
86	3	2	1.400E-12	1900.0	0.00	300.0				
87	1	1	0.000E+00							
88	3	2	8.100E-12	-270.0	0.00	300.0				
89	4	2	2.700E-28	0.0	-7.10	300.0	1.200E-11	0.0	-	
0.90			300.0	0.30	1.00					
90	4	1	4.900E-03	12100.0	0.00	300.0	5.400E+16	13830.0	0.00	
300.0			0.30	1.00						
91	1	1	0.000E+00							
92	3	2	4.300E-13	-1040.0	0.00	300.0				
93	3	2	2.000E-12	-500.0	0.00	300.0				
94	3	2	4.400E-13	-1070.0	0.00	300.0				
95	3	2	2.900E-12	-500.0	0.00	300.0				
96	3	2	4.000E-13	-200.0	0.00	300.0				
97	1	1	0.000E+00							
98	3	2	4.000E-13	-200.0	0.00	300.0				
99	3	2	1.300E-11	870.0	0.00	300.0				
100	3	2	5.100E-12	-405.0	0.00	300.0				
101	1	2	6.500E-15							
102	1	1	0.000E+00							
103	3	2	6.700E-12	-340.0	0.00	300.0				
104	4	2	2.700E-28	0.0	-7.10	300.0	1.200E-11	0.0	-	
0.90			300.0	0.30	1.00					
105	4	1	4.900E-03	12100.0	0.00	300.0	5.400E+16	13830.0	0.00	
300.0			0.30	1.00						
106	1	1	0.000E+00							
107	1	2	3.000E-13							
108	3	2	4.300E-13	-1040.0	0.00	300.0				
109	3	2	2.000E-12	-500.0	0.00	300.0				
110	3	2	4.400E-13	-1070.0	0.00	300.0				
111	3	2	2.900E-12	-500.0	0.00	300.0				
112	3	2	2.900E-12	-500.0	0.00	300.0				
113	3	2	8.700E-12	1070.0	0.00	300.0				
114	3	2	6.900E-12	230.0	0.00	300.0				
115	1	2	8.100E-13							
116	3	1	1.000E+15	8000.0	0.00	300.0				

Figure 3-1a (continued).

3. Core Model Input / Output Structures

117	1	1	1.600E+03						
118	1	2	1.500E-11						
119	3	2	1.000E-11	280.0	0.00	300.0			
120	1	2	3.200E-11						
121	3	2	6.500E-15	1900.0	0.00	300.0			
122	3	2	7.000E-13	2160.0	0.00	300.0			
123	3	2	1.040E-11	792.0	0.00	300.0			
124	4	2	1.000E-28	0.0	-0.80	300.0	8.800E-12	0.0	0.00
300.0			0.60	1.00					
125	3	2	1.200E-14	2630.0	0.00	300.0			
126	3	2	3.300E-12	2880.0	0.00	300.0			
127	1	2	2.300E-11						
128	3	2	1.000E-11	-550.0	0.00	300.0			
129	3	2	8.400E-15	1100.0	0.00	300.0			
130	3	2	9.600E-13	270.0	0.00	300.0			
131	3	2	1.800E-12	-355.0	0.00	300.0			
132	1	2	8.100E-12						
133	1	1	4.200E+00						
134	1	2	4.100E-11						
135	1	2	2.200E-11						
136	1	2	1.400E-11						
137	1	2	5.500E-12						
138	1	1	0.000E+00						
139	1	2	3.000E-11						
140	3	2	5.400E-17	500.0	0.00	300.0			
141	3	2	1.700E-11	-116.0	0.00	300.0			
142	1	2	1.700E-11						
143	1	1	0.000E+00						
144	1	2	3.600E-11						
145	3	2	2.540E-11	-407.6	0.00	300.0			
146	3	2	7.860E-15	1912.0	0.00	300.0			
147	3	2	3.030E-12	448.0	0.00	300.0			
148	1	2	1.500E-19						
149	1	2	3.360E-11						
150	1	2	7.100E-18						
151	1	2	1.000E-15						
152	1	1	0.000E+00						
153	1	2	3.600E-11						
154	3	2	1.500E-11	-449.0	0.00	300.0			
155	3	2	1.200E-15	821.0	0.00	300.0			
156	3	2	3.700E-12	-175.0	0.00	300.0			

Figure 3-1a (concluded).

```

CAMx Version      |VERSION6.4
Mechanism ID     |0
Aerosol Option   |NONE
Description      |inert test
No of gas species|1
No of aero species|0
No of reactions  |0
Prim photo rxns  |0
No of sec photo rxn|0
SrfMod #spc, #rxns|0 0
Species Records
  Gas Spec  lower bnd  H-law  T-fact  Molwt  Reactvty  Rscale
  1  TRACER  1.00E-09  1.00e-10  0.  1.00  0.0  1.

```

Figure 3-1b. Example inert chemistry parameters file (requires chemistry flag to be set false – see the description of the CAMx control file).

The section of the file that lists gas species must include the names of radical and state species, according to the selected chemical mechanism, along with each species' lower bound value, Henry's Law solubility parameters, molecular weight, and surface reactivity and resistance scaling parameters for use in the dry deposition calculations. The lower bound values set the minimum concentration "floor" for any chemical or physical process that reduces concentrations to "zero". The lower bound is also used to set initial and/or boundary conditions for species that are omitted from the initial and/or boundary condition files.

The section of the file that lists aerosol species names must include a lower-bound value, particle density, dry extinction efficiency, a hygroscopic flag, and single-scattering albedo. In the case of INERT or CF options, the user must also specify the size bin assigned to each species at the end of each particulate species record (CMU automatically applies each species to all size bins). Since the effect of aerosol water on optical parameters is taken into account through an internal relative humidity adjustment, the dry extinction efficiency for particle species PH2O must be set to zero.

CAMx supports several equations for specifying gas-phase rate constants, as shown in Table 3-3a. The type of equation used for each reaction is identified by the second parameter specified for each reaction – a number between 1 and 7 (Table 3-3a). The number of additional parameters required depends upon the expression type and varies between 2 and 13, as shown in Table 3-3b. Expression type 4 (Troe expression) allows for a complete description of dependencies on temperature and pressure; background information on Troe expressions may be found in the NASA and IUPAC rate constant compilations (NASA, 1997; IUPAC, 1992).

Rate constants can be specified in molecular units (e.g., $\text{cm}^3 \text{ molecule}^{-1} \text{ s}^{-1}$) or ppm units (e.g., $\text{ppm}^{-1} \text{ min}^{-1}$). All the rate constants must be in a single units system; CAMx will determine which units system is being used from the magnitude of the rate constants. Diagnostic information on the rate constants and units system is output by CAMx at run-time.

3.2 Photolysis Rates File

The rates for the primary photolysis reactions are supplied via the photolysis rates file in units of minute^{-1} . This file must be supplied if chemistry is invoked. The photolysis rates file comprises a large look-up table of clear-sky photolysis rates specific to the gas-phase chemistry mechanism to run. Rates are arranged in a matrix of five dimensions, including variations over 10 solar zenith angles, 5 ultraviolet (UV) surface albedos, 3 terrain heights, 11 altitudes above ground, and 5 total ozone column values. The look-up table is generated using the TUV preprocessor, which internally specifies the ranges of solar zenith (0, 10, 20, 30, 40, 50, 60, 70, 78, 86), surface UV albedo (0.04, 0.1, 0.2, 0.5, 0.9.), and terrain heights (0, 1, 3 km). The ranges of altitude above ground are controlled by the user, while the ranges of ozone column are taken from the ozone column file (Section 3.3). TUV is run with a typical aerosol profile defined by Elterman (1968).

Table 3-3a. Rate constant expression types supported in CAMx and order of expression parameters for the chemistry parameters file.

Expression Type	Description	Expression
1	Constant	$k = k_{298}$
2	UAM (Arrhenius expression)	$k = k_{298} \exp\left[E_a\left(\frac{1}{298} - \frac{1}{T}\right)\right]$
3	General temperature dependence	$k = A\left(\frac{T}{T_R}\right)^B \exp\left(-\frac{E_a}{T}\right)$
4	Troe-type temperature and pressure dependence	$k = \left(\frac{k^0[M]}{1 + k^0[M]/k^\infty}\right) F^G$ $k^0 = A\left(\frac{T}{T_R}\right)^B \exp\left(-\frac{E_a}{T}\right)$ $k^\infty = A'\left(\frac{T}{T'_R}\right)^{B'} \exp\left(-\frac{E'_a}{T}\right)$ $G = \left[1 + \left(\frac{\log(k^0[M]/k^\infty)}{n}\right)^2\right]^{-1}$
5	Equilibrium with a previously defined reaction (k_{ref})	$k = k_{ref} \left[A\left(\frac{T}{T_R}\right)^B \exp\left(-\frac{E_a}{T}\right)\right]^{-1}$
6	Lindemann - Hinshelwood as used for OH + HNO3	$k = k^0 + \frac{k_3[M]}{1 + k_3[M]/k_2}$
7	Simple pressure dependence used for OH + CO	$k = k_1 + k_2[M]$

Notes:

T is temperature (K)

TR is reference temperature of 300 K

Ea is an Arrhenius activation energy (K)

k0 is the low pressure limit of the rate constant

k∞ is the high pressure limit of the rate constant

[M] is the concentration of air

Table 3-3b. List of parameters that must be provided in the CAMx chemistry parameter file for each of the seven types of rate constant expressions. Use ppm/minute units for A and Kelvin for E_a and T_R . The variable O is the order of the reaction (1 to 3).

Expression Type	Parameters												
	1	2	3	4	5	6	7	8	9	10	11	12	13
1	O	k_{298}											
2	O	k_{298}	E_a										
3	O	A	E_a	B	T_R								
4	O	A	E_a	B	T_R	A'	E_a'	B'	T_R'	F	n		
5	O	k_{ref}	A	E_a	B	T_R							
6	O	A^0	E_a^0	B^0	T_R^0	A^2	E_a^2	B^2	T_R^2	A^3	E_a^3	B^3	T_R^3
7	O	A^1	E_a^1	B^1	T_R^1	A^2	E_a^2	B^2	T_R^2				

The photolysis rates file is a readable text format and it has the following structure:

```

TUV4.8CAMx6
Loop from 1 to nozn ozone column intervals:
  Loop from 1 to nalb UV albedo intervals:
    Loop from 1 to ntht terrain height intervals:
      ozcl, albcl, trncl          (12X, f7.3, 8X, f7.3, 11X, f7.3)
    Loop from 1 to nalt altitudes above ground:
      height                      (*)
    Loop from 1 to nphot photolysis reactions:
      (pk(n), n=1, nsol)         (1X, 10F12.0)

```

where the first record labels the version of TUV used to generate the file, and where variables have the following definitions:

ozcl	Ozone column value for the current interval (Dobson units)
albcl	UV albedo value for the current interval (unitless)
trncl	Terrain height value for the current interval (km MSL)
height	Altitude (km AGL)
pk	Photolysis rates (min^{-1}) for <i>nsol</i> solar zenith angles

Figure 3-2 presents an example of a photolysis rates file for the first several panels of data.

3.3 Ozone Column File

This file defines the intervals of total atmospheric ozone column to be used by TUV, as well as its spatial and temporal distributions for a specific CAMx domain and episode. This parameter is essential for photochemical simulations as it determines the spatial and temporal variation of photolysis rates. Therefore, this file must be supplied if chemistry is invoked.

There are two mandatory and one optional header records in the ozone column file. The first record contains an arbitrary file label. The second record defines the intervals for 5 ozone column values for the domain and temporal period to be simulated. These intervals must exactly match those defined in preparing the photolysis rates file, so the ozone column file is also read by the TUV preprocessor to define the photolysis rates lookup table (Section 3.2).

Gridded fields of time-varying ozone column follow the header records. The gridded fields are maps of the respective "codes" for each interval, as defined in the header. For example, 5 ozone column intervals are specified in TUV and in the ozone column header record, so the map must consist of a distribution of integers ranging from 1 to 5. Ozone column is supplied for the master grid only; CAMx internally assigns master cell values to all nested grids cells. Multiple maps of these codes may be provided for arbitrary time intervals that span the entire simulation period.

The ozone column file is a readable text format and it has the following structure:

text	(A)
ozname, (ozncl(n), n=1, nozn)	(A10, 5F10.0)
ozname, idt1, tim1, idt2, tim2	(A10, I10, F10.0, I10, F10.0)
Loop from j = ny master grid rows to 1	
(jozn(i, j), i=1, nx)	(9999I1)

where the variables in the ozone column file have the following definitions:

text	Text identifying file and any messages
ozname	Text string "OZONE COL"
ozncl	Ozone column (Dobson units) for each of <i>nozn</i> ozone values
idt1	Beginning date (YYJJ) of time span
tim1	Beginning hour (HHMM) of time span
idt2	Ending date of time span
tim2	Ending hour of time span
jozn	Master grid row <i>j</i> ozone column codes for <i>nx</i> master grid columns

An example of a small ozone column file is given in Figure 3-3.

emissions, initial and top boundary conditions, meteorology¹, and output concentration and deposition files share the same basic format. The input lateral boundary condition and point source emissions files are similar but include additional records specific to their data structures. The input 3D meteorological file may provide wind fields in a staggered or un-staggered grid arrangement. A flag to indicate the wind staggering is included in the second header record and is checked only when the 3D meteorological file is read.

The four header records within all CAMx binary files have the following structure:

```
name,note,itzon,nvar,ibdate,btime,iedate,etime
plon,plat,iutm,xorg,yorg,dely,dely,nx,ny,nz,iproj,istag,tlat1,tlat2,r dum
ione,ione,nx,ny
(namvar(1),l=1,nvar)
```

The header variables have the following definitions:

Record 1

name	Text string describing file contents (character*4(10) array):
	AIRQUALITY Initial and top boundary conditions
	BOUNDARY Boundary conditions
	EMISSIONS Gridded emissions
	PTSOURCE Point source emissions
	AVERAGE Average output concentrations/deposition and input meteorology/surface variables
	INSTANT Instantaneous output concentrations
note	Text string containing user note (character*4(60) array)
itzon	Integer time zone (0=UTC, 5=EST, etc.)
nvar	Integer number of variables on file
ibdate	Integer beginning date span on file (YYJJ)
btime	Real beginning decimal hour (e.g., 1:30 PM = 13.5)
iedate	Integer ending date span on file (YYJJ)
etime	Real ending decimal hour (e.g., 1:30 PM = 13.5)

Record 2

plon	Real projection pole/origin longitude (degrees; west is negative)
plat	Real projection pole/origin latitude (degrees; south is negative)
iutm	Integer UTM zone (ignored for other projections)
xorg	Real x-coordinate at southwest corner of grid (m or degrees longitude)
yorg	Real y-coordinate at southwest corner of grid (m or degrees latitude)
dely	Real cell size in x-direction (m or degrees longitude)
dely	Real cell size in y-direction (m or degrees latitude)
nx	Integer number of grid columns (east-west)
ny	Integer number of grid rows (north-south)

¹ NOTE: Starting with CAMx v6.00, all binary meteorological files have been converted to the UAM convention.

<code>nz</code>	Integer number of vertical layers
<code>iproj</code>	Integer projection index: 0 = geodetic (LATLON) 1 = Universal Transverse Mercator (UTM) 2 = Lambert Conic Conformal (LAMBERT) 3 = Rotated Polar Stereographic (RPOLAR) 4 = Polar Stereographic (POLAR) 5 = Mercator (MERCATOR)
<code>istag</code>	Integer flag to indicate wind staggering (1=staggered, 0=not staggered)
<code>tlat1</code>	Real LCP first true latitude (degrees; south is negative)
<code>tlat2</code>	Real LCP second true latitude (degrees; south is negative)
<code>rdum</code>	Real dummy variable

Record 3

<code>ione</code>	Integer dummy variable (=1)
<code>ione</code>	Integer dummy variable (=1)
<code>nx</code>	Integer number of grid columns (east-west)
<code>ny</code>	Integer number of grid rows (north-south)

Record 4

<code>namvar</code>	Text names for <i>nvar</i> variables (character*4(10, <i>nvar</i>) array)
---------------------	--

3.4.3 Input Files

The Fortran binary input files include initial/boundary conditions, gridded and elevated point source emissions, and several meteorological files. All times on input files must match the time zone specified in the CAMx control file (CAMx.in).

Initial/boundary condition files may include a single time interval covering the entire simulation period, or more detailed hour-by-hour (or other interval) variations. The time intervals are allowed to be entirely arbitrary to maximize flexibility in defining these inputs. A subset of the pollutant species to be simulated may be defined in the initial/boundary condition files; any species that are missing will be set to "lower bound" values as defined in the chemistry parameters file.

Emission inputs are usually developed at one hour intervals, but the file structures allow for any other interval as long as a consistent interval is used throughout the file (all one hour, or all three hour, but no mixing of these). The time interval on all emission files must match the emission update frequency defined in the CAMx control file. A subset of species to be simulated may be included in the emission files; zero emission rates will be applied for any species that are missing.

Meteorological fields are separated into two-dimensional and three-dimensional fields. The core meteorological file contains the basic parameters needed for most model processes, and includes winds and basic thermodynamic properties. Separate vertical diffusivity and cloud files allow for easy substitution of alternative inputs without the need to re-generate all of the core fields. The time interval on all meteorological files must match the meteorological update frequency defined in the CAMx control file.

3.4.3.1 Input Static 2-D Surface File

The static 2-D surface file contains time-invariant gridded fields of landuse and topographic elevation, and optionally leaf area index (LAI). This file must be developed for the master grid, and optionally any of the nested fine grids. The fractional distribution of 26 landuse categories, consistent with the "ZHANG03" dry deposition scheme, is supplied for each grid cell. If the "WESELY89" dry deposition option is invoked, CAMx internally maps the 26 categories to the 11 Wesely categories. The landuse categories are described in Tables 3-4 and 3-5. Landuse is used to define surface UV albedo, surface resistances for dry deposition calculations, and to set seasonal default surface roughness lengths and LAI values (if LAI is not specified in the file). Topographic elevation is used to define terrain heights for photolysis calculations. If necessary (e.g., invoking in-line oceanic iodine emissions algorithm or mercury chemistry), use the WATERMASK coverter program to allocate the "Water" category between "Water" (ocean) and "Inland Lake" (fresh) water bodies. This designation is carried through to the Wesely option within CAMx during the conversion from Zhang categories.

Table 3-4. The 11 WESELY89 landuse categories, their default UV surface albedos, and their surface roughness values (m) by season. Winter is defined for conditions where there is snow present; winter months with no snow are assigned to the Fall category. Roughness for water is calculated from the function $z_0 = 2 \times 10^{-6} w^{2.5}$, where w is surface wind speed (m/s).

Land Cover Category	Surface Roughness (meters)				UV Albedo
	Spring	Summer	Fall	Winter	
1 Urban	1.0	1.0	1.0	1.0	0.08
2 Agricultural	0.03	0.2	0.05	0.01	0.05
3 Rangeland	0.05	0.1	0.01	0.001	0.05
4 Deciduous forest	1.0	1.3	0.8	0.5	0.05
5 Coniferous forest, wetland	1.3	1.3	1.3	1.3	0.05
6 Mixed forest*	1.15	1.3	1.05	0.9	0.05
7 Water	f(w)	f(w)	f(w)	f(w)	0.04
8 Barren land	0.002	0.002	0.002	0.002	0.08
9 Non-forested wetlands	0.2	0.2	0.2	0.05	0.05
10 Mixed agricultural/range**	0.04	0.15	0.03	0.006	0.05
11 Rocky (with low shrubs)	0.3	0.3	0.3	0.15	0.05

* Roughness for mixed forest is the average of deciduous and coniferous forest.

** Roughness for mixed ag/range is the average of agricultural and rangeland.

Table 3-5. The 26 ZHANG03 landuse categories, their UV albedos, default annual minimum and maximum LAI and surface roughness (m) ranges, and mapping to the Wesely scheme (Table 3-4). Roughness for water is calculated from the function $z_0 = 2 \times 10^{-6} w^{2.5}$, where w is surface wind speed (m/s).

Land Cover Category	Wesely Mapping	Roughness (meters)		LAI		UV Albedo
		Min	Max	Min	Max	
1 Water (Ocean)	7	f(w)	f(w)	0.0	0.0	0.04
2 Ice	8	0.01	0.01	0.0	0.0	0.5
3 Inland lake (Fresh)	7	f(w)	f(w)	0.0	0.0	0.04
4 Evergreen needleleaf trees	5	0.9	0.9	5.0	5.0	0.05
5 Evergreen broadleaf trees	5	2.0	2.0	6.0	6.0	0.05
6 Deciduous needleleaf trees	4	0.4	0.9	0.1	5.0	0.05
7 Deciduous broadleaf trees	4	0.4	1.0	0.1	5.0	0.05
8 Tropical broadleaf trees	5	2.5	2.5	6.0	6.0	0.05
9 Drought deciduous trees	4	0.6	0.6	4.0	4.0	0.05
10 Evergreen broadleaf shrubs	3	0.2	0.2	3.0	3.0	0.05
11 Deciduous shrubs	3	0.05	0.2	0.5	3.0	0.05
12 Thorn shrubs	3	0.2	0.2	3.0	3.0	0.05
13 Short grass and forbs	3	0.04	0.04	1.0	1.0	0.05
14 Long grass	10	0.02	0.1	0.5	2.0	0.05
15 Crops	2	0.02	0.1	0.1	4.0	0.05
16 Rice	2	0.02	0.1	0.1	6.0	0.05
17 Sugar	2	0.02	0.1	0.1	5.0	0.05
18 Maize	2	0.02	0.1	0.1	4.0	0.05
19 Cotton	2	0.02	0.2	0.1	5.0	0.05
20 Irrigated crops	2	0.05	0.05	1.0	1.0	0.05
21 Urban	1	1.0	1.0	0.1	1.0	0.08
22 Tundra	11	0.03	0.03	0.1	2.0	0.05
23 Swamp	9	0.1	0.1	4.0	4.0	0.05
24 Desert	8	0.04	0.04	0.0	0.0	0.08
25 Mixed wood forest	6	0.9	0.9	3.0	5.0	0.05
26 Transitional forest	6	0.9	0.9	3.0	5.0	0.05

The data records for the static 2-D surface file have the following structure:

```

ibdate, btime, iedate, etime
Loop from l = 1 to nvar variables:
  ione, namvar(l), ((var(i, j), i=1, nx), j=1, ny)

```

The variables have the following definitions:

Record 1

ibdate	Integer beginning date span on file (YYJJJ)
btime	Real beginning decimal hour (e.g., 1:30 PM = 13.5)
iedate	Integer ending date span on file (YYJJJ)
etime	Real ending decimal hour (e.g., 1:30 PM = 13.5)

Record 2 through *nvar+1*

<i>ione</i>	Integer dummy variable (=1)
<i>namvar</i>	Text names for <i>nvar</i> variables (character*4(10, <i>nvar</i>) array):
	WATER Water (ocean) fraction (Zhang 1)
	ICE Ice fraction (Zhang 2)
	LAKE Lake (fresh) water fraction (Zhang 3)
	ENEEDL Evergreen needle leaf forest fraction (Zhang 4)
	EBROAD Evergreen broad leaf forest fraction (Zhang 5)
	DNEEDL Deciduous needle leaf forest fraction (Zhang 6)
	DBROAD Deciduous broad leaf forest fraction (Zhang 7)
	TBROAD Tropical broad leaf forest fraction (Zhang 8)
	DDECID Drought deciduous tree fraction (Zhang 9)
	ESHRUB Evergreen shrub fraction (Zhang 10)
	DSHRUB Deciduous shrub fraction (Zhang 11)
	TSHRUB Thorn shrub fraction (Zhang 12)
	SGRASS Short grass fraction (Zhang 13)
	LGRASS Long grass fraction (Zhang 14)
	CROPS Cropland fraction (Zhang 15)
	RICE Rice crop fraction (Zhang 16)
	SUGAR Sugar crop fraction (Zhang 17)
	MAIZE Corn crop fraction (Zhang 18)
	COTTON Cotton crop fraction (Zhang 19)
	ICROPS Irrigated cropland fraction (Zhang 20)
	URBAN Urban fraction (Zhang 21)
	TUNDRA Tundra fraction (Zhang 22)
	SWAMP Swamp fraction (Zhang 23)
	DESERT Desert fraction (Zhang 24)
	MWOOD Mixed woodland fraction (Zhang 25)
	TFOREST Transitional forest fraction (Zhang 26)
	TOPO_M Topographic elevation above sea level (m)
	LAI Optional Leaf Area Index
<i>var</i>	Real variable field values for <i>nx</i> grid columns and <i>ny</i> grid rows

3.4.3.2 Input Time-Variant 2-D Surface File

The time-variant 2-D surface file contains gridded fields of surface temperature and snow cover. This file must be developed for the master grid, and optionally any of the nested fine grids. The surface temperature is used for dry deposition calculations and to establish surface-layer atmospheric stability. Snow cover includes snow depth and age, which are used to calculate surface albedo for photochemistry, adjust surface resistances for dry deposition, and define the snow compartment for the surface chemistry model.

The data records for the time-variant 2-D surface file have the following structure and are repeated for each time interval on file:

```

ibdate, btime, iedate, etime
Loop from l = 1 to nvar variables:
  ione, namvar(l), ((var(i, j), i=1, nx), j=1, ny)

```

The variables have the following definitions:

Record 1

ibdate	Integer beginning date of time interval (YYJJ)
btime	Real beginning decimal hour (e.g., 1:30 PM = 13.5)
iedate	Integer ending date of time interval (YYJJ)
etime	Real ending decimal hour (e.g., 1:30 PM = 13.5)

Record 2 through *nvar+1*

ione	Integer dummy variable (=1)
namvar	Text names for <i>nvar</i> variables (character*4(10, <i>nvar</i>) array):
	TSURF_K Surface temperature (K)
	SNOWEW_M Snow water equivalent depth (m)
	SNOWAGE_HR Snow age since last snowfall (hr)
var	Real variable field values for <i>nx</i> grid columns and <i>ny</i> grid rows

CAMx time-interpolates surface temperature to each model timestep for each grid (but holds snow cover constant), and so the model requires that data be available on file for an additional update time at the end of the simulation. For example, in the case of hourly fields, a 24-hour simulation requires 25 input fields on file. The time interval of the data records must match the time zone and input frequency of the meteorology as specified in the CAMx.in file.

CAMx is backward-compatible with older 2-D meteorological files that may contain the snow cover variable (SNOWCOVER), which is a simple map of 0 or 1 to indicate the presence of snow in each grid cell. If the SNOWCOVER variable is found, CAMx arbitrarily assumes a snow water equivalent depth of 0.025 m (~25 cm snow depth) and snow age of 5 days.

3.4.3.3 Input Time-Variant 3-D Meteorological File

The time-variant 3-D meteorological file contains gridded fields of state meteorological parameters. This file must be developed for the master grid and optionally any fine grid nest specified for a given simulation. The layer interface heights define the vertical grid structure for each grid. The number of vertical layers and the vertical grid definition must be consistent among all grids in a simulation; otherwise CAMx will stop with an error message if this condition is not met. The layer interface heights may be specified to vary in space and/or time (e.g., to follow the layer structure of meteorological models), or they may be set to a constant field. CAMx allows the user to optionally supply wind components at cell center, in which case the model will interpolate the components to their respective positions on cell interfaces, or the user may supply these components directly on the staggered Arakawa C configuration

(recommended). In any case, the user must supply a full $nx \times ny \times nz$ array of wind values for each component (even though the CAMx Arakawa C configuration uses only $(nx-1) \times (ny-1)$ values in the horizontal). The wind staggering flag is set in the second header record. The pressure, wind, temperature, and humidity fields are used for transport, plume rise, PiG, dry and wet deposition, and chemistry calculations.

The data records for the time-variant 3-D meteorological file have the following structure and are repeated for each time interval on file:

```

ibdate, btime, iedate, etime
Loop from l = 1 to nvar variables:
  Loop from k = 1 to nz layers:
    ione, namvar(l), ((var(i, j, k), i=1, nx), j=1, ny)

```

The variables have the following definitions:

Record 1

ibdate	Integer beginning date of time interval (YYJJ)
btime	Real beginning decimal hour (e.g., 1:30 PM = 13.5)
iedate	Integer ending date of time interval (YYJJ)
etime	Real ending decimal hour (e.g., 1:30 PM = 13.5)

Record 2 through $nvar \times nz + 1$

ione	Integer dummy variable (=1)
namvar	Text names for $nvar$ variables (character*4(10, $nvar$) array):
	ZGRID_M Layer interface heights (m AGL)
	PRESS_MB Pressure (mb)
	TEMP_K Temperature (K)
	HUMID_PPM Humidity as mixing ratio (ppm)
	UWIND_MpS U-component (east-west) wind (m/s)
	VWIND_MpS V-component (north-south) wind (m/s)
var	Real layer k variable field values for nx grid columns and ny grid rows

CAMx time-interpolates these meteorological variables to each model timestep for each grid, and so the model requires that data be available on file for an additional update time at the end of the simulation. For example, in the case of hourly fields, a 24-hour simulation requires 25 input fields on file. The time interval of the data records must match the time zone and input frequency of the meteorology as specified in the CAMx.in file.

3.4.3.4 Input Time-Variant 3-D Vertical Diffusivity File

The time-variant 3-D vertical diffusivity file contains gridded fields of layer-interface diffusivity (i.e., turbulent exchange or diffusion coefficients). This file must be developed for the master grid, and optionally any fine grid nests. This file is kept separate from the main meteorological

data file to facilitate the substitution of alternative vertical mixing rates. Diffusivity is used for vertical diffusion and PiG puff growth calculations.

The data records for the time-variant 3-D meteorological file have the following structure and are repeated for each time interval on file:

```

ibdate, btime, iedate, etime
Loop from l = 1 to nvar variables:
  Loop from k = 1 to nz layers:
    ione, namvar(l), ((var(i, j, k), i=1, nx), j=1, ny)

```

The variables have the following definitions:

Record 1

ibdate	Integer beginning date of time interval (YYJJ)
btime	Real beginning decimal hour (e.g., 1:30 PM = 13.5)
iedate	Integer ending date of time interval (YYJJ)
etime	Real ending decimal hour (e.g., 1:30 PM = 13.5)

Record 2 through $nvar \times nz + 1$

ione	Integer dummy variable (=1)
namvar	Text names for $nvar$ variables (character*4(10, $nvar$) array):
	KV_M2pS Vertical diffusivity (m^2/s)
var	Real layer k variable field values for nx grid columns and ny grid rows

CAMx time-interpolates the diffusivity to each model timestep for each grid, and so the model requires that data be available on file for an additional update time at the end of the simulation. For example, in the case of hourly fields, a 24-hour simulation requires 25 input fields on file. The time interval of the data records must match the time zone and input frequency of the meteorology as specified in the CAMx.in file.

3.4.3.5 Input Time-Variant 3-D Cloud/Precipitation File

The time-variant 3-D cloud/precipitation file contains gridded fields of cloud and precipitation parameters to be used for photochemistry, aqueous chemistry, and wet/dry deposition calculations. Note that precipitation rate is not explicitly provided to the model; instead, it is internally calculated from the three precipitation water content forms provided on the cloud/rain file. This file also contains layer-specific cloud optical depth to scale down photolysis rates for layers within or below clouds to account for UV attenuation, or to scale up the rates for layers above clouds to account for UV reflection. This file must be developed for the master grid, and optionally any fine grid nests, if chemistry, dry, and/or wet deposition are invoked.

The data records for the time-variant 3-D cloud/precipitation file have the following structure and are repeated for each time interval on file:

```

ibdate, btime, iedate, etime
Loop from l = 1 to nvar variables:
  Loop from k = 1 to nz layers:
    ione, namvar(l), ((var(i, j, k), i=1, nx), j=1, ny)

```

The variables have the following definitions:

Record 1

ibdate	Integer beginning date of time interval (YYJJ)
btime	Real beginning decimal hour (e.g., 1:30 PM = 13.5)
iedate	Integer ending date of time interval (YYJJ)
etime	Real ending decimal hour (e.g., 1:30 PM = 13.5)

Record 2 through $nvar \times nz + 1$

ione	Integer dummy variable (=1)
namvar	Text names for $nvar$ variables (character*4(10, $nvar$) array):
	CLODW_GpM3 Cloud water content (g/m^3)
	RAINW_GpM3 Rain water content (g/m^3)
	SNOWW_GpM3 Snow water content (g/m^3)
	GRPLW_GpM3 Graupel water content (g/m^3)
	CLOUDOD Layer-specific cloud optical depth
var	Real layer k variable field values for nx grid columns and ny grid rows

The CAMx cloud fields are assumed to be time-averaged, so the model does not require an additional update time at the end of the simulation. For example, in the case of hourly fields, a 24-hour simulation requires only 24 cloud input fields on file. The time interval of the data records must match the time zone and input frequency of the meteorology as specified in the CAMx.in file.

3.4.3.6 Input 3-D Initial Conditions File

The input 3-D initial conditions file contains gridded concentration fields on the master grid. Initial concentration fields may be specified for a sub-set of the total number of modeled species. An initial condition file must be developed for the master grid, and contain concentration fields for at least one species. For those species not on the initial condition file, CAMx sets up uniform fields using the “lower bound” values specified in the chemistry parameters file. CAMx then interpolates all master grid initial conditions to each fine grid nest at the start of the simulation.

The data records for the initial conditions file have the following structure and are repeated for each time interval on file:

```

ibdate, btime, iedate, etime
Loop from l = 1 to nspec species:
  Loop from k = 1 to nz layers:
    ione, namspec(l), ((conc(i, j, k, l), i=1, nx), j=1, ny)

```

The variables have the following definitions:

Record 1

ibdate	Integer beginning date of time interval (YYJJ)
btime	Real beginning decimal hour (e.g., 1:30 PM = 13.5)
iedate	Integer ending date of time interval (YYJJ)
etime	Real ending decimal hour (e.g., 1:30 PM = 13.5)

Record 2 through *nspec* × *nz* + 1

ione	Integer dummy variable (=1)
namspec	Text names for <i>nspec</i> species (character*4(10, nvar) array):
conc	Real layer <i>k</i> concentration field values (ppm for gases, $\mu\text{g}/\text{m}^3$ for aerosols) for <i>nx</i> grid columns and <i>ny</i> grid rows

The time interval of the data records must match the time zone as specified in the CAMx.in file.

3.4.3.7 Input 3-D Lateral Boundary Conditions File

The input 3-D lateral boundary conditions file contains gridded concentration fields on the lateral faces of the master grid boundary. Boundary concentration fields may be specified for a sub-set of the total number of modeled species. However, if a boundary concentration is specified for a given species, it must be supplied for all four boundaries. A boundary concentration file must be developed for the master grid, and contain concentration fields for at least one species. For those species not on the boundary conditions file, CAMx sets up uniform fields using the "lower bound" values specified in the chemistry parameters file. The time span of each set of boundary data records may be set arbitrarily; e.g., a set of boundary conditions may be specified for a six hour span, followed by a set spanning just an hour.

The boundary conditions file adds an additional set of four header records, resulting in a total of eight header records altogether (note that first four records are identical to the header records described above):

```

name, note, ione, nspec, ibdate, btime, iedate, etime
plon, plat, iutm, xorg, yorg, delx, dely, nx, ny, nz, iproj, istag, tlat1, tlat2, rdum
ione, ione, nx, ny
(namspec(l), l=1, nspec)
Loop from 1 to 4 boundaries:
  ione, iedge, ncell, (icell(n), idum, idum, idum, n=1, ncell)

```

The additional header variables have the following definitions:

Records 5-8

<code>ione</code>	Integer dummy variable (=1)
<code>iedge</code>	Integer boundary edge number (1=west, 2=east, 3=south, 4=north)
<code>ncell</code>	Integer number of rows or columns on this edge
<code>icell</code>	Integer index of first cell modeled (edges 1,3), or last cell modeled (edges 2,4): if "0", this row/column is omitted from the simulation
<code>idum</code>	Integer dummy variable

The data records for the boundary conditions file have the following structure, and are repeated for each time interval on file:

```

ibdate,btime,iedate,etime
Loop from l = 1 to nspec species:
  Loop from iedge = 1 to 4 boundaries:
    ione,namspec(l),iedge,(bc(i,k,iedge,l),k=1,nz),i=1,ncell)

```

The variables have the following definitions:

Record 1

<code>ibdate</code>	Integer beginning date of time interval (YYJJ)
<code>btime</code>	Real beginning decimal hour (e.g., 1:30 PM = 13.5)
<code>iedate</code>	Integer ending date of time interval (YYJJ)
<code>etime</code>	Real ending decimal hour (e.g., 1:30 PM = 13.5)

Record 2 through $nspec \times 4 + 1$

<code>ione</code>	Integer dummy variable (=1)
<code>namspec</code>	Text names for nspec species (character*4(10,nvar) array):
<code>bc</code>	Real edge <i>iedge</i> boundary concentrations (ppm for gases, $\mu\text{g}/\text{m}^3$ for aerosols) for <i>ncell</i> grid rows/columns, and <i>nz</i> layers

The time interval of the data records must match the time zone as specified in the CAMx.in file.

3.4.3.8 Input 2-D Top Boundary Conditions File

The input 2-D top boundary conditions file contains gridded concentration fields above the top of the master grid boundary. Boundary concentration fields may be specified for a sub-set of the total number of modeled species; the sub-set of species may differ from the lateral boundary conditions. The top boundary concentration file is optional, but if supplied it must contain concentration fields for at least one species. For those species not on the boundary conditions file, CAMx sets up uniform fields using the "lower bound" values specified in the chemistry parameters file. The time span of each set of top boundary data records may be set arbitrarily; e.g., a set of boundary conditions may be specified for a six hour span, followed by a

set spanning just an hour. The time span of the top boundary conditions may differ from the lateral boundary conditions.

If the top boundary condition file is not supplied, CAMx will default to internally employing the original "zero-gradient" mixing ratio assumption, whereby the concentrations of each species in the top model layer (as mole pollutant per mole air) is assumed to also exist above the model top.

The data records for the top boundary conditions file have the following structure and are repeated for each time interval on file:

```

ibdate, btime, iedate, etime
Loop from l = 1 to nspec species:
  ione, namspec(l), ((tc(i, j, l), i=1, nx), j=1, ny)

```

The variables have the following definitions:

Record 1

ibdate	Integer beginning date of time interval (YYJJ)
btime	Real beginning decimal hour (e.g., 1:30 PM = 13.5)
iedate	Integer ending date of time interval (YYJJ)
etime	Real ending decimal hour (e.g., 1:30 PM = 13.5)

Record 2 through *nspec* × *nz* + 1

ione	Integer dummy variable (=1)
namspec	Text names for <i>nspec</i> species (character*4(10, <i>nvar</i>) array):
tc	Real concentration field values (ppm for gases, $\mu\text{g}/\text{m}^3$ for aerosols) for <i>nx</i> grid columns and <i>ny</i> grid rows

The time interval of the data records must match the time zone as specified in the CAMx.in file.

3.4.3.9 Input Elevated Point Source File

The input elevated point source emissions file contains stack parameters and emission rates for all elevated point sources, and for all emitted species, to be modeled. If elevated point sources are to be modeled, only one point source emissions file must be developed for the entire modeling domain. The point source file also flags the individual stacks to be treated by the CAMx PiG sub-model by setting the stack diameter as a negative value. The file offers the ability to optionally specify the effective plume height or the vertical plume distribution for each point source and to bypass the internal plume rise calculation.

The elevated point source file adds two additional set of header records that specify time-invariant stack parameters, resulting in a total of six header records altogether (note that first four records are identical to the header records described above):

```

name, note, ione, nspec, ibdate, btime, iedate, etime
plon, plat, iutm, xorg, yorg, delx, dely, nx, ny, nz, iproj, istag, tlat1, tlat2, rdum
ione, ione, nx, ny
(namspec(l), l=1, nspec)
ione, nstk
(xstk(n), ystk(n), hstk(n), dstk(n), tstk(n), vstk(n), n=1, nstk)

```

The additional header variables have the following definitions:

Record 5

ione	Integer dummy variable (=1)
nstk	Integer number of elevated point source stacks

Record 6

xstk	Real stack x-coordinate (m or degrees longitude)
ystk	Real stack y-coordinate (m or degrees latitude)
hstk	Real stack height (m)
dstk	Real stack diameter (m); negative value flags source for PiG
tstk	Real stack exit temperature (K)
vstk	Real stack exit velocity (m/hr)

The time-variant data records for the elevated point source file have the following structure, and are repeated for each time interval on file:

```

ibdate, btime, iedate, etime
ione, nstk
(idum, idum, kcell(n), flow(n), plmht(n), n=1, nstk)
Loop from l = 1 to nspec species:
  ione, namspec(l), (ptems(n, l), n=1, nstk)

```

The variables have the following definitions:

Record 1

ibdate	Integer beginning date of time interval (YYJJJ)
btime	Real beginning decimal hour (e.g., 1:30 PM = 13.5)
iedate	Integer ending date of time interval (YYJJJ)
etime	Real ending decimal hour (e.g., 1:30 PM = 13.5)

Record 2

ione	Integer dummy variable (=1)
nstk	Integer number of elevated point source stacks

Record 3

idum	Integer dummy variable
kcell	Zero or positive: Ignored Negative: integer flag for OSAT/PSAT source region override
flow	Zero: ignored (plume rise calculation uses time-invariant exit velocity) Positive: real stack flow rate (m^3/hr) for plume rise calculations Negative: real plume bottom (m) for vertical plume distribution override
plmht	Zero or positive: ignored (plume rise calculation is performed) Negative ($\text{flow} \geq 0$): real effective plume rise override (m) Negative ($\text{flow} < 0$): real plume top (m) for vertical plume distribution override

Record 4 through *nspec+4*

ione	Integer dummy variable (=1)
namspec	Text names for <i>nspec</i> species (character*4(10,nvar) array):
ptems	Real point emission rate (mol/time period for gases, g/time period for aerosols) for <i>nstk</i> point sources

Note that the emission time interval (the denominator for the emissions rate) is normally, but not necessarily, 1 hour. The time interval of the emission records must match the time zone and input frequency of the emissions as specified in the CAMx.in file.

3.4.3.10 Input Gridded Emissions File

The input gridded emissions file contains gridded fields of low-level (i.e., surface) emission rates for all emitted species to be modeled. If gridded emissions are to be modeled, a gridded emissions file must be developed for the master grid and optionally any nested fine grids.

The data records of the gridded emissions file have the following structure, and are repeated for each time interval on file:

```

ibdate,btime,iedate,etime
Loop from l = 1 to nspec species:
  ione,namspec(l),((emiss(i,j,l),i=1,nx),j=1,ny)

```

The variables have the following definitions:

Record 1

ibdate	Integer beginning date of time interval (YYJJ)
btime	Real beginning decimal hour (e.g., 1:30 PM = 13.5)
iedate	Integer ending date of time interval (YYJJ)
etime	Real ending decimal hour (e.g., 1:30 PM = 13.5)

Record 2 through *nspecxnz+1*

ione	Integer dummy variable (=1)
namspec	Text names for <i>nspec</i> species (character*4(10,nvar) array):

`emiss` Real gridded emission field values (mol/time period for gases, g/time period for aerosols) for n_x grid columns and n_y grid rows

Note that the emission time interval (the denominator for the emissions rate) is normally, but not necessarily, 1 hour. The time interval of the emissions record must match the time zone and input frequency of the emissions as specified in the CAMx.in file.

3.4.4 Output Files

Master and nested grid instantaneous files contain full three-dimensional fields of all species modeled, while the gridded average and deposition files contain only those species specified in the run control file. For flexibility, CAMx offers the option to write full three-dimensional average concentration fields, or just surface layer two-dimensional fields (see the "3-D average file" option in the CAMx control file). It is permissible to change the number of species on the average file, or change between 2-D and 3-D average files, from one CAMx simulation period to the next (provided the periods are configured as separate CAMx runs). As the instantaneous concentration files are used for CAMx restarts, the model only writes instantaneous fields at the end of the simulation. PiG output files possess a unique format, and are used primarily for model restarts.

3.4.4.1 Output Concentration Files

The output average files for all grids, and the coarse (master) grid instantaneous file, are all written in the CAMx Fortran binary format as described earlier. There are three differences between the output concentration files and the input initial concentration files. First, the file name given in the file description header record (header record #1) is "AVERAGE" for the average output file, "INSTANT" for the instantaneous output file, and "AIRQUALITY" for the input initial concentration file. Second, the "note" in the file description header record of the output concentration files is the message supplied in the first line of the CAMx run control file, whereas the "note" in the air quality file is set as part of the input file preparation. Third, the species lists can be different among the files: the output instantaneous file contains all species modeled (as specified in the chemistry parameters file), the average output file contains only the species specified in the run control file, and the input initial concentration file may contain any subset of modeled species as determined when that file is prepared.

Two other differences exist between the average and instantaneous output files. As noted above, the average file may contain only surface-level fields or the entire three-dimensional fields, as selected by the user. Also, gas concentration fields are output as ppm in average files, but as $\mu\text{mol}/\text{m}^3$ in instantaneous files (aerosols are in $\mu\text{g}/\text{m}^3$ in both files). Because of these differences, and because average files usually do not contain all modeled species, CAMx does not allow the average output concentration file to be used for simulation restarts.

3.4.4.2 Output Deposition Files

The output deposition file is identical in format to the two-dimensional surface-level output average concentration file. The file name given on the first record of the deposition file is "AVERAGE" so that existing post-processing software will recognize the format. However, the output deposition file differs from the output average concentration file in one important way.

The species list is identical to the list on the average concentration output files, except that four parameters are output for each species:

<code>species_DV</code>	Real 2-D dry deposition velocity field for <i>species</i> (m/s)
<code>species_DD</code>	Real 2-D dry deposited mass field for <i>species</i> (mol/ha for gases, g/ha for aerosols)
<code>species_WD</code>	Real 2-D wet deposited mass field for <i>species</i> (mol/ha for gases, g/ha for aerosols)
<code>species_LC</code>	Real 2-D precipitation liquid concentration for <i>species</i> (mol/l for gases, g/l for aerosols)

3.4.4.3 Output Surface Mass Files

The output surface model mass file is identical in format to the two-dimensional surface-level output average concentration and deposition files. The file name given on the first record of the deposition file is "AVERAGE" so that existing post-processing software will recognize the format. However, the contents of the surface mass file differ from the other files in two ways. First, the species list is defined from the section of the chemistry parameters file that explicitly lists the species to be tracked by the surface model (see Section 4.8). Second, two parameters are output for each surface model species:

<code>Sspecies</code>	Real 2-D dry mass on soil or snow for <i>species</i> (mol/ha)
<code>Vspecies</code>	Real 2-D dry mass on vegetation for <i>species</i> (mol/ha)

This file is also used for restarts to re-initialize the surface model with accumulated species mass on soil/snow and vegetative surfaces from a previous run.

3.4.4.4 Nested (Fine) Grid Instantaneous Output File

The nested (or "fine") grid Fortran binary output instantaneous file is unique and contains the three-dimensional concentration fields for all nested grids together, as opposed to separate files for each grid. All grid definition parameters given in these files are referenced relative to the master grid, so specific absolute information about grid cell size or projection coordinates for each nested grid must be determined from master grid parameters. If the user utilizes the Flexi-nesting capability of CAMx, then the gridded fields output to the nested fine grid files will change according to how nests are altered, added, and/or removed during the course of a simulation.

The header portion of the nested grid output files contain $3+n_{nest}$ records with the following structure:

```

message
nnest, nspec
(mspec(l), l=1, nspec)
Loop from 1 to nnest grid nests
  ibeg, jbeg, iend, jend, mesh, ione, nx, ny, nz, iparnt, ilevel

```

The time-variant portion of the nested grid output files have the following structure, where the following records are repeated for each output time:

```

time, idate
Loop from 1 to nnest grid nests
  Loop from l = 1 to nspec species:
    Loop from k = 1 to nz layers:
      ((conc(i, j, k, l), i=1, nx), j=1, ny)

```

The variables on the nested grid output concentration files have the following definitions:

message	Text string containing file description (character*60)
nnest	Number of fine grid nests on file
nspec	Number of species on file
mspec	Species names for nspec species
ibeg	Grid <i>n</i> x-direction starting index of grid (master grid cell)
jbeg	Grid <i>n</i> y-direction starting index of grid (master grid cell)
iend	Grid <i>n</i> x-direction ending index of grid (master grid cell)
jend	Grid <i>n</i> y-direction ending index of grid (master grid cell)
mesh	Grid <i>n</i> meshing factor (number of nested cells per master)
ione	Dummy integer = 1
nx	Grid <i>n</i> number of grid rows
ny	Grid <i>n</i> number of grid columns
nz	Grid <i>n</i> number of layers
iparnt	Grid <i>n</i> 's parent grid (grid index within which this fine grid is nested; 0 = master grid)
ilevel	Grid <i>n</i> 's grid level (depth at which this grid is nested; 1=master grid is parent)
time	Time of output (HHMM); ending hour for average output
idate	Date of output (YYJJJ)
conc	Grid <i>n</i> , species <i>l</i> , layer <i>k</i> concentrations (ppm for average gases, $\mu\text{g}/\text{m}^3$ for average aerosols, $\mu\text{mol}/\text{m}^3$ for instantaneous gas species) for <i>nx</i> grid columns, and <i>ny</i> grid rows

3.4.4.5 PiG Restart File

When the PiG option is invoked, CAMx outputs all puff parameters each hour for model restart capabilities. This file is Fortran binary and is analogous to the instantaneous gridded concentration output files in that it represents a "snapshot" of data at the top of each hour. The file format is unique and contains information for each puff, including coordinates, grid location, size specifications, age, and mass of each of the chemical species carried. While this file contains PiG information for the entire simulation, it would be of limited use for certain analyses such as plotting puff trajectories. This is because the instantaneous nature of the data,

and the dynamic memory allocation utilized in the PiG submodel, leads to insufficient information to identify and track individual puffs hour to hour.

The PiG restart file contains two records with the following structure, and these are repeated for each output time:

```

idatpig, timpig, npig, nreactr
(ingrd(n), idpig(n), xpigf(n), xpigb(n), ypigf(n), ypigb(n), zpig(n),
& axisy(n), axisz(n), sigy(n), sigx(n), sigz(n), pufftop(n), puffbot(n),
& htfms(n), htfmb(n), vtfms(n), vtfmb(n), agepigf(n), agepigb(n), fmspig(n),
& ipufmap(n), ipufgrp(n),
& ((puffrad(i, nr, n), i=1, nrad), nr=1, nreactr),
& ((puffmass(i, nr, n), i=1, nspec), nr=1, nreactr), n=1, npig

```

The variables on the PiG restart file have the following definitions:

idatpig	Date of output (YYJJJ)
timpig	Time of output (HHMM)
npig	Number of PiG puffs active at this output time
nreactr	Number of chemical reactors in each puff
ingrd	Grid index for <i>npig</i> puffs
idpig	Point source index for <i>npig</i> puffs
xpigf	x-coordinate of puff front (km from master grid SW corner) for <i>npig</i> puffs
xpigb	x-coordinate of puff back (km from master grid SW corner) for <i>npig</i> puffs
ypigf	y-coordinate of puff front (km from master grid SW corner) for <i>npig</i> puffs
ypigb	y-coordinate of puff back (km from master grid SW corner) for <i>npig</i> puffs
zpig	Puff height (m AGL) for <i>npig</i> puffs
axisy	Puff lateral width (m) for <i>npig</i> puffs
axisz	Puff vertical depth (m) for <i>npig</i> puffs
sigy	Puff Gaussian lateral dimension (m) for <i>npig</i> puffs
sigx	Puff Gaussian longitudinal dimension (m) for <i>npig</i> puffs
sigz	Puff Gaussian vertical dimension (m) for <i>npig</i> puffs
pufftop	Puff top height (m AGL) for <i>npig</i> puffs
puffbot	Puff bottom height (m AGL) for <i>npig</i> puffs
htfms	Puff horizontal turbulent flux moment, shear (m ² /s)
htfmb	Puff horizontal turbulent flux moment, buoyancy (m ² /s)
vtfms	Puff vertical turbulent flux moment, shear (m ² /s)
vtfmb	Puff vertical turbulent flux moment, buoyancy (m ² /s)
agepigf	Puff front age since release (s) for <i>npig</i> puffs
agepigb	Puff back age since release (s) for <i>npig</i> puffs
fmspig	Puff volume parameter (unitless) for <i>npig</i> puffs
ipufmap	Puff OSAT/PSAT region map pointer (unitless) for <i>npig</i> puffs
ipufgrp	Puff OSAT/PSAT group pointer (unitless) for <i>npig</i> puffs

puffrad	Puff radical concentrations (ppm) for <i>nrad</i> species, <i>nreactr</i> reactors, and <i>npig</i> puffs
puffmass	Puff pollutant mass (μmol) for <i>nspec</i> species, <i>nreactr</i> reactors, and <i>npig</i> puffs

3.4.4.6 PiG Sample Grid Files

The optional PiG sampling grid concentrations are time-averaged in the same manner as the output average concentrations provided on the computational grids. The same user-defined set of output species are written to the sampling grid files, but only two-dimensional surface layer concentrations are reported. The sampling grid file format is identical to the CAMx average and deposition files, with one file generated per sampling grid, so that they may be readily viewed and manipulated with CAMx post-processing software.

4. CORE MODEL FORMULATION

This section outlines the numerical approach employed in the core CAMx model, and describes the technical formulation of the emissions, transport and removal algorithms. The specific chemical mechanisms and their numerical solvers are discussed in detail in Section 5.

Descriptions of Plume-in-Grid and each Probing Tool are provided in Sections 6 through 10.

4.1 Numerical Approach

The physical representations and the numerical methods used for each term of the pollutant continuity equation (described in Section 1) are summarized in Table 4-1. CAMx includes peer-accepted algorithms and component formulations, and its modular framework eases the addition and/or substitution of alternative algorithms in the future.

Table 4-1. Summary of the CAMx models and methods for key physical processes.

Process	Physical Models	Numerical Methods
Horizontal advection	Eulerian continuity equation	<ul style="list-style-type: none"> • Bott (1989) • PPM (Colella and Woodward, 1984)
Horizontal diffusion	K-theory 1 st order closure	Explicit simultaneous 2-D solver
Vertical advection	Eulerian continuity equation	Implicit backward-Euler (time) hybrid centered/upstream (space) solver
Vertical diffusion	<ul style="list-style-type: none"> • K-theory 1st order closure • Non-local mixing 	<ul style="list-style-type: none"> • Implicit backwards-Euler (time) centered (space) solver • Explicit ACM2 non-local convection/diffusion (Pleim, 2007)
Gas-Phase Chemistry	<ul style="list-style-type: none"> • Carbon Bond 2005 (Yarwood et al., 2005b) • Carbon Bond 6 (Yarwood et al., 2010, 2012a, 2014; Hildebrandt Ruiz and Yarwood, 2013; Emery et al., 2015) • SAPRC07TC (Carter, 2010; Hutzell et al., 2012) • Inorganic/organic aerosol precursors 	<ul style="list-style-type: none"> • EBI (Hertel et al., 1993) • LSODE (Hindmarsh, 1983)
Aerosol Chemistry	<ul style="list-style-type: none"> • Aqueous inorganic chemistry • Inorganic thermodynamics/partitioning • Organic thermodynamics/partitioning • Static 2-mode or multi-section size models 	<ul style="list-style-type: none"> • RADM-AQ (Chang et al., 1987) • ISORROPIA (Nenes et al., 1998) • SOAP (Strader et al., 1999) or VBS (Koo et al., 2014) • Coarse/Fine (CF) 2-mode model • CMU sectional model (Pandis et al., 1993)
Dry deposition	<ul style="list-style-type: none"> • Resistance model for gases (Wesely, 1989) and aerosols (Slinn and Slinn, 1980) • Resistance model for gases (Zhang et al., 2003) and aerosols (Zhang et al., 2001) 	Deposition velocity as surface boundary condition in vertical diffusion solver
Wet deposition	Scavenging model for gases and aerosols (Seinfeld and Pandis, 1998)	Exponential decay as a function of scavenging coefficient

The continuity equation is numerically marched forward in time over a series of time steps. At each step, the continuity equation is integrated by way of an operator-splitting approach that calculates the separate contribution of each major process (emission, advection, diffusion, chemistry, and removal) to concentration change within each grid cell. The specific equations that are solved individually in the operator-splitting process are shown in order below:

$$\begin{aligned} \left. \frac{\partial c_l}{\partial t} \right|_{Emission} &= m^2 \frac{E_l}{\partial x \partial y \partial z} \\ \left. \frac{\partial c_l}{\partial t} \right|_{X \text{ advection}} &= - \frac{m^2}{A_{yz}} \frac{\partial}{\partial x} \left(\frac{u A_{yz} c_l}{m} \right) \\ \left. \frac{\partial c_l}{\partial t} \right|_{Y \text{ advection}} &= - \frac{m^2}{A_{xz}} \frac{\partial}{\partial y} \left(\frac{v A_{xz} c_l}{m} \right) \\ \left. \frac{\partial c_l}{\partial t} \right|_{Z \text{ transport}} &= \frac{\partial(c_l \eta)}{\partial z} - c_l \frac{\partial^2 h}{\partial z \partial t} \\ \left. \frac{\partial c_l}{\partial t} \right|_{Z \text{ diffusion}} &= \frac{\partial}{\partial z} \left[\rho K_v \frac{\partial(c_l/\rho)}{\partial z} \right] \\ \left. \frac{\partial c_l}{\partial t} \right|_{XY \text{ diffusion}} &= m \left\{ \frac{\partial}{\partial x} \left[m \rho K_X \frac{\partial(c_l/\rho)}{\partial x} \right] + \frac{\partial}{\partial y} \left[m \rho K_Y \frac{\partial(c_l/\rho)}{\partial y} \right] \right\} \\ \left. \frac{\partial c_l}{\partial t} \right|_{Wet \text{ Scavenging}} &= - \Lambda_l c_l \\ \left. \frac{\partial c_l}{\partial t} \right|_{Chemistry} &= \text{Mechanism – specific reaction equations} \end{aligned}$$

where c_l is species concentration ($\mu\text{mol}/\text{m}^3$ for gasses, $\mu\text{g}/\text{m}^3$ for aerosols), E_l is the local species emission rate ($\mu\text{mol}/\text{s}$ for gasses, $\mu\text{g}/\text{s}$ for aerosols), ∂t is timestep length (s), u and v are the respective east-west (x) and north-south (y) horizontal wind components (m/s), A_{yz} and A_{xz} are cell cross-sectional areas (m^2) in the y - z and x - z planes, respectively, m is the ratio of the transformed distance on the various map projections to true distance ($m=1$ for curvi-linear latitude/longitude coordinates), and Λ_l is the wet scavenging coefficient (s^{-1}).

A master driving time step for the model is dynamically determined during the simulation for the largest and coarsest (master) grid. Time steps typically range from 5-15 minutes for grid cell sizes of 10-50 km, to a minute or less for small cell sizes of 1-2 km. As a result, nested grids require multiple driving time steps per master step depending on their grid sizes relative to the master grid spacing. Furthermore, multiple transport and chemistry time steps per driving step are used as necessary to ensure accurate solutions for these processes on all grids.

The first process in each time step for a given grid is the injection of emissions from all sources. CAMx then performs horizontal and vertical advection, vertical diffusion coupled to dry deposition, horizontal diffusion, chemistry, and finally wet scavenging.

Although advection is performed separately in the x (east-west), y (north-south), and z (vertical) directions, the numerical linkage between these components has been developed in a mass consistent fashion to preserve the density field at each time step. This maintains the flexibility to allow many types of meteorological models, and modeling grid resolutions, projections, and layer structures, to characterize transport in CAMx.

Trace gases and particles are removed from the atmosphere via deposition to the ground. Dry deposition refers to the direct sedimentation and/or diffusion of material to various terrestrial surfaces and uptake into biota. Dry deposition velocities for each species are used as the surface boundary condition for vertical diffusion, which appropriately couples surface removal of pollutants through each column of cells via the vertical mixing process. Wet deposition refers to the uptake of material into cloud water and precipitation, and its subsequent transfer to the surface. The efficiency with which wet and dry deposition processes can remove pollutants from the air depends upon the physical and chemical properties of the pollutants, local meteorological conditions, the type of surface on which they are being deposited, and on the frequency, duration, and intensity of precipitation events.

4.2 CAMX Grid Configuration

4.2.1 Grid Cell Arrangement

CAMx carries pollutant concentrations at the center of each grid cell volume, representing the average concentration over the entire cell. Meteorological fields are supplied to the model to quantify the state of the atmosphere in each grid cell for the purposes of calculating transport, chemistry, and removal. CAMx internally carries these variables in an arrangement known as an "Arakawa C" grid configuration (Figure 4-1). State variables such as temperature, pressure, water vapor, and cloud water are located at cell center along with pollutant concentration, and represent grid cell average conditions. Wind components and diffusion coefficients are carried at cell interfaces to describe the transfer of mass in and out of each cell face. Note in Figure 4-1, for example, that horizontal wind components u and v are staggered from each other. This facilitates the solving of the transport equations in "flux form".

Depending upon the source of meteorological data, it is recommended that the user directly provide the gridded horizontal wind fields in the staggered Arakawa C configuration. However, this is not always feasible, and so CAMx offers the option for the user to supply all meteorological variables, including horizontal wind components, at cell center; in this case CAMx internally interpolates the winds to cell interfaces. Note that this leads to a slight smoothing effect on the horizontal wind fields.

Figure 4-1 also describes the horizontal cell indexing convention used in CAMx. Each cell is defined by the index pair (i,j) , where i ranges from 1 to nx (the number of cells in the east-west direction), and j ranges from 1 to ny (the number of cells in the north-south direction). The

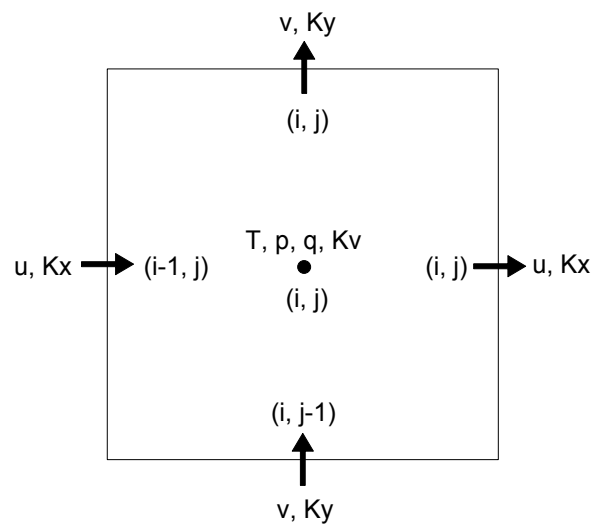


Figure 4-1. A horizontal representation of the Arakawa C variable configuration used in CAMx.

eastern and northern faces of the cell are indexed (i,j) , while the western and southern faces are indexed $(i-1,j)$ and $(i,j-1)$, respectively.

In the vertical, most variables are carried at each layer midpoint (defined as exactly half way between layer interfaces) to represent layer averages. Again the exceptions are those variables that describe the rate of mass transport across the layer interfaces, which include the vertical diffusion coefficient K_v and the vertical transport rate η . These variables are carried in the center of each cell horizontally, but are located at the top of the layer (i.e., the interface) vertically.

4.2.2 Grid Nesting

CAMx incorporates two-way grid nesting, which means that pollutant concentration information propagates into and out of all grid nests during model integration. Any number of grid nests can be specified in a single run, where horizontal grid spacing can vary from one grid nest to another (note that vertical grid structures must be consistent among all grids). The nested grid capability of CAMx allows cost-effective application to large regions in which regional transport occurs, yet at the same time providing fine resolution to address small-scale impacts in selected areas.

Each grid nest is defined over a subset of master (coarsest) grid cells. The range of master grid row and column indices that define the coverage of each nested grid must be specified in the run control file. An integer number of nested grid cells must span one master grid cell; this number is referred to as a “meshing factor”. “Buffer” cells are added around the perimeter of each nested grid to hold lateral boundary conditions. Buffer cells are added automatically within CAMx and should not be specified by the user in the run control file. All nested grid output files contain data for the entire array of computational and buffer cells; however, buffer cell concentrations are considered invalid and should be ignored. Additionally, all nested grid

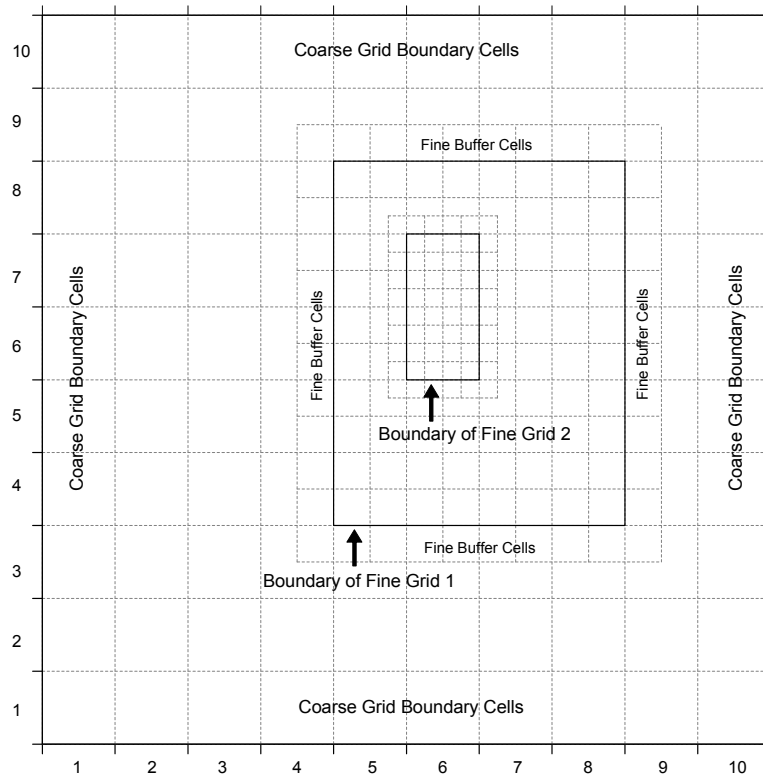


Figure 4-2. An example of horizontal grid nesting, showing two telescoping nested grids within a 10×10 cell master grid. The outer nest contains 10×12 cells (including buffer cells to hold internal lateral boundary conditions), and the inner nest contains 6×10 cells (including buffer cells).

input files must contain data for the entire array of computational and buffer cells. An example of a horizontal nesting arrangement is shown in Figure 4-2. Here, two telescoping fine grid nests are defined: one with a meshing factor of 2 spanning master grid cells (5,4) to (8,8), and one with a meshing factor of 4 spanning master grid cells (6,6) to (6,7).

Restrictions on specifying the size and resolution of all grid nests include the following:

- 1) The ratio of master grid cell size to nested grid cell size must be an integer (e.g., a “meshing factor” of 3 means that 3 nested cells span the distance of 1 master cell, resulting in an area of 9 nested cells per master cell);
- 2) For telescoping grids (a nested grid containing an even finer grid), the cell size of the finest grid must be a common denominator for all parent grids above it (e.g., a 36-12-4 km or 36-12-2 km arrangement is allowed, but a 36-12-9 km is not);
- 3) The restriction in (2) above does not apply to parallel nested grids of the same generation (e.g., 4 km and 5 km grids can be located in different areas of a master grid provided that the master cell size is some multiple of 20 km);
- 4) Nested grids cannot overlap, although they may share a common lateral boundary or edge;

- 5) Nested grids cannot extend into a lateral boundary, or non-modeled, area of the master grid;
- 6) CAMx is currently configured to allow four “generations” of nests (e.g., four levels of telescoping grids); this can be extended in the code if more than four levels of nests are required;
- 7) The total vertical depth of each nested grid must exactly match the depth of the master grid, and nested grid vertical layer structures must be consistent with the master grid in terms of the number of layers and their thicknesses;

4.2.3 Flexi-Nesting

The following Fortran binary I/O files must be provided for the master grid, and optionally provided for each nested grid:

- 2-D surface emissions;
- 2-D time-invariant surface characteristics (landuse and LAI distribution);
- 2-D time-variant surface meteorology (surface temperature, snow cover);
- 3-D time-variant state meteorology (wind, temperature, pressure, moisture, vertical grid);
- 3-D time-variant cloud and precipitation variables;
- 3-D time-variant vertical diffusivities

Any of these input files may be supplied for each nested grid, or none at all. If any of these files are not supplied for a particular nested grid, the Flexi-Nest algorithm within CAMx interpolates the missing fields from the parent grid. Clearly it is desirable to provide nested grid data whenever possible. However, the ability to interpolate data is useful for testing sensitivity to grid configurations or for situations when it is not possible to run a meteorological model for all grid nests.

The Flexi-Nest option also allows users to redefine the nested grid configuration at any point in a simulation. Nested grids can be introduced or removed only at the time of a model restart since a new CAMx user control file must be used to redefine the grid configuration. For example, the user may wish to “spin-up” the model over the first two days using just the master grid. On the third day, the user might introduce one or more nests for more detailed analysis. This would require that the model be restarted on the third day with a new control file that defines the position of the new nests and (optionally) provides any additional input fields for these grids. CAMx will internally reconcile the differences in grid structure between the restart files and the new user control file, and then interpolate any data fields not supplied to CAMx for the new nests from the parent grid(s).

4.3 Treatment of Emissions

Pollutant emissions are treated in two basic ways within CAMx: low-level (gridded) emissions that are released into the lowest (surface) layer of the model; and elevated stack-specific (point) emissions with buoyant plume rise that can be emitted into any model layer. Emission rates are held constant (not time interpolated) between reading intervals (usually 1 hour) but

are injected at every grid-specific time step during the simulation. Gridded and point emissions are provided to CAMx in separate input files. External emission processing systems are used to develop gridded and point, time- and space-resolved, chemically-speciated input files for CAMx. These external programs are not discussed in this User's Guide; see Section 2 for more information on emission systems that are used to support CAMx applications.

4.3.1 Gridded Emissions

Two-dimensional gridded low-level emissions are defined by space- and time-varying rates for each individual gas and PM species to be modeled. Gridded emissions represent sources that emit near the surface and that are not sufficiently buoyant to reach into the upper model layers. Such emission categories include:

- Low-level stack (point) emissions that are too small to result in plume rise above the model surface layer;
- Other non-point industrial sources (fugitive leaks, tanks, etc.);
- Mobile sources (cars, trucks, non-road vehicles, railroad, marine, aircraft, etc.);
- Residential sources (heating, cooking, consumer products);
- Commercial sources (bakeries, refueling stations, dry cleaners);
- Biogenic sources;
- Natural sources (small fires, wind-blown dust).

The spatial distribution of each individual source within these categories is defined by the modeling grid. Information such as population distribution, housing density, roadway networks, vegetative cover, etc. is typically used as a surrogate to distribute regional emission estimates for each source to the grid system. Processing tools are used to combine emissions from all sources into a single input file for each grid (see Sections 2 and 3).

4.3.2 Elevated Point Emissions

Similarly to gridded emissions, elevated point emissions are defined by space- and time-varying rates for each individual gas and PM species to be modeled. The only difference is that these sources emit from individual stacks with buoyant rise that may take them into upper model layers. These types of sources are almost always associated with large industrial processes, such as electric generators, smelters, refineries, large factories, etc. but can also represent natural elevated sources such as wildfires and lightning NO_x. The spatial distribution of these points is specifically given by the coordinates of the stacks themselves (grid locations are determined within CAMx). Plume rise is determined within CAMx as a function of stack parameters (height, diameter, exit velocity and temperature) and ambient meteorological conditions, so the point source file provides speciated time-resolved emission rates and stack parameters for each individual source. A single point source file provides the definition of all stacks and their emissions over the entire modeling domain (see Sections 2 and 3).

Plume rise is calculated using the multi-layer stability-dependent algorithm of Turner et al. (1986). This approach calculates the momentum and buoyant plume rise energy from the stack, takes the larger of these two values, and determines the dissipation of that energy via

mixing with ambient air according to the meteorological conditions through the host model layer. If sufficient energy remains to reach into the next model layer, the calculation for buoyant rise repeats for the meteorological conditions of that layer, and so on, until a layer is found where the plume cannot rise any farther. All emissions from this source are then injected into the grid cell directly above the stack at this layer height. This algorithm was adopted for CAMx because it provides a more realistic handling of stable layers aloft that can trap plume rise, whereas this effect would not be realized based on meteorological conditions at stack top alone.

Under neutral/unstable conditions, momentum rise at the stack top is calculated from

$$H_{mu} = \frac{3d_s v_s}{w}$$

while buoyancy rise is the lesser of

$$H_{bu} = 30(f/w)^{3/5} + z_b$$

and

$$H_{bu} = 24(f/w^3)^{3/5} [h_s + 200(f/w^3)]^{2/5} + z_b$$

In these expressions d_s is stack diameter (m), v_s is stack exit velocity (m/s), h_s is stack height (m), w is ambient wind speed (m/s), and z_b is the distance between the stack top and the base of the current model layer. A minimum wind speed of 1 m/s is specified to avoid unrealistically large plume rise. Buoyancy flux f is initially calculated from stack parameters, but is set to residual flux entering the bottom of any higher layer. The initial buoyancy flux at stack top is given by

$$f_0 = g v_s d_s^2 \left(\frac{T_s - T}{4T_s} \right)$$

where g is gravitational acceleration (9.8 m²/s), T_s is stack exit temperature (K), and T is ambient temperature (K). The residual flux calculation into the next higher layer depends on which neutral/unstable buoyancy rise equation was originally used in the current layer:

$$f = w \left(\frac{H_{bu} - z_t}{30} \right)^{5/3}$$

or

$$f = 5.5 \times 10^{-3} w^3 (H_{bu} - z_t) \left(1 + \frac{h_s}{H_{bu} - z_t} \right)^{-2/3}$$

where z_t is the distance between stack top and the top of the current model layer.

Under stable conditions, momentum rise at the stack top is calculated from the lesser of H_{mu} and

$$H_{ms} = 0.646 T^{1/2} \left(\frac{v_s^2 d_s^2}{T_s w} \right)^{1/3} \left(\frac{\partial \theta}{\partial z} \right)^{-1/6}$$

while buoyancy rise is the lesser of

$$H_{bs} = \left[\frac{1.8 f T}{w} \left(\frac{\partial \theta}{\partial z} \right)^{-1} + z_b^3 \right]^{1/3}$$

and

$$H_{bs} = \left[\frac{4.1 f T}{f_0^{1/3}} \left(\frac{\partial \theta}{\partial z} \right)^{-1} + z_b^{8/3} \right]^{3/8}$$

In these expressions, $\partial\theta/\partial z$ is the potential temperature gradient (a measure of atmospheric stability). Here also, buoyancy flux is initially calculated from stack parameters, but is set to residual flux if the plume extends into the next higher layer. The residual flux calculation depends on which stable buoyancy rise equation was originally used:

$$f = f - 0.56 \frac{\partial \theta}{\partial z} \frac{w}{T} (z_i^3 - z_b^3)$$

or

$$f = f - 0.24 \frac{\partial \theta}{\partial z} \frac{f_0^{1/3}}{T} (z_i^{8/3} - z_b^{8/3})$$

When final plume rise is reached using stable buoyancy rise, it is adjusted downward to two-thirds of the rise through the stable depth. After final plume rise is determined, the rise is further adjusted downward by stack tip downwash according to a critical Froude number and ambient wind speed. The stack Froude number is given by

$$F = \frac{T v_s^2}{g d_s (T_s - T)}$$

For $F < 3$, no downwash adjustment is made to final plume rise. Above that value, the following downwash factors (D) are applied depending upon the ambient wind speed at stack top:

$$\begin{aligned} D &= 0, & v_s < w & \text{ (no plume rise)} \\ D &= 3 \frac{v_s - w}{v_s}, & \frac{2}{3} v_s \leq w < v_s \\ D &= 1, & w < \frac{2}{3} v_s \end{aligned}$$

CAMx injects point source emissions into all model layers spanned by the plume depth at final (adjusted) rise. Plume depth is determined as a function of stack diameter, plume temperature, plume velocity, time of plume rise, and ambient wind and temperature conditions. A uniform mass distribution through plume depth is assumed. If this depth is wholly contained within a single layer, that layer receives all emission mass. If this depth spans several layers, then fractions of the emissions are injected into these layers according to the

fraction of plume depth spanning those layers. We apply the “rule-of-thumb” that plume depth equals plume rise (Turner and Schulze, 2007) as a maximum limit for plume depth.

The following equations are used to define the plume depth after reaching final rise. These are based on the approach used in the SCIPUFF model (EPRI, 2000) and were developed for use in the CAMx plume-in-grid (PiG) submodel. The plume depth D_p at final rise is given by

$$D_p = 3\left(2D_s^2 + 2Kt\right)^{1/2}$$

where D_s is stack diameter, K is plume diffusivity during rise, and t is the time of rise. The time of rise is determined by dividing final plume rise by the mean plume rise speed V_p ; the latter is set to half the stack exit velocity. A lower limit of 1 m/s is applied to the exit velocity, so the minimum value of V_p is 0.5 m/s. The plume diffusivity is determined by scaling initial plume width (according to stack diameter) by the turbulent flux moment q_p^2 :

$$K = 0.15\left(\sqrt{2}D_s\right)\sqrt{q_p^2}$$

where

$$q_p^2 = f_p V_p^2 \left[0.4 + \left(\frac{3v^2}{v^2 + V_p^2} \right) \right]$$

The turbulent flux moment is a function of the mean plume rise speed V_p , the ambient wind speed v taken at the level of final rise, and a plume entrainment coefficient f_p :

$$f_p = 1 + 4\left(\sqrt{2}D_s\right)g \left(\frac{T_p - T}{TV_p^2} \right)$$

where g is the gravitational constant (9.8 m²/s), T is ambient temperature at the level of final rise, and T_p is the mean plume temperature, taken as the mean of the stack exit temperature and the ambient temperature at final rise.

4.4 Three-Dimensional Transport

4.4.1 Resolved Transport: Advection

The CAMx advection algorithm is both mass conservative and mass consistent. Mass conservation refers to the ability to accurately account for all sources and sinks of mass in the model, with no spurious loss or gain of mass during model integration. To be mass conservative, CAMx internally carries concentrations of each species as a density (μmol/m³ for gases, μg/m³ for aerosols), and solves the advection and diffusion equations in flux form. This also serves to simplify mass budget accounting, which is used by the various source apportionment and process analysis options. Gas concentrations are internally converted to

volumetric mixing ratio (parts per million, or ppm) for the chemistry step, and when they are written to the average output files.

Mass consistency refers to the model's ability to transport pollutant mass exactly equivalent to the input atmospheric momentum field. For example, a model that is perfectly mass consistent will preserve a unity pollutant mixing ratio field in a divergent momentum field given constant unity boundary and initial conditions and zero sources and sinks. Sources of poor mass consistency in air quality models are typically related to (1) supplying meteorology that is inherently inconsistent (e.g., from an interpolative objective analysis or diagnostic model); (2) spatially interpolating or averaging meteorological model fields to a different air quality map projection or grid resolution; and (3) employing different numerical and/or physical methods in the air quality and meteorological models.

It is expected that CAMx users will prepare high quality, mass consistent meteorological fields using advanced prognostic models so as to minimize inconsistencies in the inputs themselves. The practice of developing meteorological input fields using objective analysis or "diagnostic" approaches is highly discouraged.

CAMx operates on the map projections and grid systems employed in several widely used prognostic meteorological models (e.g., WRF, MM5, and RAMS) so that translation of meteorological data to CAMx requires as little manipulation as possible. However, CAMx provides a very important flexibility that allows the air quality grid to differ in projection and resolution from the source of meteorological data. This, of course, leads to a potentially large external source of mass consistency error. The ability to drive CAMx with the output from any prognostic meteorologic model guarantees a difference in numerical methods between the two models, leading to an internal source of mass consistency error. The three dimensional advection algorithm in CAMx is designed to compensate for both external and internal sources of consistency error.

Horizontal advection uses input horizontal winds fields and is solved using the area preserving flux-form advection solver of Bott (1989) or the Piecewise Parabolic Method (PPM) of Colella and Woodward (1984) as implemented by Odman and Ingram (1993). These two finite difference schemes were incorporated into CAMx because they provide higher order accuracy with minimal numerical diffusion, yet are equivalent in execution speed compared to other simpler advection algorithms when operating on equivalent time steps. In CAMx, the Bott scheme is allowed to take larger time steps than PPM because Bott remains stable for Courant-Friedrichs-Levy (CFL) numbers up to 1 (i.e., the ratio of wind speed to grid spacing). Time steps are determined for Bott using a CFL number of 0.9, while time steps for PPM are restrained by a CFL number of 0.5. Therefore, the Bott option results in a faster simulation than the PPM option, perhaps at the price of some accuracy. We recommend testing both for your specific application.

CAMx internally calculates an instantaneous vertical velocity field from grid- and timestep-specific horizontal momentum fields as a way to balance the local atmospheric continuity equation. To calculate a vertical velocity profile for a given grid column, the divergent atmospheric continuity equation

$$\frac{\partial \rho}{\partial t} = -\nabla \cdot \rho V$$

is locally integrated through the depth of the column by imposing zero vertical velocity at the ground:

$$\rho w(z) = -\int_0^z \left(\frac{\partial \rho}{\partial t} + \nabla_H \cdot \rho V_H \right) dz$$

where the local time-rate change of atmospheric density $\partial \rho / \partial t$ in each grid cell is known from the input meteorological fields. The horizontal flux divergence of atmospheric density is calculated in a manner that is numerically consistent with the procedure used to horizontally advect pollutants:

$$\nabla_H \cdot \rho V_H = \frac{m^2}{A_{yz}} \frac{\partial}{\partial x} \left(\frac{u A_{yz} \rho}{m} \right) + \frac{m^2}{A_{xz}} \frac{\partial}{\partial y} \left(\frac{v A_{xz} \rho}{m} \right)$$

and this equation is solved using either the Bott or PPM advection solvers, as described above. In this approach, a vertical velocity profile $w(z)$ is constructed that provides a balance between the imposed density tendency and the resolved horizontal momentum divergence in each grid cell at each time step. Total three-dimensional advection thus includes resolved momentum convergence/divergence rates as well as any artificial divergences caused by the horizontal and vertical grid specifications (e.g., spatially varying vertical grid structure, or systematic distortions associated with the map projections).

The total vertical transport rate η at a particular layer interface is defined as the combination of resolved vertical velocity and the local time-rate of change of the layer interface height:

$$\eta = \frac{\partial h}{\partial t} - w$$

The total vertical transport rate is used for subsequent vertical advection calculations for all pollutants. In simple tests in which a uniform pollutant field of unity mixing ratio is transported throughout a single regional grid over several days using actual episodic meteorological inputs, this approach has been shown to provide nearly exact (to within 10^{-3} - 10^{-4} %) consistency between the density and pollutant fields.

Vertical advection is solved using a specific implicit backward-Euler integration scheme designed specifically for CAMx (Emery et al, 2011). Since implicit schemes are absolutely stable, only one solution step is necessary per driving time step. Explicit approaches require potentially many sub-steps (on the order of 10-100) to maintain a stable solution, which introduces the potential for excessive numerical diffusion.

4.4.2 Sub-Grid Turbulent Transport: Diffusion

CAMx employs a first-order eddy viscosity (or “K-theory”) approach by default to represent sub-grid turbulent diffusion (or mixing). As a “local” closure technique, K-theory only treats mass transfer cell-by-cell (horizontal) or layer-by-layer (vertical), analogously to the diffusion of heat

through a solid medium. Whereas K-theory adequately characterizes horizontal diffusion and weak vertical mixing during neutral and stable conditions, the shortcomings of K-theory are related to its inadequate treatment of deep vertical convective mixing. In actual convective situations, buoyant plumes deriving energy in the surface layer are quickly and efficiently mixed deep into the atmosphere within eddies that are usually much larger than the individual model layers. Therefore, K-theory may mix the convective boundary layer much less efficiently than commonly observed. This has been shown to have very important ramifications for chemistry, especially during transition periods between stable/neutral and convective conditions. CAMx includes the option to use K-theory vertical mixing (default) or the non-local Asymmetric Convective Model (ACM2) from Pleim (2007).

4.4.2.1 Horizontal Diffusion

As discussed by Yamartino (2000) advection solvers such as Bott and PPM reduce numerical diffusion to the point where modelers need to be concerned about including appropriate levels of explicit horizontal diffusion. Currently, there is very little information on the appropriate level of horizontal diffusion for Eulerian grid models. This issue is not limited to CAMx.

Explicit horizontal diffusion coefficients are determined within CAMx using a deformation approach based on the methods of Smagorinsky (1963):

$$K_{X/Y} = K_o + \frac{\Delta x \Delta y}{4\sqrt{2}} \left[\left(\frac{\partial u}{\partial y} + \frac{\partial v}{\partial x} \right)^2 + \left(\frac{\partial u}{\partial x} - \frac{\partial v}{\partial y} \right)^2 \right]^{1/2}$$

Separate diffusivity components are generated for fluxes in the x- and y-directions since K_x and K_y are calculated for separate cell faces in the Arakawa C grid arrangement. The value of K_o is specified according to the approach in MM5 (Anthes and Warner, 1978):

$$K_o = 3 \times 10^{-3} \frac{\Delta x \Delta y}{\Delta t}$$

A maximum value of $K_{X/Y}$ is set to maintain numerical stability for the given grid-specific timestep. A minimum value is set to $1 \text{ m}^2/\text{s}$. Horizontal diffusion is applied using an explicit simultaneous two-dimensional flux-divergence calculation.

4.4.2.2 K-theory Vertical Diffusion

The default vertical diffusion solver (K-theory) uses a standard implicit backward-Euler integration scheme. Gridded vertical diffusion coefficients (K_v) must be supplied to the model for the master grid via input file; the user may optionally supply vertical diffusion coefficients for any or all nested grids. Whereas the vertical advection step is solved in a single step, K-theory vertical diffusion is solved over potentially several sub-steps, depending upon the magnitude of the vertical diffusivity relative to the vertical layer depths (CAMx uses the smaller of the current grid time step or a maximum 5 minute sub-step). This ensures non-local diffusive coupling among all layers that exhibit high diffusivity, especially for long driving time steps on coarser grids that would otherwise only experience mixing between adjacent layers during a single step.

4.4.2.3 ACM2 Vertical Diffusion

Pleim (2007) developed the ACM2 for the Weather Research and Forecasting (WRF) meteorological model and the Community Multiscale Air Quality (CMAQ) model. The ACM2 includes: (1) mixing among adjacent layers using K-theory; (2) rapid upward non-local mixing from the surface layer to all layers through the boundary layer (the convective aspect); and (3) slower compensating downward mixing layer-by-layer from the top of the boundary layer to the surface (the asymmetric aspect). Figure 4-3 shows this approach schematically. During non-convective conditions, ACM2 reverts back to the local K-theory component. Thus, ACM2 includes the basic features of both local and the most important component of non-local exchange.

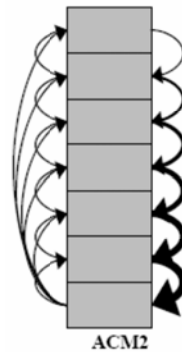


Figure 4-3. Schematic representation of the turbulent exchange among layers within a vertical grid column during convective adjustment in the ACM2 (taken from Pleim [2007]).

The ACM2 parameterization is an alternative option to the default K-theory approach. The convective component of ACM2 is invoked during unstable conditions and is solved separately using a semi-implicit scheme, whereas the K-theory component is always applied and is solved with the implicit scheme described above. All variables needed to calculate the transfer rates are available from the existing input files, or are already calculated within CAMx for other purposes. The CAMx ACM2 option does not require that ACM2 be run within the meteorological model used to derive inputs for CAMx. However, using ACM2 in both meteorological and chemistry models leads to consistent boundary layer characterization. The CAMx implementation of ACM2 supports OMP and MPI parallel processing. Runtime differences between K-theory and ACM2 are indistinguishable.

NOTE: ACM2 does not work with the Integrated Process Rate (IPR) component of the Process Analysis (PA) tool.

4.5 Wet Deposition

Wet deposition is the predominant removal process for fine particles. Particles act as cloud condensation nuclei and resulting cloud droplets grow and accrete into precipitation. Particles can also be directly scavenged by precipitation via impaction. The rates of accretion and impaction depend upon cloud type (e.g., prolonged widespread stratiform vs. brief localized

convection), condensed water phases, precipitation rate, and particle and cloud water size distributions.

Wet deposition can also be an important removal process for soluble gases through the following series of steps:

- Diffusion of gas into cloud droplets and subsequent scavenging by precipitation;
- Diffusion of gas directly into falling precipitation;
- Possible aqueous-phase reactions within cloud and rain water.

The rate at which these processes occur depends on cloud type, condensed water phase, the pollutant's solubility and its overall reaction rate once in solution. Diffusion into cloud and rain water may be reversible. Cloud water droplets can absorb a gas up to the limit of its solubility as defined by Henry's Law (the proportion of aqueous concentration to gas-phase partial pressure at equilibrium). High values for the Henry's Law constant (>10,000 M/atm) indicate a strong tendency to dissolve into water droplets, whereas low values (<100 M/atm) indicate a tendency to remain in the air (Seinfeld and Pandis, 1998). Equilibrium between air and water concentration is usually established on time scales of minutes, so equilibrium conditions can generally be assumed to exist in the atmosphere.

The CAMx wet deposition model employs a scavenging approach in which the local rate of concentration change $\partial c / \partial t$ within or below a precipitating cloud depends on a scavenging coefficient A :

$$\frac{\partial c}{\partial t} = -A c$$

Wet scavenging is calculated for each layer within a precipitating grid column from the top of the precipitation profile to the surface. Scavenging coefficients are determined differently for gases and PM based on relationships described by Seinfeld and Pandis (1998). Gas scavenging includes two rates: (1) accretion of cloud droplets containing dissolved gases into precipitation, and (2) diffusive uptake of ambient gases into precipitation, which can occur within or below cloud. PM scavenging also includes two rates: (1) accretion of cloud droplets containing particles into precipitation, and (2) impaction of ambient particles into precipitation, which occurs only below cloud. We describe these processes in more detail below.

The CAMx wet deposition model applies the following general assumptions:

- 1) Wet deposition is invoked only if precipitation is reaching the surface;
- 2) The cloud and precipitation environment exists in steady state between successive meteorological update times (usually hourly);
- 3) Liquid cloud water exists at temperatures below 273 K – a linear ramp function apportions total cloud water into liquid and ice between 233-273 K, and all cloud water is ice below 233 K;
- 4) The model considers three types of precipitating hydrometeors (rain drops, snowflakes, and graupel particles); each is separately represented by a single mean size, mass, and fall

- speed through the precipitating column and parametrically determined from the equivalent liquid surface precipitation rate;
- 5) Mixed-phased (liquid/ice) hydrometeors do not coexist within a layer – the dividing temperature between rain and the two ice forms is 273 K;
 - 6) Only a single ice hydrometeor form (snow or graupel) exists in a layer – graupel is specified if any graupel is present in that layer, otherwise snow is specified;
 - 7) A mono-disperse distribution of hydrometeors falls through a mono-disperse distribution of sub-cloud particles and cloud water droplets containing particles and dissolved gases;
 - 8) Ice hydrometeors can scavenge only liquid cloud water and cannot take up cloud ice via impaction.
 - 9) All gases dissolved in cloud water are in equilibrium with ambient air concentrations according to Henry's Law solubility, aqueous dissociation, cloud water temperature and acidity;
 - 10) All particles are taken up into cloud water (no particles exist in the interstitial air between cloud droplets) – all particle species within a particular size range (fine or coarse) are internally mixed and hydrophilic;
 - 11) Ambient gases may directly diffuse into rain, while only strong acids may diffuse into ice hydrometeors – rates depend on the hydrometeor's state of saturation as a function of pH (set to a constant value of 5), species diffusivity, and aerodynamic considerations;
 - 12) Gases may be reversibly scavenged by cloud water collection and diffusion – super-saturated gases are released back to the atmosphere according to diffusive rates in (11) above;
 - 13) Particles are irreversibly scavenged by cloud water collection and impaction.

4.5.1 Precipitation Parameters

The mean raindrop diameter d_d (m) and fall speed v_d (m/s) are taken from the empirical estimates of Scott (1978). The drop diameter is related to rainfall rate P (mm/hr), and the fall speed relationship has been modified to better agree with data provided by Seinfeld and Pandis (1998):

$$d_d = 9.0 \times 10^{-4} P^{0.21}$$

$$v_d = 3100 d_d$$

The precipitation water content L_p (g/m³) is related to rainfall rate by

$$L_p = \frac{P \rho_w}{3.6 \times 10^6 v_d}$$

where ρ_w is liquid water density (g/m³). This equation can be simplified to a dependency on just rainfall rate when the above relations for drop velocity and size are substituted. The resulting expression for rainfall rate as a function of precipitation water content is

$$P = \left(\frac{1 \times 10^7 L_p}{\rho_w} \right)^{1.27}$$

Locatelli and Hobbs (1974) developed power law equations relating average diameters, fall speeds, and masses for 15 precipitating ice "habits". We consolidated these relationships into two forms, termed "snow" and "graupel", by fitting new power law curves to the Locatelli and Hobbs data. For snow,

$$v_d = 0.83 d_d^{0.20}$$

$$m_d = 0.035 d_d^{1.8}$$

And for graupel,

$$v_d = 1.1 d_d^{0.61}$$

$$m_d = 0.059 d_d^{2.6}$$

Note that in these equations for ice, d_d is in mm and crystal mass m_d is in mg. By assuming that the number density and mass of snow/graupel crystals are equal to those for rain drops given equal precipitation water contents, we can relate the magnitudes of ice size and fall speed to equivalent liquid precipitation rate.

4.5.2 Aerosol Scavenging

Seinfeld and Pandis (1998) develop an equation that describes the scavenging rate as a mono-disperse distribution of hydrometeors falls through a mono-disperse distribution of aerosols (whether cloud water droplets or particles). After expressing the hydrometeor number density in terms of equivalent rainfall rate P (mm/hr), fall velocity v_d (m/s), and drop diameter d_d (m), the scavenging rate (s^{-1}) is

$$A = 4.2 \times 10^{-7} \frac{E P}{d_d} \quad (1)$$

where E is the collection efficiency. The scavenging rate is directly proportional to rainfall rate and inversely proportional to hydrometeor size. At higher precipitation rates, larger hydrometeors (smaller number density) limit the increase in scavenging, while at lower precipitation rates, smaller hydrometeors limit the reduction in scavenging. We use this scavenging equation for both ambient PM (A) and cloud water droplets (A_c). In the latter case we assign a collection efficiency of 0.9, which is typical for cloud droplets with sizes 10-20 μm and hydrometeors larger than 100 μm (Seinfeld and Pandis, 1998).

Within cloud layers, the model assumes that all PM exists within cloud water. Therefore, the PM scavenging rate is the same as for cloud droplets: $A = A_c$ (Equation 1 with $E=0.9$). Ambient PM scavenging below cloud depends on a collection efficiency that is a complex function of particle size (d_p) and density, hydrometeor size and fall speed, and kinematic viscosity of air and water, as expressed by Reynolds (R_e), Schmidt (S_c), and Stokes (S_t) numbers (Seinfeld and Pandis, 1998):

$$E(d_p) = \frac{4}{R_e S_c} \left(1 + 0.4 R_e^{1/2} S_c^{1/3} + 0.16 R_e^{1/2} S_c^{1/2} \right) + 4\phi \left[\frac{\mu}{\mu_w} + \phi \left(1 + 2 R_e^{1/2} \right) \right] + \left(\frac{S_t - S^*}{S_t - S^* + 2/3} \right)^{3/2}$$

where μ and μ_w are the kinematic viscosity of air ($1.8 \times 10^{-5} \text{ kg m}^{-1} \text{ s}^{-1}$) and water ($10^{-3} \text{ kg m}^{-1} \text{ s}^{-1}$), respectively, and $\phi = d_p/d_d$ is the ratio of particle size to hydrometeor size. The S^* parameter is given by

$$S^* = \frac{1.2 + \ln(1 + R_e)/12}{1 + \ln(1 + R_e)}$$

In the two-mode CF option, fine and coarse PM are treated as mono-disperse sizes according to their respective geometric mean diameters (calculated from lower and upper cut points given in the chemistry parameters file). Fine mode size and density are affected by PM water content according to the ISORROPIA model (see Section 5). Typically the fine-mode mean diameter ranges $\sim 0.3\text{-}0.5 \mu\text{m}$, which is near the minimum scavenging efficiency commonly referred to as the "Greenfield Gap". As a result, the efficiency of fine-mode particle scavenging is underrepresented by about an order of magnitude relative to integration over the entire fine-mode size distribution. Such is not the case for the coarse mode, where efficiency is consistently near 1 over all coarse sizes. Seinfeld and Pandis (1998) show differences in size-integrated PM scavenging rates between mono-disperse particles and particle size distributions with various geometric standard deviations. They show that for mean particle sizes in the sub-micron range ($0.1\text{-}1 \mu\text{m}$), size-integrated mass scavenging rates are roughly equivalent to mono-disperse scavenging rates at 10 times their size. The wet deposition model increases fine-mode geometric mean particle diameters by a factor of 10 to account for mass scavenging over the whole size distribution.

Snow presents a complication related to aerodynamic drag, which affects PM collection efficiency. To simplify the calculation for snow, the model calculates E for graupel but sets a lower limit of 1×10^{-3} based on the work of Sauter and Wang (1989).

4.5.3 Gas Scavenging

Wet scavenging of gases by precipitation occurs within and below precipitating clouds. Scavenging of both aqueous and ambient gases occur within cloud layers but at different rates. Scavenging of ambient gases alone occurs below clouds. Once again, the scavenging rate for gases in cloud water depends on the scavenging rate for cloud droplet (A_c , Equation 1 with $E=0.9$). Given the relatively short residence times of falling precipitation through a given grid cell, aqueous equilibrium between ambient gas and precipitation cannot be assumed. The model explicitly calculates diffusion of ambient gas into rain (or ice hydrometeors in the case of strong acids) following the mass balance methodology of Seinfeld and Pandis (1998). The diffusive gas scavenging rate is:

$$A_g = 1.67 \times 10^{-6} \frac{P K_c}{d_d v_d}$$

where K_c is the mass transfer coefficient (m s^{-1}) as a function of air (v) and gas (D_g) molecular diffusivity, and hydrometeor size and fall speed:

$$K_c = \frac{D_g}{d_d} \left[2 + 0.6 \left(\frac{v_d d_d}{v} \right)^{1/2} \left(\frac{v}{D_g} \right)^{1/3} \right]$$

Scavenging of ambient gas is directly proportional to diffusivity and rainfall rate, and inversely proportional to hydrometeor size and speed. Diffusive scavenging is constrained by a combination of larger hydrometeors (smaller number density) and faster fall speeds (shorter residence time) at higher precipitation rates.

4.5.3.1 Solubility Limits on Gas Scavenging

The scavenging rates Λ_c and Λ_g describe the maximum potential uptake into precipitation with no pre-existing pollutant mass. However, there is a chance for precipitation to become super-saturated with sparingly soluble gases as it falls through a grid column collecting mass. To account for this, aqueous and diffusive gas scavenging are separately calculated according to equilibrium concentrations in cloud (c_{eq}^c) and precipitation (c_{eq}^p) water, respectively, and the amount of pre-existing aqueous gas in precipitation from layers above c_0 . If $c_0 < c_{eq}^p$ (precipitation is unsaturated), a fraction of total grid cell gas concentration is added to the rain water (c_0 is augmented) and removed from the grid cell according to:

$$\Delta c = c_{eq}^c [1 - \exp(-\Lambda_c \Delta t)] + c_{eq}^p [1 - \exp(-\Lambda_g \Delta t)]$$

where c_{eq}^p accounts for the amount of total cell concentration c already taken up in cloud water ($c_{eq}^p = c - c_{eq}^c$), and Δc is limited to $c_{eq}^p - c_0$. Note that Δc , c_{eq} and c_0 are all in units of mass per air volume. If $c_0 > c_{eq}^p$ (precipitation is super-saturated) then only the diffusive term is applied and c_0 is relaxed toward c_{eq}^p by returning gas back to the atmosphere (c_0 is decremented):

$$\Delta c = (c_{eq}^p - c_0) [1 - \exp(-\Lambda_g \Delta t)]$$

The aqueous equilibrium concentration is determined by Henry's Law. The Henry's Law constant for a given gas species k_0 (M/atm) specifies the ratio of pollutant mass in aqueous solution (M or mol/l_{H2O}) to its equilibrium partial pressure (atm) at standard pressure and temperature. This constant is adjusted for temperature T and converted to a dimensionless molar ratio:

$$H = k_0 R T \exp \left[A \left(\frac{1}{298} - \frac{1}{T} \right) \right]$$

where R is the ideal gas constant (8.206×10^{-2} l atm mol⁻¹ K⁻¹), and A is the temperature dependence factor. Dissociation of ammonia, nitric acid, and sulfur dioxide as a function of water pH is also considered in the solubility calculation. The effective Henry's Law constant H

thus expresses the equilibrium ratio of the aqueous concentration c_{aq} (mass per volume of water) to the gas concentration c_g (mass per volume of air),

$$H = \frac{c_{aq}}{c_g}$$

which are related to total cell concentration c by

$$c = c_g + c_{aq} \frac{L_c}{\rho_w} = c_g + c_{eq}$$

where L_c is the cloud or precipitation water content (g m^{-3}), ρ_w is water density ($1 \times 10^6 \text{ g m}^{-3}$) and c_{eq} is equilibrium aqueous concentration as mass per volume of air.

4.6 Dry Deposition

Dry deposition can be an important removal process for many compounds. Due to the difficulty of making direct measurements of dry deposition and the need for a suitable model parameterization, dry deposition is often treated as a first-order removal mechanism, where the flux of a pollutant to the surface is the product of a characteristic deposition velocity and its concentration in the "surface layer" (i.e., the lowest model layer). Deposition velocities are derived from models that account for the reactivity, solubility, and diffusivity of gases, the sizes of particles, local meteorological conditions, and season-dependent surface characteristics. The factors affecting deposition are discussed in more detail below.

For a given species, particle size, and grid cell, CAMx determines a deposition velocity for each landuse type present in that cell and then linearly combines them according to the fractional distribution of landuse. The deposition flux is used as the lower boundary condition in the vertical diffusion algorithm. Aerosol size spectra and species-dependent properties needed for the deposition velocity calculations are externally supplied to CAMx for all pollutant species via the chemistry parameters file; gridded landuse is supplied to the master grid and optionally any nested fine grids; the season is determined by the simulation date and location on the globe.

Movement of material along a path from the atmosphere, through any plant canopy, and onto the various plant and ground surfaces within and below the canopy is typically modeled by analogy to an electrical circuit. Resistances in serial and parallel arrangements are used to represent the relative ease with which material moves through different portions of the deposition pathway. Each branch of the circuit represents a different path by which material may be deposited. For example, gaseous pollutants may transfer through the lowest layers of the atmosphere partially into a plant canopy, through the stomatal openings on plant leaves and into the plant mesophyll tissue. Alternatively, the material may travel all the way through the plant canopy and deposit on the ground surface.

CAMx offers two dry deposition options: the original approach based on the work of Wesely (1989) and Slinn and Slinn (1980); and an updated approach based on the work of Zhang et al. (2001; 2003). Both of these options are briefly described below.

4.6.1 The Wesely/Slinn Model

4.6.1.1 Dry Deposition of Gases

Wesely (1989) developed a resistance model that incorporates the major elements described above. Deposition velocity v_d is calculated from three primary resistances r (s/m) in series:

$$V_d = \frac{1}{r_a + r_b + r_s}$$

The aerodynamic resistance r_a represents bulk transport through the lowest model layer by turbulent diffusion, and operates equivalently for all gases and small particles. The magnitude of this resistance depends on the intensity of turbulent motion, which in turn depends on solar insolation, wind speed, surface roughness, and near-surface temperature lapse rate. In CAMx it is calculated from

$$r_a = \frac{1}{k u_*} \left[\ln \left(\frac{1}{z_o} \right) - \phi_h \right]$$

where u_* is friction velocity (m/s), k is von Karman's constant, z is the lowest model layer midpoint height (m), z_o is the surface roughness length (m), and ϕ_h is a stability correction term. The surface layer parameterization of Louis (1979) is used to supply friction velocity and stability correction as a function of input surface meteorology and roughness length. Roughness length is internally assigned according to season and the input gridded distribution of 11 landuse types as described in Section 3. In general, aerodynamic resistance is at a minimum on warm, sunny days with strong mixing due to surface heating and mechanical turbulence, and at a maximum on cool, calm nights when turbulent mixing is suppressed.

The quasi-laminar sublayer (or boundary) resistance r_b represents molecular diffusion through the thin layer of air directly in contact with the particular surface to which material is being deposited. It is usually assumed to depend only on the molecular diffusivity of each pollutant species, and is given by

$$r_b = \frac{2 S_c^{2/3}}{k u_*}$$

where S_c is the Schmidt number, or the ratio of air viscosity to species molecular diffusivity.

Over land, surface resistance r_s is expressed as several more serial and parallel resistances that depend upon the physical and chemical properties of the surface in question:

$$r_s = \frac{1}{\frac{1}{r_{st} + r_m} + \frac{1}{r_{uc}} + \frac{1}{r_{dc} + r_{cl}} + \frac{1}{r_{ac} + r_{gs}}}$$

where the first set of parallel resistances represents the pathway into the stomatal (r_{st}) and mesophyll (r_m) portions of active plants, the second is the pathway into the upper canopy (r_{uc}),

the third is the pathway into the lower canopy (r_{dc} and r_{cl}), and the fourth is the pathway to the ground surface (r_{ac} and r_{gs}). Many of these resistances are season- and landuse-dependent, and are built into Wesely's model; some in turn are adjusted within CAMx for solar insolation and surface wetness (vegetation is assumed to be unstressed). A few other resistances have been developed by Wesely for SO₂ and ozone, and so are scaled for each gaseous species based on the following pollutant properties:

- Molecular diffusivity (determined from molecular weight, $\sqrt{M_g / M_{H_2O}}$);
- Henry's law solubility (H);
- Chemical reactivity toward oxidation of biological substances (f).

This allows the resistance approach to be used to estimate deposition velocities for a wide range of gaseous pollutants.

The surface resistances for strong acids (e.g., nitric, sulfuric, and hydrochloric acid, peroxides) are set to zero given their strong rates of uptake by biota and other surfaces (Huebert and Robert, 1985; Wesely and Hicks, 2000). The species for which surface resistance is set to zero are defined in the CAMx chemistry parameters file.

Over water, the surface resistance for all gas species other than ozone is based on some improvements adopted by Kumar et al. (1996) following Sehmel (1980):

$$r_s = \frac{1}{3.9 \times 10^{-5} H T_s u_*}$$

where T_s is surface temperature (K). For ozone, this equation has been updated to parametrically match the tendencies of measured ozone fluxes reported by Helmig et al. (2012) from ship-borne measurements:

$$r_s^{O_3} = \frac{1}{1 \times 10^{-4} + 5 \times 10^{-6} H T_s^3 u_*}$$

where T_s is in °C rather than K. The cubic temperature dependence fits the deposition velocity response to the range of sea surface temperatures reported in the Helmig et al. data. The additional 1×10^{-4} term sets an upper limit on r_s and a lower limit on deposition velocity so that the latter does not fall much below 0.01 cm/s. A lower limit of 1500 s/m is placed on r_s such that ozone deposition over water does not exceed 6.5 cm/s, which is the upper limit in the measured data.

4.6.1.2 Dry Deposition of Aerosols

Surface deposition of particles occurs via diffusion, impaction, and/or gravitational settling. Particle size is the dominant variable controlling these processes. The resistance approach of Slinn and Slinn (1980), as implemented by Kumar et al. (1996), has been adopted in CAMx. Particle deposition velocity for a given aerosol size is calculated using the following resistance equation:

$$v_d = v_{sed} + \frac{1}{r_a + r_b + r_a r_b v_{sed}}$$

where v_{sed} is the gravitational settling (or sedimentation) velocity. This velocity is dependent on aerosol size and density:

$$v_{sed} = \frac{D^2 g C \rho_p}{18 \nu}$$

where D is the geometric-mean particle diameter (m) of a given size section, ρ_p is particle density (g/m^3), g is gravitational acceleration, and ν is the viscosity of air. The factor C is the Cunningham correction for small particles (Seinfeld and Pandis, 1998). Note that particle size and density are affected by aerosol water content, which is determined from local humidity and PM deliquescence properties according to the ISORROPIA model (see Section 5).

Aerodynamic resistance r_a is identical to the value used for gaseous dry deposition. Resistance to diffusion through the quasi-laminar sub-layer layer depends on aerosol Brownian diffusion and inertial impaction. Particles are assumed to remain on a surface once they impact, so resuspension effects are ignored. Boundary resistance r_b is given by

$$r_b = \frac{1}{u_* (S_c^{-2/3} + 10^{-3/S_t})}$$

The stokes number S_t is calculated from

$$S_t = \frac{v_{sed} u_*^2}{\nu g}$$

4.6.1.3 Specification of Season

The Wesely (1989) deposition algorithm specifies the various surface resistances by land cover type for five seasons: Spring, Summer, Fall, Winter, and Winter with snow cover. CAMx internally defines a season map to determine four of these five seasons by month and latitude (Table 4-2). Five latitude bands exist in each hemisphere:

- Tropical < 20°
- Sub-tropical 20° to 35°
- Temperate 35° to 50°
- Cool 50° to 75°
- Polar >75°

The seasons in the Northern and Southern hemispheres are offset by six months. This offset does not cause any discontinuity at the equator because all 12 months are defined as summer in the tropical band at the equator. This season map is generalized and may not be ideal for all locations. The season map is coded into data statements in the "CAMx/chmdat.f" subroutine and could be changed to better suit a specific region.

The season map shown in Table 4-2 does not consider snow cover because it is quite variable in space and time. Gridded snow cover data are specified in the time-variant 2D surface input file (see Section 3 and Section 4.7 below). Snow covered grid cells are assigned the Wesely (1989) surface resistances for the category “winter with snow cover”, regardless of the season.

Table 4-2. Relationships between season and month/latitude used in the CAMx Wesely/Slinn dry deposition model. Exception: seasons for the area within 50N-75N and 15W-15E are internally set to those of latitude band 35-50 to account for regions of Europe in which the climate is influenced by the Gulf Stream.

Month		Latitude Band				
Northern Hemisphere	Southern Hemisphere	< 20°	20° - 35°	35° - 50°	50° - 75°	> 75°
		Tropical	Sub-tropical	Temperate	Cool	Polar
Jan	Jul	Summer	Winter	Winter	Winter	Winter
Feb	Aug	Summer	Spring	Winter	Winter	Winter
Mar	Sep	Summer	Spring	Spring	Winter	Winter
Apr	Oct	Summer	Spring	Spring	Spring	Winter
May	Nov	Summer	Summer	Spring	Spring	Winter
Jun	Dec	Summer	Summer	Summer	Summer	Spring
Jul	Jan	Summer	Summer	Summer	Summer	Summer
Aug	Feb	Summer	Summer	Summer	Summer	Fall
Sep	Mar	Summer	Summer	Fall	Fall	Winter
Oct	Apr	Summer	Fall	Fall	Fall	Winter
Nov	May	Summer	Fall	Fall	Winter	Winter
Dec	Jun	Summer	Fall	Winter	Winter	Winter

4.6.2 The Zhang Model

Environment Canada's AURAMS air quality model uses a state-of-the-science deposition scheme that possesses an updated representation of non-stomatal deposition pathways (Zhang et al. 2003; Zhang et al. 2008). The approach incorporates the “leaf area index” (LAI), which is an important aspect of newer dry deposition schemes that allows for scaling of pollutant uptake into biota of varying densities. LAI is defined as the ratio of the one-sided green leaf area to a unit area of the ground. It is measured by satellite instruments at fairly high spatial resolution. The Zhang model has been tested extensively through its use in daily air quality forecasting in Canada, and has been shown to reproduce observed fluxes of ozone and SO₂ with reasonable accuracy. In CAMx, the Zhang model has tended to generate lower ozone deposition rates relative to the Wesely model, which leads to higher ozone predictions overall. This effect is seasonally dependent and will vary with the definition of LAI. Ozone is less sensitive to the source of LAI (whether Zhang defaults or satellite-enhanced) than to the choice of deposition model.

4.6.2.1 Dry Deposition of Gases

The gas resistance model of Zhang et al. (2003) invokes the same 3-resistance equation for deposition velocity as the Wesely (1989) model. The equations for aerodynamic resistance (r_a) and boundary resistance (r_b) are very similar to the Wesely (1989) formulations. However,

Zhang et al. (2003) replace the surface resistance (r_s) equation with a new relationship for the overall canopy resistance:

$$r_c = \frac{1}{\frac{1 - W_{st}}{r_{st} + r_m} + \frac{1}{r_{cut}} + \frac{1}{r_{ac} + r_{gs}}}$$

where W_{st} is the fraction of stomatal blocking under wet conditions, r_{cut} is the cuticle resistance, and all other resistances have similar meaning to the Wesely model. Stomatal resistance (r_{st}) is calculated using a sunlit/shade (so-called "two-big-leaf") stomatal resistance sub-model. Following Wesely (1989), values for r_g and r_{cut} are calculated for SO_2 and O_3 and then scaled for other gaseous species. Cuticle resistance is slightly different from that defined in traditional big-leaf models in that it also considers the aerodynamic and quasi-laminar resistances of individual leaves. This is done by parameterizing r_{cut} as a function of friction velocity, similar to the concept of overall cuticle uptake considered in a multi-layer model framework.

LAI is used in functions for r_{ac} and r_{cut} , where the LAI for any given day is linearly interpolated from monthly default LAI as a function of landuse type. To account for LAI effects on surface roughness (z_0), a similar daily LAI interpolation is applied to that parameter. Hence, the Zhang model does not require the specification of season, as all resistance equations are continuous over each month (note that CAMx automatically applies the 6-month offset for applications in the southern hemisphere).

For snow on the ground and leaves, both r_{gs} and r_{cut} are adjusted by a snow cover fraction, which is calculated from snow depth, snow age, and landuse type as described in Section 4.7. Snow cover is defined through the input 2D surface file, as described in Section 3. For surfaces without canopies, r_{gs} is defined as the resistance to any surface (e.g. soil, ice, snow and water), r_{ac} is set to zero, and very large values are used for r_{st} , r_m and r_{cut} .

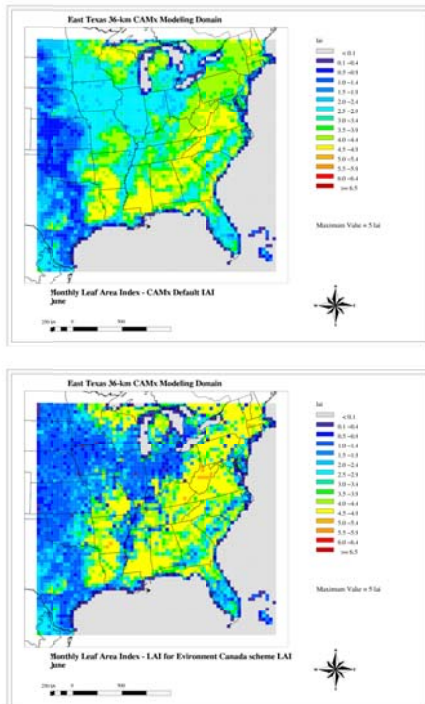
Over water, the updated temperature-dependent ozone surface resistance equation described above for the Wesely scheme is also used for the Zhang scheme.

The Zhang model includes a set of embedded annual surface roughness ranges and monthly LAI specific to each of the 26 landuse categories. The capabilities of the scheme were extended by adding the option to use episode-specific (i.e., satellite-derived) LAI data. Satellite-based LAI data from MODIS (MODerate-resolution Imaging Spectroradiometer)² can be processed into gridded LAI fields that are passed to CAMx as an optional record in the time-invariant 2D surface input file (see Section 3). The optional gridded LAI fields are used to scale the default landuse-specific LAI values. For each grid cell, a landuse-weighted default LAI is determined according to the landuse fractions present. An LAI scaling factor is then determined as the ratio of the input LAI to the landuse-weighted default LAI. This factor is used to scale the individual default LAI values for each landuse type in the grid cell, subject to the annual maximum to

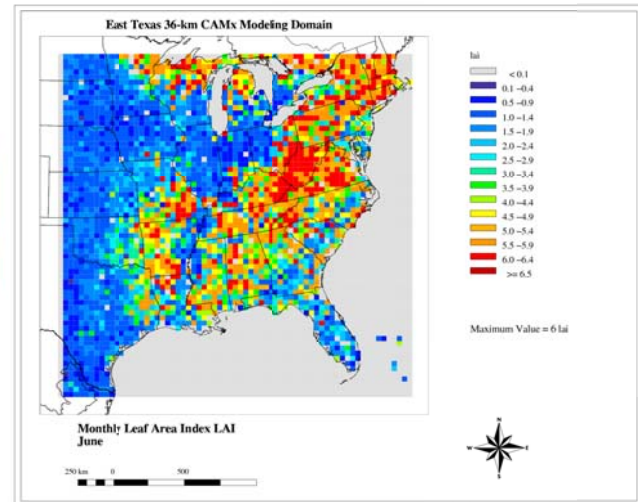
² MODIS provides LAI at 250 meter spatial resolution and 16 day temporal resolution.

minimum range among the monthly default values. Figure 4-4 illustrates how the use of satellite LAI data introduces additional episode-specific variation into the LAI field.

Zhang Embedded LAI Data



LAI from Satellite



Modified LAI using Satellite Data

Figure 4-4. Comparison of monthly LAI data embedded in the Zhang dry deposition scheme against episode-specific LAI for June 2005.

4.6.2.2 Dry Deposition of Aerosols

Theoretically, particles in the size range $0.1\text{--}1.0\ \mu\text{m}$ deposit at rates much less than $0.01\ \text{cm/s}$, but such values are comparable only to laboratory (wind tunnel) studies. According to Zhang et al. (2001), much higher values have been obtained in many field studies, including for sub-micron sulfate in which deposition velocities of one to two orders of magnitude higher have been measured. For example, Gallagher et al. (1997) state that much higher deposition velocity values, typically $1\ \text{cm/s}$ or more for sub-micron aerosol deposition to a forest, are consistent across the aerosol size spectrum. The Zhang et al. (2001) study developed a simple parameterization of particle dry deposition as a function of aerosol size and landuse that predicts higher deposition velocities for sub-micron aerosols, especially over rough vegetated surfaces.

The deposition of aerosols is based on the model of Slinn (1982), but using simplified empirical parameterizations to replace detailed canopy information. The aerosol deposition velocity is defined as:

$$v_d = v_{sed} + \frac{1}{r_a + r_b}$$

where v_{sed} and r_a have identical meanings as the Slinn and Slinn (1980) definition described earlier for the Wesely/Slinn deposition model. Note that in this case, the virtual serial resistance $r_a \cdot r_b \cdot v_{sed}$ has been removed, which results in higher values of deposition velocity. The quasi-laminar boundary resistance is given by

$$r_b = \frac{1}{\varepsilon_0 u_* (E_B + E_{IM} + E_{IN}) R_1}$$

where the variable E includes the collection efficiencies for Brownian diffusion, impaction, and interception, respectively, R_1 is a factor representing the fraction of particles that stick to the surface, and ε_0 is an empirical constant that is set to a value of 3. The Brownian collection efficiency depends on the Schmidt number, while the impaction efficiency and R_1 depend on the Stokes number.

The collection efficiency by interception also exists if the particle passes an obstacle at a distance shorter than its physical dimensions (e.g., large particles passing near hairy leaves). Zhang et al. (2001) adopted a simple equation for this term that is a function of particle diameter and a characteristic radius, for which default values are given for different landuse and seasonal categories.

Figure 4-5 compares estimated particle deposition velocities from the Zhang model, the Slinn and Slinn (1980) model, and the AERMOD model (EPA, 1998). Calculations were made for daytime, neutrally stable conditions for a range of wind speeds and landuse categories. Figure 4-5 shows that the Zhang model increases deposition velocities over forest by roughly an order of magnitude for the 0.1-1 μm range, yet reduces deposition velocities above 1 μm .

4.7 Snow Cover and Surface Albedo

Surface albedo for snow-covered grid cells is calculated according to snow depth, snow age, and land cover type. The approach is based on literature describing the evolution of snow albedo in the WRF/NOAH land surface model (Ek et al., 2003; Wang and Zeng, 2010; Livneh et al., 2010; and Barlage et al., 2010).

Fractional snow cover (f_s) accounts for the effects of surface roughness elements (shrubs, trees, rocks and other structures) extending above thin/patchy snow:

$$f_s = 1 - \exp\left(-\alpha \frac{W}{W_c}\right) + \frac{W}{W_c} \exp(-\alpha)$$

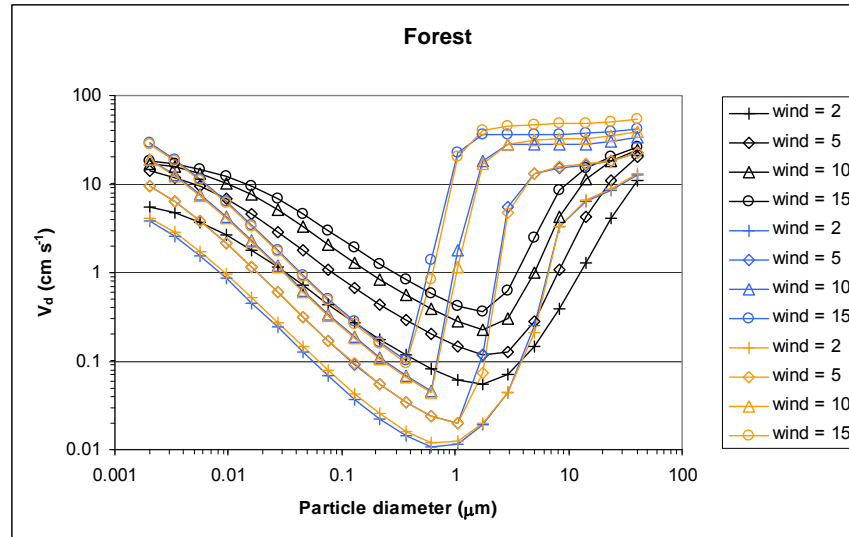


Figure 4-5. Comparison of particle dry deposition velocities as a function of size and wind speeds (m/s) for three models: black – Zhang et al. (2001); blue – Slinn and Slinn (1980); orange – AERMOD (EPA, 1998). Results are shown for a forest landuse category during daytime neutral stability. Particle density was set at 1.5 g/cm^3 .

where $\alpha = 2.6$, W is snow water equivalent depth (SWE), and W_c is the threshold SWE above which $f_s = 100\%$. Following Wang and Zeng (2010) and Linveh et al. (2010), W_c is set to 0.01 m for barren or low vegetation (grasslands and agriculture) and to 0.2 m for tall vegetation (forests), except an intermediate value of 0.02 m is assigned to shrub lands where vegetation is typically higher than grasses, and a value of 0.05 m is assigned to urban (Table 4-4).

Throughout CAMx we apply a common approximation that actual snow depth is $10 \times \text{SWE}$.

Snow albedo (a_s) is allowed to evolve to account for the optical effects of melting and accumulation of dirt/soot, following the approach of Linveh et al. (2010):

$$a_s = a_{max} A^{t^B}$$

where a_{max} is the maximum fresh snow albedo (0.85; Barlage et al., 2010), t is the number of days since the last snowfall, $A = 0.94$ (0.82) and $B = 0.58$ (0.46) during the accumulation (ablation) phase. Accumulation occurs during cold periods when surface temperature is below 273 K, whereas ablation occurs during melting periods when surface temperature is at 273K. Snow albedo is constrained to a lower bound of 0.4. Snow age is refreshed to zero (and snow albedo to 0.85) when SWE accumulates by more than 0.001 m/hr (accumulating snow depth > 1 cm/hr).

The resultant grid-cell average surface albedo (a) is a linear combination of snow albedo (a_s) and terrestrial (non-snow) albedo (a_t):

$$a = f_s a_s + (1 - f_s) a_t$$

where a_t is defined according to landuse type (Tables 3-4, 3-5). In case a distribution of multiple landuse types exists within a given grid cell, a linear weighting scheme is employed to account for variable snow cover fractions for each individual landuse type:

$$a = \sum_n f_n \times \{f_s(n)a_s(n) + [1 - f_s(n)]a_t(n)\}$$

where the sum is over all landuse types, f_n is the fractional coverage of landuse n , $a_t(n)$ is the default terrestrial albedo for landuse n , $f_s(n)$ is the fractional snow cover for landuse n , and $a_s(n)$ is the calculated snow albedo for landuse n . Figure 4-6 shows an example of grid-cell albedo evolution for a hypothetical 20-day springtime snow event (assuming ablation conditions) for low and tall vegetation grid cells with a terrestrial (non-snow) albedo of 0.05. Several snow accumulation events are specified to occur over the first 12 days, followed by rapid melting to zero depth by day 20. While total albedo increases to peak values of 0.85 quite rapidly for low-vegetation, the value for tall vegetation lags and peaks just above 0.5 at maximum snow depth. Both cases indicate effects from snow depth (fractional snow cover) and snow age.

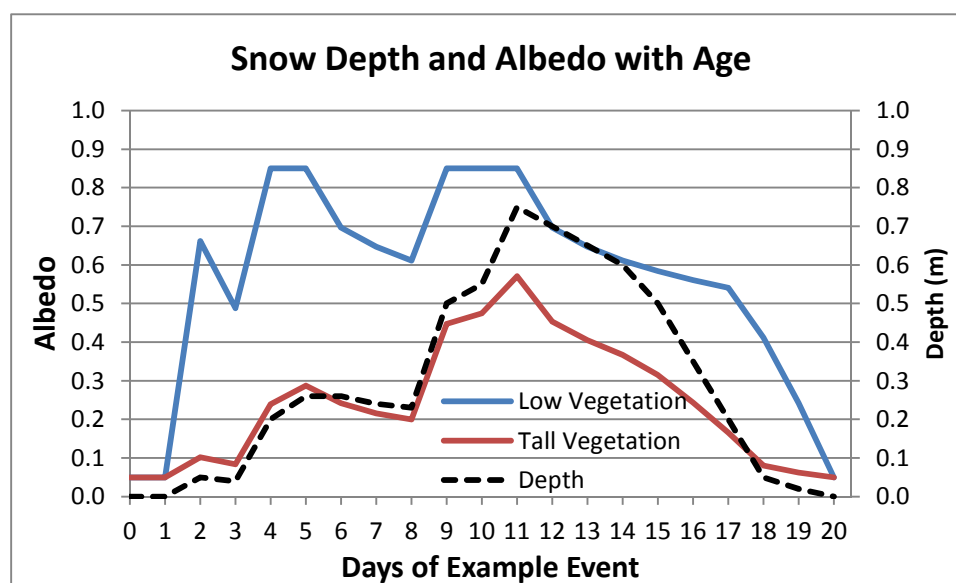


Figure 4-6. Example of grid-cell albedo evolution for a hypothetical 20-day springtime snow event (assuming ablation conditions) for low and tall vegetation grid cells with a terrestrial (non-snow) albedo of 0.05.

4.8 Surface Model for Chemistry and Re-Emission

The CAMx surface model is an optional capability that treats: (1) chemical degradation and/or transformation of deposited pollutant mass on soil, vegetation and an overlying snowpack; (2) volatilization of chemical products back into the air (re-emission); and (3) loss from leaching into soil, penetration into plant tissue, and uptake into snow melt water. The surface model

treats any subset of species listed in the core model's chemical mechanism. Limitations of the current implementation include:

- The surface model cannot be used with the Plume-in-Grid treatment;
- Deposition to water surfaces is assumed to be irreversible and thus is not tracked by the surface model;
- Wet deposition does not contribute to surface mass, as compounds in aqueous solution are assumed to be immediately lost to surface water processes (absorption, runoff, etc.).

4.8.1 Surface Model Algorithms

Figure 4-7 displays the surface model processes schematically and Table 4-3 defines parameters that are referred to in Figure 4-7. While core model algorithms are used to deposit compounds to the surface and re-emit them to the atmosphere, the surface model tracks the accumulation of mass on terrestrial surface media (soil, vegetation and snow), subsequent chemical transformation (both heterogeneous and photolysis), re-emission to the atmosphere, and physical removal.

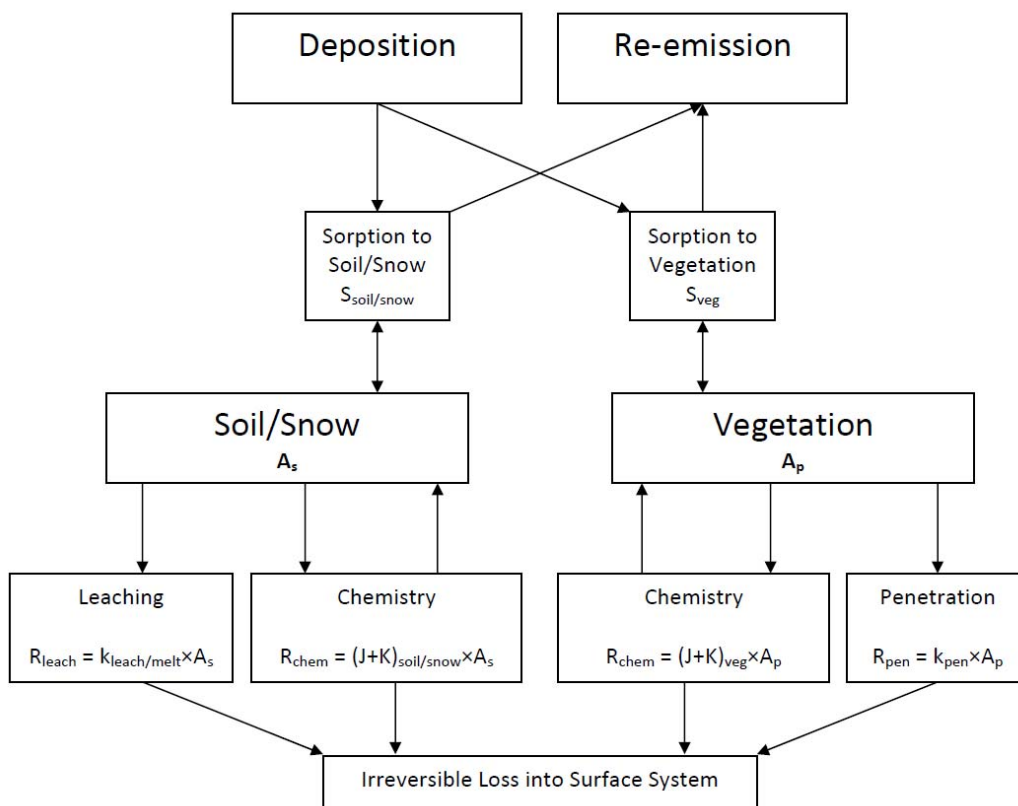


Figure 4-7. Schematic of the CAMx surface model.

Table 4-3. Description of CAMx surface model variables shown in Figure 4-7.

Variable	Definition	Units
A_s	Areic mass of compound on soil or snow	mol ha ⁻¹
A_p	Areic mass of compound on vegetation	mol ha ⁻¹
S_{soil}	Soil-air partitioning coefficient	unitless
S_{snow}	Snow-air partitioning coefficient	unitless
S_{veg}	Vegetation-air partitioning coefficient	unitless
k_{leach}	Soil leaching rate coefficient	min ⁻¹
K_{melt}	Snow melt loss rate coefficient	min ⁻¹
k_{pen}	Leaf penetration rate coefficient	min ⁻¹
J	Photolysis chemistry rate coefficient	min ⁻¹
K	Heterogeneous chemistry rate coefficient	min ⁻¹
R_{leach}	Leaching or snow melt loss rate	mol ha ⁻¹ min ⁻¹
R_{pen}	Leaf penetration rate	mol ha ⁻¹ min ⁻¹
R_{chem}	Chemistry rate	mol ha ⁻¹ min ⁻¹

After deposition to a snow-free surface grid cell is calculated each time step, the newly deposited mass increments are divided among soil and vegetation compartments and added to total surface mass in each compartment accumulated during the run. The net soil/vegetation split for a given grid cell is determined by the combination of the fractional coverage of each landuse type in that cell and landuse-specific split factors. The fractional coverage of 11 (Wesely) or 26 (Zhang) landuse categories in each grid cell is an external input to CAMx (Section 3). The soil/vegetation splits assigned to each landuse category are internally defined within CAMx and assumed to be seasonally constant. Values for soil/vegetation splits are estimated based on simple conceptual considerations of the amount of annual-averaged vegetation (i.e., leaf area index) typical of each category (Table 4-4).

Snow is activated in the surface model when snow depth is sufficiently deep to cover exposed soil. The lower limit on snow depth is 10 cm to be consistent with the approach described in Section 4.7 in which a 10 cm depth completely covers low-vegetation landuse. In such cases, the soil/vegetation split is replaced by the snow cover fraction such that the soil fraction is entirely snow-covered and the vegetation fraction is progressively covered with deeper snow depth. The soil compartment transitions to a snow compartment; sorption coefficients and rates for chemistry and loss convert to the values set for snow (as described below). With very deep snow exceeding 200 cm, high vegetation is completely covered and the surface model reduces to a single compartment for snow.

The surface model uses partitioning (equilibrium) coefficients to calculate the amount of accumulated material sorbed to soil/snow and vegetation. The sorbed fraction is subject to chemical reactions and physical removal associated with soil leaching, plant penetration, and

Table 4-4(a). Wesely landuse categories and associated annual-averaged soil/vegetation split factors, UV albedo, and SWE W_c .

Category Number	Land Cover Category	Surface Parameters		
		Soil Fraction	UV Albedo	Snow W_c (m SWE)
1	Urban	0.7	0.08	0.05
2	Agricultural	0.2	0.05	0.01
3	Rangeland	0.5	0.05	0.01
4	Deciduous forest	0.1	0.05	0.2
5	Coniferous forest, wetland	0.1	0.05	0.2
6	Mixed forest	0.1	0.05	0.2
7	Water	n/a	0.04	n/a
8	Barren land	1.0	0.08	0.01
9	Non-forested wetlands	0.2	0.05	0.01
10	Mixed agricultural/range	0.3	0.05	0.01
11	Rocky (with low shrubs)	0.5	0.05	0.01

Table 4-4(b). Zhang landuse categories and associated annual-averaged soil/vegetation split factors, UV albedo, and SWE W_c .

Category Number	Land Cover Category	Surface Parameters		
		Soil Fraction	UV Albedo	Snow W_c (m SWE)
1	Water (Ocean)	n/a	0.04	n/a
2	Ice	n/a	0.5	0.01
3	Inland lake (Fresh)	n/a	0.04	n/a
4	Evergreen needleleaf trees	0.1	0.05	0.2
5	Evergreen broadleaf trees	0.1	0.05	0.2
6	Deciduous needleleaf trees	0.1	0.05	0.2
7	Deciduous broadleaf trees	0.1	0.05	0.2
8	Tropical broadleaf trees	0.1	0.05	0.2
9	Drought deciduous trees	0.1	0.05	0.2
10	Evergreen broadleaf shrubs	0.5	0.05	0.02
11	Deciduous shrubs	0.5	0.05	0.02
12	Thorn shrubs	0.5	0.05	0.02
13	Short grass and forbs	0.5	0.05	0.01
14	Long grass	0.3	0.05	0.02
15	Crops	0.2	0.05	0.01
16	Rice	0.2	0.05	0.01

17	Sugar	0.2	0.05	0.01
18	Maize	0.2	0.05	0.01
19	Cotton	0.2	0.05	0.01
20	Irrigated crops	0.2	0.05	0.01
21	Urban	0.7	0.08	0.05
22	Tundra	0.2	0.05	0.01
23	Swamp	0.2	0.05	0.01
24	Desert	1.0	0.08	0.01
25	Mixed wood forest	0.1	0.05	0.2
26	Transitional forest	0.1	0.05	0.2

snow melt. The un-sorbed fraction is available for re-emission. Separate chemical-specific soil-air, vegetation-air, and snow-air partitioning coefficients are set in the CAMx chemistry parameters file. They represent the equilibrium ratio of chemical on a surface to chemical in air at the air-surface interface. For example, a compound with a partitioning coefficient of 10,000 (unitless) has an equilibrium concentration on the surface that is 10,000 times more than that in air.

Chemistry can simply decay deposited material as a removal process, or it can generate products that can subsequently re-emit depending on the products' partitioning coefficient. All surface removal processes are assumed to be irreversible and result in a permanent removal of mass. Chemistry, soil leaching, plant penetration, and snow melt loss are dependent on chemical properties of the compounds and also on numerous site-specific factors such as soil, vegetation, and snow properties, highly transient meteorological conditions, etc. Often these factors are unknown or fall within a range. The rates of these processes are defined as the process rate coefficient (k) times the mass on the surface area, or areic mass (A):

$$R_{process} = k_{process} \times A_{surface}$$

When the actual rate coefficients (or inversely, the half-lives, $t_{1/2}$) are unknown for the substance, they can be generalized by 5 classes:

- | | | | | |
|----|------------|----------------------------|---------------------------|---|
| 1. | Very fast: | $t_{1/2} = 0.04 \text{ d}$ | $k = 17 \text{ d}^{-1}$ | $= 1.2 \times 10^{-2} \text{ min}^{-1}$ |
| 2. | Fast: | $t_{1/2} = 0.21 \text{ d}$ | $k = 3.3 \text{ d}^{-1}$ | $= 2.3 \times 10^{-3} \text{ min}^{-1}$ |
| 3. | Moderate: | $t_{1/2} = 1.0 \text{ d}$ | $k = 0.69 \text{ d}^{-1}$ | $= 4.8 \times 10^{-4} \text{ min}^{-1}$ |
| 4. | Slow: | $t_{1/2} = 5.0 \text{ d}$ | $k = 0.14 \text{ d}^{-1}$ | $= 9.7 \times 10^{-5} \text{ min}^{-1}$ |
| 5. | Very slow: | $t_{1/2} = 25 \text{ d}$ | $k = 0.03 \text{ d}^{-1}$ | $= 2.1 \times 10^{-5} \text{ min}^{-1}$ |

A 6th class can be added by setting the k -value to zero or a de minimis value to effectively remove the process from consideration. In this manner chemicals can be modeled with an estimated half-life that is unique for each process.

Note that all partitioning coefficients and rates other than photolysis are fixed and ignore dependence on various environmental conditions (e.g., temperature, pressure, surface type, surface moisture, etc.). Photolysis rates are specified by the user to represent peak direct-exposure clear-sky values at zero zenith (solar noon) and are internally adjusted for solar angle, cloud attenuation (as calculated for atmospheric photolysis), and shade effects using multiplicative factors. A multiplicative “shade factor” is defined to reduce photolysis rates within/below vegetation. Snow cover reduces shading effects to account for enhanced reflection and internal UV scattering within the snowpack.

Losses by soil leaching, plant penetration, and snow melt are arbitrarily accelerated during rain events, such that a 1 mm/hr rainfall rate results in an e-folding loss of surface mass in 1 hour. Mass loss within the snowpack by melting alone occurs only when surface temperature is at 273 K. Snowpack loss also occurs during snowfall such that a 1 cm/hr accumulation results in an e-folding loss of surface mass in 24 hours by successively burying pollutant mass and limiting its ability to diffuse through the snowpack. The model assumes that no surface mass is re-introduced as snow depth/fraction decrease during sublimation or melting (i.e., irreversible loss of surface mass as implemented for soil and vegetation).

The approach for re-emission of volatilized (un-sorbed) mass is consistent with the CAMx dry deposition algorithm. Since water surfaces are not considered by the surface model, re-emission fluxes from water are ignored in this implementation. Dry deposition of material from the lowest model layer to the surface is treated as an irreversible (fully sorbed) first-order flux through the use of a dry deposition velocity. Re-emission of volatilized (un-sorbed) mass is also treated as a first-order 1-way flux using an “effective” velocity that is similar in form to deposition:

$$v_e = \frac{1}{r_a + r_b}$$

where r_a is the aerodynamic resistance to turbulent transfer through the lowest model layer, and r_b is the resistance to molecular diffusion through the laminar sub-layer in contact with surface elements. The deposition surface resistance term r_s is missing since only the pre-determined un-sorbed fraction of surface mass is considered for surface-to-air transfer. The r_a and r_b terms are calculated by the surface model in exactly the same manner as the values used for dry deposition to ensure consistency.

4.8.2 Running CAMx With the Surface Model

The CAMx surface model parameters that need to be specified for each compound or surface reaction to be tracked are as follows:

S_{soil}	Soil-air partitioning coefficient	unitless
S_{veg}	Vegetation-air partitioning coefficient	unitless
S_{snow}	Snow-air partitioning coefficient	unitless
k_{leach}	Soil leaching rate coefficient	min^{-1}
k_{pen}	Leaf penetration rate coefficient	min^{-1}
k_{melt}	Snow melt loss rate coefficient	min^{-1}
J_{soil}	Soil photolysis rate coefficient	min^{-1}
K_{soil}	Soil heterogeneous chemistry rate coefficient	min^{-1}
J_{veg}	Vegetation photolysis rate coefficient	min^{-1}
K_{veg}	Vegetation heterogeneous chemistry rate coefficient	min^{-1}
J_{snow}	Snow photolysis rate coefficient	min^{-1}
K_{snow}	Snow heterogeneous chemistry rate coefficient	min^{-1}

These values are set at the end of the CAMx chemistry parameters file; an example of the chemistry parameters file format is shown in Figure 4-8. A control record is also needed at the top of the chemistry parameters file to define the number of species and reactions to track.

A CAMx namelist control file variable called "SURFACE_MODEL" must be set to "true" in order to invoke the surface model. When the surface model is invoked, the surface model section of the chemistry parameters file is read and the respective equilibrium and rate variables are set accordingly.

```

CAMx Version      |VERSION6.4
Mechanism ID      |2
Aerosol Option    |NONE
Description       |CB6r2 (r98/30/13 version) + ECH4
No of gas species |75
No of aero species|0
No of reactions   |216
Prim photo rxns  |23 1 8 9 21 27 28 38 43 47 50 56 88 92 97 98 108 112 114 117
                  |119 128 129 161
No of sec photo rxn|6
ID, prim ID, scale|64 56 1.0
                  |90 88 1.0
                  |163 1 0.07
                  |196 1 0.015
                  |197 1 0.08
                  |201 1 0.08
SrfMod #spc, #rxns|3 2
.
.
.
Surface Model
Species           SoilSorb SoilLeach VegSorb VegPen SnoSorb SnoMlt
1 HNO3            1.00E+10 1.00E-10 1.00E+10 1.00E-10 1.00E+10 9.70E-05
2 PNA             1.00E+10 1.00E-10 1.00E+10 1.00E-10 1.00E+10 9.70E-05
3 HONO            1.00E+00 1.00E-10 1.00E+00 1.00E-10 1.00E+00 9.70E-05
Rxn Precursor Product Soil K Soil J Veg K Veg J Snow K Snow J
1 HNO3 HONO 0.00E+00 0.00E+00 0.00E+00 0.00E+00 0.00E+00 1.00E-03
2 PNA HONO 0.00E+00 0.00E+00 0.00E+00 0.00E+00 1.00E-01 0.00E+00

```

Figure 4-8. The portions of the CAMx chemistry parameters file (highlighted) to support the surface model. In this example, 3 gases are treated, where nitric acid (HNO₃) and peroxyntic acid (PNA) react to form nitrous acid (HONO). All three are subject to decay by soil leaching, plant penetration, and snow melt loss. The values shown here are for illustrative purposes only and do not represent any known surface chemistry mechanism.

5. CHEMISTRY MECHANISMS

The photochemical mechanisms currently supported in CAMx are listed in Table 5-1. All are balanced for nitrogen conservation so that predicted NO_y can be calculated as the sum of nitrogen containing species. Mechanisms 2 through 6 can be linked to optional modal (CF) and size-segregated (CMU) primary and secondary particulate matter (PM) treatments. CAMx includes algorithms for inorganic aqueous aerosol chemistry (RADM-AQ), inorganic gas-aerosol partitioning (ISORROPIA), and organic oxidation and gas-aerosol partitioning (VBS or SOAP). The PM treatments require additional gas species as PM precursors and use products from the gas-phase photochemistry for the production of sulfate, nitrate, and condensable organic gases. The CF PM treatment also supports several optional mercury species. Additionally, there is an interface that allows a simpler user-defined chemical mechanism to be employed in the model (Mechanism 10). A listing of all reactions and rate expressions for supported photochemical mechanisms are provided in the appendices.

Table 5-1. Gas-phase chemical mechanisms currently implemented in CAMx v6.4.

Mechanism ID	Description
6	CB05 (Yarwood et al., 2005b). 156 reactions among 51 species (38 state gases, 13 radicals).
2	CB6 "Revision 2" (CB6r2; Yarwood et al., 2010; Yarwood et al., 2012a; Hildebrandt Ruiz and Yarwood, 2013). 216 reactions among 75 species (55 state gases, 20 radicals).
3	CB6r2 with updates to include reactions involving oceanic halogen compounds (CB6r2h; Yarwood et al., 2014). 304 reactions among 115 species (88 state gases, 27 radicals).
4	CB6 "Revision 4" (CB6r4) that combines temperature- and pressure-dependent NO ₂ -organic nitrate branching (Emery et al., 2015) with a condensed set of reactions involving ocean-borne inorganic iodine (Emery et al., 2016). 229 reactions among 86 species (61 state gases, 25 radicals).
5	A version of SAPRC07 that includes updates to support toxics and numerical expressions of rate constants to support the current chemistry mechanism compiler (SAPRC07TC; Carter, 2010; Hutzell et al., 2012). 565 reactions among 117 species (72 state gases, 45 radicals).
10	A user-defined simple chemistry mechanism can be developed for any gas and/or particulate species, which is defined by a "Mechanism 10" parameters file and solved within a user-supplied subroutine called "chem10.f."

The selection of which mechanism to run in CAMx is determined by the "chemistry parameters" input file. This file defines the number of gas and aerosol species and the number of reactions for the mechanism, lists the species by name with associated physical-chemical properties, lists the reaction rate constants and temperature dependencies for each reaction, and defines which reactions are photolytic. Chemistry parameters input files are provided with CAMx and should not be modified by users. See Section 3 for additional information on the format and usage of these files. Chemistry parameters files are specific to versions of CAMx. Always use chemistry parameters files distributed with each CAMx version, do not attempt to use files from different CAMx versions.

5.1 Gas-Phase Chemistry

5.1.1 Carbon Bond

The Carbon Bond IV (CB4) mechanism was first developed by Gery et al. (1989), and was subsequently updated in the 1990's to include revised PAN chemistry, additional radical-radical termination reactions and updated isoprene chemistry (Carter 1996; Whitten et al., 1996). Additional CB4 updates were then made to expand ozone modeling from urban to regional/rural environments and to support secondary aerosol chemistry, mercury and toxics (Yarwood et al., 2005a).

Several newer Carbon Bond versions are available in CAMx as described below. Table 5-2 lists chemical species names and properties common to all CAMx Carbon Bond mechanisms.

5.1.1.1 Carbon Bond 2005

Mechanism 6 is the 2005 version of Carbon Bond (CB05) developed for EPA atmospheric modeling studies (Yarwood et al., 2005b). Updates in CB05 include:

- Updated rate constants based on 2003 – 2005 IUPAC and NASA evaluations.
- An extended inorganic reaction set for urban to remote tropospheric conditions.
- NO_x recycling reactions to represent the fate of NO_x over multiple days.
- Explicit organic chemistry for methane and ethane.
- Explicit methylperoxy radical, methyl hydroperoxide and formic acid.
- Lumped higher organic peroxides, organic acids and peracids.
- Internal olefin (R-HC=CH-R) species called IOLE.
- Higher aldehyde species ALDX making ALD2 explicitly acetaldehyde.
- Higher peroxyacyl nitrate species from ALDX called PANX.
- Lumped terpene species called TERP.

CB05 was evaluated against smog chamber data from the Universities of North Carolina and California at Riverside. The new higher aldehyde and internal olefin species improve mechanism performance for these species and produce oxidants more rapidly at low VOC/NO_x ratios. The new terpene species improves simulation of oxidants and PM from biogenic emissions. Several new organic peroxide species improve the simulation of oxidants that are involved in PM sulfate formation. The addition of explicit methylperoxy radical improves the simulation of hydrogen peroxide under low NO_x conditions.

5.1.1.2 Carbon Bond Version 6

Carbon Bond version 6 (CB6) was developed by Yarwood et al. (2010). Since then, several revisions have been made to CB6, as described below. Mechanism 2 is CB6 revision 2 (CB6r2; Hildebrandt Ruiz and Yarwood, 2013).

Several organic compounds that are long-lived and relatively abundant, namely propane, acetone, benzene and ethyne (acetylene), were added explicitly in CB6 to improve oxidant formation from these compounds as they are oxidized slowly at the regional scale. Alpha-dicarbonyl compounds (glyoxal and analogs), which can form from secondary organic aerosol (SOA)

Table 5-2. Species names and descriptions common to all Carbon Bond Mechanisms in CAMx.

Species	Description	Carbon #	C	H	O	Mol. Wt.
BZO2	Peroxy radical from OH addition to benzene	6	6	7	5	159.1
C2O3	Acetylperoxy radical	2	2	3	3	75.0
CRO	Alkoxy radical from cresol	7	7	7	1	107.1
CXO3	C3 and higher acylperoxy radicals	3	3	5	3	89.0
EPX2	Peroxy radical from EPOX reaction with OH	5	5	9	5	149.1
HCO3	Adduct from HO2 plus formaldehyde	1	1	3	3	63.0
HO2	Hydroperoxy radical	1	1		1	28.0
ISO2	Peroxy radical from OH addition to isoprene	5	5	9	3	117.1
MEO2	Methylperoxy radical	1	1	3	2	47.0
NO3	Nitrate radical				3	62.0
O	Oxygen atom in the O ³ (P) electronic state				1	16.0
O1D	Oxygen atom in the O ¹ (D) electronic state				1	16.0
OH	Hydroxyl radical			1	1	17.0
OPO3	Peroxyacyl radical from OPEN	4	4	3	4	115.0
RO2	Operator to approximate total peroxy radical concentration		4	7	2	87.1
ROR	Secondary alkoxy radical	1	4	7	1	71.1
TO2	Peroxy radical from OH addition to TOL	7	7	9	5	173.1
XLO2	Peroxy radical from OH addition to XYL	8	8	11	5	187.1
XO2	NO to NO2 conversion from alkylperoxy (RO2) radical		4	7	2	87.1
XO2H	NO to NO2 conversion (XO2) accompanied by HO2 production		4	7	2	87.1
XO2N	NO to organic nitrate conversion from alkylperoxy (RO2) radical		4	7	2	87.1
AACD	Acetic acid	2	2	4	2	60.0
ACET	Acetone	3	3	6	1	58.1
ALD2	Acetaldehyde	2	2	4	1	44.0
ALDX	Propionaldehyde and higher aldehydes	3	3	6	1	58.1
BENZ	Benzene	6	6	6		78.1
CAT1	Methyl-catechols	7	7	8	2	124.1
CO	Carbon monoxide	1	1		1	28.0
CH4	Methane	1	1	4		16.0
CRES	Cresols	7	7	8	1	108.1
CRON	Nitro-cresols	7	7	7	3	153.1
EPOX	Epoxide formed from ISPX reaction with OH	5	5	10	3	118.1
ETH	Ethene	2	2	4		28.0
ETHA	Ethane	2	2	6		30.1
ETHY	Ethyne	2	2	2		26.0
ETOH	Ethanol	2	2	6	1	46.1
FACD	Formic acid	1	1	2	2	46.0
FORM	Formaldehyde	1	1	2	1	30.0
GLY	Glyoxal	2	2	2	2	58.0
GLYD	Glycolaldehyde	2	2	4	2	60.0

Species	Description	Carbon #	C	H	O	Mol. Wt.
H2O2	Hydrogen peroxide			2	2	34.0
HNO3	Nitric acid			1	3	63.0
HONO	Nitrous acid			1	2	47.0
HPLD	hydroperoxyaldehyde	5	5	8	3	116.1
INTR	Organic nitrates from ISO2 reaction with NO	5	5	9	4	147.1
IOLE	Internal olefin carbon bond (R-C=C-R)	4	4	8		56.1
ISOP	Isoprene	5	5	8		68.1
ISPD	Isoprene product (lumped methacrolein, methyl vinyl ketone, etc.)	4	4	6	1	70.1
ISPX	Hydroperoxides from ISO2 reaction with HO2	5	5	10	3	118.1
KET	Ketone carbon bond (C=O)	4	4	8	1	72.1
MEOH	Methanol	1	1	4	1	32.0
MEPX	Methylhydroperoxide	1	1	4	2	48.0
MGLY	Methylglyoxal	3	3	4	2	72.0
N2O5	Dinitrogen pentoxide				5	108.0
NO	Nitric oxide				1	30.0
NO2	Nitrogen dioxide				2	46.0
NTR	Organic nitrates	4	4	9	3	119.1
O3	Ozone				3	48.0
OLE	Terminal olefin carbon bond (R-C=C)	3	3	6		42.1
OPAN	Peroxyacyl nitrate (PAN compound) from OPO3	4	4	3	6	161.0
OPEN	Aromatic ring opening product (unsaturated dicarbonyl)	4	4	4	2	84.0
PACD	Peroxyacetic and higher peroxy-carboxylic acids	2	2	4	3	76.0
PAN	Peroxyacetyl Nitrate	2	2	3	5	121.0
PANX	C3 and higher peroxyacyl nitrate	3	3	5	5	135.0
PAR	Paraffin carbon bond (C-C)	1	5	12		72.1
PNA	Peroxynitric acid			1	4	79.0
PRPA	Propane	3	3	8		44.1
ROOH	Higher organic peroxide		4	10	2	90.1
SO2	Sulfur dioxide				2	64.0
SULF	Sulfuric acid (gaseous)			2	4	98.0
TERP	Monoterpenes	10	10	16		136.2
TOL	Toluene and other monoalkyl aromatics	7	7	8		92.1
XOPN	Aromatic ring opening product (unsaturated dicarbonyl)	5	5	6	2	98.1
XYL	Xylene and other polyalkyl aromatics	8	8	10		106.2
NTR1	Simple organic nitrates		4	9	3	119.1
NTR2	Multi-functional organic nitrates		4	9	4	135.1
ECH4	Emitted methane (to enable tracking separate from CH4)	1	1	4		16.0
XPRP	Operator for organic nitrates from PRPA	3	3	7	2	89.1
XPAR	Operator for organic nitrates from PAR	1	5	11	2	117.1
CRNO	Nitro-cresol oxy radical	7	7	6	3	152.1

Species	Description	Carbon #	C	H	O	Mol. Wt.
CRN2	Nitro-cresol peroxy radical	7	7	6	4	168.1
CRPX	Nitro-cresol hydroperoxide	7	7	7	4	169.1
CAO2	Ring-opening product from methyl catechol	7	7	9	5	173.1

via aqueous-phase reactions (Carlton et al., 2007), were added in CB6 to improve support for SOA modeling. Precursors to alpha-dicarbonyls in CB6 are aromatics, alkenes and ethyne. CB6 included several updates to peroxy radical chemistry that improved formation of hydrogen peroxide (H_2O_2) and therefore sulfate aerosol formation. The gas-phase reaction of dinitrogen pentoxide (N_2O_5) with water vapor is slower in CB6 than CB05, which reduced nighttime formation of nitric acid, although heterogeneous reactions on aerosol surfaces may dominate nitric acid formation at night (Brown et al., 2006). CB6 included the calculation of the heterogeneous N_2O_5 hydrolysis rate as a function of nitrate, chloride, and water concentrations in particles (Bertram and Thornton, 2009) when PM is explicitly simulated; if no PM chemistry is included, CAMx sets the heterogeneous rate to the IUPAC (2015) N_2O_5 hydrolysis rate.

The core inorganic chemistry mechanism for CB6 was based on evaluated data from the IUPAC tropospheric chemistry panel as of January, 2010 (Atkinson et al., 2010). IUPAC also was the primary source for photolysis data in CB6 with some data from the 2006 NASA/JPL data evaluation (Sander et al., 2006) or other sources for photolysis of some organic compounds. There were changes to the organic chemistry for alkanes, alkenes, aromatics and oxygenates. The most extensive changes were for aromatics and isoprene. Chemistry updates for aromatics were based on the updated toluene mechanism (CB05-TU) developed by Whitten et al. (2010) extended to benzene and xylenes. The isoprene mechanism was revised based on several recently published studies (Paulot et al., 2009a,b; Peeters et al., 2009).

CB6 was evaluated using 339 experiments from several chambers at the University of California at Riverside and the Tennessee Valley Authority. The performance of CB6 and CB05 in simulating chamber studies was comparable for alkanes, alkenes, alcohols and aldehydes with both CB6 and CB05 performing well and exhibiting 20% or less bias for maximum ozone. For species that were explicitly added in CB6 (ethyne, benzene and ketones), CB6 performed much better than CB05. For aromatics, CB6 improved upon CB05 by reducing under prediction bias in maximum ozone to about 10% for benzene, toluene and xylene. For isoprene, both CB05 and CB6 show little bias for maximum ozone (less than 5%) but CB6 tended to form ozone too slowly. CB6 improved upon CB05 for simulating mixtures of VOCs. For mixtures without aromatics, both CB05 and CB6 showed minimal bias for maximum ozone. For mixtures including aromatics, both CB05 and CB6 under predicted maximum ozone but bias was reduced from about 30% for CB05 to about 20% for CB6.

CB6 revision 1 (CB6r1) included revised chemistry for isoprene and aromatic hydrocarbons and more NO_x -recycling from the degradation of organic nitrates (Yarwood et al., 2012a). Revision 2 (CB6r2) increased detail in the formation and fate of organic nitrates (ON), including organic nitrate destruction by reactions in aerosols (Hildebrandt Ruiz and Yarwood, 2013). ONs are formed when VOCs degrade in the presence of NO_x and are important in the atmosphere because they sequester NO_x and can contribute to organic aerosol (OA). NO_2 is released when

ONs degrade by photolysis in the gas-phase, returning NO_x to the atmosphere where it may contribute to ozone production. CB6r2 differentiates organic nitrates between simple alkyl nitrates that remain in the gas-phase and multi-functional ONs that can partition into OA (Hildebrandt Ruiz and Yarwood, 2013). ONs present in aerosols are then assumed to undergo hydrolysis to nitric acid with a lifetime of approximately 6 hours based on laboratory experiments and ambient data. These changes tend to reduce regional concentrations of ozone and ONs, and increase nitric acid. Regional modeling simulations using CAMx with CB6r2 show that accounting for ON hydrolysis in aerosols improve performance for ozone and in simulating the partitioning of NO_y between ONs and nitric acid.

5.1.1.3 Carbon Bond Version 6 with Halogen Chemistry

Mechanism 3 is an extension of CB6r2 chemistry that adds reactions involving ocean-borne halogen compounds (CB6r2h; Yarwood et al., 2014). Bromine reactions were integrated with previously developed reactions for iodine (Yarwood et al., 2012b) and chlorine (Tanaka et al., 2003; Koo et al., 2012) with rate constants updated to currently accepted values (IUPAC, 2014a and b) and mechanism revisions to promote consistency. The additional halogen compounds and reactions added to CB6r2 are listed in Appendix B.

The chlorine (Cl) reaction mechanism is based on Koo et al. (2012) with the following updates:

- Reaction rate constants updated to IUPAC (2014a and b) as necessary;
- Cl-atoms with organic compounds are limited to alkanes and isoprene
- Added ClO radical reactions with BrO and IO
- Added ClNO₃ hydrolysis to HOCl on aerosols
- Cl-atom reactions with organic compounds limited to alkanes and isoprene

Reactions of Cl-atoms with organic compounds are limited to alkanes and isoprene. Cl-atom production from the photolysis of chloromethanes is included only for those halomethanes that are included as sources of Br from seawater. Degradation of anthropogenic chlorocarbons (e.g., HCFCs) is not included in the mechanism. The dominant source of atmospheric Cl is expected to be sea salt emissions. Hydrochloric acid (HCl) is displaced into the gas phase when sea salt aerosols are acidified by nitric and sulfuric acids. The HCl formed from sea salt can react with dinitrogen pentoxide (N₂O₅) on aerosol surfaces to produce nitryl chloride (ClNO₂) which photolyzes to produce Cl-atoms. When PM is explicitly modeled, the heterogeneous reaction rate for N₂O₅ + HCl is calculated using the parameterization developed by Bertram and Thornton (2009).

The bromine (Br) reaction mechanism is similar to the mechanisms of Yang et al. (2005), Smoydzin and von Glasow (2009) and Parrella et al. (2012) and is more compact than the mechanisms of Vogt et al. (1999), Whitten and Yarwood (2008) and Ordóñez et al. (2012). Reaction rate constants for the Br mechanism are from IUPAC (2014a and b). Hydrolysis of BrNO₃ is included as pseudo gas-phase reaction with a rate constant comparable to hydrolysis of N₂O₅. The largest source of atmospheric Br is sea salt aerosol (Yang et al., 2005) although the mechanism by which sea salt Br enters the gas-phase differs from that for Cl depletion under acid conditions (discussed above) and this can also occur at neutral pH. Other sources of

atmospheric Br included in the mechanism are decomposition of the halomethanes CHBr_3 , CH_2Br_2 , CH_2BrCl , CHBr_2Cl and CHBrCl_2 .

The iodine (I) reaction mechanism is based on Yarwood et al. (2012b) with the following updates:

- Reaction rate constants updated to IUPAC (2014a and b) as necessary
- Added IO radical reactions with ClO and BrO
- Added INO_3 hydrolysis to HOI on aerosols
- Removed INO and related reactions

Reactions of INO were removed because INO concentrations were found to be small (Yarwood et al., 2012b). Hydrolysis of INO_3 is included as pseudo gas-phase reaction with a rate constant comparable to hydrolysis of N_2O_5 .

Emissions from oceans are the major source of atmospheric iodine (Carpenter, 2003), including methyl iodide (CH_3I), other iodo-methanes (CH_2I_2 , CH_2ICl , CH_2IBr), larger alkyl iodides, and molecular iodine (I_2). Iodine emissions result both from biological and photochemical processes in ocean water (Moore and Tokarczyk, 1993; Moore and Zafirou, 1994). Photochemical processes that cause iodine emissions are linked to reactions of dissolved ozone and thereby to enhanced ozone deposition to oceanic waters (Ganzeveld et al., 2009; Helmig et al., 2012).

Reactions among the radicals ClO, BrO, and IO are included to interconnect the mechanisms for different halogens. Atmospheric reactions of Cl-atoms, Br-atoms and I-atoms can produce or destroy tropospheric ozone through a series of catalytic cycles, where each halogen atom is regenerated in the reactions and therefore one atom can potentially destroy many O_3 molecules. Catalytic destruction of O_3 by Cl and Br is terminated only when deposition removes reservoir species, e.g., by dry or wet deposition of HCl and HBr. The atmospheric reactions of I-atoms differ from Br and Cl in several ways:

- I-atoms do not abstract H from organic compounds in contrast to Br and Cl-atoms;
- Formation of oxides is more extensive for I (IO, OIO, I_2O_2 , IxOy) than for Br (BrO) or Cl (ClO);
- Larger iodine oxides (IxOy) form aerosols whereas Cl and Br oxides remain in the gas phase.

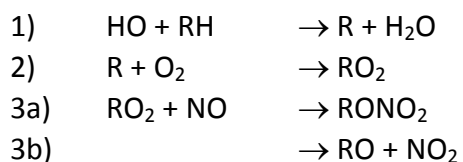
Aerosol formation by larger iodine oxides is a sink for reactive I that can terminate O_3 destruction by reactive I.

5.1.1.4 Carbon Bond Version 6, Revision 4

Mechanism 4 is CB6 revision 4 (CB6r4), which combines temperature- and pressure-dependent NO_2 -alkyl nitrate branching originally developed as CB6r3 (Emery et al., 2015) with a condensed set of reactions involving ocean-borne inorganic iodine (Emery et al., 2016). CB6r4 is supported by a new in-line parameterization that computes inorganic iodine emissions flux caused by ozone deposition to seawater (Section 5.1.1.5). See Appendix D for a complete listing of reactions, rate expressions, and VOC properties.

Alkyl nitrates (RONO_2) can influence ozone production because both nitric oxide (NO) and radicals (specifically RO_2) are removed by alkyl nitrate formation. However, the temperature dependence of alkyl nitrate formation is omitted from current photochemical mechanisms such as CB05-TU (Whitten et al., 2010), CB6r2 (Hildebrandt Ruiz and Yarwood, 2013), SAPRC11 (Carter and Heo, 2013), RACM2 (Goliff et al., 2013) and the Master Chemical Mechanism (Saunders et al., 2003). Lee et al. (2014) considered how cold winter conditions affect alkyl nitrate branching and concluded that omitting the temperature dependence may cause a 15% high bias in ozone formation.

Alkyl nitrates are formed when alkanes are oxidized in the atmosphere in the presence NO. Alkanes are compounds of hydrogen and carbon with only single bonds connecting the atoms, e.g., methane (CH_4), ethane (C_2H_6), propane (C_4H_8), etc. Analyses of air samples collected in western US oil and gas development basins during wintertime ozone events show that alkanes dominate the organic gases present in the air. The formation of alkyl nitrates from alkanes can be described by the following reactions in which an alkane (RH) reacts with hydroxyl radical (HO) and oxygen (O_2) to form an alkyl peroxy radical (RO_2) that has two potential reaction pathways with NO:



Perring et al. (2013) have reviewed the atmospheric impacts of RONO_2 formation. The yield of RONO_2 is determined by the branching ratio between reactions 3a and 3b, which depends on both temperature and pressure (Atkinson et al., 1983). The association reaction of RO_2 with NO in reaction 3a is favored over reaction 3b by lower temperatures and higher pressures.

Emery et al. (2015) developed the CB6r3 chemical mechanism from CB6r2 to improve applicability to winter conditions. Temperature and pressure dependent formation of RONO_2 was implemented for propane (CB6 species "PRPA") and larger alkanes (CB6 species "PAR") using the parameterization of Yeh and Ziemann (2014). CB6r3 was designed to produce the same RONO_2 yields as CB6r2 at room temperature and pressure (298 K and 1 atm). CAMx simulations with CB6r3 for the Uintah Basin of Utah confirmed the directionality of the ozone effect described by Lee et al. (2014).

Iodine compounds emitted from ocean waters can cause ozone depletion of several ppb per day within the marine boundary layer (Mahajan et al., 2010 and references therein). Iodine depletes ozone catalytically, meaning that a single iodine atom can destroy many ozone molecules (Chameides and Davis, 1980; Mahajan et al., 2009). Emissions of inorganic iodine compounds (I_2 and HOI, or collectively Ix) are caused by deposition of ozone to ocean waters (Garland and Curtis, 1981; Carpenter et al., 2013), whereas emissions of organic iodine compounds result from biological processes (Carpenter, 2003).

The iodine portion of CB6r2h includes 30 reactions (Yarwood et al., 2014) but the extra computational burden motivated subsequent development of a compact mechanism. Emery et al.

(2016) developed a more efficient condensed iodine mechanism involving 16 reactions among 9 inorganic iodine species that are most important to the dynamics of the full iodine mechanism, and that are consistently the key drivers of ozone depletion across a range of I_x emission. The Source Apportionment Probing Tool was updated to account for an additional ozone destruction pathway by iodine and conversion of nitrogen tracer classes involving iodine nitrate (INO₃).

Emery et al. (2016) showed that the efficiency of ozone depletion by iodine is highly dependent on the amount of iodine enrichment; therefore, accurately representing important iodine precursors (e.g., HOI) is critical for the fidelity of simulating ozone depletion by iodine. In CAMx simulations for Texas, the full halogen and 16-reaction iodine mechanisms produced similar peak ozone decrements of 5-7 ppb over the Gulf of Mexico. While the condensed mechanism was faster than CB6r2h, it remained disproportionately slow relative to CB6r2 because of stiff reactions involving the species I, IO and OIO. We implemented and tested a faster iterative EBI solution for these species. We updated the chemical mechanism compiler (CMC) for CAMx to automatically apply this solver strategy (called the IO_x solver) for CB6r4, CB6r2h and any future halogen mechanisms in CAMx. While developing the IO_x solver we also restructured the loop over species in the main CAMx EBI solver to improve efficiency for all chemical mechanisms.

CB6r4 also adds pseudo-heterogeneous hydrolysis of isoprene-derived organic nitrate (INTR). Aerosol uptake of organic nitrate followed by particle-phase hydrolysis to HNO₃ formation can be an important pathway for loss of atmospheric NO_x (Hildebrandt Ruiz and Yarwood, 2013; Jacobs et al., 2014; Fisher et al., 2016). CB6r4 assumes the same lifetime (1 hour) against particle-phase hydrolysis of INTR as Fisher et al. (2016). Partitioning of organic nitrate into particle phase is modeled using a two-product parameterization based on ambient measurement data during the 2010 CalNex (Rollins et al., 2013). If PM is not explicitly modeled, equal partitioning between the gas and particle phases is assumed.

Finally, all 8 reactions of volatile organic compounds (VOC) with oxygen atoms (O) were deleted from the mechanism. O-atom reactions with VOC were included in CB mechanisms because they can matter for smog chamber simulations used for mechanism development, but they have negligible impact in atmospheric simulations.

5.1.1.5 In-Line Inorganic Iodine Emissions

The CAMx in-line I_x emissions algorithm incorporates recent findings on the feedback between ozone deposition to ocean waters and emission flux of iodine (Prados-Roman et al., 2015; Garland and Curtis, 1981). The algorithm follows the parameterization developed by Carpenter et al. (2013), as implemented in the CAM-Chem global chemistry-climate model (Lamarque et al., 2012), for aqueous iodine in ocean surface water, and I₂ and HOI air emissions:

$$E(HOI) = [O_3] \times \left[4.15 \times 10^5 \left(\frac{\sqrt{[I_{aq}^-]}}{w} \right) - \left(\frac{20.6}{w} \right) - 2.36 \times 10^4 \sqrt{[I_{aq}^-]} \right]$$

$$E(I_2) = [O_3] \times [I_{aq}^-]^{1.3} \times (1.74 \times 10^9 - 6.54 \times 10^8 \ln w)$$

where the units of E are $\text{nmol m}^{-2} \text{day}^{-1}$, w is wind speed (m s^{-1}), $[O_3]$ is surface ozone concentration (ppb), and $[I_{aq}^-]$ is aqueous iodide concentration (mol dm^{-3}). Sea surface temperature (SST , K) is used as the basis for estimating $[I_{aq}^-]$ (MacDonald et al., 2014):

$$[I_{aq}^-] = 1.46 \times 10^6 e^{\left(\frac{-9134}{SST}\right)}$$

Aqueous iodide concentrations exhibit a strong exponential sensitivity to SST, resulting in similarly strong Ix emissions sensitivity to SST and wind speed and a linear Ix emissions response to ambient ozone concentrations. For conditions typical of the Gulf of Mexico, HOI contributes 91-99% of the total Ix emissions flux with I_2 contributing the remainder. Prados-Roman et al. (2015) note that the parameterization for $[I_{aq}^-]$ above yields lower concentrations than the SST^2 dependence of Chance et al. (2014), and that ozone deposition rates are related to ocean biogeochemistry (Ganzeveld et al., 2009). Including these factors would enhance Ix emissions, particularly in regions with elevated ozone and high oceanic iodide concentrations. With these considerations in mind, Prados-Roman et al. (2015) conclude that Ix fluxes estimated from the parameterizations above should be regarded as lower limits.

This algorithm is invoked by setting the namelist flag "Inline_Ix_Emissions" to ". TRUE." Oceanic Ix emissions are calculated for any grid cells containing ocean water bodies, as determined by the CAMx input landuse file. Section 3.4.3.1 describes the procedures to follow to ensure that your input landuse file correctly distinguishes between ocean and fresh water bodies. In-line emission fluxes of I_2 and HOI are added to the CAMx deposition output files so that they can be plotted and analyzed. In-line emissions eliminate the need to supply oceanic Ix emissions in your input gridded emissions files. If Ix (i.e., I_2 and/or HOI) emissions are present on your input files, CAMx will stop with an error to avoid double-counting. If in-line emissions are not invoked, you may continue to use externally-derived halogen emissions from the SEASALT pre-processor.

5.1.2 SAPRC 2007

The 2007 update to the SAPRC chemistry mechanism, called SAPRC07 (Carter, 2010), replaced the dated SAPRC99 mechanism. The version implemented in CAMx is SAPRC07TC, which includes additional model species to explicitly represent selected toxics and reactive organic compounds and uses numerical expressions of rate constants that are compatible with the current chemistry mechanism solver (Hutzell et al., 2012). Chlorine chemistry is not included in the CAMx implementation. See Appendix E for a complete listing of reactions, rate expressions, species definitions, and VOC properties.

5.1.3 Implicit Gas-Phase Species

All photochemical mechanisms in CAMx employ fixed concentrations for molecular oxygen (O_2), molecular hydrogen (H_2), and methane (CH_4). Concentrations for these compounds are set to the following constant mixing ratios (i.e., they are not impacted by the chemical solution):

$$\begin{aligned}[\text{O}_2] &= 2.095 \times 10^5 \text{ ppm} \\ [\text{H}_2] &= 0.60 \text{ ppm} \\ [\text{CH}_4] &= 1.75 \text{ ppm}\end{aligned}$$

Mechanisms 2, 3 and 4 (CB6 variants) include a species named ECH4 to represent emitted methane over and above the global background of 1.75 ppm.

5.1.4 Photolysis Rates

The rates of atmospheric photolysis reactions depend upon solar irradiance and therefore are sensitive to the amount of solar radiation transmitted through the atmosphere as well as reflected from the earth's surface (albedo). Photolysis rates are externally derived assuming clear-sky conditions as a function of five parameters: solar zenith angle, altitude above ground, total ozone column, surface albedo, and terrain height. The rates are provided to CAMx as a large lookup table that spans the range of conditions for each of the five dimensions. The lookup table is developed using a CAMx pre-processor that incorporates the Tropospheric Ultraviolet and Visible (TUV) radiative transfer model (NCAR, 2011). TUV employs a standard atmosphere density profile for Rayleigh scattering and other absorbers such as oxygen. User-specified ozone column values are used to scale a typical vertical ozone profile within TUV. A default aerosol profile from Elterman (1968) is combined with typical aerosol optical properties within TUV to account for haze.

The CAMx version of TUV is modified to output photolysis rate information in a format directly compatible with all CAMx photochemical mechanisms. See Sections 2 and 3 for more information on developing photolysis inputs.

As CAMx runs, the lookup rates are interpolated to the specific conditions in each grid cell. They are then adjusted for any local cloud cover and local aerosol attenuation (if PM is simulated). Additionally, solar angle-dependent temperature and pressure adjustments are applied to five key photolysis reactions (NO_2 , O_3 , acetaldehyde, and two formaldehyde reactions).

5.1.4.1 Cloud and Aerosol Adjustments

Photochemistry is strongly influenced by the presence of clouds, which can both attenuate and enhance the actinic flux of ultraviolet (UV) and visible radiation responsible for photolysis. Their specific radiative impacts depend on many factors, including height, depth and fractional sky cover; water content; and water phase (i.e., liquid droplets or ice crystals). Aerosols also influence photochemistry according to their optical properties and mass loading as a function of altitude and depth. CAMx includes a fast in-line version of TUV (Emery et al., 2010) to calculate photolysis adjustment profiles through each cloudy, aerosol-laden grid column.

The in-line TUV is run twice for each grid column: first for non-cloudy conditions with the same Elterman (1968) aerosol profile used in the full-science TUV pre-processor, and second with clouds and simulated aerosols to derive a vertical profile of the cloudy:clear actinic flux ratio (in the case that aerosols are not run in CAMx, the Elterman profile is used consistently). This ratio is then applied as a multiplicative factor to the clear-sky value in each grid cell. This approach

maintains accuracy in the calculation of clear-sky photolysis rates, while allowing clouds and aerosols to be directly involved in radiative transfer calculations through each grid column.

TUV includes a calculation of integrated atmospheric density above the CAMx domain, based on the U.S. standard atmosphere, so that atmospheric attenuation of the UV stream is properly calculated entering the model top. Other aspects of the in-line TUV model were substantially streamlined to minimize runtimes. First, radiative calculations are performed for only a single representative wavelength (350 nm). Second, since absorption by gases occurs in rather narrow UV bands relative to the broad-band influence of clouds, the absorption from oxygen, ozone, nitrogen dioxide and sulfur dioxide were removed. Third, the extraterrestrial flux was not needed as it cancels out in the calculation of the cloudy: clear ratio. Finally, the plane-parallel version of the delta-Eddington approach was used in lieu of the more complex and expensive pseudo-spherical geometry. Preliminary tests against the full-science TUV showed that the streamlined version resulted in less than 1% differences in actinic flux ratio for a range of cloudy conditions (Emery et al., 2010).

Optical depth τ expresses the reduction of incident light I_0 through a light attenuating medium of depth Δz according to

$$I = I_0 e^{-\tau}$$

The in-line TUV adjustment scheme utilizes cloud optical depth fields provided by the CAMx cloud/rain file, and aerosol optical depths calculated from the PM mass concentrations simulated by CAMx.

The CAMx meteorological interface pre-processors generate cloud water and optical depth fields from the variable fields present in the raw meteorological output files. Cloud optical depth is calculated in each model grid cell according to the approach of Del Genio et al. (1996) and Voulgarakis et al. (2009), which satisfactorily approximates the effects of random cloud overlap according to

$$\tau = \frac{3L\Delta z}{2\rho_w r_d} (F_c)^{3/2}$$

where L is cloud liquid water content (g/m^3), Δz is the cell depth containing cloud water, ρ_w is the density of liquid water (10^6 g/m^3), and F_c is fractional cloud cover. The mean cloud droplet radius r_d is not dependent on water phase, and is assumed to be a typical tropospheric value of $1.5 \times 10^{-5} \text{ m}$ for liquid cloud water. TUV assumes constant Mie scattering parameters for clouds: a single scattering albedo of 0.99, and an asymmetry factor of 0.85.

When CAMx is run with PM, vertical haze opacity profiles are calculated from simulated aerosol concentration fields. When CAMx is run with only gas-phase chemistry without aerosols, photolysis rates are only adjusted for clouds. Aerosol optical parameters are best determined from Mie theory, but in the interest of minimizing impacts to model speed and considering the degree of uncertainty in the simulated aerosol concentrations themselves, a simpler method

was adopted. Aerosols are assumed to exist as an external mixture of their component chemical species. Aerosol light extinction (scattering and absorption) is a function of each species' concentration, extinction efficiency, and affinity for hygroscopic growth. Total aerosol optical depth is determined by summing extinction over all species and multiplying by layer depth.

Dry extinction efficiencies and single-scattering albedos for each aerosol species, valid at 350 nm, are externally defined in the CAMx chemistry parameters file. While these can be altered by the user, the chemistry parameters files that are provided with the CAMx distribution include default values according to Takemura et al. (2002), as shown in Table 5-3.

Table 5-3. Default dry extinction efficiency and single-scattering albedo at 350 nm (Takemura et al., 2002) in the distributed CAMx chemistry parameters file.

Species	Dry Extinction Efficiency (m ² /μg)	Single-Scattering Albedo
Sulfate	7×10 ⁻⁶	0.99
Nitrate	7×10 ⁻⁶	0.99
Ammonium	7×10 ⁻⁶	0.99
Organics	7×10 ⁻⁶	0.80
Elemental Carbon	18×10 ⁻⁶	0.25
Crustal (Fine+Coarse)	0.4×10 ⁻⁶	0.70
Sea salt (Na+Cl)	1.5×10 ⁻⁶	0.99

Takemura et al. (2002) provide extinction efficiencies and single-scattering albedos for sulfate, organics, soot, total dust, and sea salt; we have extended the sulfate values to nitrate and ammonium. The asymmetry factor is internally set to a default value of 0.61 regardless of the composition of the aerosols.

Hygroscopic aerosols are also flagged in the chemistry parameters file. For each flagged species, an internal growth factor is applied to the dry extinction efficiencies according to the relative humidity conditions in each grid cell. The growth curve is taken from the Phase I report of the Federal Land Managers' Air Quality Related Values Workgroup (FLAG, 2000). By default, the relative humidity growth factor is flagged for sulfate, nitrate, ammonium and sea salt; a single growth factor is applied for all hygroscopic species (Figure 5-1). Minimum and maximum limits on relative humidity are set at 1% and 95%, respectively.

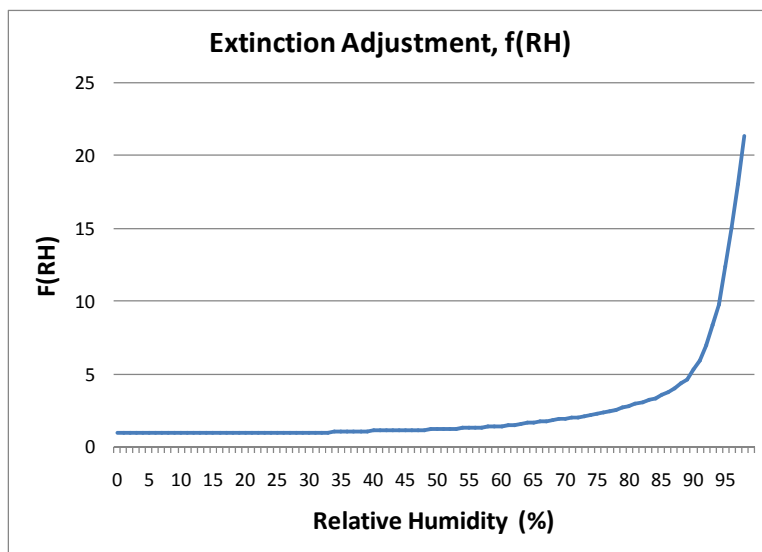


Figure 5-1. Relative humidity adjustment factor applied to the dry extinction efficiency for hygroscopic aerosols (FLAG, 2000).

5.1.4.2 Effects of Surface Albedo and Snow Cover

Photolysis rates depend on the amount of solar radiation reflected from the Earth's surface (albedo). UV albedo is assigned within CAMx according to the distribution of gridded landuse provided by the time-invariant 2D surface file (Tables 3-4 and 3-5). Snow-free UV albedos fall in the range 0.04 to 0.08 and are constant in time. Analyses of reflected UV radiation recorded in satellite data (Herman and Celarier, 1997) report similar UV albedo values in the range 0.02-0.08 for typical terrestrial and water surfaces. Snow is much more reflective than other types of surfaces and so it is important to characterize the effect of snow cover on photolysis rates.

The CAMx photolysis rate input file is generated for five surface albedos, two of which represent the non-snow range (0.04 – 0.10) and four that represent the snow range (0.1 – 0.2 – 0.5 – 0.9). CAMx determines the landuse- and snow-weighted average surface albedo in each grid cell (Section 4.7) and interpolates photolysis rates between the five albedos.

5.1.5 Gas-Phase Chemistry Solvers

Solving the time evolution of gas-phase chemistry requires numerically integrating a set of ordinary differential equations (ODEs) and is among the most computationally expensive operations performed in a photochemical grid model. One reason for this is that the ODEs describing tropospheric chemistry are “stiff” – meaning that the chemical species involved have widely varying production and/or decay times. The computational efficiency of the gas-phase chemistry solver strongly influences the overall efficiency of a grid model. CAMx includes two chemistry solvers that offer trade-offs between accuracy and efficiency.

The most accurate solution methods available for stiff ODEs are “Gear” type implicit solvers (Gear, 1971) such as LSODE (Hindmarsh, 1983). Gear solvers are stable when applied to “stiff” problems, such as gas-phase chemistry, but are generally too slow for routine use in grid model

applications. Hertel et al. (1993) developed an implementation of the Euler Backward Iterative (EBI) method that is very efficient and also accurate because it utilizes explicit algebraic formulae to solve several important groups of species (HO_x, NO_x, etc.).

5.1.5.1 LODE

CAMx includes the double precision version of the Livermore Solver for Ordinary Differential Equations (LSODE; Hindmarsh, 1983) distributed by the Netlib repository of numerical algorithms (<http://www.netlib.org/>). LODE is too slow for everyday use but valuable as a reference method within CAMx. LODE is based on Gear's method with numerical refinements to improve efficiency and ease of use (Radhakrishnan and Hindmarsh, 1993). Gear methods (Gear, 1971) are implicit and employ backwards-differentiation formulae to step forward in time by taking multiple steps. The converged solutions at each step are saved in a history matrix and used to predict the next solution. Thus, LODE must initially take short time steps to build the history matrix and may then take progressively longer steps. LODE is most efficient for long integration times (and inefficient for short integration times) and therefore least burdensome for coarse grid model applications that have relatively long coupling times between gas-phase chemistry and other processes, e.g., advection.

User-supplied information required by LODE is essentially the error control parameters and the functions defining the system of ODEs, $\mathbf{f}(\mathbf{y},t)$, where \mathbf{y} is the vector of species concentrations and t is time. Supplying a subroutine to evaluate the time derivatives of species concentrations ($\mathbf{f} = d\mathbf{y}/dt$) is mandatory. Supplying a function to evaluate the Jacobian matrix ($\mathbf{J} = d\mathbf{f}/d\mathbf{y}$) is optional since, if not supplied, LODE can derive a numerical Jacobian by finite difference between repeated evaluations of \mathbf{f} . Supplying an algebraic Jacobian ensures accuracy, although a numerical Jacobian may be equally accurate if adequate precision (e.g., double precision) is employed. Supplying an algebraic Jacobian is more efficient when \mathbf{J} is sparse, but for condensed mechanisms such as CB05 \mathbf{J} is not sparse and the numerical Jacobian method is faster. CAMx uses the numerical Jacobian method with a relative error tolerance of 10^{-7} and an absolute error tolerance of 10^{-10} .

5.1.5.2 EBI Solver

The backward Euler method solves concentrations (\mathbf{y}) as $\mathbf{y}(t+h) = \mathbf{y}(t) + h\mathbf{f}$, where \mathbf{f} is the time derivative of species concentrations ($\mathbf{f} = d\mathbf{y}/dt$) evaluated at $t+h$. The method must be iterated to convergence in $\mathbf{y}(t+h)$ because species concentrations are interdependent. The basic EBI method is not efficient for stiff problems such as tropospheric chemistry because convergence is slow and the step size (h) must be short. Hertel et al. (1993) greatly improved the efficiency and accuracy of the method by developing analytical solutions to the EBI equation for groups of species that are strongly coupled (e.g. HO_x and NO_x/O₃). Time steps of up to 3 minutes are taken by the Hertel EBI solver in CAMx.

5.2 Aerosol Chemistry

The gas-phase chemistry is run alone (no aerosols) by supplying CAMx with a chemistry parameters file with the aerosol option keyword set to "NONE", the number of aerosol species set to zero, and the entire list of aerosol species parameters omitted (see Section 3). Aerosols

are treated by supplying CAMx with a chemistry parameters file with the aerosol keyword set to "INERT", "CF", "CF_SOAP2", "CF_VBS" or "CMU". In all such cases, the number of aerosol species, the number of size sections and their size ranges, and various aerosol parameters are specified. The aerosol keyword "INERT" allows the user to define any number of arbitrarily-named inert particulate species to be carried by the model during a photochemical simulation (e.g., modeling the dispersion of only wind-blown dust).

Aerosol chemistry processes can be run together with gas-phase chemistry using two options for treating aerosol size distributions: the CF scheme and CMU scheme. The CF scheme divides the size distribution into two static modes (coarse and fine). Primary species can be modeled as fine and/or coarse particles, while all secondary (chemically-formed) species are modeled as fine particles only. The CMU scheme employs a sectional approach that dynamically models the size evolution of each primary and secondary aerosol constituent across a number of fixed size sections. The CF and CMU options require a minimum set of specific aerosol species with associated chemistry. Aerosol water is explicitly treated in both CF and CMU options, which affects aerosol size and density.

5.2.1 Additional Gas-Phase Species

When either the CF or CMU aerosol option is selected, the following gas-phase species are added to model gas-aerosol interactions:

- 1) Ammonia (NH₃) as a precursor for inorganic aerosol.
- 2) Hydrogen chloride (HCL) as a product of acidified sea salt aerosol.
- 3) Separately-tracked emitted ("primary") VOCs that form intermediate organic condensable gas (CG) species via oxidation reactions: benzene, toluene, xylene, isoprene, monoterpenes, sesquiterpenes, and intermediate-volatility organic compounds (IVOC).
- 4) Several intermediate CG species that may condense to secondary organic aerosol (SOA) or are products of SOA volatilization.

5.2.2 Aerosol Processes

Aerosol chemical and thermodynamic processes include the following:

- 1) Aqueous sulfate and nitrate formation in resolved cloud water using the RADM aqueous chemistry algorithm (Chang et al., 1987) with updated SO₂ oxidation reaction rates and metal-catalyzed oxidation mechanism (Ibusuki and Takeuchi, 1987; Martin and Good, 1991; Jacobson, 1997); aqueous formation of SOA from glyoxal, methyl glyoxal and glycolaldehyde (Ortiz-Montalvo et al., 2012; Lim et al., 2013) is also handled by the RADM module.
- 2) Partitioning of inorganic aerosol constituents (sulfate, nitrate, ammonium, and natural minerals) between the gas and aerosol phases using the ISORROPIA thermodynamic module (Nenes et al., 1998, 1999); uptake of SO₂ and HNO₃ onto crustal aerosols and subsequent conversion to sulfate and nitrate aerosol is calculated outside of ISORROPIA.

- 3) Organic aerosol-gas partitioning and oxidation chemistry using two options:
 - a. A semi-volatile equilibrium scheme called SOAP (Strader et al., 1999) that forms a condensed "organic solution phase";
 - b. A hybrid 1.5-dimension volatility basis set (1.5-D VBS) approach (Koo et al., 2014) providing a unified framework for gas-aerosol partitioning and chemical aging of both primary and secondary organic aerosols.

Organic aerosol treatments are described in more detail in separate sub-sections below.

Aqueous chemistry is not explicitly applied to sub-grid clouds; clouds are assumed to either occupy the entirety of a grid cell volume, or be completely absent from it. The cell-averaged effect of sub-grid clouds is treated in the CAMx meteorological preprocessors that generate three-dimensional gridded cloud input fields. Cloudy grid cells are determined by cloud liquid water contents above a threshold of 0.05 g/m^3 . Aqueous chemistry is calculated for each cloud grid cell at each model time step.

In cloudy grid cells undergoing aqueous chemistry, the ISORROPIA equilibrium algorithm is called every time step to ensure that rapidly evolving sulfate, nitrate and neutralizing cations are in balance with the local environment. In cloud-free grid cells, ISORROPIA is called on a unique aerosol "coupling" time step that is defined within the chemistry parameters file. By default, the aerosol coupling time step is 15 minutes, and this is used for all master and nested grids in a simulation regardless of the grid-specific driving time step.

Uptake of SO_2 and HNO_3 by mineral dust particles is another potentially important heterogeneous reaction pathway. Gas-phase SO_2 molecules are transported to the surface of crustal aerosols and react with oxidants on the particle surface. The heterogeneous reaction of SO_2 was implemented in CAMx assuming a pseudo first-order reaction with the humidity-dependent uptake coefficient by Zheng et al. (2015). HNO_3 reacts with calcium in soil dust particles to form calcium nitrate. Based on Saharan dust study (Astitha et al., 2009), we estimate about 6% mass fraction of calcium carbonate (CaCO_3) in fine dust particles (FCRS), and half of it is assumed to be replaced by calcium nitrate. Since the current ISORROPIA implementation in CAMx does not consider mineral cations other than sodium, the heterogeneous reactions of SO_2 and HNO_3 are treated external to ISORROPIA.

Table 5-4 shows the inorganic aerosol species that can be included with the CF scheme. Some species must be present for this scheme ("Mandatory Species") to establish linkages between gas and aerosol phase chemistry. Other species are optional (meaning that they can be removed from the chemistry parameters input file), except that sodium and chloride must always be present or absent together (i.e., one cannot be present without the other). If sodium and chloride are not modeled then default background values are used within CAMx.

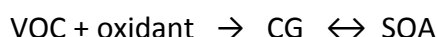
In the CMU scheme, CRST is used to identify all primary inert material, which replaces the CF species FPRM, FCRS, CPRM, and CCRS in Table 5-4. Individual aerosol species names specify both the constituent and the size section using a set naming convention, e.g., PSO_4_1 refers to particle sulfate in size section 1. The CMU scheme requires that the complete list of all aerosol species be present in the chemistry parameters file (i.e., no aerosol species are optional).

Table 5-4. List of inorganic PM species for the CAMx CF aerosol option.

Internal Label	Name	Mandatory Species
PSO4	Sulfate	X
PNO3	Particulate Nitrate	X
PNH4	Particulate Ammonium	X
PH2O	Aerosol Water Content	X
NA	Sodium	
PCL	Particulate Chloride	
PEC	Primary Elemental Carbon	
FPRM	Fine Other Primary (diameter≤2.5 μm)	
FCRS	Fine Crustal (diameter≤2.5 μm)	
CPRM	Coarse Other Primary	
CCRS	Coarse Crustal	

5.2.2.1 SOAP

SOAP is the default SOA chemistry/partitioning module when the aerosol keyword is set to "CF", "CF_SOAP2" or "CMU" in the chemistry parameters input file. Directly emitted (primary) organic aerosol is treated by SOAP as a single non-volatile species called POA that does not chemically evolve. However, POA does influence the evolution of SOA. SOA species exist in equilibrium with condensable gasses (CG) that can be produced by VOC oxidation:



The SOAP module consists of two parts: gas-phase oxidation chemistry that forms CG products, and equilibrium partitioning between gas and aerosol phases for each CG/SOA pair. CG formation from VOC oxidation reactions is handled within the SOAP module rather than the main gas-phase chemistry, as described below. This approach has the following advantages: (1) it separates the VOC precursors and lumping schemes for oxidant chemistry and SOA formation (e.g., for aromatics, different lumping schemes may be appropriate for oxidant and SOA formation); (2) it allows the same SOA mechanism to be used with different oxidant mechanisms; (3) it allows inclusion of SOA precursors without explicitly defining oxidant reactions (e.g., sesquiterpenes are explicit in the SOA module but their oxidant formation may be represented by surrogate species).

Each precursor produces three CG species: more-volatile, less-volatile and non-volatile products. The more- and less-volatile CG products from all anthropogenic precursors are lumped to CG1 and CG2, respectively. The CG products from all biogenic precursors are similarly lumped to CG3 and CG4. No CG is needed to represent non-volatile products as they are instantly condensed to form SOA (SOPA and SOPB from anthropogenic and biogenic precursors, respectively). The physical properties of the SOAP species are shown in Table 5-5.

Polymerization reactions in organic aerosol phases will increase the molecular weight of the condensed aerosol and reduce the volatility. Detailed descriptions of polymerization depend upon the chemical composition of the organic and inorganic aerosol phases (e.g., aerosol acidity). SOAP assumes that semi-volatile SOAs are polymerized to form non-volatile SOAs

Table 5-5. SOA parameters for SOAP

SOA species	VOC precursor	Aerosol mass yield ¹	C* [$\mu\text{g}/\text{m}^3$] at 298K	$\Delta\text{H}^{\text{vap}}$ [kJ/mol]	MW [g/mol]
SOA1	Benzene	0 / 0.605	48	20	150
	Toluene	0 / 0.137			
	Xylene	0 / 0.093			
	IVOC	0 / 0			
SOA2	Benzene	0 / 0.036	1.6	24	150
	Toluene	0 / 0.064			
	Xylene	0 / 0.036			
	IVOC	0.224 / 0.200			
SOPA	Benzene	0.37 / 0.019	0	-	220
	Toluene	0.30 / 0			
	Xylene	0.36 / 0.00006			
	IVOC	0.348 / 0.183			
SOA3	Isoprene	0.209	140	24	180
	Monoterpene	0.626			
	Sesquiterpene	1.885			
SOA4	Isoprene	0.035	2.9	57	180
	Monoterpene	0.062			
	Sesquiterpene	0.431			
SOPB	Isoprene	0.004	0	-	220
	Monoterpene	0			
	Sesquiterpene	0			

¹ Mass-based yields of CG products from VOC precursors (low-NOx yield / high-NOx yield)

(SOPA and SOPB) with a half-life of 20 hours (Kalberer et al., 2004). In-cloud SOA formation by the RADM module is added to SOPB. Total SOA is the sum of SOA1-4 plus SOPA and SOPB. Total organic aerosol is the sum of total SOA and the single POA species.

CAMx provides an alternative set of SOA parameters based on new aerosol yield data that corrects for vapor wall losses in smog chamber experiments (Zhang et al., 2014; Hodzic et al., 2016). This option is enabled by the aerosol keyword "CF_SOAP2" in the chemistry parameters input file. With this option, water solubility of the CG species is enhanced based on a new parameterization of volatility-dependent Henry's law constants (Hodzic et al., 2014; Knote et al., 2015), and polymerization of biogenic SOA is disabled assuming that the biogenic SOA polymerization has already been accounted for in the new yield data. Table 5-6 presents the alternative SOA parameters for SOAP2.

Emissions of SOA precursors must be provided separately from the emissions of oxidant (CB or SAPRC) precursors, e.g., isoprene emissions must be speciated both as ISOP for oxidant chemistry and ISP for SOA chemistry. This "double counting" of emissions is correct because the species (e.g., ISOP and ISP) serve different purposes. Ideally, emissions processors will develop VOC speciation schemes that suit both oxidant and SOA modeling. In the absence of more refined information, emissions of SOA precursors may be set equal to emissions of oxidant precursors as follows: ISP = ISOP; TRP = TERP; BNZA = BENZ; TOLA = TOL or ARO1; XYLA = XYL or ARO2. SOAP also models SOA formation from anthropogenic IVOC precursors (IVOA). However, current emission inventories are generally missing IVOC emissions. Users can omit

Table 5-6. SOA parameters for SOAP2

SOA species	VOC precursor	Aerosol mass yield ¹	C* [$\mu\text{g}/\text{m}^3$] at 300K	$\Delta\text{H}^{\text{vap}}$ [kJ/mol]	MW [g/mol]
SOA1	Benzene	0.487 / 0.248	14	116	150
	Toluene	0.663 / 0.304			
	Xylene	0.291 / 0.084			
	IVOC	0 / 0.012			
SOA2	Benzene	0.167 / 0.391	0.31	147	150
	Toluene	0.345 / 0.293			
	Xylene	0.306 / 0.049			
	IVOC	0.275 / 0.225			
SOPA	Benzene	0 / 0	0	-	220
	Toluene	0.262 / 0.044			
	Xylene	0.294 / 0.025			
	IVOC	0.277 / 0.129			
SOA3	Isoprene	0.156 / 0.076	26	118	180
	Monoterpene	0.140 / 0.155			
	Sesquiterpene	0.136 / 0.092			
SOA4	Isoprene	0.029 / 0.023	0.45	123	180
	Monoterpene	0.281 / 0.156			
	Sesquiterpene	0.400 / 0.328			
SOPB	Isoprene	0.011 / 0	0	-	220
	Monoterpene	0.124 / 0.029			
	Sesquiterpene	0.270 / 0.175			

¹ Mass-based yields of CG products from VOC precursors (low-NOx yield / high-NOx yield)

them or estimate them from total non-methane organic compound (NMOC) emissions as described in the next section.

Some emitted VOCs are semi-volatile (SVOCs) and can condense directly to SOA, e.g., biogenic emissions of oxygenated VOCs. SOA formation from SVOC emissions may be accounted for by including the SVOC in the CAMx emissions as one of the CGs listed in Table 5-6. Choose a CG that has appropriate volatility properties, and account for any molecular weight difference between the SVOC and surrogate CG (moles CG emitted = moles SVOC \times MW_{SVOC}/MW_{CG}).

5.2.2.2 1.5-D VBS

The VBS organic aerosol (OA) chemistry/partitioning module is selected when the aerosol keyword is set to "CF_VBS" in the chemistry parameters input file. VBS works with the 2-mode CF size option but is not currently compatible with the CMU sectional size option.

The VBS approach (Donahue et al., 2006; Robinson et al., 2007) provides a unified framework for gas-aerosol partitioning and chemical aging¹ of both POA and SOA. It uses a set of semi-volatile OA species with volatility equally spaced in a logarithmic scale (the basis set). VBS member species are allowed to react further in the atmosphere (chemical aging) to describe volatility changes (i.e., shifting between volatility bins). First generation VBS models use one-dimensional basis sets (1-D VBS) wherein organic compounds are grouped only by volatility and thus are unable to describe varying degrees of oxidation observed in atmospheric OA of similar volatility. To overcome this shortcoming, a two dimensional VBS (2-D VBS) was developed where organic compounds are grouped by oxidation state as well as volatility (Donahue et al.,

2011, 2012). However, use of 2-D VBS in a 3-D PGM has been limited due to high computational cost.

A hybrid VBS approach is implemented in CAMx, called 1.5-D VBS, which combines the simplicity of the 1-D VBS with the ability to describe evolution of OA in the 2-D space of oxidation state and volatility (Koo et al., 2014). Figure 5-2 shows a schematic diagram of the 1.5-D VBS scheme currently implemented in CAMx. This scheme uses five basis sets to describe varying degrees of oxidation in ambient OA: two basis sets for chemically aged oxygenated OA (OOA; anthropogenic and biogenic) and three for freshly emitted OA (hydrocarbon-like OA [HOA] from meat-cooking and other anthropogenic sources and biomass burning OA [BBOA]).

Each basis set has five volatility bins ranging from 10^{-1} to 10^3 $\mu\text{g m}^{-3}$ in saturation concentration (C^*), which roughly covers the volatility range of semi-volatile organic compounds (SVOCs). An effective heat of vaporization (ΔH^{vap}) value of 35 kJ mole^{-1} is used for all SOA species. For POA, ΔH^{vap} is estimated using the following empirical formulas:

$$\Delta H^{\text{vap}} = -4 \log_{10}(C_{298\text{K}}^*) + 85 \text{ kJ mole}^{-1} \quad (\text{For biomass burning; May et al., 2013c})$$

$$\Delta H^{\text{vap}} = -11 \log_{10}(C_{298\text{K}}^*) + 85 \text{ kJ mole}^{-1} \quad (\text{For other primary; Ranjan et al., 2012})$$

Table 5-7 lists the model OA compounds assigned to the volatility bins. Their molecular structures were determined by placing them on the 2-D volatility space defined by Donahue et al. (2011, 2012). The 1.5-D VBS scheme adjusts oxidation state as well as volatility in response to chemical aging by simplifying the 2-D VBS model. Chemical aging of SOA and oxygenated POA is modeled by shifting OA mass along a pre-defined pathway of the OOA basis set, which reduces volatility while increasing oxidation state. POA aging, which would require different pathways from the HOA (or BBOA) basis set to the OOA basis set, is simplified in this 1.5-D VBS scheme where oxidation products of POA are represented as a mixture of POA and OPOA in the next lower volatility bins. The gas-phase OH reaction rates for POA and anthropogenic SOA are assumed to be 4×10^{-11} and $2 \times 10^{-11} \text{ cm}^3 \text{ molecule}^{-1} \text{ s}^{-1}$, respectively. Aging of biogenic SOA is disabled in our implementation based on previous modeling studies that found aging biogenic SOA led to a significant over-prediction of OA in rural areas (Lane et al., 2008; Murphy and Pandis, 2009). Additional details on the 1.5-D VBS model can be found elsewhere (Koo et al., 2014; Hildebrandt Ruiz et al., 2015). Total OA is the sum of all OA in the five volatility bins from primary formation (PAP + PCP + PFP) and from secondary formation (PAS + PBS).

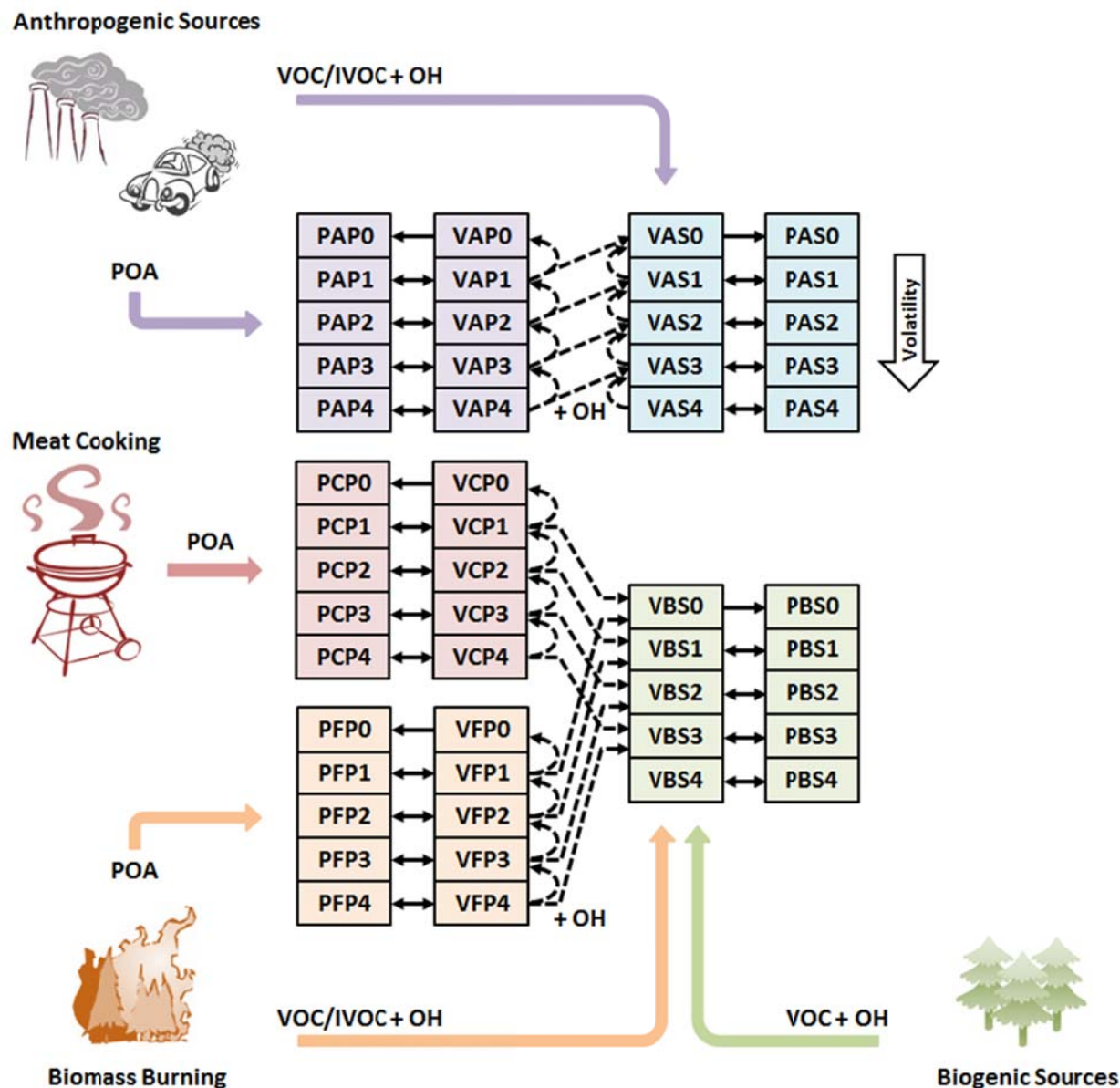


Figure 5-2. Schematic diagram of the CAMx VBS module. The model VBS species name consists of 4 characters that indicate the phase (P – particle; V – vapor), the source (A – anthropogenic; B – biogenic; C – cooking; F – fire), the formation (P – primary; S – secondary), and the volatility bin number. The solid and dashed arrows represent gas-aerosol partitioning and chemical aging, respectively. The thick colored arrows represent POA emissions or oxidation of SOA precursors.

Table 5-7. Molecular properties of the 1.5-D VBS species.

Basis Set	Model Species Name ^a	C* ^b ($\mu\text{g m}^{-3}$)	$\overline{\text{OS}}_c$ ^c	C #	O #	MW (g mole ⁻¹)	OA/OC
OOA	PAS0 & PBS0	0 ^d	0.102	7	4.90	172	2.05
	PAS1 & PBS1	1	-0.188	7.25	4.38	167	1.92
	PAS2 & PBS2	10	-0.463	7.5	3.84	163	1.81
	PAS3 & PBS3	100	-0.724	7.75	3.30	158	1.70
	PAS4 & PBS4	1000	-0.973	8	2.74	153	1.59
HOA	PAP0 & PCP0	0 ^d	-1.52	17	2.69	278	1.36
	PAP1 & PCP1	1	-1.65	17.5	2.02	275	1.31
	PAP2 & PCP2	10	-1.78	18	1.34	272	1.26
	PAP3 & PCP3	100	-1.90	18.5	0.632	268	1.21
	PAP4 & PCP4	1000	-2.00	19	0.0	266	1.17
BBOA	PFPO	0 ^d	-0.704	10	4.32	205	1.71
	PFP1	1	-1.02	11	3.60	208	1.58
	PFP2	10	-1.29	12	2.85	211	1.47
	PFP3	100	-1.52	13	2.08	213	1.37
	PFP4	1000	-1.73	14	1.27	215	1.28

a: See Figure 5-2 for the model species naming convention.

b: Effective saturation concentration.

c: Average oxidation state of carbon.

d: Properties of the lowest volatility bins were estimated assuming $C^* = 0.1 \mu\text{g m}^{-3}$, but they actually represent all OA with $C^* \leq 0.1 \mu\text{g m}^{-3}$, and are treated as non-volatile in the model.

Table 5-8 lists input emission species users need to prepare for the 1.5-D VBS OA scheme. In addition to the traditional anthropogenic and biogenic VOC precursors as used by SOAP, source-specific IVOC emissions need to be provided. The CAMx VBS scheme allocates POA emissions from five source types to the PAP, PCP, and PFP species based on emission factors (Table 5-9) determined from laboratory experiments. VBS uses source-specific volatility distribution factors for gasoline vehicles (POA_GV), diesel vehicles (POA_DV), meat cooking (POA_MC), and biomass burning (POA_BB) based on recent chamber studies (May et al., 2013a,b,c; Woody et al., 2015). For other POA emissions (POA_OP), VBS applies distribution factors estimated by Robinson et al. (2007).

Emissions of intermediate-volatility organic compounds (IVOCs; $10^4 \leq C^* \leq 10^6$) make important contributions to OA in the atmosphere but generally are missing from emission inventories because neither VOC nor POA emission factors account for IVOCs. A pre-processor (PREPVBS) can be used to map source-specific POA emissions to the five distinct POA emission species for VBS, and to scale IVOC emissions from total non-methane organic compound (NMOC) emissions based on smog chamber data (Jathar et al., 2014).

Table 5-8. Input species for 1.5-D VBS scheme.

Species	Description	Notes
TOLA	Toluene	Anthropogenic VOC precursors
XYLA	Xylene	
BNZA	Benzene	
ISP	Isoprene	Biogenic VOC precursors
TRP	Monoterpenes	
SQT	Sesquiterpenes	
IVOG	IVOC from gasoline engines	IVOC precursors
IVOD	IVOC from diesel engines	
IVOA	IVOC from other anthropogenic sources	
IVOB	IVOC from biomass burning	
POA_GV	POA from gasoline vehicles	POA precursor emissions assigned to PAP and PFP modeled species
POA_DV	POA from diesel vehicles	
POA_MC	POA from meat cooking	
POA_OP	POA from other anthropogenic sources	
POA_BB	POA from biomass burning	

Table 5-9. Volatility distribution factors used to allocate POA emissions from five different source types to the five PAP, PCP, and PFP volatility bins.

POA species	Emission Fraction for volatility bin with C* of				
	0	1	10	100	1000
POA_GV	0.27	0.15	0.26	0.15	0.17
POA_DV	0.03	0.25	0.37	0.24	0.11
POA_MC	0.35	0.35	0.1	0.1	0.1
POA_OP	0.09	0.09	0.14	0.18	0.5
POA_BB	0.2	0.1	0.1	0.2	0.4

5.2.3 Aerosol Sectional Approach

Unlike the CF scheme, where each species is represented by a single particle size, the CMU scheme institutes an additional step to distribute the bulk aerosol concentrations from the aqueous/aerosol chemistry modules into each size bin. For inorganic aerosol species, ISORROPIA yields the bulk aerosol composition at equilibrium. The aerosol size distribution is then determined by distributing the change in aerosol mass during the time step into each size bin using a weighting factor (Pandis et al., 1993). The fraction $f_{i,k}$ of total flux of species i between gas and aerosol phases that condenses onto or evaporates from an aerosol size section k is given by,

$$f_{i,k} = \frac{2\pi N_k d_k D_i (c_i - c_i^{eq}) / (\beta_k + 1)}{\sum_k 2\pi N_k d_k D_i (c_i - c_i^{eq}) / (\beta_k + 1)}$$

where N_k and d_k are the number and mean diameter of particles in the section k , respectively, D_i , c_i , and c_i^{eq} are the diffusivity, bulk gas-phase concentration, and equilibrium concentration at the particle surface of species i , respectively, $\beta_k = 2\lambda / ad_k$, λ is the mean free path of air, and a is

the accommodation coefficient (Pandis et al., 1993). Assuming that c_i^{eq} is independent of particle size, the fraction is reduced to,

$$f_{i,k} = \frac{N_k d_k / (\beta_k + 1)}{\sum_k N_k d_k / (\beta_k + 1)} = f_k.$$

The above weighting factor then depends on the surface area only.

For organic aerosols, SOAP calculates the bulk equilibrium composition. Using the pseudo-ideal solution assumption (Strader et al., 1999), the effect of chemical composition of the particle can be incorporated into the weighting factor:

$$f_{i,k} = \frac{N_k d_k (c_i - x_{i,k} c_i^*) / (\beta_k + 1)}{\sum_k N_k d_k (c_i - x_{i,k} c_i^*) / (\beta_k + 1)}.$$

where $x_{i,k}$ is the mole fraction of species i in the section k and c_i^* is the effective saturation concentration of species i . Since the fraction determines the composition of each size section, the above equation should be solved iteratively at each time step. Assuming that the chemical composition changes slowly during a time step, however, the mole fractions can be approximated with those from the previous time step (Koo et al., 2003).

For cloud/fog droplets, RADM is used to calculate sulfate, nitrate and SOA formation in the bulk aqueous phase. The added mass is then distributed into each size bin by a weighting factor which is based on the size-resolved aqueous chemistry model simulation results (Fahey and Pandis, 2001).

In addition, mathematical descriptions of nucleation and coagulation have been added to the CMU scheme. The nucleation model employs the nucleation rate parameterization proposed by Russell et al. (1994). The model assumes a linear sulfuric acid vapor concentration variation for the given time step of the aerosol module based on the initially available sulfuric acid and assigns all the nucleated mass to the first section of the distribution. The coagulation rate of the aerosol particles is modeled according to Seinfeld and Pandis (1998). A high-resolution distribution is used for the coagulation calculations by subdividing each section of the original distribution into 3 additional sections.

5.3 Mercury Chemistry

Mercury exists in the atmosphere as elemental mercury, Hg(0), and oxidized mercury, Hg(II) (Schroeder and Munthe, 1998). Hg(II) can be inorganic (e.g., mercuric chloride, HgCl₂) or organic (e.g., methyl mercury, MeHg). It can also be present as particulate mercury (e.g., mercuric oxide, HgO, or mercury sulfide, HgS). In the global atmosphere, Hg(0) is the dominant form. Hg(II) typically constitutes a few percent of total mercury and is predominantly in the gas phase. MeHg concentrations in the atmosphere are negligible, about a factor of 10 to 30 lower than Hg(II) concentrations, based on analysis of precipitation samples conducted by Frontier

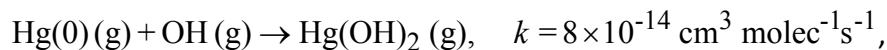
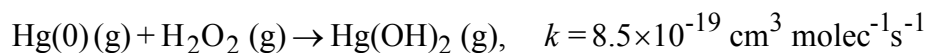
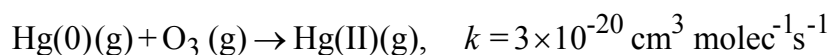
Geosciences, Inc. (e.g., Seigneur et al., 1998). However, Hg(II) becomes methylated in water bodies, where it can bioaccumulate in the food chain. Hg(0) is sparingly soluble and is not removed significantly by wet deposition; its dry deposition velocity is also believed to be low. As a result, Hg(0) has a long atmospheric lifetime, on the order of several months, that is governed by its oxidation to Hg(II). On the other hand, Hg(II) is quite soluble; it is consequently removed rapidly by wet and dry deposition processes. Particulate mercury, Hg(p), is mostly present in the fine fraction of particulate matter (PM_{2.5}), although some Hg(p) may be present in coarse PM (e.g., Landis and Keeler, 2002).

Known transformations among inorganic mercury species include the gas-phase oxidation of Hg(0) to Hg(II), the aqueous-phase oxidation of Hg(0) to Hg(II), the aqueous-phase reduction of Hg(II) to Hg(0), various aqueous-phase equilibria of Hg(II) species, and the adsorption of Hg(II) to PM in both the gas-phase and aqueous-phase. The inorganic mercury chemistry modules implemented in CAMx are based on our current knowledge of these transformations. However, it should be noted that our knowledge of mercury chemistry continues to evolve as new laboratory data become available, and the Hg chemical kinetic mechanisms in CAMx and other models that treat the atmospheric fate of mercury will need to be revised accordingly.

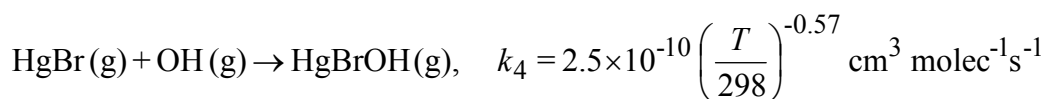
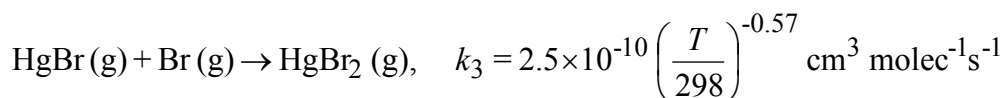
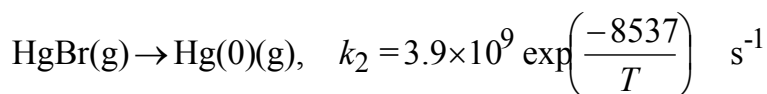
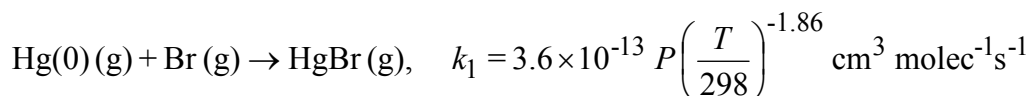
Below, we provide additional details on the gas- and aqueous-phase mercury chemistry mechanisms implemented in CAMx, and the implementation approach.

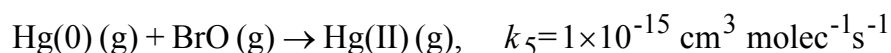
5.3.1 Gas-Phase Chemistry

The gas-phase transformations include the oxidation of Hg(0) to Hg(II) by ozone (O₃) (Hall, 1995), hydrogen peroxide (H₂O₂) (Tokos et al., 1998) hydroxyl radicals (OH) (Sommar et al., 2001; Pal and Ariya, 2003; 2004), bromine (Br) (Ariya et al., 2002), and hypobromite (BrO) (Raofie and Ariya, 2003). The oxidation of Hg(0) by O₃, H₂O₂, and OH are given by the following three reactions:



while oxidation by Bromine is based on a sequence of 5 reactions (Seigneur and Lohman, 2008):





The reaction rate constants provided above are for temperatures in the range of 20 to 25°C; no temperature dependence information is available. For the bromine reactions, T is the temperature in degrees Kelvin, and P is the pressure in atmospheres. The five reactions are treated as a single reaction, with an effective Hg(0) first-order rate constant that is a function of the individual reaction rates and the concentrations of Br, BrO and OH based on the assumption that Br, BrO and OH concentrations don't change by their reactions with mercury. This treatment is similar to that of Holmes et al. (2006), who considered the oxidation of Hg(0) by bromine atoms with a set of three reactions. The effective first-order rate constant is calculated by the following expression:

$$k_{\text{eff}} = \frac{k_1 [\text{Br}] (k_3 [\text{Br}] + k_4 [\text{OH}])}{k_2 + k_3 [\text{Br}] + k_4 [\text{OH}]} + k_5 [\text{BrO}] \quad \text{s}^{-1}$$

5.3.2 Adsorption of Hg(II) on PM

In the first implementation of mercury in CAMx, Hg(II) adsorption on PM was considered only in the aqueous phase (see below), using an adsorption coefficient derived from available experimental data (Seigneur et al., 1998; Ryaboshapko et al., 2002). It is essential to also consider the adsorption of gaseous Hg species to PM because gas/particle conversion also affects Hg deposition (Lindberg et al., 2007). Rutter and Schauer (2007a) reported results of laboratory work measuring the adsorption of reactive gaseous mercury (RGM) to atmospheric and synthetic particles as a function of temperature. Their experimental results suggest that surface area rather than PM mass controls the partitioning process. They reported three surface-area adsorption coefficients for urban PM (collected in Milwaukee, WI, and Riverside, CA), ammonium sulfate and adipic acid, respectively. They expressed the surface-area adsorption coefficient (K_{sa}) as follows:

$$K_{sa} = \text{Hg}_{p,ads} / (\text{RGM} \cdot A_{sp} \cdot \text{PM})$$

where K_{sa} is in $\text{m}^3 \text{m}^{-2}$, $\text{Hg}_{p,ads}$ and RGM are in pg m^{-3} , A_{sp} is the specific surface area of ambient PM in $\text{m}^2 \mu\text{g}^{-1}$ and PM is the ambient urban PM concentration in $\mu\text{g m}^{-3}$. Here, $\text{Hg}_{p,ads}$ refers only to the adsorbed RGM, i.e., it does not include non-volatile primary particulate mercury. Rutter and Schauer (2007a) also found that the K_{sa} obtained for urban PM falls between that of ammonium sulfate (more RGM adsorption) and adipic acid (less RGM adsorption). Their laboratory experiments lead to the following value for K_{sa} as a function of temperature (in K) for adsorption to urban PM:

$$K_{sa} = 10^{(4250/T - 10)} \quad (1)$$

Rutter and Schauer's (2007b) experimental results also show a ten-fold increase in adsorption of RGM to sodium chloride compared to ammonium sulfate and organic particulate compounds

(a larger increase was observed for sodium nitrate). Thus, the adsorption coefficient for RGM adsorption to sea-salt is about 10 times that for urban PM:

$$K_{sa} = 10^{(4250/T-9)} \quad (2)$$

Following the approach used in Vijayaraghavan et al. (2008), we treat all non-sea-salt PM as urban PM for simplicity and use Equation (1) to simulate RGM adsorption to all non-sea-salt PM. The adsorption to sea-salt PM is calculated using Equation (2). Thus, the effective adsorption coefficient for each aerosol size section is calculated as:

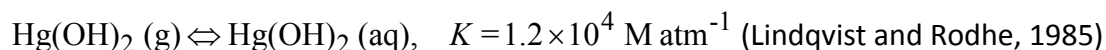
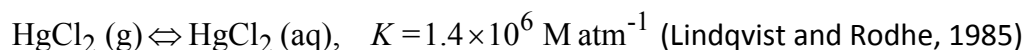
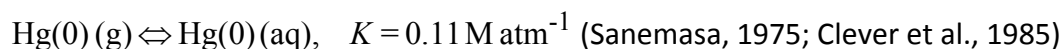
$$K_{sa,eff} = 10^{(4250/T-9)} F_{ss} + 10^{(4250/T-10)} (1 - F_{ss})$$

where F_{ss} is the fraction of sea-salt in that size section. In the CAMx implementation, we assume that RGM is adsorbed on primary fine and coarse PM.

5.3.3 Aqueous-Phase Chemistry

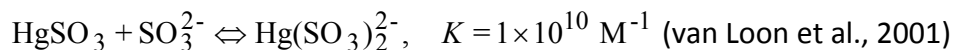
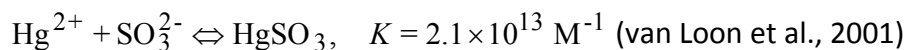
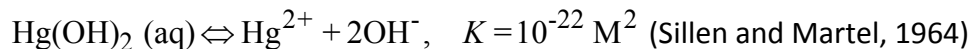
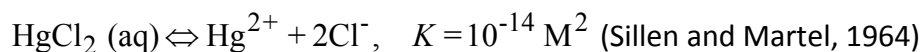
The aqueous-phase chemistry includes the reduction of Hg(II) to Hg(0) via reaction with hydroperoxy radicals (HO_2) and by the formation of the sulfite complexes (at low HCl concentrations), HgSO_3 and $\text{Hg}(\text{SO}_3)_2^{2-}$, as well as the oxidation of Hg(0) to Hg(II) by dissolved O_3 , OH, and Cl_2 . Adsorption of Hg(II) species on atmospheric particulate matter (PM) is simulated using an adsorption coefficient ($K = 34 \text{ L g}^{-1}$) recommended by Seigneur et al. (1998). The relevant reactions are listed below. Note that the gas-liquid equilibria and ionic equilibria of the non-mercury species (e.g., SO_2 , O_3) involved in the mercury aqueous-phase chemistry are not shown here, since they are identical to those in the other CAMx mechanisms.

5.3.2.1 Gas-liquid Equilibria

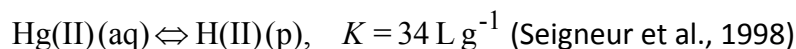


The Henry's Law constants listed above are for temperatures in the range of 20 to 25°C. Temperature dependence information is available for the Hg(0) Henry's Law constant but the validity of this information for temperatures below 0°C is not established.

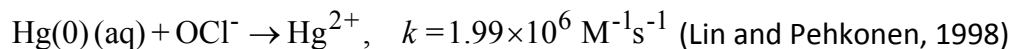
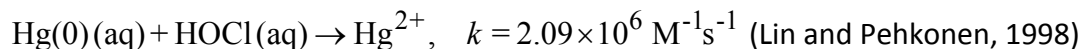
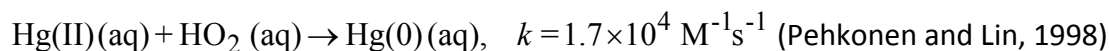
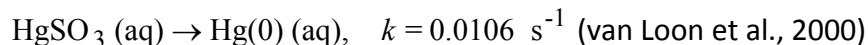
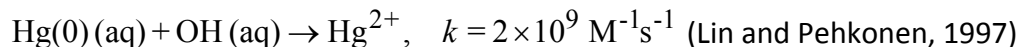
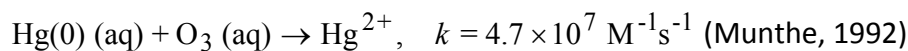
5.3.2.2 Aqueous-phase Equilibria



5.3.2.3 Adsorption of Hg(II) on PM in the Aqueous Phase



5.3.2.4 Aqueous-phase Kinetics



In the last two reactions listed above, HOCl and OCl⁻ come from the dissolution and subsequent dissociation of molecular chlorine (Cl₂). Note that Hg(II) (aq) refers to all divalent Hg species in solution (i.e., Hg²⁺ + HgCl₂(aq) + Hg(OH)₂(aq) + HgSO₃ + Hg(SO₃)₂²⁻). The rate constants listed for the aqueous-phase kinetics are for temperatures in the range of 20 to 25°C. Temperature dependence information is available for the HgSO₃ reduction reaction.

As mentioned previously, the gas- and aqueous-phase Hg transformations presented above represent the state of the science from a decade ago (Ryaboshapko et al., 2002; Seigneur et al., 2001a, 2004) and our knowledge of mercury chemistry continues to evolve. For example, Gardfeldt and Johnson (2003) challenged the aqueous-phase reduction of Hg(II) to Hg(0) by dissolved HO₂, suggesting that this pathway is unimportant. There also seems to be some circumstantial evidence of reduction of Hg(II) to Hg(0) in power plant plumes from various experimental studies that is not accounted for in current treatments of Hg chemistry (e.g., Edgerton et al., 2001; Seigneur et al., 2001b). Additional details are provided in a scoping study for mercury deposition conducted for the Midwest Regional Planning Organization by Seigneur et al. (2003).

5.3.4 Implementation Approach

The approach used to implement the mercury transformation pathways, discussed above, into CAMx is based on the assumption that the mercury species concentrations are much smaller than those of the species with which they react. Thus, the concentrations of the non-mercury species can be assumed to be constant during the mercury chemistry calculations and analytical solutions are available for both the gas-phase and aqueous-phase conversions.

The mercury chemistry discussed in the previous sections requires the concentrations of the following non-mercury species: O₃, H₂O₂, OH, SO₂, HO₂, Cl₂, HCl, Br, BrO and atmospheric particulate matter (PM). The concentrations of most of these species are available from CAMx. However, the halogen compounds Cl₂, Br, and BrO are only included for one specific gas-phase

mechanism (CB6r2h, Mechanism 3) and otherwise not explicitly simulated. Since the mercury chemistry is currently not linked to any halogens that might be available from the gas-phase chemistry, we specify typical vertical profiles of Cl_2 , Br, and BrO concentrations. The Cl_2 concentrations are prescribed to be non-zero over oceans and zero elsewhere. Also, daytime Cl_2 concentrations are lower than nighttime values to account for the fact that Cl_2 is photolyzed during the day. The zenith angle is used for the determination of night/day. A 2-D array of integer values (1 if ocean, 0 if not) is used to determine if the grid column is predominantly over ocean. This array is initialized at the beginning of the simulation from an input file and is specific for the modeling domain and grid. For Br and BrO, vertical profiles over land and ocean are prescribed, with higher values over ocean than over land. During the night, the concentrations of these species are assumed to be zero, since the photolysis of Br_2 is the primary source for these radicals.

The mercury aqueous-phase chemistry module also requires the specification of cloud liquid water content (LWC) and cloudwater pH. Both these variables are available from CAMx – the mercury aqueous-phase chemistry module is invoked after the CAMx PM aqueous-phase chemistry calculations are performed, so the cloudwater pH has already been calculated. Note that the PM aqueous-phase module (based on the RADM aqueous-phase chemistry module that is also used in Models-3/CMAQ) does not explicitly simulate the cloud chemistry of OH and HO_2 radicals. The concentrations of these radicals can be reduced by their heterogeneous chemistry within clouds (e.g., Jacob, 2000; Jaegle et al., 2001). In the CAMx implementation, we account for this by reducing the concentrations of OH and HO_2 radicals by factors of 2 and 10, respectively.

5.3.5 Chemistry Parameters for Mercury

The mercury chemistry module requires total PM concentrations, so mercury can only be modeled in conjunction with PM chemistry. Mercury chemistry is selected by including mercury species among the list of modeled species. The CAMx mercury species names are:

- HG0 – elemental gaseous mercury, or Hg(0)
- HG2 – reactive gaseous mercury, or Hg(II)
- HGP – primary particulate mercury, or Hg(P)
- HGIIP – reactive gaseous mercury, or Hg(II) adsorbed onto fine PM
- HGIIPC – reactive gaseous mercury, or Hg(II) adsorbed onto coarse PM

CAMx requires that all five or none of these species be included in a simulation. Therefore, mercury chemistry is not required for PM modeling, but if mercury chemistry is selected then all five mercury species must be modeled. All of the rate constants and equilibrium constants for the mercury chemistry module are hard-coded and so no mercury reaction rate data are included in the chemistry parameters input file (see Section 3). This is similar to the RADM aqueous chemistry and ISORROPIA inorganic aerosol equilibrium modules.

Several physical properties of the mercury species must be specified on the chemistry parameters file (see Figure 3-3a). The physical properties specified for the gas species (Henry's Law, molecular weight, surface reactivity) influence the deposition characteristics. The Henry

constant for HG2 is assumed to be similar to that of HNO_3 because these two gases have similar solubility. The HG2 species represents HgCl_2 and $\text{Hg}(\text{OH})_2$; the Henry constant for the former is $1.4 \times 10^6 \text{ M atm}^{-1}$ and for the latter it is $1.2 \times 10^4 \text{ M atm}^{-1}$. The surface resistance factor is set to zero for strong acids, such as HNO_3 , that have a strong tendency to stick to surfaces – this forces the surface resistance calculated in the dry deposition algorithms to zero. The reactivity parameter for HG2 is set to 0, as for HNO_3 .

The dry deposition of HG0 is set to zero by choosing a very low Henry constant (similar to CO). This is based on the assumption that natural emissions and dry deposition of HG0 balance each other over the modeling domain. This assumption is justified by the fact that the atmospheric lifetime of HG0 (about 1 year) greatly exceeds its residence time (days to weeks) within a regional modeling domain. If natural emissions of HG0 are not included in the mercury emissions inventory, the dry and wet deposition of HG0 should be zero by setting a Henry constant of smaller than $1 \times 10^{-8} \text{ M atm}^{-1}$. However, if natural emissions of $\text{Hg}(0)$ are used in the CAMx simulation, the Henry constant should be set to 0.111 with a temperature factor of -4970 K (Clever et al., 1985).

5.4 Simple Chemistry Via Mechanism 10

The chemical mechanisms in CAMx require significant effort to prepare emissions data and can result in extensive run times. There are many cases when air pollution problems could be investigated with a much simpler chemistry scheme. An example of this would include modeling SO_2 from a few specific sources over a relatively small region, and treating conversion to sulfate by assuming a representative decay rate. CAMx provides an option to configure a simple and flexible scheme that can be used for modeling chemical reactions other than the ozone or secondary PM reactions treated by the full-science mechanisms.

The simple chemistry scheme is selected by specifying 10 for the mechanism ID in the chemistry parameters input file. The user must develop specific chemical reactions and code them into the subroutine `CAMx/chem10.f`; an example subroutine is available in the source code directory. Follow the guidelines in that subroutine to implement your specific set of reactions. This approach requires some knowledge from the user, but also provides complete flexibility.

6. PLUME-IN-GRID SUBMODEL

Photochemistry is a highly non-linear problem because chemical reaction rates among most compounds depend upon their ambient concentrations. In Eulerian air quality models, ambient concentrations depend on how well the modeling grid resolves emissions, transport, and chemical history. Thus, grid resolution plays a vital role in the ability of the model to properly characterize photochemical conditions. Increasing resolution should in theory lead to a better model as the time/space discretization tends toward a continuum. However, practical and theoretical considerations suggest that the lower limit on horizontal grid spacing is about 1000 meters for Eulerian air quality models such as CAMx. Nevertheless, even higher resolution is often necessary to adequately simulate chemistry within concentrated point source plumes.

Plume-in-grid treatments have been developed to track individual plume segments (or puffs) in a Lagrangian sense, accounting for plume-scale dispersion and chemical evolution until such time as puff mass can be adequately represented within the larger grid model framework. Then the puff mass is added to the grid system as a virtual source, and that mass is subsequently carried by the grid model processes. It is important to understand that the inclusion of a Lagrangian puff model within an Eulerian grid model is a forced construct. The formulations among the various modeling approaches are fundamentally different and there is no theoretically "correct" methodology.

The CAMx Plume-in-Grid (PiG) sub-model addresses the size and chemical evolution of point source plumes. Two PiG options are available that vary in their chemical complexity. Both approaches share common design features for puff initialization, puff structure, transport, and growth. They deviate in how they treat chemistry and when they transfer mass from puffs to grid cells. This section details the structure and functionality of both options.

- 1) **GREASD PiG:** The Greatly Reduced Execution and Simplified Dynamics PiG option is aimed at treating the early chemical evolution of large NO_x plumes when mostly inorganic gas-phase reactions are operative. GREASD PiG works with OSAT/PSAT because of the simplified approach employed and because compatibility with source apportionment was an explicit design objective.
- 2) **IRON PiG:** The Incremental Reactions for Organics and NO_x PiG option treats the full suite of gas-phase photochemistry for all types of point sources. Gas-phase chemistry is simulated within each plume segment using an "incremental chemistry" approach (EPRI, 2000), whereby puffs carry the incremental contributions of the puff relative to the grid concentrations. IRON PiG supports the Reactive Tracer (RTRAC) Probing Tool, but it does not work with other Probing Tools and it does not treat PM.

6.1 CAMx PiG Formulation

6.1.1 Basic Puff Structure and Diffusive Growth

Both GREASD and IRON PiG sub-models share a common physical structure and growth algorithm. A stream of plume segments (puffs) is released from a designated point source. Each puff possesses a longitudinal length and directional orientation defined by the separation of a leading and a trailing point. Initial separation of these points is determined by the wind

vector at final plume rise. Each point is then subsequently and independently transported through the gridded wind fields, which directly accounts for puff stretching and changes to centerline orientation due to deforming shears. The "position" of each puff is defined at the center point of each puff between the endpoints, and is used to identify the grid cell in which the puff resides for the calculation of diffusive growth and chemistry.

Like other puff models, the shape of each puff is characterized by a spread tensor, which is defined from a set of Gaussian standard deviations (σ) along the three spatial axes (σ_x , σ_y , σ_z). Diffusive growth is described by the evolution of these values. The total cross-sectional width extends $\pm 1.5\sigma_y$ from puff centerline. Similarly, the total cross-sectional depth extends $\pm 1.5\sigma_z$ from puff centerline (with limits placed on depth by the ground and by capping stable layers aloft). The total longitudinal length is the distance between the puff endpoints with an additional $\pm 1.5\sigma_x$ added in each direction. Horizontal area and total volume are calculated using the formulae for an ellipse. Figure 6-1 presents a schematic representation of each puff in horizontal cross-section.

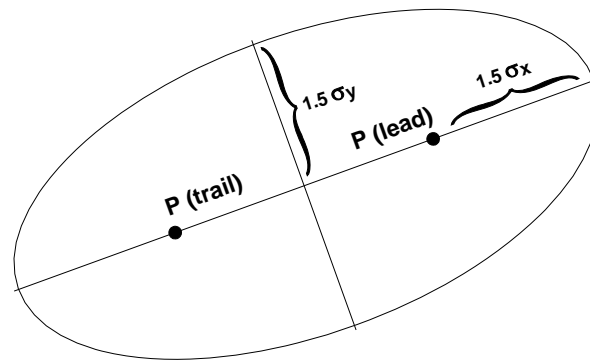


Figure 6-1. Schematic representation of CAMx PiG puff shape in the horizontal plane. Directional orientation of the puff is arbitrary, and evolves according to wind direction, shears and diffusive growth along its trajectory.

PiG puff growth is based on SCICHEM theory and concepts (EPRI, 2000), but includes some simplifications. SCICHEM solves predictive spatial moment equations with second-order closure that relate the evolution of the puff spread tensor ($\sigma_{ij} = \sigma_i \times \sigma_j$) to resolved mean shears and turbulent velocity statistics. The Reynolds-averaged second-moment transport equation is given as

$$\frac{d\sigma_{ij}}{dt} = \sigma_{ik} \frac{\partial \bar{u}_j}{\partial x_k} + \sigma_{jk} \frac{\partial \bar{u}_i}{\partial x_k} + \frac{\langle x'_i \bar{u}'_j c' \rangle}{Q} + \frac{\langle x'_j \bar{u}'_i c' \rangle}{Q}$$

where \bar{u} is the mean wind vector component, the primed values represent turbulent fluctuations from the mean, and the angle brackets denote integrals over space. The Reynolds averaging process always introduces higher-order fluctuation correlations, and this is given by the turbulent flux moments $\langle x'u'c' \rangle$, where $\bar{u}'c'$ represents the turbulent flux of concentration. It is these last two diffusion terms that SCICHEM solves in its second-order closure scheme.

For sub-puff scale turbulence, SCICHEM employs the restriction that the only active off-diagonal component of $\langle x'u'c' \rangle$ is the symmetric horizontal term ($i=x, j=y$), but it is applied only for the large-scale (meso to synoptic) contribution to puff deformation when puff scales reach such dimensions. In CAMx, we ignore this off-diagonal flux moment term altogether since puffs are ultimately terminated when puff scales approach much smaller grid scales (typically < 50 km). SCICHEM also makes the assumption that the horizontal turbulence is isotropic, $\langle x'u'c' \rangle = \langle y'v'c' \rangle$. This results in a single diffusivity equation for both x and y directions, and a single diffusivity for the z direction:

$$K_x = K_y = \frac{\langle y'v'c' \rangle}{Q}$$

$$K_z = \frac{\langle z'w'c' \rangle}{Q}$$

The SCICHEM second-order tendency equations are used to model the time-evolution of PiG puff turbulent flux moments (represented by diffusivities $K_x=K_y$ and K_z) and their contribution to the evolution of puff spread (represented by the diagonal components of the puff spread tensor, σ_x^2 , σ_y^2 and σ_z^2). Puff spread is defined for puff depth (σ_z), puff width (σ_y), and puff length (σ_x). We account for the effects of grid-resolved shears of horizontal wind in the evolution of lateral and longitudinal spread. But we assume that the evolution of vertical spread is solely the result of turbulent fluxes, which are orders of magnitude larger than grid-resolved shears of vertical wind.

The resulting Reynolds-averaged second-moment transport equations for CAMx PiG are:

$$\begin{aligned} \frac{d\sigma_z^2}{dt} &= 2K_z \\ \frac{d\sigma_y^2}{dt} &= 2\sigma_y^2 D + 2\sigma_y\sigma_z S_y + 2K_x \\ \frac{d\sigma_x^2}{dt} &= 2\sigma_x^2 D + 2\sigma_x\sigma_z S_x + 2K_x \end{aligned}$$

where D is total explicit (grid-resolved) horizontal shear of horizontal wind (i.e., “deformation”, see Section 4.4). S is the explicit vertical shear of horizontal wind, which is broken down into puff-relative lateral (y) and longitudinal (x) components:

$$S_x = |\cos(\theta - \phi)| \left(\frac{du^2}{dz} + \frac{dv^2}{dz} \right)^{1/2}$$

$$S_y = |\sin(\theta - \phi)| \left(\frac{du^2}{dz} + \frac{dv^2}{dz} \right)^{1/2}$$

The difference between θ and ϕ represents the relative angle between the puff's longitudinal orientation and the direction of vertical shear, respectively; a cross-puff shear results in more lateral spread while along-puff shear results in more longitudinal spread. The explicit shear terms containing D and S may be toggled by the user: (1) shear effects are always applied to puff growth rates; (2) shear effects are applied only within the boundary layer but never above; or (3) shear effects are never applied.

The SCICHEM tendency equation for the horizontal turbulent flux moment is

$$\frac{d}{dt} \langle y' \overline{v' c'} \rangle = Qq^2 - A \frac{q}{\Lambda} \langle y' \overline{v' c'} \rangle$$

where $A = 0.75$, $q^2 = \overline{v' v'}$, and Λ is the horizontal turbulent length scale. Separate equations are given for two different boundary layer turbulence scales (shear- and buoyancy-produced), such that

$$\langle y' \overline{v' c'} \rangle = \langle y' \overline{v' c'} \rangle_{shear} + \langle y' \overline{v' c'} \rangle_{buoyancy}$$

Within the surface-based boundary layer, the horizontal velocity variance is given by

$$q_{buoyancy}^2 = 0.13 w_*^2 [1 + 1.5 \exp(z / z_i)]$$

$$q_{shear}^2 = 2.5 u_*^2 (1 - z / z_i)$$

where u_* is the friction velocity, w_* is the convective velocity scale, z is height above the surface, and z_i is the height of the surface-based boundary layer. The horizontal turbulent length scale is given by

$$\frac{1}{\Lambda_{shear}^2} = \frac{1}{(0.3 z_i)^2} + \frac{1}{(0.65 z)^2}$$

$$\Lambda_{buoyancy} = 0.3 z_i$$

In the stable boundary layer, only the shear components of q^2 and Λ are applied. Above the boundary layer, SCICHEM applies rough approximations for the velocity variance and turbulent length scale. In CAMx we have set these values to $q^2 = 0.1 \text{ m}^2/\text{s}^2$, and $\Lambda = 300 \text{ m}$.

The SCICHEM tendency equation for the vertical turbulent flux moment is

$$\frac{d}{dt} \langle z' \overline{w' c'} \rangle = A \frac{q_v}{\Lambda_v} \left(Q K_z^{eq} - \langle z' \overline{w' c'} \rangle \right)$$

where $q_v^2 = \overline{w' w'}$, Λ_v is the vertical turbulent length scale, and K_z^{eq} is the equilibrium diffusivity. Whereas a specific equation for K_z^{eq} is formulated for SCICHEM, we have chosen to specify the value of this parameter from the gridded fields of vertical diffusivity in CAMx. Again SCICHEM gives separate equations for shear- and buoyancy-produced turbulence scales.

Within the surface-based boundary layer, the vertical velocity variance is given by

$$q_v^2 \Big|_{shear} = 1.5 u_*^2 (1 - z/z_i)$$

$$q_v^2 \Big|_{buoyancy} = 1.1 w_*^2 (z/z_i)^{2/3} (1.05 - z/z_i)$$

The vertical turbulent length scale for both shear and buoyancy is equal to Λ_{shear} given above for horizontal length scale. Above the boundary layer, SCICHEM applies rough approximations for the velocity variance and turbulent length scale and we have adopted these for CAMx: $q_v^2 = 0.01 \text{ m}^2/\text{s}^2$, and $\Lambda_v = 10 \text{ m}$.

The external variables needed by PiG to complete the dispersion calculations include z_i , u_* and w_* . All of these are available from an internal module in CAMx that calculates these boundary layer similarity theory parameters. Thus, no additional parameters are needed to be input to the model.

6.1.2 Puff Transport

A fresh set of new puffs are released from all PiG point sources within the modeling domain for the duration of the smallest time step among the master and all nested grids. The length of each puff is determined by the combination of the mean total wind speed at the height of final plume rise and time step. Limits are placed on maximum extruded length based on half the finest resolution in the given simulation. If winds and time-steps are such that the maximum allowed length is violated, then several puffs are automatically emitted from a given stack per time step. The user can also set a maximum time interval of release if more puffs (better plume resolution) are desired over the default automated release interval. The orientation of the puff length is along the total wind vector. Total puff volume is determined by stack volumetric flow rate in conjunction with growth due to turbulent entrainment following the SCICHEM approach. Initially, $\sigma_x = \sigma_y$ and σ_z values are explicitly calculated from this entrainment calculation.

The effects of resolved wind shear on plume deformation (i.e., at plume scales larger than individual puff scales) are treated using a “chained puff” approach (Figure 6-2). Points at the leading and trailing edges of the puff centerline are individually transported through the gridded wind fields, which directly accounts for puff stretching and changes to centerline orientation due to deforming shears. Since puffs can extend over multiple layers, layer density-weighted average wind components are determined for each endpoint based on the vertical coverage of the puff. The “chain” aspect means that at least initially (as puffs are emitted from the stack) the trailing point of a puff emitted at time t will be the leading point of a puff emitted at time $t+dt$. However, as the puffs are advected downstream, the leading point of one puff will deviate from the trailing point the puff behind it due to evolving puff depth and wind fields.

The “position” of each puff is defined by its center point between the endpoints. This position defines the grid domain and grid cell in which the puff resides for the calculation of diffusive growth and chemistry. This definition holds even if the puff is sufficiently long that the endpoints are in different grid cells (or even different nested grids if near a nest boundary). With our definition for termination when horizontal area approaches grid cell area, the puff length should not extend across more than two grid cells.

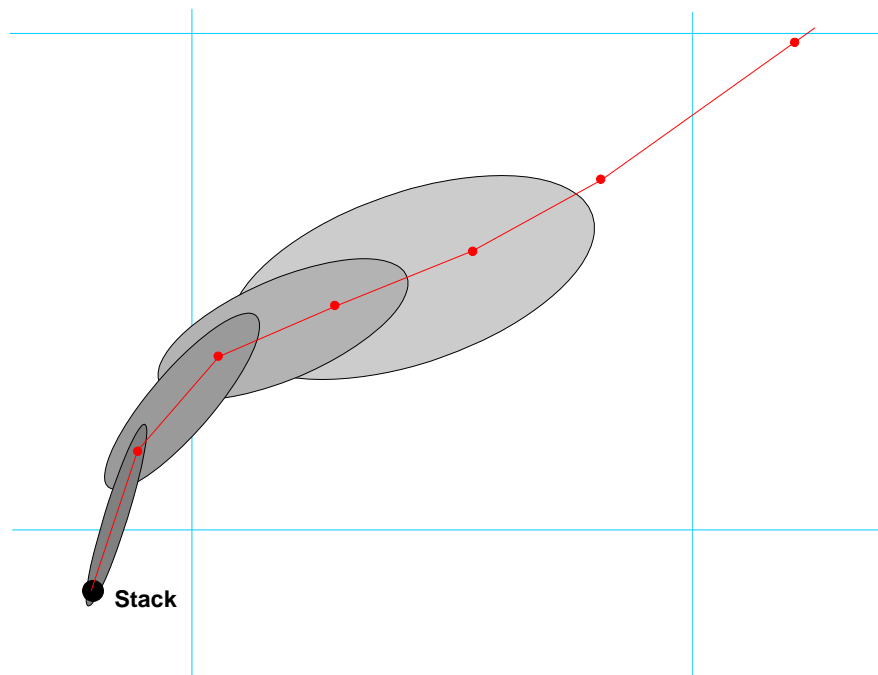


Figure 6-2. Plan-view schematic representation of a chain of PiG puffs emitted from a point source into an evolving gridded wind field. The red line connected by dots represents puff centerlines, with dots representing leading and trailing points of each puff. The CAMx computational grid is denoted by the blue lines.

6.2 GREASD PiG

The GREASD PiG is designed for large NO_x point sources, where only inorganic chemistry is operative during early plume evolution. The intention of GREASD PiG is to more properly age emitted NO_x within the confined plume volume to mitigate the artificially rapid chemical processing of fresh NO to NO₂ to ozone that would otherwise occur if immediately released into a large grid volume. A condensed inorganic chemical mechanism is employed in GREASD PiG that includes 23 reactions involving oxidation of NO_x and SO_x. Therefore, GREASD PiG should not be used for VOC sources. Chemical limitations applied within GREASD PiG cause puffs to transfer their mass to the grid before oxidant production from VOCs is no longer suppressed; this can occur before puffs reach a size threshold determined by the grid spacing.

The chemical evolution of large NO_x point source plumes can be characterized in three stages (EPRI, 2000), as described below:

- Stage 1: Early plume conditions where NO_x concentrations are very high and radical concentrations are negligible – simple NO/NO₂/O₃ photostationary state applies along with the NO-NO self reaction;
- Stage 2: Mid-range plume conditions where radical concentrations are sufficiently large to generate secondary inorganic acids like nitrate and sulfate;
- Stage 3: Long-range plume conditions where sufficient mixing with the ambient air leads to the full range of gas-phase reactions involving VOC oxidation and ozone formation.

The objective for GREASD PiG is to transfer mass to the grid at about the time when radical production via organic chemistry starts to become important, so GREASD PiG treats plume chemistry during Stages 1 and 2. We define the onset of Stage 3 chemistry when the following criterion is met:

$$\frac{k_{OH}[CO] + k_{OH}[SO_2]}{k_{OH}[NO_2]} > 1$$

At this point GREASD puffs transfer all of their mass to the grid before the onset of Stage 3. This specific design constraint is also compatible with the requirements of the source apportionment Probing Tools.

Kumar and Russell (1996) and Karamchandani et al. (1998) found that PiG models with simplified inorganic chemistry produced results that were very similar to full chemistry. The chemical mechanism for GREASD PiG includes 23 reactions listed in Table 6-1 that were selected as follows:

- Reactions for the NO-NO₂-O₃ photo-stationary state established in sunlight (1-3)
- Self-reaction of NO important only at very high NO concentrations (4)
- Production of OH by photolysis of O₃ and HONO in sunlight (5-9)
- Production of nitric acid in sunlight (10)
- Formation of NO₃ and N₂O₅ at night (11-17)

Table 6-1. List of 23 reactions for GREASD PiG including correspondence to CAMx reaction numbers in the CB05, CB6 and SAPRC07TC mechanisms.

Chemical Mechanism for GREASD PiG		Corresponding Reaction Number for Grid Chemistry		
Number	Reaction	CB05	CB6	S07
1	$\text{NO}_2 = \text{NO} + \text{O}$	1	1	1
2	$\text{O} + \text{O}_2 + \text{M} = \text{O}_3 + \text{M}$	2	2	2
3	$\text{O}_3 + \text{NO} = \text{NO}_2$	3	3	7
4	$\text{NO} + \text{NO} + \text{O}_2 = 2 \text{NO}_2$	22	24	10
5 ¹	$\text{NO} + \text{NO}_2 + \text{H}_2\text{O} = 2 \text{HONO}$	23	41	N/A
6	$\text{O}_3 = \text{O}_1\text{D}$	9	9	18
7	$\text{O}_1\text{D} + \text{M} = \text{O} + \text{M}$	10	10	21
8	$\text{O}_1\text{D} + \text{H}_2\text{O} = 2 \text{OH}$	11	11	20
9	$\text{HONO} = \text{NO} + \text{OH}$	25	43	23
10	$\text{NO}_2 + \text{OH} = \text{HNO}_3$	28	45	25
11	$\text{NO}_2 + \text{O}_3 = \text{NO}_3$	7	26	8
12	$\text{NO}_3 = \text{NO}_2 + \text{O}$	14	27	17
13	$\text{NO}_3 = \text{NO}$	15	28	16
14	$\text{NO}_3 + \text{NO} = 2 \text{NO}_2$	16	29	9
15	$\text{NO}_3 + \text{NO}_2 = \text{NO} + \text{NO}_2$	17	30	15
16	$\text{NO}_3 + \text{NO}_2 = \text{N}_2\text{O}_5$	18	36	11
17	$\text{N}_2\text{O}_5 = \text{NO}_3 + \text{NO}_2$	21	37	12
18 ²	$\text{N}_2\text{O}_5 + \text{H}_2\text{O} = 2 \text{HNO}_3$	19	39	13
19	$\text{SO}_2 + \text{OH} = \text{SULF} + \text{HO}_2$	63	52	44
20	$\text{OH} + \text{CO} = \text{HO}_2$	66	123	29
21	$\text{FORM} = 2 \text{HO}_2 + \text{CO}$	75	97	204
22	$\text{FORM} = \text{CO}$	76	98	205
23	$\text{HO}_2 + \text{NO} = \text{OH} + \text{NO}_2$	30	25	31

1. Rate for GREASD PiG reaction 5 is set to zero when used with SAPRC07TC.
2. Rate for GREASD PiG reaction 18 may be enhanced by reaction on aerosol.

- Production of nitric acid at night (18)
- Production of sulfuric acid in sunlight (19)
- Removal of OH by CO (20)
- Production of OH by photolysis of formaldehyde (21-22)
- Conversion to OH of any HO₂ formed in 20-22 (23)

These reactions dominate gas-phase chemistry in plumes from major NO_x emitters during stages 1 and 2. Table 6-1 also shows the correspondence between GREASD PiG reactions and the complete gas-phase chemical mechanisms implemented in CAMx. This mapping is used in CAMx to set the rate constants and photolysis rates for GREASD PiG reactions from corresponding reactions in the grid chemical mechanisms. This implementation ensures consistency with these chemical mechanisms. The GREASD PiG performs gas-phase chemistry

for only those chemical species emitted directly into the plume, and does not include the influence from any background compounds on the grid except for ozone, carbon monoxide, and formaldehyde. Assuming zero background for gas species is reasonable for the early stages of NO_x plumes because puff concentrations are orders of magnitude larger than ambient concentrations. On the other hand, background ozone, carbon monoxide, and formaldehyde are the primary sources of oxidants in the condensed mechanism that drive inorganic processing of plume NO_x to other forms of oxidized nitrogen (NO_z), so these are handled as “incremental” species as described below for IRON PiG. The Livermore Solver for Ordinary Differential Equations (LSODE) is used to solve the condensed mechanism in double-precision.

6.3 Particulate Matter In PiG

Non-linear effects and errors in gas-phase chemistry are transmitted to (and potentially amplified by) the PM aqueous chemistry and partitioning algorithms. The implementation of PM and PSAT in PiG prompted the need to limit the impact of such issues similarly to the constraints imposed by OSAT for gas-phase chemistry. Therefore, PM and PSAT can only be run using the GREASD PiG option. As for gas-phase chemistry, only inorganic PM chemistry is treated by GREASD PiG. Note also that the PiG PM treatment was designed specifically for the static 2-mode PM chemistry only (CF), and will not operate for the multi-section PM chemistry (CMU).

The GREASD PiG gas-phase chemistry oxidizes NO_x and SO_x emissions to nitric and sulfuric acids, which are PM precursors. To maintain consistency with the grid chemistry, aqueous PM chemistry (RADM-AQ) is then performed at every time step if the puff resides in a cloudy grid cell. However, inorganic gas/PM partitioning (performed by ISORROPIA) among sulfate, nitrate and ammonia is not performed by GREASD PiG, but is delayed until the masses of these compounds are dumped to the grid. Additionally, chemistry and partitioning for secondary organic aerosols is not performed.

6.4 IRON PiG

The IRON PiG model incorporates a complete treatment of gas-phase chemistry in point source pollutant plumes, while secondarily adding additional features central for treating toxic pollutants not normally carried by the standard CAMx chemical mechanisms. Therefore the IRON PiG can treat a wide variety of point source emissions, including VOC sources.

IRON PiG adopts the “incremental chemistry” concept from the SCICHEM model (EPRI, 2000), whereby each puff carries concentrations relative to ambient background. This results in the possibility of both positive and negative puff concentrations depending on how the chemistry evolves. The full gas-phase chemistry mechanism chosen for a given run is solved twice for each puff at each time step: first for the vertically-averaged background concentrations from the grid cells vertically spanned by the puff; and second for the sum of puff and background concentrations. The LSODE solver is used to solve both chemistry steps. After both steps are completed, the updated background concentrations are subtracted from the updated puff+background concentrations, yielding the new puff incremental concentrations. Note that the updated background concentrations are used for reference only in the puff incremental

chemistry algorithm; the actual grid concentrations are not affected and are separately solved by the grid chemistry routine.

6.5 PiG Features

This section describes specific features of the PiG submodel; certain features are always active while others can be optionally invoked for a particular CAMx run. The IRON PiG sub-model includes two constructs designed specifically to facilitate the incremental chemistry approach:

- The concept of “virtual dumping” to handle the chemical impacts of large puffs that can overlap other puffs within a given grid column;
- The concept of multiple puff “reactor” cells to account for the chemical effects of concentration distributions within each puff.

Each of these is described below.

6.5.1 Puff Layer Spanning (IRON and GREASD)

The PiG is designed to chemically process point source plume mass within streams of puffs until such time that each puff can be adequately resolved on the horizontal grid. Puffs are allowed to vertically span multiple grid model layers before they reach horizontal grid scales. This introduces technical implications for defining “background” concentrations and ambient conditions for puff chemistry, as well as for transferring plume incremental mass to the grid. The solution employed is to:

- 1) Assume that the vertical distribution of puff concentration is always uniform;
- 2) Distribute puff mass transfer (via “leaking” and “dumping”) to the grid according to the puff fractional coverage across each model layer and by density-weighting; and
- 3) Determine mean background concentrations and other ambient conditions (e.g., temperature, humidity, etc.) over the puff vertical span via similar fractional layer-density weighting.

Horizontally, the mean background concentration and ambient conditions are taken from the single host grid column containing each puff center point, even if the puff is large and/or spans a horizontal cell interface. As described earlier, puffs are considered to be elliptical in the horizontal, with the minor axis spanning the cross-wind puff width (defined as $\pm 1.5\sigma_y$), and the major axis spanning the along-wind puff length (defined as length $\pm 1.5\sigma_x$ on each end).

However, given the complications associated with multiple layers spanning and mass-weighting of ambient inputs and dumped mass, puffs are rectangular and uniform in the vertical, with total puff depth defined as $\pm 1.5\sigma_z$.

6.5.2 Puff Overlap and the Idea of Virtual Dumping (IRON only)

The chemical effects of puff overlap were considered to be an important attribute of IRON PiG. However, we wished to maintain a relatively simple approach, while appropriately accounting for the largest probable effects. We assume that the largest effect is the condition in which older expansive puffs span significant fractions of their host grid cell, thereby potentially

overlapping all other puffs contained within the same cell. Instead of geometrically determining fractional overlap puff-by-puff, we instead introduce a process that we refer to as “virtual dumping.”

For a given grid column, the mass from all puffs determined to be “sufficiently” large are temporarily dumped to the column, distributed according to each puff’s vertical layer span, and added together along with the pre-existing grid concentrations. This process is referred to as a “virtual dump” of puff mass to the grid column. The criteria to determine a “sufficiently” large puff is the same that initiates puff mass leaking to the grid (as described below). In this approach, all large puffs contribute to the background chemistry step for other puffs occupying the same grid column. Double-counting is avoided by not including a puff’s contribution to the background while its specific background and incremental chemical calculations are performed.

6.5.3 Multiple Puff Reactors (IRON only)

Accounting for full chemistry potentially introduces significant non-linear effects that are highly dependent upon the distribution of pollutant mass within each puff. Especially for ozone, aircraft flights through power plant plumes have often recorded wide concentration variations relative to ambient conditions: within the plume core where NO_x remains concentrated, ozone is often depressed and follows NO-NO₂-ozone equilibrium, whereas on plume fringes where NO_x is dilute and mixes with ambient VOC, ozone concentrations can exhibit concentration maxima. Past models have accounted for cross-plume chemistry variations through the use of reactors, with approaches ranging from multiple rectangular slabs to concentric shells.

The user may select multiple reactors as well to sub-divide the puff. Any number of reactors may be chosen (the default is 1). Multiple reactors simply divide the total puff volume evenly, and the initial mass assignments for newly emitted puffs are made using the standard error function that results in an initial Gaussian-like mass/concentration distribution among the reactors. This provides a mechanism for simulating the differing chemical processing that takes place in various concentration regimes. As the purpose of the reactors is merely to represent the range of photochemical conditions that are likely to occur at various locations within the puff as it undergoes differential shearing and mixing, there is no particular physical orientation assigned to these reactors with respect to each other or to the puff as a whole. Thus, there is no communication (i.e., diffusional mass exchange) between the reactors. The same background concentration chemistry applies to all reactors of a given puff. When puff mass is leaked or dumped, all reactors shed the same relative fraction of mass.

In summary, chemistry is solved for each puff “reactor” in three steps:

- 1) The layer-mean background (grid + overlapping puff) concentrations and environmental conditions over the volume occupied by the puff are stored and then chemically updated via the LSODE gas-phase chemistry mechanism;
- 2) The pre-updated mean background concentrations are added to the puff increments and the total concentrations are chemically updated; and
- 3) The updated results from step 1 are subtracted from the updated results of step 2 to provide the updated incremental concentrations.

6.5.4 Puff Dumping (IRON and GREASD)

Mass transfer from puff to grid can happen in two ways: slowly, termed “leaking”, or suddenly, termed “dumping.” As described earlier, all mass is transferred to the vertical grid structure in a density-weighted fashion according to each puff’s fractional layer coverage. The process of leaking ensures that puff mass is transferred to the grid continuously, rather than in discrete lumps of pollutants with very different concentrations than those in the grid. Sudden dumping can cause unphysical numerical shocks in the grid and can lead to unrealistic gridded concentration patterns that appear as “bulls-eyes”. The idea behind puff leakage is to account for turbulent shearing of mass from the main plume and its subsequent dispersion to the grid scale. This rate of transfer should be directly proportional to the puff size relative to the grid scale.

Puff leakage is controlled by comparing the horizontal area of a puff to a specified leakage parameter, defined as a fraction of horizontal grid cell area. When a puff is first emitted there is no leakage. As the puff grows in volume the concentrations within the reactors are reduced accordingly by dilution. When the puff area exceeds the leakage onset parameter, a fraction of the mass in each puff reactor is transferred to the grid. This fraction is determined by the relative exceedance of the leakage parameter; initial leakage is slow as the exceedance is relatively small, but leakage rates grow as the puff continues to grow beyond the leakage parameter.

The reduced mass from leakage is compensated by a reduced effective volume, so that concentrations are not artificially diluted by leakage (an essential chemical imperative). Thus, two distinct volumes are tracked: the actual volume (defined by the puff spread σ) and the effective volume. While these are identical before leakage, they deviate after leakage is initiated, and thereafter the relative deformation of the actual puff volume (via diffusion, shearing, etc.) is used to scale the deformation of effective puff volume.

Eventually the horizontal span of the puff will exceed the grid cell area, and the remaining mass is then dumped all at once to the grid. However, because of the combination of photochemical processing and leakage, by the time a puff dumps the potential for producing numerical shocks is much reduced. Furthermore, if the puff exceeds a user-defined maximum age, puff mass is transferred to the grid at the rate of 10% per timestep.

6.5.5 PiG Rendering (IRON and GREASD)

While the mass confined to the puffs at any given time has not yet affected the grid concentrations, it will eventually, so it can be somewhat misleading to sequester this mass from visualizations of a model simulation. The puff mass can be optionally incorporated into the model average output files for visualization purposes (referred to as “PiG rendering”). Rendering employs a “virtual dump” of the puff masses into the average output concentration array each time step. As described for chemistry, virtual puff mass is added as an increment over the entire grid column according to fractional layer-density weighting over puff depth, thus diluting its concentrations relative to that within the puff. The actual puff mass remains within each puff over the course of its lifetime, and the actual grid mass is unaffected until puffs are killed and their masses truly dumped into the grid. This visualization is available for

either 2-D surface or 3-D average output files, and can produce some rather startling effects in output displays, including very narrow virtual plumes, or streaks, representing mass moving through the grid in sub-grid puffs, but not subject to grid-scale eddy diffusion.

6.5.6 High Resolution Puff Sampling (IRON and GREASD)

PiG optionally employs surface-layer puff sampling on a user-defined grid of arbitrary horizontal resolution, similarly to the way nested grids are defined. Sampling grids are entirely passive, and intended to provide a display of the plume concentrations at scales much smaller than typically used for the finest computational grids (i.e., <1 km), primarily around and downwind of a source complex. Sampled PiG concentrations are time-averaged like the output concentrations provided on the computational grids, and are written to files with similar format so that they may be readily viewed and manipulated with CAMx post-processing software. Additional information on configuring and using PiG sampling grids is provided in Sections 2 and 4.

Given that the puffs constantly evolve via diffusive growth and reshaping due to deforming shears, the sampling procedure includes trigonometric calculations to define which sampling points are influenced by each puff. This influence is determined according to the puffs' two-dimensional horizontal Gaussian shape shown in Figure 6-1. To include a sufficiently large percentage of mass across each puff for sampling, limits of $\pm 3\sigma_{x/y}$ in both horizontal dimensions are used to define the puffs' total elliptical area coverage. Puffs are only sampled if they extend vertically within 10 m of the ground.

Sampling grids are defined in the CAMx control file (see Section 2), and array dimensions must be set sufficiently large in the CAMx Fortran parameters file in `./Includes/camx.prm` (see Section 2). An example of the type of plume detail that can be visualized using a sampling grid is provided in Figure 6-3. In this case, a very fine 200 m sampling grid is set within a 4-km computational grid.

6.6 Deposition

The CAMx PiG treats the removal of gas and PM species from each puff via deposition processes. Both dry and wet deposition calculations presented unique implementation issues for puffs. The most difficult issue for both forms of deposition was how to manage deposition exchange between puffs and the ground in the case of negative puff concentration increments.

6.6.1 Dry Deposition

Dry deposition needs to consider the following: (1) the point at which puffs begin to deposit to the surface; (2) how to handle deposition through potentially deep puffs that may straddle several layers of varying stability since the puffs do not themselves resolve these stratifications or vertical concentration distributions; (3) managing deposition fluxes of negative concentration increments. Our solution to issue (1) was to ignore dry deposition within puffs until they diffusively grow to the ground, although in reality deposition occurs on roughness elements that extend some distance above the ground (trees, buildings, etc.). We implemented a criterion that the bottom of the puff must extend to or below the midpoint of the surface layer, or below 10 m (whichever is larger), in order for dry deposition to be active.

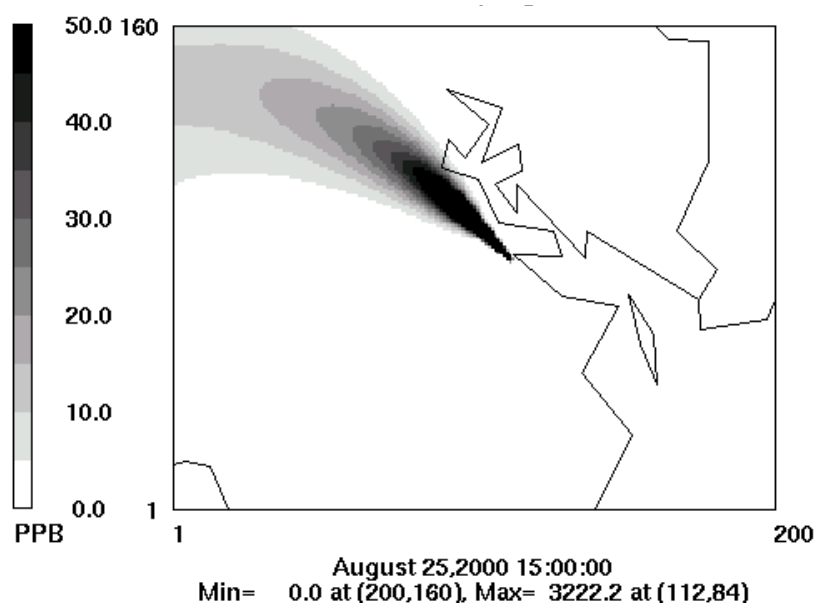


Figure 6-3. Example of a single point source PiG plume as depicted by a sampling grid with 200 m resolution (shown by the extent of the plot; 40 km by 32 km total extent). This sampling grid was set within a CAMx computational grid with 4-km resolution. The source location is arbitrary and is emitting an inert tracer.

Issue (2) can be handled in a variety of ways and complexity. The current implementation institutes a simpler solution and we will consider more complicated improvements for future developments if evidence suggests that they would be necessary. PiG utilizes pre-computed species-dependent deposition velocities derived for the grids. Each puff in a particular grid cell is provided the host cell's deposition velocities for each species, and these are used to determine the flux of mass through the fraction of puff depth occupying the model's surface layer.

Issue (3) is unique to the incremental chemistry concept introduced with IRON PiG. The flux of material depositing to the ground is given by $F = c \cdot v_d$, where by the normal definition a positive deposition velocity v_d leads to a positive deposition flux to the ground. If the puff increment c is negative, then a negative flux is calculated (flux from ground to puff). This is appropriate if we consider the following argument. Dry deposition applied to a grid cell removes some pollutant mass from the entire volume. If there is a puff existing in that cell with a negative concentration increment, then the amount of mass removed from the cell was over estimated if we consider the puff's contribution to total cell mass. The negative deposition flux calculated for this puff leads to the addition of mass to the puff increment. Adding mass to a negative increment reduces the magnitude of the increment, as expected for a deposition process. This mass is taken from the grid cell's accumulated deposited mass to maintain accurate mass accounting within the model.

6.6.2 Wet Deposition

Wet deposition needs to consider the following: (1) how to handle scavenging of pollutants through potentially deep puffs that may straddle several layers of varying cloud and precipitation conditions but that do not themselves resolve vertical concentration distributions; (2) managing deposition fluxes of negative concentration increments in combination with the potential for mass to move in and out of rainwater as it falls (e.g., for slightly soluble gasses); (3) accounting for the initial pollutant concentrations in rainwater as they enter the top of each puff.

It was important to maintain consistency between the treatment of wet deposition and the approach for puff chemistry. The chemistry relies on the assumption of vertically well-mixed puff reactors that can span multiple layers, and this is why layer-density weighted average ambient conditions are passed to the chemistry routines. To maintain this assumption for wet deposition, a single scavenging rate is applied through the entire puff depth as effectively a single layer of pollutant. This was found to be the simplest implementation approach. This single scavenging rate is calculated according to layer-density weighted average ambient cloud and precipitation conditions.

Wet scavenging is performed throughout the entire depth of the puff to determine the amount of flux in or out of rainwater. Total concentrations (puff + background) are used to determine species-dependent scavenging rates using the identical algorithm as for grid removal. The rates are used to derive removal fractions, and these fractions are then applied directly to the puff incremental mass for each species. Removal fractions are considered positive for the standard case of mass moving from puff to rain.

We further assume that the top boundary condition for rainwater entering the top of each puff is zero. This means that the removal fraction is always positive (from puff to rain) in the single-layer puff. In contrast, for gridded concentrations the layer-by-layer buildup of slightly soluble species can lead to a reversal of fluxes (from rain to grid) if super saturation is diagnosed in a particular layer.

Note that negative puff mass increments in combination with a positive removal fraction lead to a reversal of the flux direction (rain to puff), but that is not allowed and in such cases wet scavenging is set to zero. We account for impacts on the mass budget appropriately by adding to the wet deposition mass array according to the net fluxes into rainwater.

6.7 PiG Configuration

Selecting the individual elevated point sources to receive the PiG treatment is accomplished by setting their stack diameters negative within the header (time-invariant point list) section of the CAMx input point source file. CAMx will run correctly with these negative diameters even if the PiG algorithm is not invoked. CAMx preprocessors exist to ease the procedure of ranking elevated point sources by emission rate and flagging the sources that the user wishes to treat.

Invoking the CAMx PiG sub-model is controlled by keywords in the CAMx control file (`CAMx.in`), as described in Section 2. The choices are:

```

PiG_Submodel = 'NONE',
PiG_Submodel = 'GREASD',
PiG_Submodel = 'IRON',

```

Note that the single choice between GREASD and IRON applies to all flagged point sources. It is not possible to make a single CAMx run with IRON PiG applied to a certain group of sources, and GREASD PiG applied to another group. Also note that GREASD must be selected to run PiG with OSAT, PM and PSAT; IRON must be selected to run PiG with the RTRAC Probing Tool. Several additional parameters are used to configure the PiG. It is important to note that all PiG configuration parameters exist in the CAMx Fortran parameters file (`./Includes/camx.prm`), as described in Section 2. PiG parameters are grouped together and briefly described at the end of that file. By configuring the PiG submodel in the code, the default PiG configuration (as recommended by the model developers) is preset within the model distribution and alleviates the need for users to select settings on their own.

The default values are shown below:

```

parameter ( MXPIG      = 50000 )
parameter ( MXRECTR    = 1 )
parameter ( FLEAK      = .25 )
parameter ( LEAKON     = .FALSE. )
parameter ( LVISPIG   = .FALSE. )
parameter ( OVERLAP   = .FALSE. )
parameter ( DXYMAX     = -10000. )
parameter ( AGEMAX     = 18.*3600. )
parameter ( PIGMXDT   = 300. )
parameter ( SHRFLG     = 1 )

```

Users should exercise thoughtful consideration when altering these default values. A description of each of the remaining parameters is provided below, along with guidance in setting values.

6.7.1 Guidance on the Use of CAMx PiG

6.7.1.1 PiG Keyword

The PiG keyword controls whether the PiG option is to be invoked in a CAMx simulation, and whether the emissions are treated with the GREASD or IRON options. This keyword can be switched from NONE to GREASD or IRON on a model restart to invoke the PiG treatment at any point during a multi-day simulation. To allow for this, it is not mandatory to provide CAMx with a pre-existing PiG output file upon a model restart – CAMx will not stop if this file is missing. It is recommended that this file be provided on all subsequent restarts since the PiG output file is needed to reinitialize the PiG module, otherwise all mass contained in puffs at the end of the previous run will be lost. If the PiG keyword is switched to NONE on a model restart, CAMx will continue the simulation without PiG, but all mass contained in puffs at the end of the previous run will be lost.

- Guidance:
 - Invoke GREASD or IRON PiG at any point during a multi-day simulation, or none at all. Once PiG is started, provide CAMx with the PiG output file from the previous run for all subsequent model restarts so that no point source mass is lost.
 - GREASD PiG should be invoked for large NO_x point sources only, since it does not provide any organic chemistry. GREASD PiG supports PM chemistry (CF but not CMU). It can be run in conjunction with the OSAT/PSAT. It does not support DDM, PA, or RTRAC.
 - IRON PiG can be invoked for any point source to treat gas-phase chemical evolution using any of the CAMx photochemical mechanisms. IRON PiG does not treat particulate chemistry. It can be run in conjunction with the RTRAC Probing Tool. It does not support OSAT/PSAT, DDM, or PA.

Both GREASD and IRON options use the LSODE chemistry solver exclusively, so users will notice an impact on run time, particularly if many (thousands) puffs are to be tracked, and IRON PiG is invoked (2 solutions of full photochemistry for each puff), and IRON puffs are configured with many puff reactor cells (full photochemistry solutions each). Since GREASD chemistry is simpler and the lifetime of GREASD puffs are much shorter than their IRON counterparts, GREASD PiG will run faster than IRON PiG for the same number of flagged sources. PiG chemistry is internally parallelized using OMP to maximize PiG speed performance.

6.7.1.2 Number of PiG Puffs

MXPIG sets the maximum number of PiG puffs to be expected during a simulation. It is used to statically allocate memory arrays for the PiG sub-model. A value of 10,000 is usually sufficient for most applications in which PiG is used; set this parameter to 1 if PiG is not used to conserve memory. If this parameter is exceeded during a simulation, the model will halt. If this happens, simply increase MXPIG, recompile the model executable, and restart the simulation.

- Guidance: Use the default value for most simulations, or set to 1 if PiG is not to be used. If the model stops because MXPIG is exceeded, increase its value, recompile, and restart the model.

6.7.1.3 Number of PiG Reactors (IRON only)

MXRECTR sets the number of puff reactors; when greater than 1, each puff is separated into that number of reactor cells and primary emissions are apportioned among them using a Gaussian distribution. Since chemistry is performed for each individual reactor cell (both background and puff+background), this parameter can affect the speed of chemical computations in the PiG. We have not seen a significant sensitivity to values greater than 1, but testing for each application is warranted.

- Guidance: Use the default of 1 for initial simulations, but test the sensitivity to this parameter for each unique application.
- Reactors greater than 1 are not allowed for GREASD PiG.

6.7.1.4 Leakage Parameters

FLEAK, LEAKON, and DXYMAX together control puff leakage to the computational grid and ultimately puff termination. When LEAKON is true, FLEAK and DXYMAX control when puffs begin to leak portions of reactor mass to the grid along their trajectory. When LEAKON is false, no leaking is performed and puffs maintain all of their mass until they reach sizes for termination, at which point all mass is directly introduced to the grid at that point. DXYMAX sets the maximum dimension that puff size will be compared to for leaking and termination: when it is zero, puff size will be compared to grid area only; when it is positive, puff size will be compared to the value of DXYMAX regardless of grid resolution; when it is negative, puff size will be compared to DXYMAX or grid resolution, whichever is smaller. FLEAK is the relative fraction of horizontal puff area to cell area (or DXYMAX) above which leaking will begin and continue until sufficient mass is shed and the puff is terminated. In the example above, puffs will begin to leak mass when they reach 25% of the host grid cell's area.

- Guidance: If LEAKON is set to true, maintain FLEAK at the default value of 0.25. Then test model sensitivity to different values of FLEAK and/or DXYMAX.
- Guidance: We suggest leaving DXYMAX = -10000, meaning puffs will be terminated when they reach the grid scale or 10 km, whichever is smaller. Puffs exceeding this size are usually well-aged and go beyond reasonable assumptions of puff coherence (also see AGEMAX parameter below).
- Leaking is not allowed when PiG is run with PM.

6.7.1.5 Overlap Flag (IRON only)

OVERLAP controls whether puff overlap is to be treated in the background chemistry step. As stated earlier, puffs only overlap if they meet the size criteria for leaking; all puffs smaller than this size do not overlap any other puffs in the same grid cell.

- Guidance: We recommend that the OVERLAP flag remain set to the default value of "false".
- Overlap is not allowed for GREASD PiG.

6.7.1.6 Virtual Puff Rendering

LVISPIG is a flag that turns on puff "rendering" to the computational grid average concentrations. When it is false, the chemical effects of puff mass are not seen on the output average files until they either begin to leak mass to the grid and/or they are terminated and their mass is entirely introduced to the computation grid. However, when the flag is true, all puff mass that resides in each grid column is summed, apportioned vertically to each grid cell according to puff vertical extent (via density and layer-depth weighting), converted to concentrations, and added to the average gridded concentrations for output. This process is referred to as rendering since the effects of all puff mass can be readily visualized in the CAMx output.

- Guidance: This option has no impact on the actual CAMx chemical solution. However, output average concentration files will be affected by puff rendering, and therefore could impact graphics of CAMx results and model performance measures.
- Virtual dumps are not allowed when PiG is run with PM.

6.7.1.7 Maximum Puff Age

AGEMAX is the age limit for all PiG puffs (IRON and GREASD). When puffs reach this age limit, they are terminated and all of their mass is transferred to the host grid. The assumption of a stream of coherent puffs becomes less valid with time as horizontal and vertical wind shears increase plume spread. At some point the plume mass is better resolved on the grid than within puffs. The maximum puff age provides a safety check to ensure that puffs do not persist for unrealistic times in stable environments. The maximum puff age should be set long enough to allow puffs to persist overnight, but a lifetime of longer than a day is probably not realistic.

- Guidance: limit puff age to 12-24 hours – we find that 18 hours works best since it will allow puffs emitted in the late afternoon to last through the night and into the following morning. Twelve hours is seen to be too short in this regard; puffs usually do not reach 24 hours of age before being terminated by grid constraints.

6.7.1.8 Maximum Puff Release Interval

PIGMXDT sets the maximum frequency of release and by default is set to 300 seconds (5 minutes). This value should be adequate for most applications. However, if the user wishes to improve plume resolution by increasing the number of puffs, the frequency of release can be increased by reducing the value of PIGMXDT. This value supersedes the automated puff release rate that is determined by wind speed and grid size.

- Guidance: Maintain the default value of 300 s and allow PiG to use the automated PiG release frequency. Set to a lower value if better plume resolution is desired; note that more puffs will be released and this could slow the model markedly.

6.7.1.9 Effects of Wind Shear on Puff Growth Rates

SHRFLG sets the approach by which to apply the effects of explicitly resolved (grid scale) wind shear on puff growth rates. There are three options available to the user:

- 0 = shear is never applied;
- 1 = shear is applied only within the boundary layer;
- 2 = shear is always applied.

- Guidance: The application of wind shear can lead to large growth rates, especially above the boundary layer where stability squelches turbulent growth, and this may over-dilute puff concentrations, lead to early transfer of puff mass to the grid, and have markedly reduced impacts downwind. Shear has less relative impact on growth rates in neutral/unstable conditions because turbulent growth on its own leads to rapid plume dilution. For these reasons, the default is to ignore the effects of shear when puffs are above the boundary layer.

7. SOURCE APPORTIONMENT

Photochemical grid models are often used to develop emission reduction strategies to attain air quality objectives. Traditional methods involve running numerous iterative reduction or “zero-out” simulations (i.e., “brute force” methods) to identify the contributions from specific pollutants, source categories and source regions. This process quickly becomes impractical, but the lack of such information might lead to implicating sources that contribute little to high pollutant levels or, conversely, not properly identifying sources that do contribute.

CAMx includes a source apportionment (SA) or attribution capability that estimates the contributions from multiple source areas, categories, and pollutant types to the spatial and temporal distribution of ozone and PM in a single model run. The main challenges in implementing a methodology to track the relationships between separate groups of precursor emissions and subsequent non-linear formation of target pollutants include:

- Accounting not only for the presence of precursors from a given source region at a given receptor location, but also accurately estimating their cumulative contribution to target pollutants while they were en-route to the receptor;
- Ensuring compatibility with the underlying air quality model formulation so that derived source-receptor relationships are consistent with model results for total concentrations;
- Providing sufficient spatial and temporal resolution while managing, within practical constraints, the computer resources required to run the source apportionment tool.

SA uses sets of tracer species to track the fate of precursor emissions and the ozone and PM compounds formed from these emissions. The tracers operate as “spectators” to the normal CAMx calculations so that the underlying relationships between total emissions and concentrations are not perturbed. SA tracers are not “passive”: rather they track the effects of chemical reaction, transport, diffusion, emissions and deposition within a CAMx simulation and are thus referred to as “reaction tracers.” A source can be defined in terms of geographical area (or region) and/or emission category (or group). Figure 7-1 provides an example of the way a CAMx domain can be sub-divided into multiple source areas – 40 in this example. Also, the emission inventory could be sub-divided into several source categories; for example, three emission categories (mobile, industrial, biogenic) over 40 source regions would produce 120 separate sets of tracers. All sources of precursors, ozone, PM must be accounted for, so CAMx initial and boundary conditions are also tracked as separate source groups. The methodology is designed such that all ozone, PM and precursor concentrations are attributed among the selected source regions/groups at all times and throughout all grids. The methodology also estimates the fractions of ozone formed en-route under VOC- or NO_x-limited conditions, indicating whether ozone at a particular time and locations will respond to reductions in VOC or NO_x precursor emissions.

An important feature of the reaction tracer approach is that the normal CAMx calculations are not perturbed; thus, SA estimates the same total ozone, PM and precursor concentrations as CAMx. Further, since the same inputs are used for meteorology, emissions etc., and the same numerical methods are employed throughout the model, the source-receptor relationships

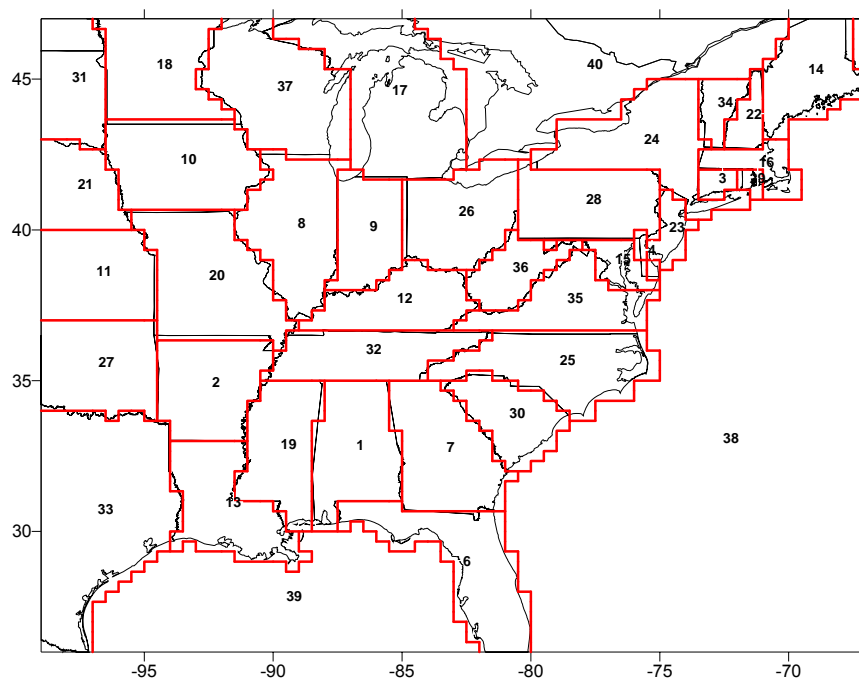


Figure 7-1. Example of the sub-division of a CAMx domain into separate areas for geographic source apportionment.

developed by SA inherently have a high degree of consistency with those generated by CAMx. The biggest limitation of this (or any other) source apportionment approach relates to non-linear chemical interactions between emissions from different sources, which by extension means that any perturbation to the emission inventory changes source-receptor relationships and attribution in a non-linear way. Thus, for pollutants like ozone and some PM, SA results only apply to a particular emissions scenario, and cannot be used to extrapolate effects resulting from emission changes among the tracked source regions/groups.

7.1 Ozone Source Apportionment

Yarwood et al (1996a,b) developed an ozone source attribution approach that has become known as the “Ozone Source Apportionment Technology” (OSAT). This method was originally implemented in the Urban Airshed Model (UAM) and was built into the first version of CAMx. The second version (OSAT2 – although this term was not widely used) was released with CAMx v4.20 in 2005 along with the addition of Particulate Source Apportionment Technology (PSAT). The OSAT2 update accounted for simultaneous production and destruction of ozone by photochemistry and tended to allocate less ozone to long-range transport (because of destruction during transport) and more to local production. The third version (OSAT3) was released with CAMx v6.30 in 2016, and includes an improved approach to handle NO_x recycling (Yarwood and Koo, 2015). The OSAT3 update tends to allocate more ozone to long-range transport (due to contributions from NO_x during downwind transport) and less to local production.

7.1.1 OSAT Formulation

The original OSAT uses four tracers per source region/group to account for contributions to ozone formation. Ozone formation involves both NO_x and VOC, and OSAT uses two tracer families (N_i and V_i) to apportion NO_x and VOC by source region/group *i*. The ozone formation process is controlled by the relative availability of NO_x and VOC, and so ozone formation is described either as NO_x-limited or VOC-limited, respectively. The ratio of the production rates of hydrogen peroxide (H₂O₂) and nitric acid (HNO₃) is the indicator used to classify ozone formation as being instantaneously limited by NO_x or VOC. Ozone formation is classified as being NO_x-limited when $P(\text{H}_2\text{O}_2)/P(\text{HNO}_3) < 0.35$ (Sillman, 1995). When ozone production at a given location and time is NO_x-limited, it makes sense to attribute that production to source region/groups based on their contributions to the local NO_x, and similarly to attribute production based on VOC contributions when ozone formation is VOC-limited. Consequently, separate ozone tracer families (O3N_i and O3V_i) are used to track ozone formed under NO_x and VOC-limited conditions.

The OSAT tracers by source region/group *i* are:

- N_i Nitric oxide (NO) and nitrogen dioxide (NO₂) emissions
- V_i VOC emissions
- O3N_i Ozone formed under NO_x-limited conditions from N_i
- O3V_i Ozone formed under VOC-limited conditions from V_i

The original OSAT tracer scheme is illustrated in Figure 7-2. Net ozone change due to chemistry (ΔO_3) is tracked by the tracer families O3N and O3V. Ozone destruction ($\Delta\text{O}_3 < 0$) reduces all O3N and O3V proportionately. Ozone production ($\Delta\text{O}_3 > 0$) is classified either as NO_x-limited or VOC-limited using the indicator $\Delta\text{H}_2\text{O}_2/\Delta\text{HNO}_3$ and assigned either to O3N or O3V, respectively, in proportion to the precursor tracers present, respectively N or V. The precursor tracers N and V are removed by chemical decay.

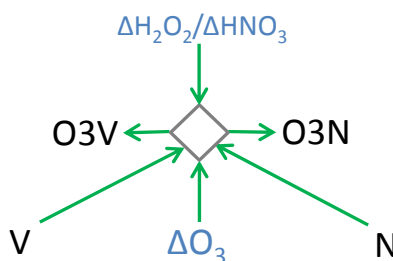


Figure 7-2. The original OSAT scheme for ozone apportionment. Information flows along arrows. Changes in core model species are shown in blue, OSAT tracers are in black, the diamond represents the OSAT algorithm that determines ozone tracer changes. $\Delta\text{H}_2\text{O}_2/\Delta\text{HNO}_3$ is the indicator ratio used to determine NO_x- or VOC-limited ozone production.

7.1.2 OSAT2 Formulation

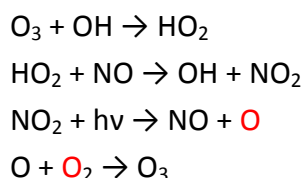
The original OSAT algorithm allocated the net ozone change (ΔO_3) to tracers O3N and/or O3V. However, ozone production and destruction reactions operate simultaneously and so the net ozone change is the balance of production and destruction. For example, VOC oxidation can cause photochemical ozone production at the same time that $O_3 + \text{VOC}$ reactions directly consume ozone, and these processes may lead to a net ozone increase or decrease depending mainly upon availability of NOx and sunlight.

OSAT2 accounts for the following ozone destruction mechanisms:

- 1) $O_3 + \text{VOC}$ reactions since these remove ozone;
- 2) $O(^3P) + \text{VOC}$ reactions since these effectively remove ozone;
- 3) $O(^1D) + H_2O$ reaction since this effectively removes ozone;
- 4) HOx + O_3 reactions that do not re-form ozone.

Ozone destruction is calculated as the smaller (i.e., more negative) of the sum of these four mechanisms or ΔO_3 . Ozone production is then calculated as the difference between ΔO_3 and the ozone destruction. The O3V and O3N tracers are adjusted first for ozone destruction (applied to all tracers) and second for ozone production (applied using the OSAT rules).

The amount of ozone destruction is calculated from the time-integrated rates of the four chemical processes listed above. It is easy to account for processes 1-3 since the ozone destroyed is simply the time-integral of the reactions involved. Process 4 is less easy to quantify because ozone can be re-formed. For example:



However, process 4 is an important ozone destruction mechanism in low NOx (e.g., rural) environments. Therefore, accounting for process 4 is important to understanding long-range ozone transport. The main reaction pathways between ozone and HOx (OH and HO_2) are shown in Figure 7-3.

The ozone destruction rate due to $O_3 + \text{HOx}$ reactions is computed from:

$$O_3 \text{ Destruction} = \text{Rate}(O_3 + HOx) \times \left(\frac{\text{Rate}(HO_2 \text{ term})}{\text{Rate}(HO_2 + NO) + \text{Rate}(HO_2 \text{ term})} \right)$$

The OSAT2 tracers are the same as the original OSAT. The OSAT2 scheme for ozone apportionment is illustrated in Figure 7-4. Ozone production and destruction are treated separately and can occur simultaneously. Ozone destruction ($-\Delta O_3$) reduces all O3N and O3V proportionately. Ozone production ($+\Delta O_3$) is classified either as NOx-limited or VOC-limited

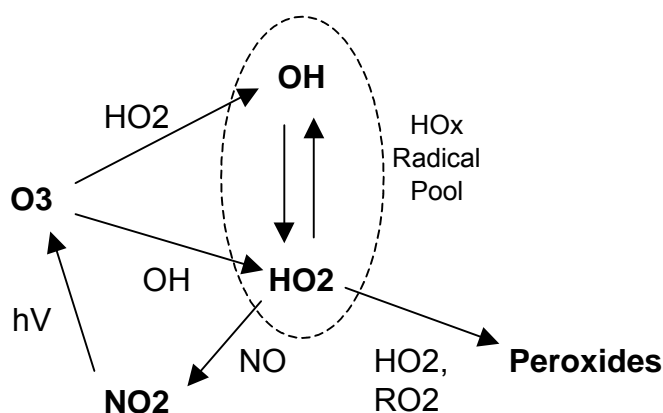


Figure 7-3. Daytime reactions of ozone with HOx (OH and HO₂) showing potential for reformation of ozone or ozone destruction via peroxide formation.

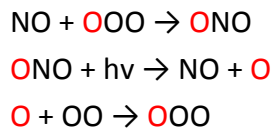


Figure 7-4. The OSAT2 scheme for ozone apportionment. Information flows along arrows. Changes in core model species are shown in blue, OSAT tracers are in black, the diamond represents the OSAT algorithm that determines ozone tracer product. $\Delta\text{H}_2\text{O}_2/\Delta\text{HNO}_3$ is the indicator ratio used to determine NO_x- or VOC-limited ozone production.

using the indicator $\Delta\text{H}_2\text{O}_2/\Delta\text{HNO}_3$ and assigned either to O₃N or O₃V, respectively, in proportion to the precursor tracers present, respectively N or V. The precursor tracers V and N are removed by chemical decay.

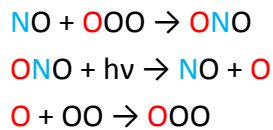
7.1.3 OSAT3 Formulation

OSAT3 improves the accuracy of the OSAT methods by keeping track of the source(s) of ozone removed by reaction with NO to form NO₂ and subsequently returned as ozone when NO₂ is destroyed by photolysis. Accomplishing this objective requires maintaining source attribution of odd-oxygen through the chemical reactions that link ozone, NO and NO₂. This is illustrated in the following chemical reactions where ozone is written as OOO, NO₂ is written as ONO, and the source attributed odd-oxygen is shown in red:



Source attribution of the odd-oxygen content of NO_2 is performed by tracer families OON and OOV that are introduced in OSAT3. Two tracer families are needed in order to keep track of the source profile of ozone consumed, which was represented by O3V and O3N.

Source attribution of the nitrogen in NO and NO_2 must also be performed in order to apply the apportionment algorithms that track ozone production using O3N and O3V. Accordingly, OSAT3 simultaneously attributes both the N and odd-oxygen in NO_2 to sources, and the source signatures of these two apportionments will almost always differ. This is illustrated below, where chemical source attribution is shown in blue for nitrogen and red for odd-oxygen:



The chemical conversion pathways between oxidized nitrogen species (NO_y) in CB6 are summarized in Figure 7-5. Arrows show the direction of conversion, which is bi-directional in some cases. Other chemical mechanisms have similar NO_y conversion pathways to CB6. Also shown in Figure 7-5 are the OSAT3 tracer families. Color coding shows the correspondence between OSAT3 tracer families and the NO_y species that they represent (note that the purpose for color coding in Figure 7-5 is different from colors used in the chemical reactions above).

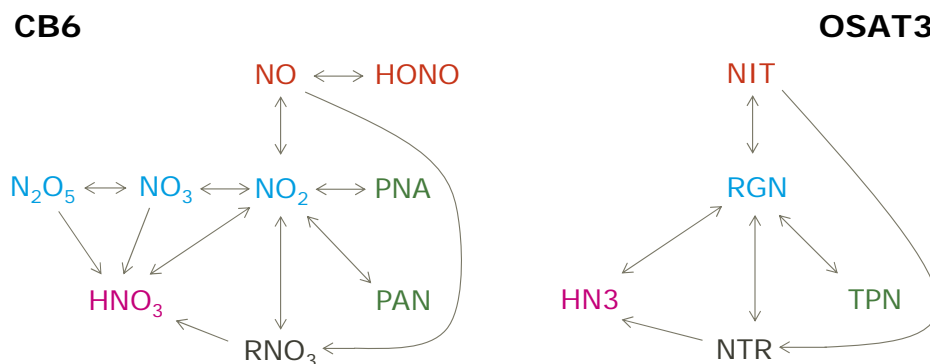


Figure 7-5. Correspondence between NO_y species in CB6 and tracer families in OSAT3 with conversions between species/tracers shown by arrows.

Tracking source attribution of nitrogen through all forms of NO_y enables OSAT3 to account for NO_x recycling when NO_x is converted to another form of NO_y (e.g., PAN or HNO₃) and later converted back to NO_x. OSAT3 uses the following 10 tracers by source region/group *i*:

V _{<i>i</i>}	VOC emissions
NIT _{<i>i</i>}	Nitric oxide (NO) and nitrous acid (HONO) emissions
RGN _{<i>i</i>}	Nitrogen dioxide (NO ₂), nitrate radical (NO ₃) and dinitrogen pentoxide (N ₂ O ₅)
TPN _{<i>i</i>}	Peroxy acetyl nitrate (PAN), analogues of PAN and peroxy nitric acid (PNA)
NTR _{<i>i</i>}	Organic nitrates (RNO ₃)
HN3 _{<i>i</i>}	Gaseous nitric acid (HNO ₃)
O3N _{<i>i</i>}	Ozone formed under NO _x -limited conditions from N _{<i>i</i>}
O3V _{<i>i</i>}	Ozone formed under VOC-limited conditions from V _{<i>i</i>}
OON _{<i>i</i>}	Odd-oxygen in NO ₂ formed from O3N _{<i>i</i>}
OOV _{<i>i</i>}	Odd-oxygen in NO ₂ formed from O3V _{<i>i</i>}

The OSAT3 scheme for ozone apportionment is illustrated in Figure 7-6. The VOC precursor tracer family V is unchanged in OSAT3 and removed by chemical decay, while the tracer N is replaced with NIT. The fate of NO_x emissions is tracked by the nitrogen tracer families NIT, RGN, TPN, NTR and HN3. Ozone production and destruction are treated separately and can occur simultaneously (as in OSAT2). Ozone production (+ΔO₃) is classified either as NO_x-limited or VOC-limited using the indicator ΔH₂O₂/ΔHNO₃ and assigned either to O3N or O3V, respectively, in proportion to the precursor tracers present, respectively NIT or V. Ozone destruction (-ΔO₃) reduces all O3N and O3V proportionately. When ozone destruction results from reaction with NO to form NO₂, the amounts of O3N and O3V removed are transferred to the respective odd-oxygen tracers OON and OOV. When NO₂ is removed by photolysis to form ozone, the amounts of OON and OOV removed are transferred to the respective tracers O3N and O3V.

7.1.4 Alternative Ozone Apportionment Using APCA

An alternative ozone apportionment technique called Anthropogenic Precursor Culpability Assessment (APCA) differs from OSAT in recognizing that certain emission categories are not controllable (e.g., biogenic emissions) and that apportioning ozone production to these categories does not provide information that is relevant to development of control strategies. To address this, in situations where OSAT would attribute ozone production to non-controllable emissions, APCA re-allocates that ozone production to the controllable precursors that participated in ozone formation with the non-controllable precursor. For example, when ozone formation is due to biogenic VOC and anthropogenic NO_x under VOC-limited conditions (a situation where OSAT would attribute ozone production to biogenic VOC), APCA attributes ozone production to the anthropogenic NO_x present. Using APCA instead of OSAT results in more ozone formation attributed to anthropogenic NO_x sources and less ozone formation attributed to biogenic VOC sources.

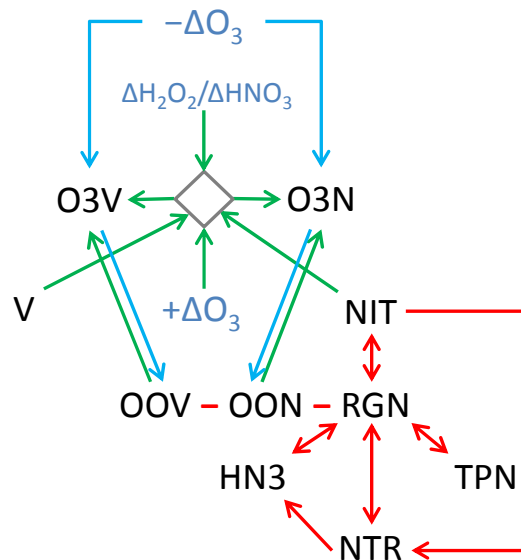


Figure 7-6. The OSAT3 scheme for ozone apportionment. Information flows along arrows. Changes in core model species are shown in blue, OSAT tracers are in black, the diamond represent the OSAT algorithms that determine ozone tracer production. $\Delta H_2O_2 / \Delta HNO_3$ is the indicator ratio used to determine NO_x- or VOC-limited ozone production. RGN apportions the nitrogen in NO₂ whereas OON and OOV apportion the odd-oxygen in NO₂.

The only difference between APCA and OSAT is the algorithm used to allocate ozone production under VOC or NO_x-limited conditions. The OSAT3 update does not revise the allocation of ozone production under VOC or NO_x-limited conditions and therefore the APCA algorithm works with the OSAT3 update.

7.2 Particulate Source Apportionment

Particulate Source Apportionment (PSAT) uses multiple tracer families to track the fate of primary and secondary PM (Yarwood et al., 2004). PSAT is designed to apportion the following classes of CAMx PM species (CF mode only):

- Sulfate (PSO4)
- Particulate nitrate (PNO3)
- Ammonium (PNH4)
- Secondary organic aerosol (SOA)
- Particulate mercury (HgP)
- Six categories of primary PM:
 - Elemental carbon (PEC)
 - Primary organic aerosol (POA)
 - Crustal fine (FCRS)

- Other fine (FPRM)
- Crustal coarse (CCRS)
- Other coarse (CPRM)

A single tracer family can apportion primary PM species whereas secondary PM species require several tracer families to track the relationship between gaseous precursors and the resulting PM. PNO₃ and SOA are the most complex PM categories to apportion because the emitted precursor gases (NO, VOC) are several steps removed from the resulting PM species (PNO₃, SOA).

The PSAT “reactive tracers” for each type of PM by source region/group *i* are described below. PSAT tracer names for particulate species begin with the letter “P.”

Sulfur

- SO_{2i} Primary SO₂ emissions
- PS_{4i} Particulate sulfate from primary emissions plus secondarily formed sulfate

Nitrogen

- NIT_i Nitric oxide (NO) and nitrous acid (HONO)
- RGN_i Nitrogen dioxide (NO₂), nitrate radical (NO₃), and dinitrogen pentoxide (N₂O₅)
- TPN_i Peroxyl acetyl nitrate (PAN), analogues of PAN and peroxy nitric acid (PNA)
- NTR_i Organic nitrates (RNO₃)
- HN_{3i} Nitric acid (HNO₃)
- PN_{3i} Particulate nitrate from primary emissions plus secondarily formed nitrate
- NH_{3i} Ammonia (NH₃)
- PN_{4i} Particulate ammonium (NH₄)

Secondary Organics

- ARO_i Aromatic (benzene, toluene, xylene, IVOC) secondary organic aerosol precursors
- ISP_i Isoprene secondary organic aerosol precursors
- TRP_i Terpene secondary organic aerosol precursors
- SQT Sesquiterpene secondary organic aerosol precursors
- CG_{1i} Condensable gases from aromatics (high volatility products)
- CG_{2i} Condensable gases from aromatics (low volatility products)
- CG_{3i} Condensable gases from biogenic (high volatility products)
- CG_{4i} Condensable gases from biogenic (low volatility products)
- PO_{1i} Particulate organic aerosol associated with CG₁
- PO_{2i} Particulate organic aerosol associated with CG₂
- PO_{3i} Particulate organic aerosol associated with CG₃
- PO_{4i} Particulate organic aerosol associated with CG₄
- PPA_i Anthropogenic organic aerosol polymers (SOPA)

PPB_i Biogenic organic aerosol polymers (SOPB)

Mercury

HG0_i Elemental Mercury vapor

HG2_i Reactive gaseous Mercury vapor

PHG_i Particulate Mercury

Primary Particulates

PEC_i Primary Elemental Carbon

POA_i Primary Organic Aerosol

PFC_i Fine Crustal PM

PFN_i Other Fine Particulate

PCC_i Coarse Crustal PM

PCS_i Other Coarse Particulate

Both ozone and PNO3 are associated with NOx emissions. The oxidized nitrogen tracer families for OSAT3 and PSAT are equivalent with the only difference being the additional tracer for particulate species in PSAT. Therefore, PSAT uses the same OSAT3 tracer family for oxidized nitrogen.

PSAT includes a total of 40 tracers for each source region/group if applied to all PM types. Since source apportionment may not always be needed for all species, the PSAT implementation is flexible and allows source apportionment for any or all of the chemical classes in each CAMx simulation (i.e. the PSO4, PNO3, PNH4, SOA, HgP and primary PM classes listed above). For example, source apportionment for sulfate, nitrate and ammonium requires just 10 tracers per source region/group.

A fundamental assumption in PSAT is that PM should be apportioned to the primary precursor for each type of PM. For example, PSO4 is apportioned to SOx emissions, PNO3 is apportioned to NOx emissions, PNH4 is apportioned to NH3 emissions, etc. As a source apportionment method, PSAT must account for all modeled sources of a PM species. Consider two model species A and B that are apportioned by reactive tracers a_i and b_i , respectively. Reactive tracers must be included for all sources of A and B including emissions, initial and boundary conditions so that complete source apportionment is obtained, i.e., $A = \sum a_i$ and $B = \sum b_i$.

In PSAT, the general approach to modeling change over a model time step Δt is illustrated for a chemical reaction $A \rightarrow B$.
The general equation for species destruction is:

$$a_i(t + \Delta t) = a_i(t) + \Delta A \frac{a_i}{\sum a_i}$$

Here, the relative apportionment of A is preserved as the total amount changes. This equation applies to chemical removal of A and also to physical removal of A by processes such as deposition or transport out of a specific grid cell.

The general equation for species production (e.g., chemical production by the chemical reaction $A \rightarrow B$) is:

$$b_i(t + \Delta t) = b_i(t) + \Delta B \frac{a_i}{\sum a_i}$$

Here, production of B inherits the apportionment of the precursor A . The same equation applies for "production" of B in a specific grid cell due to emissions or transport. For the case where B increases due to emissions, a_i is the apportionment of the emissions inventory. For the case where B increases due to transport, a_i is the apportionment of the upwind grid cell.

In some cases, source category specific weighting factors (w_i) must be added to the equation for species destruction:

$$a_i(t + \Delta t) = a_i(t) + \Delta A \frac{w_i a_i}{\sum w_i a_i}$$

An example is chemical decay of the aromatic VOC tracers (ARO), which must be weighted by the average OH rate constant of each ARO_{*i*}. ARO tracers for different source groups have different average VOC reactivities because the relative amounts of benzene, toluenes and xylenes differ between source categories.

In some cases, source category specific weighting factors (w_i) must be added to the equation for species production:

$$b_i(t + \Delta t) = b_i(t) + \Delta B \frac{w_i a_i}{\sum w_i a_i}$$

An example is chemical production of condensable gases (CG1 or CG2) from aromatic VOC tracers, which must be weighted by aerosol yield weighting factors. The aerosol yield weighting factors depend upon the relative amounts of benzene, toluenes and xylenes in each source group.

Several aerosol reactions are treated as equilibria, $A \leftrightarrow B$. If A and B reach equilibrium at each time step, it follows that their source apportionments also reach equilibrium:

$$a_i(t + \Delta t) = [a_i(t) + b_i(t)] \left(\frac{A}{A + B} \right)$$

$$b_i(t + \Delta t) = [a_i(t) + b_i(t)] \left(\frac{B}{A + B} \right)$$

Examples are the equilibrium between gas phase nitric acid and aerosol nitrate, gas phase ammonium and aerosol ammonium, and condensable organic gases (CG) and secondary organic aerosols (SOA).

7.3 Running CAMx With SA

7.3.1 CAMx Control File

Source apportionment is invoked similarly to the other Probing Tools within the CAMx control file. In the `&CAMx_Control` namelist module, the variable `Probing_Tool` must be set to "SA" if OSAT, APCA or PSAT are to be run. An additional namelist module called `&SA_Control` must then be provided in the control file to configure the SA portion of the model. The additional namelist module is described below. The order of the variables follows the template available with the source code. Several examples of the SA portion of the CAMx run control file are shown in Figures 7-7a-c.

Description of SA Control in the CAMx Run Control File

<code>&SA_Control</code>	Label for the Probing Tool namelist module that configures the SA option; it must begin in column 2
<code>&</code>	Flag ending a namelist module; it must be in column 2
<code>SA_Summary_Output</code>	Logical flag used to limit the species written to the tracer concentration file to a subset of the SA tracers. If set to true, the output will be restricted to O3N and O3V for OSAT/APCA, and the following species for PSAT: PS4, PN3, PN4, PO1, PO2, PO3, PO4, PO5, PO6, PO7, POH, PPA, PPB, PEC, POA, PFC, PFN, PCC, PCS, HGO, HG2, PHG
<code>SA_Treat_SULFATE_Class</code>	Logical flag to turn on the sulfate class of tracer species
<code>SA_Treat_NITRATE_Class</code>	Logical flag to turn on the nitrate class of tracer species
<code>SA_Treat_SOA_Class</code>	Logical flag to turn on the SOA class of tracer species
<code>SA_Treat_PRIMARY_Class</code>	Logical flag to turn on the primary PM class of tracer species
<code>SA_Treat_MERCURY_Class</code>	Logical flag to turn on the mercury class of tracer species
<code>SA_Treat_OZONE_Class</code>	Logical flag to turn on the ozone class of tracer species (uses OSAT attribution by default)
<code>SA_Use_APCA</code>	Logical flag to use APCA attribution rather than OSAT (<code>SA_Treat_OZONE_Class</code> must be set to TRUE)
<code>SA_File_Root</code>	Character root output path/filename
<code>SA_Stratify_Boundary</code>	Logical flag to stratify boundary types (TRUE=separate tracer types will be used for the North, South, East, West and Top boundaries, FALSE=a single tracer type will be used for all 5 boundaries)

SA_Deposition_Output	Logical flag to output deposited tracer mass to a file (TRUE=output deposited tracer mass, FALSE=do not generate a tracer deposition output file)
SA_Number_of_Source_Regions	Integer number of source regions for this run. This must be the same as the number of source areas defined in the SA_Source_Area_Map file
SA_Number_of_Source_Groups	Integer number of emission groups (categories) for this run. Together with the Use_Leftover_Group flag, this determines the number of paired gridded and point emission files that must be supplied (additional details below)
Use_Leftover_Group	Logical flag to define a "leftover" emissions group (TRUE= calculate a "leftover" emissions group from the difference between the sum of the emission group files and the regular CAMx emission files, FALSE=do not calculate a "leftover" emissions group)
SA_Receptor_Definitions	Character input SA receptor definition path/filename. (This is an optional file)
SA_Source_Area_Map	Character array (by CAMx grid) input SA original source area definition path/filename uniquely assigning each grid cell to a single source region (required for master grid, optional for nested grids)
SA_Use_Partial_SourceMap	Logical flag for fractional (or partial) source region (or area) maps (TRUE= use fractional maps, FALSE = use original source area definition only)
Partial_Source_Area_Map	Character array (by SA emissions group and CAMx grid) input SA fractional source area definition path/filename assigning each grid cell to multiple source regions by emission group (optional)
SA_PT_Override	Logical flag to allow point source override (TRUE = look for and use the point source override flags in sector-specific point source files, FALSE = ignore point source override flags)
SA_Master_Restart	Character input master grid SA restart path/filename (ignored if Restart=FALSE)
SA_Nested_Restart	Character input nested grid SA restart path/filename (ignored if Restart=FALSE or Number_of_Grids=1)
SA_Points_Group	Character array (by source group) input SA elevated point source emissions path/filename (optional, ignored if Point_Emissions=FALSE)

SA_Emiss_Group_Grid	Character array (by source group, by CAMx grid) input SA gridded emissions path/filename (optional, ignored if Gridded_Emissions=FALSE)
---------------------	---

Each partial source area map to be used in the run must be listed by source group and grid: e.g., Partial_Source_Area_Map(3,2) refers to SA emissions group 3 and grid 2. These map files must be listed in the same order as the group emission input files (i.e., the map assigned to category 1 must be consistent with the emissions assigned to category 1).

7.3.2 Specifying Emission Groups

SA can apportion ozone, PM and precursor concentrations among several emission categories (or "groups"). To achieve this, the emissions for each group must be supplied in separate emission files, both for low level (gridded) emissions for the master and each nested grid, and for elevated point sources. The additional emission files must be in the CAMx gridded and point emission file formats, as described in Section 3. If a category does not include point sources (e.g. biogenics), the point source file name for the group can be left blank. If a category has no gridded emissions, the gridded file name for the group can be left blank for all grids.

APCA requires at least two emission groups, and the first group must be biogenic emissions.

For example, in the case where emissions are tracked by three groups, three sets of emission files should be supplied that when summed equal the total emissions in the regular CAMx emission files supplied to the core model. CAMx also allows for an alternative option: two sets of files could be supplied and the third group can be calculated from the "leftover" emissions (i.e., the difference between the regular CAMx emissions and the two specified emission groups). The leftover option is set according to the input flag "Use_Leftover_Group". If the leftover option is selected, the model verifies that the leftover group is not too small to calculate within the numerical precision of the computer (this also traps cases where the flag was set in error). If the leftover option is not selected, the model verifies that the total emissions for the groups supplied are equal to the regular model emissions, i.e., that a leftover group is not needed. In both cases, if appropriate conditions are not met, the model stops with a descriptive error message.

The number of emission files that need to be supplied for different model configurations is summarized in Table 7-1; the table also shows how the emissions groups are numbered, which is reflected in the tracer species names (defined below).

Table 7-1. Numbers of emission file sets (i.e., gridded files and point source file) needed for different model configurations. APCA requires at least two emission groups, and the first group must be biogenic emissions.

Number of Emission Groups	Use Leftover Group	Number of Emission File Sets Needed	Numbering of Emission Groups and Tracer Species
n=1	Not Applicable	0	0
n>1	False	n	1,2,3,...n
n>1	True	n-1	1,2,3,...n


```

&SA_Control

SA_File_Root           = './OSAT_output/CAMx.OSAT.020603',

SA_Summary_Output     = .true.,
SA_Stratify_Boundary  = .false.,
SA_Deposition_Output  = .false.,
SA_Number_of_Source_Regions = 19,
SA_Number_of_Source_Groups = 1,
Use_Leftover_Group    = .false.,
SA_Treat_SULFATE_Class = .false.,
SA_Treat_NITRATE_Class = .false.,
SA_Treat_SOA_Class    = .false.,
SA_Treat_PRIMARY_Class = .false.,
SA_Treat_MERCURY_Class = .false.,
SA_Treat_OZONE_Class  = .true.,
SA_Use_APCA           = .false.,

SA_Receptor_Definitions = './OSAT_input/receptor.cities ',
SA_Source_Area_Map(1)   = './OSAT_input/OSAT.source.area.map',
SA_Source_Area_Map(2)   = ' ',
SA_Use_Partial_SourceMap = .false.,
Partial_Source_Area_Map(1,1) = ' ', ! Map for SA group 1, grid 1
Partial_Source_Area_Map(1,2) = ' ', ! Map for SA group 1, grid 2
SA_PT_Override          = .false.,

SA_Master_Restart      = ' ',
SA_Nested_Restart      = ' ',

SA_Points_Group(1)     = ' ',

SA_Emiss_Group_Grid(1,1) = ' ',
SA_Emiss_Group_Grid(1,2) = ' ',

&

```

Figure 7-7a. An example of SA input records in the CAMx run control file. The options for this OSAT run are as follows: this is a two-grid run, master and nested grid surface concentrations are written to file, a single tracer type is to be used for all boundaries, 19 source regions, and one emission group (i.e., zero additional emission files and no leftover group). This is the first day of the simulation (i.e., restart is false), so no OSAT restart files are supplied.

```

&SA_Control

SA_File_Root           = './OSAT_output/CAMx.OSAT.020604',

SA_Summary_Output      = .true.,
SA_Stratify_Boundary   = .false.,
SA_Deposition_Output   = .false.,
SA_Number_of_Source_Regions = 19,
SA_Number_of_Source_Groups = 3,
Use_Leftover_Group     = .true.,
SA_Treat_SULFATE_Class = .false.,
SA_Treat_NITRATE_Class = .false.,
SA_Treat_SOA_Class     = .false.,
SA_Treat_PRIMARY_Class = .false.,
SA_Treat_MERCURY_Class = .false.,
SA_Treat_OZONE_Class   = .true.,
SA_Use_APCA            = .false.,

SA_Receptor_Definitions = './OSAT_input/receptor.cities ',
SA_Source_Area_Map(1)   = './OSAT_input/OSAT.source.area.map',
SA_Source_Area_Map(2)   = ' ',
SA_Use_Partial_SourceMap = .false.,
Partial_Source_Area_Map(1,1) = ' ', ! Map for SA group 1, grid 1
Partial_Source_Area_Map(1,2) = ' ', ! Map for SA group 1, grid 2
SA_PT_Override          = .false.,

SA_Master_Restart      = './OSAT_output/CAMx.OSAT.020603.sa.inst',
SA_Nested_Restart      = './OSAT_output/CAMx.OSAT.020603.sa.finst',

SA_Points_Group(1)     = ' ',
SA_Points_Group(2)     = './OSAT_input/utils.020604',

SA_Emiss_Group_Grid(1,1) = './OSAT_input/bio.grd1.020604',
SA_Emiss_Group_Grid(1,2) = './OSAT_input/bio.grd2.020604',
SA_Emiss_Group_Grid(2,1) = './OSAT_input/util.grd1.020604',
SA_Emiss_Group_Grid(2,2) = './OSAT_input/util.grd2.020604',

&

```

Figure 7-7b. As in Figure 7-7a, but in this case the run is a continuation day of a run with three emission groups. The three emission groups are defined by supplying extra emission files for point and area sources for each grid (emission groups 1 and 2), and setting the “Use_Leftover_Group” flag to TRUE so that the model calculates the third group internally. The point source group 1 filename is blank because group 1 is a category with no point source emissions (e.g., biogenics).

```

&SA_Control

SA_File_Root                = './OSAT_output/CAMx.APCA.020604',

SA_Summary_Output           = .true.,
SA_Stratify_Boundary        = .false.,
SA_Deposition_Output        = .false.,
SA_Number_of_Source_Regions = 19,
SA_Number_of_Source_Groups  = 3,
Use_Leftover_Group          = .false.,
SA_Treat_SULFATE_Class      = .true.,
SA_Treat_NITRATE_Class      = .true.,
SA_Treat_SOA_Class          = .false.,
SA_Treat_PRIMARY_Class      = .false.,
SA_Treat_MERCURY_Class      = .false.,
SA_Treat_OZONE_Class        = .true.,
SA_Use_APCA                 = .true.,

SA_Receptor_Definitions    = './OSAT_input/receptor.cities ',
SA_Source_Area_Map(1)      = './OSAT_input/OSAT.source.area.map',
SA_Source_Area_Map(2)      = ' ',
SA_Use_Partial_SourceMap   = .false.,
Partial_Source_Area_Map(1,1) = ' ',      ! Map for SA group 1, grid 1
Partial_Source_Area_Map(1,2) = ' ',      ! Map for SA group 1, grid 2
SA_PT_Override              = .false.,

SA_Master_Restart           = './OSAT_output/CAMx.APCA.020603.sa.inst',
SA_Nested_Restart           = './OSAT_output/CAMx.APCA.020603.sa.finst',

SA_Points_Group(1)         = ' ',
SA_Points_Group(2)         = './OSAT_input/utils.020604',
SA_Points_Group(2)         = './OSAT_input/other.020604',

SA_Emiss_Group_Grid(1,1)   = './OSAT_input/bio.grd1.020604',
SA_Emiss_Group_Grid(1,2)   = './OSAT_input/bio.grd2.020604',
SA_Emiss_Group_Grid(2,1)   = './OSAT_input/util.grd1.020604',
SA_Emiss_Group_Grid(2,2)   = './OSAT_input/util.grd2.020604',
SA_Emiss_Group_Grid(3,1)   = './OSAT_input/othr.grd1.020604',
SA_Emiss_Group_Grid(3,2)   = './OSAT_input/othr.grd2.020604',

&

```

Figure 7-7c. This figure follows from Figure 7-7b: it is a continuation day of a 2-grid run with three emission groups, and all three emission groups are defined explicitly by supplying extra emission files; therefore, the “Use_Leftover_Group” flag is set to FALSE. The point source group 1 filename is blank because group 1 is a category with no point source emissions (e.g., biogenics). APCA is used to attribute ozone sources, so biogenic emissions MUST be present as group 1. PSAT will trace PM sulfate and nitrate species.

When specifying point source files to resolve source categories, the list of point sources on each file must be identical (i.e., same number of sources, same order) to the regular model point source file. This formal restriction is necessary to ensure that point sources are correctly cross-referenced within CAMx. Thus, a point source file for a specific source group may need to contain records for sources that are not in the group: these records should have zero emissions.

7.3.3 Source Area Mapping

SA can apportion ozone, PM and precursor concentrations among several geographic regions within the modeling domain, as shown in Figure 7-1. SA requires a digital map of the modeling grid that defines how tracers are allocated spatially – this “source area map” file assigns each grid cell to one or more geographic source regions. A source area map must be defined for the master grid and optionally any nested grids. The source area map formats are identical among all grids, but maps for nested grids **must include the boundary (“buffer”) rows and columns**. The source regions defined on each nest take precedence over those defined for the master grid. If a source area map is not provided for a specific nest then the source region definition will be defined by the source area map for the parent grid.

There are two ways to define source area maps. The first (original) approach is to uniquely assign the entirety of each grid cell to a single geographic region with which to apportion all source categories present in that grid cell. The second option allows for the fractional allocation of each grid cell to multiple regions, for example, in cases where several geopolitical boundaries intersect within a single cell. Furthermore, separate fractional area maps may be developed that uniquely define source region distributions for each emission category to be tracked by SA. The original source area maps are required to run SA, but can be superceded by the optional fractional source area maps. The original maps provide the default SA region definition in case a fractional region map file is not provided for one or more source categories. If no fractional area maps are provided to CAMx, then the entire SA treatment defaults back to the original area map definition. CAMx includes reports in the output diagnostic file to allow the user to review the SA region configuration.

The original SA map format is simple: an array of 3-digit integers (*i3*) spanning the entirety of a particular CAMx grid. Figure 7-8 shows the source area mapping file for the single grid corresponding to Figure 7-1. Since the CAMx domain in Figure 7-1 has 63 rows and 64 columns of cells, the file shown in Figure 7-8 has 63 lines with 64 numbers on each line. The first number in the top left corner always corresponds to the northwest corner of the domain. This file is typically generated using GIS software by overlaying the modeling grid onto geopolitical maps and using the dominant coverage in each grid cell as its source region assignment.

To facilitate multiple intersecting regions within each grid cell, a fractional area map for a single grid may include multiple “panels”, where the total number of panels is determined by the maximum number of region overlaps found among all grid cells. For example, if a particular grid cell contains a grid-wide maximum of four overlapping regions, then the fractional map contains four panels, each listing one of the four regions and its fractional coverage in that cell.

The fractional SA map file has the following format:

Loop over number of panels	
/SRCMAPnn-mm/	Header keyword, where nn is source category/group ID, mm is panel ID
Loop from <i>n_y</i> grid rows to 1	
(<i>regn</i> (<i>i</i> , <i>j</i>), <i>frc</i> (<i>i</i> , <i>j</i>), <i>i</i> =1, <i>n_x</i>)	Loop over <i>n_x</i> grid columns, 500(<i>i3</i> ,1x,f5.1)
End loop over rows	
End loop over panels	
/END/	End of file keyword

The integer variable array *regn* is the region index that exists in cell (*i*, *j*) and the real variable array *frc* is the fraction (percent) of cell (*i*, *j*) covered by that region. For non-zero cell fractions, both *regn* and *frc* must be listed, otherwise *regn* is shown as 0 and *frc* is blank to maximize visual clarity of the file. The total coverage among all regions in each grid cell equals 100.0% when summed over all panels. An example is shown in Figure 7-9 for a small grid of 10x10 cells.

The original source area map, and possibly even the fractional map, may not adequately resolve the region to which certain point sources should be assigned. To provide finer control of point source assignments to geographic areas, the region index can be specified for any point source using the *kcell* variable in the point source file (see file description in Section 3). This feature is referred to as “point source override.”

7.3.3.1 Generating Fractional Area Maps From SMOKE Reports

A Fortran tool called REGNMAP has been developed to support the development of fractional area maps using information derived from the Sparse Matrix Operator Kernel Emissions (SMOKE) processing system. SMOKE can be configured to output information to “report files” that list the spatial allocation of county-level emissions to a particular modeling grid by criteria pollutant (NO_x, VOC, SO_x, and PM). A separate fractional area map can be developed for each

```

/SRCMAP03-01/
 5 100.0 5 100.0 5 100.0 5 100.0 5 25.0 6 100.0 6 100.0 6 100.0 6 100.0 6 100.0
 5 100.0 5 100.0 5 100.0 5 100.0 5 25.0 6 100.0 6 100.0 6 100.0 6 100.0 6 100.0
 5 100.0 5 100.0 5 100.0 5 100.0 5 30.0 6 100.0 6 100.0 6 100.0 6 100.0 6 100.0
 5 100.0 5 100.0 5 100.0 5 100.0 5 35.0 6 100.0 6 100.0 6 100.0 6 100.0 6 100.0
 5 100.0 5 100.0 5 100.0 5 100.0 5 50.0 6 100.0 6 100.0 6 100.0 6 100.0 6 100.0
 5 100.0 5 100.0 5 100.0 5 100.0 5 60.0 6 100.0 6 100.0 6 100.0 6 100.0 6 100.0
 5 100.0 5 100.0 5 100.0 5 100.0 5 80.0 6 100.0 6 100.0 6 100.0 6 100.0 6 100.0
 5 100.0 5 100.0 5 100.0 5 100.0 5 100.0 5 20.0 6 100.0 6 100.0 6 100.0 6 100.0
 5 100.0 5 100.0 5 100.0 5 100.0 5 100.0 5 50.0 6 100.0 6 100.0 6 100.0 6 100.0
 5 100.0 5 100.0 5 100.0 5 100.0 5 100.0 5 60.0 6 100.0 6 100.0 6 100.0 6 100.0
/SRCMAP03-02/
 0 0 0 0 6 75.0 0 0 0 0 0
 0 0 0 0 6 75.0 0 0 0 0 0
 0 0 0 0 6 60.0 0 0 0 0 0
 0 0 0 0 6 65.0 0 0 0 0 0
 0 0 0 0 6 50.0 0 0 0 0 0
 0 0 0 0 6 40.0 0 0 0 0 0
 0 0 0 0 6 20.0 0 0 0 0 0
 0 0 0 0 0 80.0 0 0 0 0 0
 0 0 0 0 0 6 50.0 0 0 0 0 0
 0 0 0 0 0 6 40.0 0 0 0 0 0
/END/

```

Figure 7-9. Example fractional area map file for a small (10x10) grid. This file is for source category/group #3 and includes 2 map panels. The grid covers source region #5 and #6 and these regions overlap in the middle of the domain. Panel 2 shows just the remaining overlap information for region #6.

source sector or group of sectors depending on how the user runs SMOKE and configures the list of sectors to be tracked for SA (e.g., consider spatial differences between urban area sources and agricultural non-road sources). SMOKE spatial allocation reports must be invoked in order to utilize the REGNMAP program to develop fractional area maps for CAMx.

Mobile emissions are not spatially allocated in the same way as non-road and stationary sources, so SMOKE reports are not available for the on-road sector if SMOKE-MOVES is used. Therefore, the on-road sector must continue to be tracked in SA using the original source area map. Additionally, SMOKE does not allocate elevated point sources to the modeling grid like surface county-level sources, and so SMOKE spatial allocation reports are not available for point sources. All category-specific point source files to be tracked by SA are assigned to the original region map definition by default, except for those individual point sources flagged for source region override (see Section 3).

REGNMAP reads SMOKE spatial allocation reports for a specific modeling grid and source category (or group of categories), extracts emissions data by grid cell and state/county Federal Information Processing Standards (FIPS) code, and generates a fractional area map file for that grid and source category/group. The list of SA regions to process are externally defined as a county or group of counties, a state or group of states, or all other undefined areas. REGNMAP provides an option to select among the criteria pollutants NO_x, VOC, SO_x, or PM_{2.5} as the basis to define the fractional grid cell areas in case the specific source category/group to be processed is uniquely characterized by one of these species (e.g., NO_x for mobile sources, SO_x for power plants). Alternatively, the user may select "All" criteria pollutants, in which case the

fractional allocation is based on the sum of all emissions reported per grid cell for that source category/group. Additional information on how to run REGNMAP is provided with the program.

7.3.4 Receptor Definition

Tracer concentrations can be optionally output to a text file for selected receptor locations at the model's output frequency (usually 1 hour). The receptors for each model run are defined in the "receptor definition" input file. Three types of receptors are supported:

POINT	a point specified in the CAMx projection coordinate system. Concentrations at the point are determined by bi-linear interpolation of the surrounding four surface grid cells.
SINGLE CELL	a single surface grid cell identified by grid cell index.
CELL AVERAGE	a group of surface grid cells identified by a range of grid indices that are averaged together to provide multi-cell average tracer concentrations.
WALL OF CELLS	a group of grid cells identified by a range of grid and layer indices that define a wall (i.e., a flux plane).

For the receptor types that are defined by grid cell it is necessary to specify the grid containing the receptor on the receptor definition record. Grid numbers are defined using the internal CAMx grid ordering. The grid numbering as defined by CAMx is shown in a table in the `.diag` file. Each receptor can be identified by a 10 character name. The formats for specifying each receptor type are given in Table 7-2. An example receptor file is shown below:

POINT	City 1	1024.0	-272.0	
SINGLE CELL	Cell 1	1	45	18
CELL AVERAGE	Region 10	2	8	
	31	19		
	32	19		
	33	19		
	34	19		
	31	18		
	32	18		
	33	18		
	34	18		
WALL OF CELLS	Boundary1	2	10	20
			18	18
			1	5

7.3.5 Output File Formats

SA writes several output files that are in the CAMx Fortran binary format, as described in Section 3. These include the master and nested grid tracer instantaneous concentration files (`.sa.inst` and `.sa.finst`), the grid-specific surface tracer average concentration file (`.sa.grdnn`), and the grid-specific surface deposited mass file (`.sa.depn.grdnn`). In

Table 7-2. Format for the receptor definition file.

Receptor Type	Line	Columns	Data
POINT	1	1-15	The word "POINT"
	1	21-30	Receptor name
	1	31-40	X co-ordinate
	1	41-50	Y co-ordinate
SINGLE CELL	1	1-15	The word "SINGLE CELL"
	1	21-30	Receptor name
	1	31-40	Grid Number
	1	41-50	X cell number
CELL AVERAGE	1	51-60	Y cell number
	1	1-15	The words "CELL AVERAGE"
	1	21-30	Receptor name
	1	31-40	Grid number
	1	41-50	The number of cells to average (M)
	2-M	1-10	X cell number
2-M	11-20	Y cell number	
WALL OF CELLS	1	1-15	The words "WALL OF CELLS"
	1	21-30	Receptor name
	1	31-40	Grid number
	1	41-50	X-cell begin
	1	51-60	X-cell end
	2	41-50	Y-cell begin
	2	51-60	Y-cell end
	3	41-50	Z-cell begin
3	51-60	Z-cell end	

addition, SA writes out tracer concentrations for selected receptor locations to a text file (.sa.receptor). The naming conventions for tracer species and the format of the receptor concentration file are discussed below.

7.3.5.1 Tracer Species Names

The names of tracer species uniquely identify the information carried by each species and together identify the SA configuration. Species names have less than ten characters, consistent with the CAMx convention. The naming conventions are as follows:

Emission Sources **SSSeeerrr**

where:

SSS Species type, e.g., NOX, VOC, O3V, O3N, PSO4, etc.

eee Emissions group:

 Single group, always 000

 Multiple groups, 001, 002, etc.

rrr Region tracer released from, 001, 002, 003, etc.

Initial/Boundary **SSSeeerrr**

where:

SSS Species type, e.g., NOX, VOC, O3V, O3N, PSO4, etc.

eee Initial Concentrations: always 000
 Boundary Concentrations not stratified by boundary: always 000
 Boundary Concentrations stratified by boundary: WST, EST, STH, NTH,
 TOP indicating boundary of origin

rrr IC for Initial Concentrations, BC for Boundary Concentrations

Examples: NOX000015, VOC002015, O3V000IC, O3NTOBPC

7.3.5.2 Receptor Concentration File

Tracer concentrations at user-specified receptor locations are output to the “receptor concentration” file. The file is in comma delimited text format suitable for importing into a spreadsheet. An example output file is shown in Figure 7-10. Two header lines at the top of the file identify the model version and the date the run was performed. Next, two lines identify the time period covered by the file and the averaging interval (generally one hour, determined by the CAMx simulation control file). Next, three lines define the SA configuration, followed by the numbers of tracer species that result from this configuration. The names of each tracer species are listed by tracer type: the order in which species are listed here is the same as the order in which tracer concentrations are given later in the file.

The tracer species names are followed by the number of receptors and receptor names as specified in the “receptor definition” file. The tracer concentrations are reported in blocks with a date and time stamp at the head of each block. Within each block, receptors are reported in numerical order. For each receptor, there are data for the tracer species identified at the heading “Tracer Names”. All values are in CAMx units of ppm for gases and $\mu\text{g}/\text{m}^3$ for PM.

7.3.6 Postprocessing

The tracer concentrations in the gridded surface concentration files can be displayed using any post-processing software normally used for displaying CAMx average file output formats.

The receptor concentration file contains information for all receptors and all hours within the model run that created the file. It is left to the user to develop post-processing tools to analyze the information contained in this file.

7.4 Steps In Developing Inputs And Running SA

Below is a simple methodological list of steps to follow in setting up and running SA. The process is similar among the OSAT/APCA, PSAT, and DDM Probing Tools.

- 1) Define the source groups and regions that you wish to track. Keep in mind that memory resources increase dramatically as the number of tracers grows. Probing Tool applications with large numbers of tracers, tracer classes, nested grids or grid cells may exceed available memory.
- 2) Build a source region map (Figure 7-8) that defines the spatial allocation of tracer emissions. For small domains or small number of regions, this can be done by hand. We suggest using GIS software to develop complex source region maps on large grids.

CAMx, CAMx 6.30 Test Problem -- Mech6 CF CB05 SA.OMP, Source Apportionment, SA 160408,
Thu Mar 31 13:18:53 2016

File Duration , 02154, 0.00, 02154, 24.00,
Average Interval , 1.0000

Number of timing periods , 0
Number of source areas , 4
Number of emission groupings , 4
Number of tracer species , 180
Number of VOC species , 18
Number of O3N species , 18
Number of O3V species , 18
Number of OON species , 18
Number of OOV species , 18
Number of NIT species , 18
Number of RGN species , 18
Number of TPN species , 18
Number of NTR species , 18
Number of HN3 species , 18
Number of INERT TIME species , 0
Number of DECAY TIME species , 0

Tracer Names,

VOC000IC , VOC000BC, VOC001001, VOC001002, VOC001003, VOC001004, VOC002001, ...
O3N000IC , O3N000BC, O3N001001, O3N001002, O3N001003, O3N001004, O3N002001, ...
O3V000IC , O3V000BC, O3V001001, O3V001002, O3V001003, O3V001004, O3V002001, ...

(List continues for remaining tracer species names)

Number of receptors , 4
No, Name, Type, Grid#, Xloc, Yloc,
1, City 1 , 0, , 1024.0, -272.0,
2, Cell 1 , 1, 1, 45, 18,
3, Region 10, 8, 2, 31, 19,
32, 19,
33, 19,
34, 19,
31, 18,
32, 18,
33, 18,
34, 18,
4, Boundary1, 3, 2, 10, 20,
18, 18,
1, 5,

Time Varying Tracer Data,

Data for Period, 02154, 0.00, 02154, 1.00,
Receptor, 1,
1.3265E-02, 1.3544E-09, 1.0000E-16, 1.0974E-15, 1.0000E-16, 1.0000E-16, ...
1.2237E-01, 3.3869E-08, 1.0000E-16, 1.6165E-14, 1.0000E-16, 1.0000E-16, ...
8.7304E-02, 1.1926E-08, 1.0000E-16, 1.0000E-16, 1.0000E-16, 1.0000E-16, ...
9.0300E-02, 1.5269E-08, 1.0188E-16, 2.6997E-15, 1.0213E-16, 1.0162E-16, ...
1.0036E-16, 4.0640E-15, 1.0036E-16, 1.0036E-16, 1.0036E-16, 1.0029E-16, ...
1.0000E-16, 3.7563E-15, 1.0000E-16, 1.0000E-16, 1.0000E-16, 1.0000E-16, ...
Receptor, 2,

(File continues with data for remaining receptors and hours)

Figure 7-10. Example receptor concentration file. Lines ending with “...” are truncated to fit the page, and the file would continue with data for additional receptors and hours in the same format.

- 3) Process the emissions inventory into the separate source group files that you want to track (e.g., mobile, area, point, biogenic, etc.).
 - a) Consideration of potential source apportionment or sensitivity applications prior to any emissions processing can be very beneficial so that files by group are available for later use.
 - b) Elevated point sources will automatically be assigned to the source region in which they reside. However, you may override the region to which each individual point source is assigned (see the definition of `kcell` in Section 3, Elevated Point Source File). A point source region does not need to be defined in the source region map, e.g., you could have a map with two regions that split the domain in half, with a third region assigned arbitrarily to represent elevated point sources only.
- 4) Edit the CAMx control namelist file (Section 2).
 - a) Set the `Probing_Tool` variable to "SA"; this will activate the `&SA_Control` namelist module.
 - b) Edit or add the `&SA_Control` namelist module (described earlier). Provide the required information, including:
 - output paths
 - whether to stratify boundary conditions
 - flags to turn on specific ozone or PM classes
 - number of source regions
 - number of source groups
 - whether to use the leftover group option
 - receptor definitions
 - list of input emission files by group.
 - c) Note that APCA **requires** that the biogenic emission files for each grid are listed first. Several examples are shown in Figure 7-7.
- 5) Configure the CAMx source code to define the number of tracers, and build an executable. This will ensure that you have sufficient memory for the Probing Tool application.
 - a) Edit the file `Includes/camx.prm`
 - b) Change the parameter `MXTRSP`, following the instructions provided in the file. CAMx is distributed with `MXTRSP=1` to minimize memory requirements for standard applications of the model. If you run SA with an insufficient value, the model will stop and tell you the required value of `MXTRSP` for your application.
 - c) Execute the `CAMx Makefile` to build an executable program (Section 2).
- 6) Run CAMx and review the diagnostic output files to ensure that the model is correctly interpreting and running the Probing Tool configuration that you have specified. Ensure that CAMx is generating the proper output files that you are expecting. Review the table of emissions by source group and region.

- 7) Review gridded tracer fields using commonly available plotting programs. Utilities such as PAVE or Verdi will read Probing Tool files directly. Use of any other software may require specialized re-formatting procedures.
- 8) You may post-process and analyze SA receptor files using your own spreadsheet or database software.
- 9) Probing Tool gridded tracer output files are written in the same Fortran binary format as the regular CAMx concentration output files. You can post-process gridded output fields using any software that reads CAMx files, or you can adapt those programs or build your own software to generate specialized analysis and graphical products.

8. DECOUPLED DIRECT METHOD FOR SENSITIVITY ANALYSIS

Photochemical modelers have traditionally used sensitivity analysis both for model performance evaluation and emission control strategy design. The simplest approach to sensitivity analysis, often referred to as the “brute-force” approach, involves changing a model input parameter, rerunning the model, and then evaluating the change in model output for each parameter to be investigated. For example, a model performance evaluation may use sensitivity simulations to evaluate the impact of changing initial or boundary conditions (ICs and BCs), biogenic emissions, anthropogenic emissions, etc. Control strategy evaluation may reduce VOC and NO_x emissions to determine whether VOC and/or NO_x reduction strategies are the most effective path to reduce ozone.

The advantages of the “brute force” method for sensitivity analysis are:

- Applicable to any model input parameter;
- Results are conceptually easy to explain and interpret.

The limitations of the “brute force” method are:

- Computationally inefficient;
- Sensitivity depends upon the magnitude of the perturbation if the model response is non-linear;
- Sensitivity derived from small perturbations may contain significant levels of uncertainty (numerical noise).

The last two points bear further explanation. If the model response to an input parameter depends upon non-linear components within the model (e.g., chemistry), then the relative magnitude or even sign of the output response may change for perturbations of different sizes. An example is the ozone response to NO_x reductions in a VOC-limited environment: smaller reductions in NO_x emissions increase ozone levels whereas larger NO_x reductions decrease ozone.

This situation can be illustrated mathematically. We define a “sensitivity coefficient” (s) which represents the change in concentration (c) with respect to some input parameter (λ), evaluated relative to the base state ($\lambda=\lambda_0$),

$$s = \left. \frac{\partial c}{\partial \lambda} \right|_{\lambda_0}$$

In general, λ can be a vector (denoted as $\underline{\lambda}$), which contains multiple parameters related to processes in the model (e.g., rate constants) or inputs to the model (e.g., emissions). The concentration response to a change in $\underline{\lambda}$ can be represented by a Taylor series of sensitivity coefficients:

$$\begin{aligned}
 c(\underline{x}, t; \underline{\lambda}) &= c(\underline{x}, t; \underline{\lambda}_{i0}) + \sum_{i=1}^n \left. \frac{\partial c}{\partial \lambda_i} \right|_{\underline{\lambda}_{i0}} (\lambda_i - \lambda_{i0}) \\
 &+ \frac{1}{2} \sum_{i=1}^n \sum_{j=1}^n \left. \frac{\partial^2 c}{\partial \lambda_i \partial \lambda_j} \right|_{\underline{\lambda}_{i0}} (\lambda_i - \lambda_{i0})(\lambda_j - \lambda_{j0}) \\
 &+ \text{third and higher order terms...}
 \end{aligned}$$

where n is the number of $\underline{\lambda}$ vector elements, \underline{x} is the spatial dimension vector, and t is time. In the ozone sensitivity example above, the non-linear ozone response to large NO_x emission reductions indicates that high-order sensitivity coefficients (curvatures and inflections) are significant relative to the first order sensitivity (linear response). As the magnitude of the input perturbation tends to zero, the output response will become dominated by the first-order sensitivity. Therefore, very small changes in the input parameter may be required to use the “brute force” method to estimate the first-order (local) sensitivity. The practical limitation to this approach is that since the change in output must be determined from the difference between two simulations, small levels of numerical uncertainty (noise) in two very similar outputs will contaminate the sensitivity calculation.

An alternative methodology for evaluating model sensitivity was developed by Dunker (1980, 1981) called the decoupled direct method (DDM). The DDM can be used to calculate the same type of sensitivity coefficient as the “brute force” method. The difference is that with DDM, sensitivity coefficients are calculated explicitly by specialized algorithms implemented in the host model. Thus, the DDM offers several advantages over the brute force method:

- Improved computational efficiency, especially as multiple sensitivities can be calculated simultaneously;
- Improved accuracy since sensitivities are not contaminated by numerical noise.

8.1 Implementation

The original CAMx implementation of the DDM considered only first-order sensitivity for gas-phase species. Dunker et al. (2002) performed a rigorous analysis of DDM and demonstrated excellent agreement against brute force tests. High-order DDM (HDDM; Hakami et al., 2003; Cohan et al., 2005) has since been implemented in CAMx. HDDM enables CAMx to calculate second-order sensitivities along with first-order values for gas-phase species (Koo et al., 2007a, 2008). The first-order DDM sensitivity has been extended to PM species (Koo et al., 2007b, 2009). In the following discussion we use the term DDM generically to mean first and/or higher order sensitivity.

The CAMx DDM calculates concentration sensitivity to several sources (i.e., emissions, ICs and BCs) and to chemical rate constants. The sensitivity to be evaluated may bear a simple relationship to a model input parameter, such as scaling ozone BCs by a factor ($BC_{new} = \lambda \times BC_0$), or additively increasing the ozone BC's by a constant amount everywhere ($BC_{new} = \lambda + BC_0$). To allow complete flexibility, the sensitivity perturbations are specified by providing additional IC, BC, and/or emission input files with the same format as the regular model input files.

As a result, the user can perform many different sensitivity calculations in a single run according to the content of the DDM input files. For example, if the same BC file is specified for both CAMx and DDM, the output sensitivity fields represent the sensitivity of the predicted concentrations to those particular BCs. Simply scaling the output sensitivity coefficients fields provides the incremental concentrations resulting from scaling the BCs. If a DDM BC file contains constant concentrations everywhere, the sensitivity will correspond to a uniform absolute increase in the BCs rather than a percentage increase as described above. Another possibility includes a DDM BC file with a different spatial pattern than the CAMx input file. The sensitivity coefficient would then correspond to changing both the geographic distribution and magnitude of BCs. In short, the DDM input files can be arbitrary – different from the CAMx input file in the overall magnitude of concentrations or emissions, different in the geographic and temporal distribution, and different in the relative proportions of the chemical species. However, the user must understand what perturbations are being considered in order to properly interpret the resulting output sensitivity coefficient fields.

In mathematical terms, a regular model input file, for example the BC input file, represents some set of functions of space and time $f_i(\underline{x}, t)$, where each chemical species i can be defined by a unique function. An additional input file provided to the DDM represents another set of functions of space, time, and chemical species $g_i(\underline{x}, t)$ that can be different from the regular input file. The scalar parameter λ_i is then defined by

$$F_i(\underline{x}, t) = f_i(\underline{x}, t) + \lambda_i \times g_i(\underline{x}, t).$$

Here, $\lambda_i \times g_i(\underline{x}, t)$ is the perturbation, and the user desires information on how the model would respond if the input $f_i(\underline{x}, t)$ is replaced by the input $F_i(\underline{x}, t)$. In the case of sensitivity to rate constants, no user-defined input file is provided and the perturbation is always defined as $\lambda_i \times \underline{k}$ where \underline{k} is a vector of selected rate constants. The DDM calculates the first-order sensitivity $s_i^{(1)}(\underline{x}, t)$ and second-order sensitivity $s_i^{(2)}(\underline{x}, t)$ with respect to the scalar parameter λ_i . The Taylor series to second order then gives the estimate:

$$c_i(\underline{x}, t; \lambda_i) = c_i(\underline{x}, t; \lambda_i=0) + \lambda_i \times s_i^{(1)}(\underline{x}, t) + \frac{1}{2} \lambda_i^2 \times s_i^{(2)}(\underline{x}, t)$$

where $c_i(\underline{x}, t; \lambda_i)$ is the estimated model result for species i when $F_i(\underline{x}, t)$ is used as input, and $c_i(\underline{x}, t; \lambda_i=0)$ is the base case model result when $f_i(\underline{x}, t)$ is used as input.

For example, to calculate the sensitivity of the predicted ozone concentration to scaling boundary ozone by a factor, CAMx would be provided with a DDM BC file that has the same ozone values as the regular model BC file. The sensitivity coefficient fields output by CAMx could then be used to estimate the resulting ozone concentration if the ozone BCs were increased by 20%, as follows (for simplicity hereafter, the dependence on space, time, and chemical species will be omitted):

$$c_{\lambda=0.2} = c_{\lambda=0} + 0.2 \times s^{(1)} + \frac{1}{2} \times 0.2^2 \times s^{(2)}$$

To calculate the sensitivity of the predicted ozone concentration to increasing boundary ozone by 10 ppb, CAMx would be provided with a DDM BC file that has a constant ozone value of 10 ppb. The sensitivity coefficient fields could be used to estimate the ozone concentration if the ozone BCs were increased by 10 ppb as follows:

$$c_{\lambda=1.0} = c_{\lambda=0} + 1 \times s^{(1)} + \frac{1}{2} \times 1^2 \times s^{(2)}$$

where each sensitivity is calculated according to the 10 ppb addition carried in the DDM BC file (thus sensitivities are scaled by unity). An alternative approach would be to provide CAMx with a DDM BC file that has a constant ozone value of 1 ppb, and to estimate ozone response if the ozone BCs were increased by 10 ppb would require that each sensitivity above be scaled by 10.

These are examples of relatively simple sensitivities. A more complex example would be to calculate ozone sensitivity to scaling morning (6-9 AM) NO_x emissions in a specific group of grid cells. In this case you would provide CAMx with a DDM emissions file where all values are zero except for the NO_x emissions in the selected grid cells between 6 AM and 9 AM, which would have the same value as the regular emissions file. The sensitivity coefficient could be used to predict the concentration after a scalar change (λ) in the morning NO_x emissions using the same general equation as given above:

$$c_{\lambda} = c_{\lambda=0} + \lambda \times s^{(1)} + \frac{1}{2} \lambda^2 \times s^{(2)}$$

Any type of sensitivity perturbation can be described via an input file. However, the CAMx user interface also provides easy ways to define some sensitivities that are likely to be used frequently. In the first example above, the DDM BC file was described as having the "same ozone values as the regular model BC file." To avoid the effort of preparing an input file that is trivially different from the regular model file, the user interface allows you to select specific species from an input file to track - in this case ozone. It is possible to separately track the sensitivity to more than one species from the same file (e.g. ozone and NO). It is also possible to track the combined sensitivity to a group of species, such as NO_x, VOC, HRVOC, or ALL. The user interface also provides a simple way to track sensitivities to emissions from specific grid cells or groups of cells (sub-regions).

8.1.1 Tracking Sensitivity Coefficients Within CAMx

DDM sensitivity coefficients are calculated in parallel to the core CAMx processes (emissions, advection, diffusion, chemistry, deposition, etc.) that step the three-dimensional concentration fields forward in time. For some processes (e.g., chemistry and horizontal advection), the sensitivity routines make use of information saved from the corresponding core model routines in cases where the results depend non-linearly upon species concentrations. In other cases, the sensitivity algorithm is identical to the CAMx algorithm (e.g., horizontal diffusion) and both concentrations and sensitivity coefficients can be processed by the single routine. Finally, there are cases where a specialized module has been written for the sensitivity coefficients to improve the computational efficiency (e.g., vertical advection).

Priorities in the DDM coding implementation were:

- Ensuring accuracy by using consistent numerical methods for the concentrations and sensitivities;
- Ensuring accuracy by calculating the concentrations and sensitivities within the chemistry solvers over the same chemistry sub-steps (for original DDM);
- Optimizing the efficiency of the sensitivity coefficient calculations without compromising accuracy;
- Providing a flexible User Interface that allows calculation of sensitivities to all sources and precursors;
- Ensuring that the DDM algorithms have minimal impact on computer resource requirements (memory and CPU time) when the DDM is not being used.

DDM and HDDM can be used with either of the two horizontal advection solvers available in CAMx. The original first-order DDM implementation was developed only for the EBI chemistry solver; it cannot be used with LSODE. However, HDDM can be used with EBI or LSODE.

DDM and HDDM algorithms are not currently implemented for the CAMx Plume-in-Grid (PiG) submodel or the in-line iodine emissions algorithm.

8.1.2 Flexi-DDM

Although DDM is computationally much more efficient than the Brute-Force method, it does require much more additional CPU time and memory space over and above a standard CAMx run, which can be significant especially when many first and second-order sensitivities are requested for a nested grid run with multiple source categories and multiple source regions. The increased computational cost may not always be worthwhile if only part of the modeling domain is of interest. One way to enhance computational efficiency in such cases is to use one-way nesting, where BCs for a nested grid are extracted from the parent grid, and so subsequent runs with sensitivities are performed without outer grids. However, differences between the two nesting schemes (i.e. 1-way vs. 2-way) sometimes cause discrepancies in the model results. An alternative approach is to run the full 2-way nested model while “turning off” sensitivity calculations outside nested grids of interest.

CAMx provides a feature called “Flexi-DDM”, which allows the user to turn off sensitivity calculations for selected grids (normally grids far outside the area of interest) to improve computational efficiency of DDM runs (at the expense of accuracy). This reduces CPU times but will not reduce memory requirements. Also, note that turning off sensitivity calculations for outer grids is only appropriate for certain types of sensitivity calculations: e.g., sensitivity to master grid BCs cannot be calculated with Flexi-DDM.

8.2 Running CAMx With DDM and HDDM

The DDM user interface was designed along similar lines to the Source Apportionment (SA) user interface. This makes it easier to learn how to use both options and promotes consistency in analyses performed using SA and DDM. DDM is invoked similarly to the other Probing Tools

within the CAMx control file. In the `&CAMx_Control` namelist module, the variable `Probing_Tool` must be set to either "DDM" to utilize the original first-order implementation, or "HDDM" to utilize the high-order implementation. An additional namelist module called `&DDM_Control` must then be provided in the control file to configure the DDM portion of the model. The additional namelist module is described below. The order of the variables follow the template available with the source code. An example of the DDM portion of the CAMx run control file is shown in Figure 8-1.

Description of DDM Control in the CAMx Run Control File

<code>&DDM_Control</code>	Label for the Probing Tool namelist module that configures the DDM option; it must begin in column 2
<code>&</code>	Flag ending a namelist; it must be in column 2
<code>DDM_File_Root</code>	Character root output path/filename
<code>DDM_Stratify_Boundary</code>	Logical flag to stratify boundary types (TRUE=separate sensitivity types will be used for the N, S, E, W, and Top boundaries, FALSE=a single sensitivity type will be used for all 5 boundaries)
<code>DDM_Number_of_Source_Regions</code>	Integer number of source regions to be tracked. This must be the same as the number of source areas defined in the <code>DDM_Source_Area_Map</code> file. This value must be greater than zero when sensitivity to emissions is requested.
<code>DDM_Number_of_Source_Groups</code>	Integer number of emission groups to be tracked. This determines the number of emission files that must be supplied (additional details below). This value must be greater than zero when sensitivity to emissions is requested.
<code>Number_of_IC_Species_Groups</code>	Integer number of species or species groups in the initial conditions to be tracked. This number may be between zero and the number of species being simulated plus four (allowing for the four species groups VOC, HRVOC, NOX, ALL).
<code>IC_Species_Groups</code>	Character array (by IC group) names of the species or species groups in the initial conditions to be tracked. Allowed names are any species being simulated by the mechanism in use (e.g., O3, PAR, NO, etc.) plus the species groups NOX, VOC, HRVOC, and ALL. It is permissible to specify both a species and a group containing that species, e.g., both NO and NOX. Each name may have up to 10 characters. Note that if you select a species that is not present on the IC file provided, the initial sensitivities

for that species will be set to zero. This variable may be left blank if the number of initial condition species groups is zero.

Number_of_BC_Species_Groups	Integer number of species or species groups in the boundary conditions to be tracked. This number may be between zero and the number of species being simulated plus four (allowing for the four species groups VOC, HRVOC, NOX, ALL).
BC_species_Groups	Character array (by BC group) names of the species or species groups in the boundary conditions to be tracked. See description for IC_Species_Group above.
Number_of_EM_Species_Groups	Integer number of species or species groups in the emissions to be tracked. This number may be between zero and the number of species being simulated plus four (allowing for the four species groups VOC, HRVOC, NOX, ALL).
Emis_Species_Groups	Character array (by emissions group) names of the species or species groups in the emissions to be tracked. See description for IC_Species_Group above.
Number_of_Rate_Const_Groups	Integer number of reaction rate sensitivity groups to be tracked. This number may be zero.
Rate_Const_Groups	Character string containing each reaction rate sensitivity group name and reaction numbers that belong to the group. Group name and reaction numbers are separated by colon (:) and each reaction number is separated by comma (,).
Number_of_HDDM_Sens_Groups	Integer number of second-order sensitivity groups to be tracked (additional details below). This number may be zero.
HDDM_parameters	Character array names of the first-order sensitivity parameters to which second-order sensitivity is computed. The naming of the first-order parameters is the same as the long name of sensitivities with the first 4 characters omitted (see DDM sensitivity naming conventions/formats below). For each HDDM sensitivity group, two first-order parameters are required (the same can be used twice). All the first-order parameters must be included in the modeling.
DDM_Receptor_Definitions	Character input DDM receptor definition path/filename. (This is an optional file).
DDM_Source_Area_Map	Character array (by CAMx grid) input DDM source area definition path/filename (required for master grid, optional for nested grids). Source regions are defined using a map in the same format as the integer SA source area map (Section 7);

fractional source area maps are not supported by DDM. Unlike SA, DDM does not require that all parts of the modeling domain be tracked, therefore it is permissible to define an area numbered zero in the source area map (emissions from those areas will not be tracked). The non-zero source region numbers must be between 1 and the number of regions.

DDM_PT_Override	Logical flag to allow point source override (TRUE = look for and use the point source override flags in sector-specific point source files, FALSE = ignore point source override flags)
DDM_Calc_Grid	Logical array containing Flexi-DDM flag for each grid (.TRUE. = calculate sensitivities in the grid; .FALSE. = do not calculate sensitivities in the grid).
DDM_Initial_Conditions	The name of the sensitivity initial condition file. Leave the file name blank for restart days or if sensitivity to initial conditions is not being calculated.
DDM_Boundary_Conditions	The name of the sensitivity lateral boundary condition file. Leave the file name blank if sensitivity to lateral boundary conditions is not being calculated.
DDM_Top_Concentrations	The name of the sensitivity top boundary condition file. Leave the file name blank if sensitivity to top boundary conditions is not being calculated.
DDM_Master_Restart	Character input master grid DDM restart path/filename (ignored if Restart=FALSE)
DDM_Nested_Restart	Character input nested grid DDM restart path/filename (ignored if Restart=FALSE or Number_of_Grids=1)
DDM_Points_Group	Character array (by source group) input DDM elevated point source emissions path/filename (optional, ignored if Point_Emissions=FALSE)
DDM_Emiss_Group_Grid	Character array (by source group, by CAMx grid) input DDM gridded emissions path/filename (optional, ignored if Gridded_Emissions=FALSE)

```

&DDM_Control

DDM_File_Root           = './DDM_output/CAMx.020604',
DDM_Stratify_Boundary   = .false.,
DDM_Number_of_Source_Regions = 4,
DDM_Number_of_Source_Groups = 2,

Number_of_IC_Species_Groups = 1,
IC_Species_Groups(1)      = 'O3',
Number_of_BC_Species_Groups = 1,
BC_species_Groups(1)      = 'O3',
Number_of_EM_Species_Groups = 2,
Emis_Species_Groups(1)    = 'NOX',
Emis_Species_Groups(2)    = 'VOC',
Number_of_Rate_Const_Groups = 1,
Rate_Const_Groups(1)     = 'RXN1: 120,121,122',
Number_of_HDDM_Sens_Groups = 3,
HDDM_parameters(1,1)     = 'EM0201NOX_',
HDDM_parameters(1,2)     = 'EM0201NOX_',
HDDM_parameters(2,1)     = 'EM0201VOC_',
HDDM_parameters(2,2)     = 'EM0201VOC_',
HDDM_parameters(3,1)     = 'EM0201NOX_',
HDDM_parameters(3,2)     = 'EM0201VOC_',

DDM_Receptor_Definitions = './DDM_input/receptor.cities',
DDM_Source_Area_Map(1)   = './DDM_input/source_map.DDM.4areas',
DDM_Source_Area_Map(2)   = ' ',
DDM_PT_Override          = .false.,
DDM_Calc_Grid(1)         = .true.,
DDM_Calc_Grid(2)         = .true.,

DDM_Initial_Conditions   = './DDM_input/IC.020603',
DDM_Boundary_Conditions = './DDM_input/BC.020604',
DDM_Top_Concentrations   = './DDM_input/TC.020604',
DDM_Master_Restart       = './DDM_output/CAMx.020603.ddm.inst',
DDM_Nested_Restart       = './DDM_output/CAMx.020603.ddm.finst',

DDM_Points_Group(1)      = ' ',
DDM_Points_Group(2)      = './DDM_input/utils.020604',

DDM_Emiss_Group_Grid(1,1) = './OSAT_input/bio.grd1.020604',
DDM_Emiss_Group_Grid(1,2) = './OSAT_input/bio.grd2.020604',
DDM_Emiss_Group_Grid(2,1) = './OSAT_input/util.grd1.020604',
DDM_Emiss_Group_Grid(2,2) = './OSAT_input/util.grd2.020604',

&

```

Figure 8-1. Example of DDM inputs in the CAMx control file. CAMx is run with two grids, and DDM is configured to track emissions from four source regions and two source groups. Sensitivity to ozone initial and boundary conditions are tracked, while sensitivities to NO_x and VOC emissions are tracked. Sensitivity for a single rate constant group will be calculated involving mechanism reaction numbers 120, 121, and 122. Three groups of second-order sensitivities to anthropogenic NO_x and VOC emissions (from emissions group 2, source region 1) will be computed (d^2/dNO_x^2 , $d^2/dVOC^2$ and d^2/dNO_xdVOC). No source region map is provided for the nested grid (the region assignments on the nest are defined by the master grid). Only the group 2 point sources are tracked (no biogenic point sources are available).

8.3 DDM Output Files

The output file types for a DDM simulation are described in Table 8-1. These files have the same format as corresponding concentration output files, described in Section 3.

Table 8-1. DDM output file suffix names.

File Name Suffix	DDM File Type
.ddm.inst	Binary master grid instantaneous sensitivity file at end of simulation (used for restart), 3-D, all sensitivities, in $\mu\text{mol m}^{-3}$ for gases and $\mu\text{g m}^{-3}$ for PM.
.ddm.finst	Binary nested grid instantaneous sensitivity file at end of simulation (used for restart), 3-D, all sensitivities, in $\mu\text{mol m}^{-3}$ for gases and $\mu\text{g m}^{-3}$ for PM.
.ddm.grdnn	Binary average sensitivity file for grid <i>nn</i> , 2-D, surface layer sensitivities only for affected species requested in the CAMx average file, in ppm for gases and $\mu\text{g m}^{-3}$ for PM.
.ddm.receptor	Text hourly average sensitivities at user specific receptor locations. This file is in comma delimited text format suitable for importing into a spreadsheet.

8.4 DDM Sensitivity Coefficient Names

Each DDM sensitivity coefficient tracks the influence of a species from a specific source (the *influencing species*) on a predicted concentration (the *affected species*). The sensitivity coefficient names are constructed to show this relationship, as follows:

$$\{\text{Affected Species}\}\{\text{Pollutant Source}\}\{\text{Influencing Species}\}$$

This is a lot of information to encode in a name that must conform to the ten character limit imposed by the binary I/O file formats. Because of this, two naming systems are used in CAMx:

- Long Names - these names are easy to read, but since they are more than ten characters in length they cannot be used in sensitivity coefficient binary output files. If an alternate I/O format is implemented in the future it may be possible to use the long names on sensitivity output files.
- Short Names - these convey the same information as the long names but require more practice to learn. They are used in the sensitivity coefficient binary output files.

At the start of each CAMx run a concordance of Long and Short sensitivity coefficient names is written to the diagnostic output file (.diag file). An example concordance is shown in Figure 8-2, and a detailed explanation of the naming convention follows.

Affected Species	Influencing Species	Source Type	Group	Region	Long Name	Short Name
NO	ALL	EM	1	2	NO_EM0102ALL_	0160102ALL
NO2	ALL	EM	1	2	NO2_EM0102ALL_	0170102ALL
O3	ALL	EM	1	2	O3_EM0102ALL_	0180102ALL
PAN	ALL	EM	1	2	PAN_EM0102ALL_	0190102ALL
PANX	ALL	EM	1	2	PANXEM0102ALL_	0200102ALL
PNA	ALL	EM	1	2	PNA_EM0102ALL_	0210102ALL
FACD	ALL	EM	1	2	FACDEM0102ALL_	0220102ALL
FORM	ALL	EM	1	2	FORMEM0102ALL_	0230102ALL
H2O2	ALL	EM	1	2	H2O2EM0102ALL_	0240102ALL
HNO3	ALL	EM	1	2	HNO3EM0102ALL_	0250102ALL
HONO	ALL	EM	1	2	HONOEM0102ALL_	0260102ALL
IOLE	ALL	EM	1	2	IOLEEM0102ALL_	0270102ALL
ISOP	ALL	EM	1	2	ISOPEM0102ALL_	0280102ALL
ISPD	ALL	EM	1	2	ISPDDEM0102ALL_	0290102ALL
MEOH	ALL	EM	1	2	MEOHEM0102ALL_	0300102ALL
MEPX	ALL	EM	1	2	MEPXEM0102ALL_	0310102ALL
MGLY	ALL	EM	1	2	MGLYEM0102ALL_	0320102ALL
AACD	ALL	EM	1	2	AACDEM0102ALL_	0330102ALL
ALDX	ALL	EM	1	2	ALDXEM0102ALL_	0340102ALL
CO	ALL	EM	1	2	CO_EM0102ALL_	0350102ALL
ALD2	ALL	EM	1	2	ALD2EM0102ALL_	0360102ALL
NTR	ALL	EM	1	2	NTR_EM0102ALL_	0370102ALL

Figure 8-2. Example concordance of long and short sensitivity coefficient names from the CAMx diagnostic output file.

8.4.1 Initial Condition Sensitivity Names

Long Name **NNNNIC_____MMMM**

where:

NNNN Affected species name with trailing underscore to pad blanks
IC Indicates the sensitivity coefficient is for initial conditions
_____ Four underscores to pad the name to 14 characters
MMMM Influencing species name with trailing underscore to pad blanks

Examples: O3__IC____O3__
 HNO3IC____NOX_
 ETH_IC____HRVO

Short Name **nnnI_____mmm**

where:

nnn Affected species number
I Indicates the sensitivity coefficient is for initial conditions
_____ Three underscores to pad the name to 10 characters
mmm Influencing species number or name of a species group (NOX, VOC, HRVOC or ALL).

Examples: 018I___018 (where O3 is species number 18)
 025I___NOX (where HNO3 is species number 25)
 042I___HRV (where ETH is species number 42)

8.4.2 Boundary Condition Sensitivity Names

Long Name **NNNNBCRRR_MMMM**

where:

NNNN Affected species name with trailing underscore to pad blanks
BC Indicates the sensitivity coefficient is for boundary conditions
RRR NTH, STH, EST, WST or TOP if stratified by boundary; ALL if not stratified by boundary
_ Underscore to pad the name to 14 characters
MMMM Influencing species name with trailing underscore to pad blanks

Examples: O3__BCTOP_O3__
 HNO3BCEST_NOX_
 ETH_BCALL_HRVO

Short Name **nnnBRRRmmm**

where:

nnn Affected species number
B Indicates the sensitivity coefficient is for initial conditions
RRR NTH, STH, EST, WST or TOP if stratified by boundary; ALL if not stratified by boundary
mmm Influencing species number or name of a species group (NOX, VOC, HRVOC or ALL)

Examples: 018BTOP018 (where O3 is species number 18)
 025BESTNOX (where HNO3 is species number 25)
 042BALLHRV (where ETH is species number 42)

8.4.3 Emissions Sensitivity Names

Long Name **NNNEMGRRMMMM**

where:

NNNN Affected species name with trailing underscore to pad blanks
EM Indicates the sensitivity coefficient is for emissions
GG Emissions group number
RR Emissions region number
MMMM Influencing species name with trailing underscore to pad blanks

Examples: O3__EM010103__
HNO3EM0201NOX_
ETH_EM0103HRVO

Short Name **nnnGRRmmm**

where:

nnn Affected species number
GG Emissions group number
RR Emissions region number
mmm Influencing species number or name of a species group (NOX, VOC, HRVOC or ALL)

Examples: 0180101018 (where O3 is species number 18)
0250201NOX (where HNO3 is species number 25)
0420103HRV (where ETH is species number 42)

8.4.4 Reaction Rate Sensitivity Names

Long Name **NNNNRATE__MMM**

where:

NNNN Affected species name with trailing underscore to pad blanks
RATE Indicates the sensitivity coefficient is for rate constants
__ Two underscores to pad the name to 14 characters
MMM Reaction rate sensitivity group name with trailing underscore to pad blanks

Examples: NO__RATE__RXN1
O3__RATE__R28__

Short Name **nnnRATEmmm**

where:

nnn Affected species number
RATE Indicates the sensitivity coefficient is for rate constants
mmm Reaction rate sensitivity group number

Examples: 016RATE001 (where NO is species number 16)
018RATE002 (where O3 is species number 18)

8.4.5 HDDM Sensitivity Names

Long Name **NNNNHDDMLLLMMM**

where:

NNNN	Affected species name with trailing underscore to pad blanks
HDDM	Indicates the sensitivity coefficient is second-order
LLL	The index of the first 1 st -order sensitivity parameter in the internal list of the 1st-order parameters
MMM	The index of the second 1 st -order sensitivity parameter in the internal list of the 1st-order parameters

Examples: NO__HDDM001001
 O3__HDDM001002

Short Name **nnnH111mmm**

where:

nnn	Affected species number
H	Indicates the sensitivity coefficient is second-order
111	The index of the first 1 st -order sensitivity parameter in the internal list of the 1st-order parameters
mmm	The index of the second 1 st -order sensitivity parameter in the internal list of the 1st-order parameters

Examples: 016H001001 (where NO is species number 16)
 018H001002 (where O3 is species number 18)

8.5 Steps In Developing Inputs And Running DDM

Below is a simple methodological list of steps to follow in setting up and running DDM. The process is similar among the SA and DDM Probing Tools.

- 1) Define the source groups and regions that you wish to track. Keep in mind that memory resources increase dramatically as the number of sensitivities grows. Probing Tool applications with large numbers of sensitivities, nested grids or grid cells may exceed available memory.
- 2) Build an integer source region map (see Section 7) that defines the spatial allocation of emission sensitivities. For small domains or small number of regions, this can be done by hand. We suggest using GIS software to develop complex source region maps on large grids.
- 3) Process the emissions inventory into the separate source group files that you want to track (e.g., mobile, area, point, biogenic, etc.).

- a) Consideration of potential source apportionment or sensitivity applications prior to any emissions processing can be very beneficial so that files by group are available for later use.
 - b) Elevated point sources will automatically be assigned to the source region in which they reside. However, you may override the region to which each individual point source is assigned (see the definition of `kcell` in Section 3, Elevated Point Source File). A point source region does not need to be defined in the source region map, e.g., you could have a map with two regions that split the domain in half, with a third region assigned arbitrarily to represent elevated point sources only.
- 4) Edit the CAMx control namelist file (Section 2).
- a) Set the `Probing_Tool` variable to the technology you wish to use (DDM, HDDM). This will activate the `&DDM_Control` namelist module.
 - b) Edit or add the `&DDM_Control` namelist module (described earlier). Provide the required information, including:
 - output paths
 - whether to stratify boundary conditions
 - number of source regions
 - number of source groups
 - numbers and names of IC, BC, emissions, rate constant, and HDDM groups
 - receptor definitions
 - IC/BC input files
 - list of input emission files by group.
- 5) Configure the CAMx source code to define the number of tracers, and build an executable. This will ensure that you have sufficient memory for the Probing Tool application.
- a) Edit the file `Includes/camx.prm`
 - b) Change the parameters `MXTRSP` and `MXFDDM`, following the instructions provided in the file. CAMx is distributed with `MXTRSP = 1` and `MXFDDM = 1` to minimize memory requirements for standard applications of the model. If you run DDM with an insufficient value, the model will stop and tell you the required value of `MXTRSP` and `MXFDDM` for your application.
 - c) Execute the `CAMx Makefile` to build an executable program (Section 2).
- 6) Run CAMx and review the diagnostic output files to ensure that the model is correctly interpreting and running the Probing Tool configuration that you have specified. Ensure that CAMx is generating the proper output files that you are expecting. Review the table of concordance of long and short sensitivity coefficient names.
- 7) Review gridded tracer fields using commonly available plotting programs. Utilities such as PAVE or Verdi will read Probing Tool files directly. Use of any other software may require specialized re-formatting procedures.
- 8) Probing Tool gridded tracer output files are written in the same Fortran binary format as the regular CAMx concentration output files. You can post-process gridded output fields using any software that reads CAMx files, or you can adapt those programs or build your own software to generate specialized analysis and graphical products.

9. PROCESS ANALYSIS

Process Analysis (PA) allows for in-depth analysis of photochemical model performance by revealing the contributions from individual physical and chemical processes operating within the model (Jeffries and Tonnesen, 1994). Using PA, one can more fully understand the complex interactions between the different processes, explain simulation results within the context of the model formulation, and improve the design of control strategies.

A conventional model performance evaluation employs statistical and graphical methods to analyze predicted concentrations against observed concentrations. This answers the basic question: "How well is the model replicating measurements?" While such comparisons are necessary to summarize performance, they are far from sufficient to determine whether the model is adequately representing the real situation. This is because compensating errors among various model processes can result in predictions that serendipitously agree with limited observations but for the wrong reasons. In contrast PA provides information on how the specific model predictions were obtained, which can be interpreted to improve model performance and/or inform control strategy decisions.

9.1 Process Analysis In CAMx

Three components of PA are implemented in CAMx:

- 1) **Integrated Processes Rate (IPR) analysis.** The IPR method provides detailed process rate information for each physical process in CAMx (i.e., advection, diffusion, deposition, emissions, and chemistry) for selected grid cells and selected species (Wang, Langstaff, and Jeffries, 1995). The IPR outputs can be analyzed to determine what processes governed the model-predicted concentrations at any time and place. IPR information has often been plotted as a time series of process contributions for specific cells or groups of cells. IPR outputs have also been used to check the mass balance in the host model, i.e., to determine whether model concentrations are fully explained by the diagnosed process information or whether unexpected artifacts are occurring. The IPR data are relatively easy to interpret and can be analyzed using simple tools such as spreadsheets. IPR works for all gas and PM mechanisms and with PiG. IPR does not work with the ACM2 vertical diffusion option.
- 2) **Integrated Reaction Rate (IRR) analysis.** The IRR method provides detailed reaction rate information for all reactions in the chemical mechanism for selected grid cells (Jeffries and Tonnesen, 1994). The IRR data can be analyzed to determine how the chemical changes occurring in the model are related to the chemical mechanism. For example, by analyzing rate information over groups of reactions it is possible to quantify chemically meaningful attributes such as radical initiation rates, radical propagation efficiencies, chain lengths, etc. Since these analyses tend to be complex, IRR data generally require post-processing to be useful. IRR is implemented for the CB05 chemical mechanism, and partially for CB6r2; it is not implemented for other CB6 variants or for SAPRC07 (see Chapter 5, Table 5-1).

- 3) **Chemical Process Analysis (CPA).** CPA is related to the IRR method but is designed to be more user friendly and accessible. With CPA, a selection of useful parameters is calculated from IRR data within CAMx and then output to gridded files for entire grids (Tonnesen and Dennis, 2000). The gridded CPA files use the same format as the gridded concentration outputs and can be visualized and processed using standard post-processing tools. CPA is implemented for the CB05 chemical mechanism, and partially for CB6r2; it is not implemented for other CB6 variants or for SAPRC07 (see Chapter 5, Table 5-1).

9.1.1 Integrated Process Rate Analysis

The specific processes that are reported by IPR are listed in Table 9-1. This information is output for each chemical species selected for inclusion in the average concentration output file, and for each grid cell selected for analysis. The process rates are integrated across each model output time interval (normally hourly). Taken together, this information provides a complete description of how the species concentration changed across the output time interval and the magnitude of all of the processes that caused this change. Information is output in the concentration units used internally within CAMx ($\mu\text{mole}/\text{m}^3$ for gases, $\mu\text{g}/\text{m}^3$ for PM species). A gas conversion factor ($\text{ppm}/\mu\text{mole}/\text{m}^3$) specific to the grid cell/time period is also output to allow conversion to mixing ratio (ppm) for comparison of gas species with CAMx average concentration outputs. For PM species, the conversion factor is always 1. Grid cell volume is also output to allow aggregation across grid cells.

For most of the process rates listed in Table 9-1 the interpretation is straightforward, the rate is simply the concentration change caused by the named process across the output time interval. The sign convention is such that a positive flux always tends to increase the cell concentration. Further explanation is provided for several processes below:

Plume-in-Grid change: The grid cell concentration change caused by Plume-in-Grid puffs that transferred mass to the grid cell during the output time interval.

Point source emissions: Does not include point sources selected for PiG treatment as these are reported in Plume-in-Grid Change.

Dilution in the vertical: CAMx allows for layer interface heights to change over time which can lead to a "dilution" term for affected grid cells.

Boundary diffusion: In some cases this term will be zero by definition, namely: the bottom boundary of surface layer grid cells; the top boundary of top layer grid cells; any lateral boundary that coincides with a nest boundary.

Dry deposition: This term is zero by definition for all grid cells above the surface layer.

Table 9-1. Process information reported by the IPR option.

IPR Parameter	Process Information	Units ^a
1	Initial concentration	$\mu\text{mole}/\text{m}^3$ ($\mu\text{g}/\text{m}^3$)
2	Gas phase chemistry	$\mu\text{mole}/\text{m}^3$ ($\mu\text{g}/\text{m}^3$)
3	Gridded emissions	$\mu\text{mole}/\text{m}^3$ ($\mu\text{g}/\text{m}^3$)
4	Point source emissions	$\mu\text{mole}/\text{m}^3$ ($\mu\text{g}/\text{m}^3$)
5	Plume-in-Grid change	$\mu\text{mole}/\text{m}^3$ ($\mu\text{g}/\text{m}^3$)
6	West boundary advection	$\mu\text{mole}/\text{m}^3$ ($\mu\text{g}/\text{m}^3$)
7	East boundary advection	$\mu\text{mole}/\text{m}^3$ ($\mu\text{g}/\text{m}^3$)
8	South boundary advection	$\mu\text{mole}/\text{m}^3$ ($\mu\text{g}/\text{m}^3$)
9	North boundary advection	$\mu\text{mole}/\text{m}^3$ ($\mu\text{g}/\text{m}^3$)
10	Bottom boundary advection	$\mu\text{mole}/\text{m}^3$ ($\mu\text{g}/\text{m}^3$)
11	Top boundary advection	$\mu\text{mole}/\text{m}^3$ ($\mu\text{g}/\text{m}^3$)
12	Dilution in the vertical	$\mu\text{mole}/\text{m}^3$ ($\mu\text{g}/\text{m}^3$)
13	West boundary diffusion	$\mu\text{mole}/\text{m}^3$ ($\mu\text{g}/\text{m}^3$)
14	East boundary diffusion	$\mu\text{mole}/\text{m}^3$ ($\mu\text{g}/\text{m}^3$)
15	South boundary diffusion	$\mu\text{mole}/\text{m}^3$ ($\mu\text{g}/\text{m}^3$)
16	North boundary diffusion	$\mu\text{mole}/\text{m}^3$ ($\mu\text{g}/\text{m}^3$)
17	Bottom boundary diffusion	$\mu\text{mole}/\text{m}^3$ ($\mu\text{g}/\text{m}^3$)
18	Top boundary diffusion	$\mu\text{mole}/\text{m}^3$ ($\mu\text{g}/\text{m}^3$)
19	Dry deposition	$\mu\text{mole}/\text{m}^3$ ($\mu\text{g}/\text{m}^3$)
20	Wet deposition	$\mu\text{mole}/\text{m}^3$ ($\mu\text{g}/\text{m}^3$)
21	Inorganic aerosol chemistry	$\mu\text{mole}/\text{m}^3$ ($\mu\text{g}/\text{m}^3$)
22	Organic aerosol chemistry	$\mu\text{mole}/\text{m}^3$ ($\mu\text{g}/\text{m}^3$)
23	Aqueous aerosol chemistry	$\mu\text{mole}/\text{m}^3$ ($\mu\text{g}/\text{m}^3$)
24	Final concentration	$\mu\text{mole}/\text{m}^3$ ($\mu\text{g}/\text{m}^3$)
25	Units conversion	$\text{ppm}/(\mu\text{mole}/\text{m}^3)$ (N/A) ^b
26	Average cell volume	m^3

a Units in the parentheses are for PM species.

b Unit conversion factor for PM species is always 1.

9.1.2 Integrated Reaction Rate Analysis

IRR provides the integrated rate of each gas-phase chemical reaction in units of ppm hr^{-1} for each grid cell selected for process analysis. Reaction rates are accumulated (integrated) within the chemistry solver at the time steps being used to solve the chemical equations, and output at the CAMx output time interval (usually 1 hour).

9.1.3 Chemical Process Analysis

The CPA method calculates a pre-determined set of parameters as listed in Table 9-2. The CPA parameters are calculated for all grid cells in either the surface layer or all layers. The selection between surface layer or all layer CPA outputs is determined by the "3-D average file" flag specified in the CAMx Control File (see Section 2). This is based on the premise that 3-D CPA information will be interpreted in conjunction with 3-D concentration fields.

Table 9-2. Chemical Process Analysis (CPA) variables calculated in CAMx for the CB05 and CB6r2 mechanisms. Concentrations are ppb; production and destruction are ppb/hr; photolysis rates are hr⁻¹, ratios are unitless.

CB05	CB6r2	Description
Ozone and Oxidant Production and Loss		
OxProd	OxProd	Production of Ox = Ozone + NO _y -NO
OxLoss	OxLoss	Destruction of Ox
PO3_net	PO3_net	Net ozone produced
PO3_VOCsns	PO3_VOCsns	Net ozone produced under VOC sensitive conditions
PO3_NOxsns	PO3_NOxsns	Net ozone produced under NO _x sensitive conditions
PH2O2_PNH3	PH2O2_PNH3	Ratio of H ₂ O ₂ produced / HNO ₃ produced. Greater than 0.35 means NO _x sensitive ozone production
O3_dest	O3_dest	Ozone destruction by chemical reactions
Radical Initiation		
OH_new		New OH produced (initiated)
HO2_new		New HO ₂ produced
HOx_new		New HO _x (HO _x = OH+HO ₂) produced
newOH_O1D		Production of OH from ozone photolysis
newOH_HONO		Production of OH from HONO photolysis
nOH_O3_OLE		Production of OH from ozone-alkene reactions
nwHO2_HCHO		Production of HO ₂ from formaldehyde photolysis
RO2_new		New RO ₂ produced
Radical Propagation		
OHw_CO	OHw_CO	OH reacted with carbon monoxide
OHw_CH4	OHw_CH4	OH reacted with methane
	OHw_ECH4	OH reacted with locally emitted methane
OHw_ETHA	OHw_ETHA	OH reacted with alkanes
OHw_PAR	OHw_PAR	
	OHw_PRPA	OH reacted with propane
	OHw_BENZ	OH reacted with benzene
OHw_TOL	OHw_TOL	OH reacted with toluene and mono-substituted aromatics
OHw_XYL	OHw_XYL	OH reacted with xylenes and poly-substituted aromatics
OHw_ETH	OHw_ETH	OH reacted with ethene
	OHw_ETHY	OH reacted with ethylene
OHw_OLE	OHw_OLE	OH reacted with terminal alkenes (R-HC=CH ₂ , e.g. propene)
OHw_IOLE	OHw_IOLE	OH reacted with internal alkenes (R-HC=CH-R, e.g. 2-butene)
OHw_ISOP	OHw_ISOP	OH reacted with isoprene
OHw_TERP	OHw_TERP	OH reacted with terpenes
OHw_all_HC	OHw_all_HC	OH reacted with all organic compounds (including CO)
ISOPwOx		Isoprene reacted with O ₃ , NO ₃ and O(³ P)
TERPwOx		Terpenes reacted with O ₃ , NO ₃ and O(³ P)
OH_rctd	OH_rctd	Total OH reacted
HO2_rctd		Total HO ₂ reacted
HOx_rctd		Total HO _x reacted
RO2_rctd		Total RO ₂ reacted

CB05	CB6r2	Description
OHfromHO2		OH produced from reactions of HO ₂
Y_OHperHO2		Yield of OH per HO ₂ reacted (= OHfromHO2 / HO2_rctd)
Radical Termination and HOx Chain Length		
OH_term		OH terminated
HO2_term		HO ₂ terminated
HOx_term		HOx terminated
RO2_term		RO ₂ terminated
HOx_CL		HOx chain length (= HOx_rctd / {2 x HOx_new})
Formaldehyde Production		
HCHOp_eth		Formaldehyde produced from ethene
HCHOp_ole		Formaldehyde from terminal alkenes (R-HC=CH ₂ , e.g. propene) in the first generation of products
HCHOp_iole		Formaldehyde from internal alkenes (R-HC=CH-R, e.g. 2-butene) in the first generation of products
HCHOp_terp		Formaldehyde from terpenes in the first generation of products
HCHOp_isop		Formaldehyde from isoprene in the first generation of products
HCHOp_ispd		Formaldehyde from isoprene daughter products (isoprod, methacrolein and methylvinylketone)
HCHOp_Tot		Total formaldehyde produced
NOy Reactions		
HNO3_OHNO2	HNO3_OHNO2	Nitric acid produced from OH reacting with NO ₂
HNO3_NO3HC	HNO3_NO3HC	Nitric acid produced from NO ₃ reacting with organics
HNO3_N2O5	HNO3_N2O5	Nitric acid produced from N ₂ O ₅ reacting with water
PANprodNet		Net PAN produced
PANlossNet		Net PAN destroyed
	NTR1_prod	Organic nitrate production
	NTR2_prod	Organic nitrate production
	INTR_prod	Organic nitrate production
	NTR1toNTR2	Organic nitrate conversion
	INTRtoNTR2	Organic nitrate conversion
RNO3_prod		Organic nitrates (RNO ₃) produced
NOxrecycl	NOxrecycl	Nitrates (HNO ₃ and RNO ₃) recycled to NOx
NOw_HO2		NO reacted with HO ₂ (forming NO ₂)
NOw_RO2s		NO reacted with RO ₂ (forming NO ₂)
NOw_RCO3s		NO reacted with RCO ₃ (forming NO ₂)
Photolysis		
J_NO2	J_NO2	NO ₂ photolysis rate
J_O3O1D	J_O3O1D	O ₃ photolysis rate to O(¹ D) atoms
J_CLDADJ	J_CLDADJ	Cloud/haze adjustment factor
Radical Concentrations		
OH	OH	OH radical concentration
HO2	HO2	HO ₂ radical concentration

9.2 Running Process Analysis

PA can be used with most of the physical options available for the “core” CAMx model, e.g., the various advection and chemistry mechanisms/solvers. However, PA cannot be used at the same time as the other CAMx “Probing Tool” options (e.g., SA, DDM, or RTRAC) because the Probing Tools share internal data structures to minimize the total memory resources required by CAMx. IPR cannot be used with the ACM2 diffusion option.

PA is invoked similarly to the other Probing Tools within the CAMx control file. In the `&CAMx_Control` namelist module, the variable `Probing_Tool` must be set to either “PA” (generates all PA output), “IPR”, or “IRR”. Table 9-3 summarizes the types of process analysis performed for each keyword and the output files that are produced.

Table 9-3. Process analysis keywords and associated CAMx output files.

Process Analysis Key Word			Output Filename	File Contains
IPR	IRR	PA		
Yes	No	Yes	*.ipr	Integrated process rate (IPR) information for all selected cells
No	Yes	Yes	*.irr	Integrated reaction rate (IRR) information for all selected cells
No	Yes	Yes	*.cpa.grdnn	Chemical process analysis (CPA) parameters for grid <i>nn</i>

An additional namelist module called `&PA_Control` must then be provided in the control file to configure the PA portion of the model. The additional namelist module is described below. The order of the variables follow the template available with the source code. An example of the PA portion of the CAMx run control file is shown in Figure 9-1.

The rules for defining PA sub-domains are as follows:

- 1) They must be contained within a single CAMx grid;
- 2) They may not include cells that contain a nested grid;
- 3) They may contain as few as 1 grid cells;
- 4) They may contain up to all of the grid cells in a CAMx grid provided that this does not violate the second rule;
- 5) They may intersect or overlap – the same grid cell may be in several process analysis domains.

Description of PA Control in the CAMx Run Control File

<code>&PA_Control</code>	Label for the Probing Tool namelist module that configures the PA option; it must begin in column 2
<code>&</code>	Flag ending a namelist; it must be in column 2
<code>PA_File_Root</code>	Character root output path/filename
<code>Number_of_PA_Domains</code>	Integer number of PA analysis domains to be evaluated during the simulation.
<code>Within_CAMx_Grid</code>	Integer array (by PA domain) pointer into the CAMx grid within which the PA domain exists (1=master grid, etc.). Use the CAMx internal grid number reported in the *.diag file. Note that this may differ from the nest order provided by the user in the CAMx control file.
<code>PA_Beg_I_Index</code>	Integer array (by PA domain) grid column containing western edge of PA domain.
<code>PA_End_I_Index</code>	Integer array (by PA domain) grid column containing eastern edge of PA domain.
<code>PA_Beg_J_Index</code>	Integer array (by PA domain) grid row containing southern edge of PA domain.
<code>PA_End_J_Index</code>	Integer array (by PA domain) grid row containing northern edge of PA domain.
<code>PA_Beg_K_Index</code>	Integer array (by PA domain) grid layer containing bottom of PA domain.
<code>PA_End_K_Index</code>	Integer array (by PA domain) grid layer containing top of PA domain.

```

&PA_Control

  PA_File_Root          = 'CAMx.OTAG.950707.PA',

  Number_of_PA_Domains = 2,
  Within_CAMx_Grid(1)  = 1,
  PA_Beg_I_Index(1)    = 8,
  PA_End_I_Index(1)    = 12,
  PA_Beg_J_Index(1)    = 9,
  PA_End_J_Index(1)    = 13,
  PA_Beg_K_Index(1)    = 1,
  PA_End_K_Index(1)    = 5,

  Within_CAMx_Grid(2)  = 2,
  PA_Beg_I_Index(2)    = 107,
  PA_End_I_Index(2)    = 110,
  PA_Beg_J_Index(2)    = 78,
  PA_End_J_Index(2)    = 82,
  PA_Beg_K_Index(2)    = 1,
  PA_End_K_Index(2)    = 7,

&

```

Figure 9-1. Example section of a CAMx control file specifying options for Process Analysis.

9.2.1 Setting CAMx Parameters

PA stores information in data structures that are dimensioned using Fortran parameter statements. These parameters must be large enough to accommodate the PA configuration specified in the CAMx control file. If one of these parameters is exceeded CAMx will stop with an error message stating that a parameter must be changed and the model recompiled. It is always a good idea to do a complete rebuild (use the Unix command “make clean”) when a parameter is changed. The parameters that may need to be changed are in two include files, “procan.inc” and “camx.prm”.

procan.inc

MXPADOM – The maximum number of Process Analysis domains.

MXPACEC – The maximum number of Process Analysis cells over all domains

camx.prm

MXTRSP – This parameter defines gridded data structures that are used by several probing tools. For PA the data structures store chemical process analysis (CPA) variables, so MXTRSP must be set to at least the value of MXCPA (set in procan.inc) which is 99.

9.2.2 Output File Formats

CAMx may output up to four files containing PA information according to the PA option selected (see Table 9-3). All of these files are in Fortran binary format to conserve disk space. Two files (the `*.ipr` and `*.irr` files) contain information for just the grid cells selected for PA. The formats for these files are not described here since two Fortran post-processor programs are provided to extract data from these files in a comma-delimited text format. The files containing CPA information (the `*.cpa.grdnn`) are gridded files covering the same area as the regular model average files (`*.avrg.grdnn`). The gridded CPA files have the same format as a regular model average file as described in Section 3.

9.3 Postprocessing

Two post-processors are provided to read the binary `*.ipr` and `*.irr` output files and extract PA data for further analysis. The CPA output files can be visualized directly.

9.3.1 IPR Output Files

The Fortran program “`ext_ipr`” extracts IPR data from one or more CAMx `*.ipr` binary files and reformats the data to comma delimited text format (`.csv`) suitable for subsequent analysis (e.g., using spreadsheets). The “`ext_ipr`” program performs the following tasks:

- Reads and outputs the descriptive header of the `*.ipr` file;
- Optionally combines data from several consecutive `*.ipr` files to provide multi-day output;
- Selects data for an individual cell within a PA sub-domain or aggregates data over multiple cells within a PA sub-domain;
- Outputs the selected IPR data in `.csv` format in either ppb or molar units for gas species; PM species are in either $\mu\text{g}/\text{m}^3$ or mass units.

A sample script to run the “`ext_ipr`” program is provided with its source code, and the script includes a description of how to use the program.

The “`ext_ipr`” program can combine IPR information across several cells. This is useful for analyzing the contributions of model processes to a geographic area that spans multiple cells and layers (e.g., an urban area). For simplicity, the multi-cell area must be defined as a rectangular box. The capability of aggregating IPR information across vertical layers is particularly important during the day because vertical columns of cells within the mixed layer become strongly coupled on time scales shorter than one hour. Thus, if the process contributions for a surface grid cell are analyzed during the day vertical diffusion will often completely dominate all other processes. In this situation, it is more informative to analyze a column of cells extending from the surface to the approximate height of the mixed layer. When the “`ext_ipr`” program aggregates information across grid cells it accounts for differences in cell volume. If the output for aggregate cells is requested in ppb units, the output from CAMx in micromole/volume units is converted to ppb using the volume-weighted average units conversion factor for the cells being aggregated.

One useful approach to analyzing IPR data is to plot the contributions of several processes as a time series. Figure 9-2 presents an example as an illustration of how PA can be used.

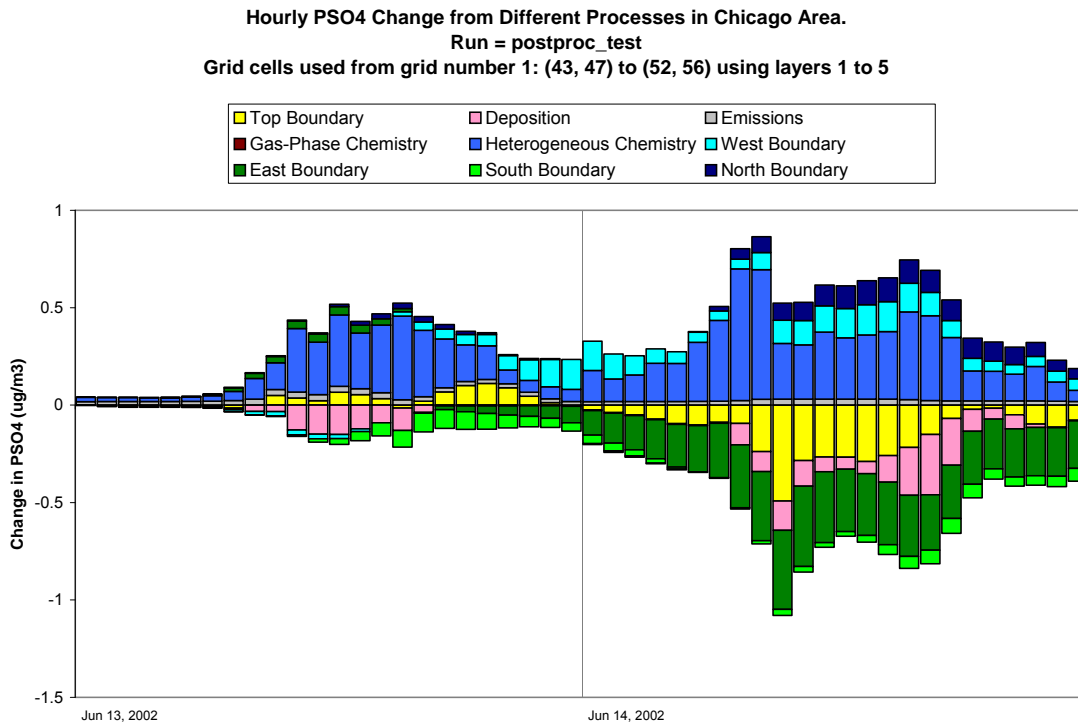


Figure 9-2. Example IPR time series analysis for PSO4; lateral boundary and chemistry terms are not aggregated.

9.3.2 IRR Output Files

The Fortran program “ext_irr” extracts IRR data from one or more CAMx *.irr binary files and reformats the data for subsequent analysis. The “ext_irr” program performs the following tasks:

- Reads and outputs the descriptive header of the *.irr file;
- Optionally combines data from several consecutive *.irr files to provide multi-day output;
- Selects data for an individual cell or multiple cells within a PA sub-domain;
- Optionally, outputs the selected IRR data to a .csv format text file;
- Optionally, outputs the selected IRR data to a UAM average format binary file.

The text IRR data are suitable for subsequent analysis (e.g., using spreadsheets). The binary IRR output from "ext_irr" can be displayed using any post-processing software that can display CAMx average concentration outputs.

9.3.3 CPA Output Files

CPA results are output from CAMx as gridded files in the same format as the average concentration files, and therefore can be visualized using any post-processing software that can display CAMx concentration outputs. These files may optionally include just the surface layer or all layers according to how the "3-D output" flag is set in the CAMx control file. Surface layer species concentrations reflect the balance between several model processes including surface emissions/deposition, vertical mixing, and chemical reactions in surface (and possibly aloft) grid cells. In contrast, the CPA output data are grid cell specific and reflect chemical change in single grid cells. The fact that vertical mixing tends to average species concentrations over multiple layers whereas CPA variables are layer specific may complicate and bias the interpretation of CPA results. A solution is to place both the concentrations and CPA variables on a comparable basis by averaging them over all layers within the planetary boundary layer.

A post-processor (VERTAVG) was developed to average CPA variables and concentrations over multiple layers contained within the depth of the planetary boundary layer (PBL). The PBL depth varies in space and time according to the strength and vertical extent of turbulent mixing. Vertical turbulent mixing is specified for CAMx by the input diffusivity (Kv) fields. The VERTAVG processor reads CAMx Kv, height, temperature, and pressure input files, and then calculates the PBL depth for each grid column at each hour. VERTAVG also reads a CAMx 3-D output file of CPA variables (or species concentrations) and calculates air-mass weighted PBL values for each grid column at each hour. The output from VERTAVG is a 2-D file in average file format where the single layer represents the PBL average values rather than surface layer values.

VERTAVG appends two extra variables to the file being processed to aid with interpretation and to make clear that the data have been vertically averaged. The added variables are:

- PBL_Z is the diagnosed height of the PBL for each grid column.
- PBL_I is the layer index of the top layer within the diagnosed PBL for each grid column.

CAMx must be run using the option to create 3-D species concentration (and therefore CPA) output files in order to use VERTAVG.

10. REACTIVE TRACERS

The CAMx reactive tracer algorithm provides a flexible approach for simulating the emission, dispersion, chemistry, and deposition of multiple trace gas and particulate tracers on the computational grid(s) and within the IRON PiG treatment. Originally developed to model air toxics, it was extended and generalized to be able to track a variety of user-defined organic and inorganic species.

Reactive tracers are carried separately from the core model photochemical/PM chemistry mechanisms, and thus can be used to address a variety of issues, separately or in combination:

- Reactive and inert gaseous and particle air toxic compounds;
- Chemical decay of individual VOC compounds into multiple generations of daughter products;
- Source tagging of primary emitted inert and reactive compounds from specific source types/classes, or from individual stacks, facilities and/or complexes.

The reactive tracer algorithm is implemented as a CAMx "Probing Tool" and thus shares model data structures with other Probing Tools such as the SA, DDM and PA. This streamlines the CAMx code, improves efficiency, and maximizes consistency with the core model since it allows reactive tracer calculations for emissions, transport, and deposition to use the existing CAMx algorithms. However, this means that reactive tracers cannot be used simultaneously with other Probing Tools.

The reactive tracer implementation employs two approaches to define tracer chemistry. The original approach, referred to as RTRAC, allows tracers to decay and form multiple generations of daughter products through photolysis and user-specified thermal reactions with ozone and radicals (OH, NO₃) that are extracted from the core model's gas-phase chemistry (CB or SAPRC). A second approach, referred to as the RTRAC Chemical Mechanism Compiler (RTCMC), allows the user to externally define a full chemistry mechanism with no limits on complexity (within available computer resources). RTCMC can also access any gas-phase concentrations from the core gas-phase mechanism as well. Neither option allows chemistry for particulate tracers.

10.1 Description of RTRAC

Reactive tracers are defined for each CAMx run by providing an RTRAC chemistry parameters file similar to that used for the core model. The example in Figure 10-1 illustrates an example RTRAC air toxics application (ENVIRON, 2002; Morris et al., 2003). The number and names of the tracers are arbitrary; i.e. information on the tracer species' chemical identities, structure, reaction pathways, and kinetics are kept separate from the core model. Consistent with the chemistry parameters files used for the core model's photochemistry, the physical characteristics for each reactive tracer must be specified for deposition calculations, and their reaction pathways and rates must be defined.


```

CAMx Version      |VERSION6.3
Description       |Example RTRAC Chemsitry for Toxics
No of gas tracers |6
No of aero tracers|8
No photolysis rxns|4
No thermal rxns  |12
Gas Tracers
No. Name         P/S  SNAM  lower bnd  H-law  T-fact  Molwt  Reactvty  Rscale
1  PACET         PRIM 1.00E-12  6.30e+03 -6492.  44.00  0.0      1.0
2  HCHO          PRIM 1.00E-12  6.30e+03 -6492.  30.00  0.0      1.0
3  BENZ          PRIM 1.00E-12  1.80e-01  0.      78.00  0.0      1.0
4  BUTA          PRIM 1.00E-12  1.00e-02  0.      54.00  0.0      1.0
5  SACET         SEC  ALD2  1.00E-12  6.30e+03 -6492.  44.00  0.0      1.0
6  SFORM         SEC  FORM  1.00E-12  6.30e+03 -6492.  30.00  0.0      1.0
Aero Tracers
No. Name         lower bnd  Density  Low cut  Upper cut
7  DSLF          1.00E-09  1.5      0.10    2.50
8  ECF           1.00E-09  1.5      0.10    2.50
9  CRF           1.00E-09  1.5      0.10    2.50
10 CR6F          1.00E-09  1.5      0.10    2.50
11 DSLC          1.00E-09  1.5      2.50    10.00
12 ECC           1.00E-09  1.5      2.50    10.00
13 CRC           1.00E-09  1.5      2.50    10.00
14 CR6C          1.00E-09  1.5      2.50    10.00
Photolysis reactions
Toxic  Rxn #  Factor
PACET  108    1.0
SACET  108    1.0
HCHO   98     1.6
SFORM  98     1.6
Thermal reactions and rates
Toxic  React A (ppm-lmin-1)  Ea (K)  B  Tref
PACET  OH  8.2015E+03 -3.1099E+02  0.0  300.0
PACET  NO3 2.0689E+03 1.8599E+03  0.0  300.0
HCHO   OH  1.6699E+03 -6.4815E+02  2.0  300.0
HCHO   NO3 4.1377E+03 2.5161E+03  0.0  300.0
BENZ   OH  3.6944E+03 1.9978E+02  0.0  300.0
BUTA   OH  2.1871E+04 -4.4787E+02  0.0  300.0
BUTA   O3  4.8766E+01 2.5000E+03  0.0  300.0
BUTA   NO3 2.1871E+04 1.4890E+03  0.0  300.0
SACET  OH  8.2015E+03 -3.1099E+02  0.0  300.0
SACET  NO3 2.0689E+03 1.8599E+03  0.0  300.0
SFORM  OH  1.6699E+03 -6.4815E+02  2.0  300.0
SFORM  NO3 4.1377E+03 2.5161E+03  0.0  300.0

```

Figure 10-1. Example RTRAC chemistry input file for modeling specific toxic species.

The structure of the RTRAC tracer definition provides complete flexibility in the selection of the compounds and tracers to be included in each analysis. The user is able to easily alter or expand the compounds as needed.

For gas species, the required deposition parameters are the Henry's Law constant and molecular weight M_g , the latter of which defines a diffusivity parameter according to $\sqrt{M_g / M_{H_2O}}$. The deposition calculation for gases that react in plant tissue also needs a reactivity parameter that describes whether a species reacts when dissolved inside leaf tissues (Wesely, 1989). This parameter is intended for modeling the deposition of reactive species, such as ozone, and should be set to zero for air toxics. The deposition calculation for gasses

also uses an "Rscale" factor to adjust the surface resistance. This is used to set the surface resistance to zero for strong acids (e.g., HNO₃) and should be set to 1.0 for modeling air toxics.

The deposition calculation for particles requires the particle density and size associated with each species. The particle size is calculated as the geometric mean of the lower and upper cut points (see Figure 10-1). If possible, the particle size and density should be based on the measured size of particles associated with each RTRAC species (e.g., for a compound associated with soot particles, use a density and size representing the soot).

The emission rates for the RTRAC species are provided by an extra set of emission files (surface and/or point source). Emissions of gases are in moles per time period (normally moles/hour), whereas particles are in grams per time period. The emissions file format is the same as for a regular CAMx emissions file, as described in Section 3.

10.1.1 RTRAC Gas-Phase Chemistry

The RTRAC chemistry calculations use a special chemistry module. Chemistry may be modeled for primary and secondary gas species, meaning that tracers can be formed from the decay of primary tracers or from the decay of host model species (e.g., secondary formaldehyde). The chemical decay of gaseous tracers can account for thermal reactions with ozone (O₃), hydroxyl radical (OH) and nitrate radical (NO₃), as well as photolysis. The algorithms are coded so that all chemical decay pathways are zero by default and only become non-zero if decay rates are explicitly specified in the input file (see Figure 10-1). The example RTRAC chemistry input file in Figure 10-1 shows how thermal reactions are specified by naming the tracer and oxidant, and providing reaction rate parameters. Note that the RTRAC chemical reaction rates depend on the rates and parameters provided in the RTRAC input file, and not the rates in the host model chemical mechanism; however the host model does provide the oxidizing species concentrations (i.e., O₃, OH, and NO₃).

10.1.1.1 Thermal Reactions

Thermal reactions with oxidants are modeled as second order reactions:

$$R = k[\text{tracer}][\text{oxidant}]$$

where R is the decay rate and the rate constant k is defined using the generalized temperature dependent rate expression:

$$k = A \left(\frac{T}{300} \right)^B \exp \left(\frac{-E_a}{T} \right)$$

The Arrhenius factor (A) must be in units (ppm⁻¹min⁻¹), the activation energy (E_a) must be Kelvin and B is dimensionless. This is the same as expression 3 in Table 3-3a. Oxidant concentrations for the decay calculation are obtained from the CAMx photochemical simulation for each grid cell at each time step. RTRAC can be used with any of the photochemical mechanisms that are available in the current version of CAMx (see Section 5). Choosing between the core

mechanisms will influence the RTRAC chemical decay rates by changing the oxidant concentrations in the host model.

10.1.1.2 Photolysis

Photolysis reactions are specified by naming the tracer undergoing photolysis and providing a ratio of the tracer photolysis rate to one of the photolysis reactions in the host photochemical mechanism. For example, Figure 10-1 shows that there are both primary and secondary acetaldehyde reactive tracers (PACET and SACET) and the photolysis rate for both species is set equal to CB6r2 reaction 108 (photolysis of ALD2), which is based on acetaldehyde. Figure 10-1 also shows that there are two types of formaldehyde (PFORM and SFORM). Modeling the photolysis of formaldehyde with RTRAC is complicated by the fact that the CB6r2 mechanism includes two photolysis reactions for formaldehyde (reactions 97 and 98). The solution shown in Figure 10-1 is to model formaldehyde photolysis as 1.6 times the rate of reaction 98. The CAMx host mechanisms are discussed in Section 5 and are defined by the text chemistry parameters files (Section 3) and mechanism listings distributed with CAMx and available from the CAMx web page (www.camx.com).

10.1.1.3 Secondary Species

RTRAC allows for formation of secondary/daughter products related to the chemical decay of one of the primary tracers. Secondary species can also be subject to chemical decay, just like primary species, if the user desires. Therefore, the RTRAC chemistry module allows decay reactions (thermal and photolysis) to be specified for secondary species using the same method as for primary species. In this manner, concentrations of secondary species are determined by the balance between chemical production and destruction. RTRAC requires that any secondary daughter tracers must be specified after their parent tracer in the chemistry parameters input file.

RTRAC also allows tracers that track the secondary formation of any species that is included in the host chemical mechanism. For example, in Figure 10-1 the species SFORM is used to track secondary formaldehyde, and so SFORM is defined as a secondary species and identified with the host species FORM. This means that the RTRAC chemistry module will identify the chemical production of FORM in each grid cell at each time step, and add this chemical production to the SFORM tracer. Since SFORM is intended to track only secondary formaldehyde, no primary emissions should be included for SFORM.

10.1.1.4 Chemical Decay Rates for Near-Source Modeling

The RTRAC algorithm can output hourly chemical decay rates at user-specified locations to support external analyses, for example, as input to a Gaussian plume/puff model. The user provides the locations of each receptor using the CAMx Probing Tools receptor file input format. Figure 10-2 displays an example RTRAC receptor input file for the five locations. At each grid cell, hourly decay rates for each RTRAC compound and every vertical layer are output and can then be interfaced with a user-selected plume model.

SINGLE CELL	Test Cell	1	42	44
SINGLE CELL	Test Cell	1	41	36
SINGLE CELL	Test Cell	1	39	36
SINGLE CELL	Test Cell	1	50	43
SINGLE CELL	Test Cell	1	34	48

Figure 10-2. Example RTRAC receptor input file identifying the grid cells with locations where hourly decay rates will be output for subgrid-scale point source modeling (see format for SA receptor file in Table 7-2).

Separate families of reactive tracer compounds can be simulated by providing separate emission inputs similarly to SA (see Section 7). Tracking separate families of RTRAC tracers allows for source apportionment and can be used to avoid double counting when an external plume model is used to obtain near-source impacts. For example, separate families of air toxic tracers can be specified for each point source complex to be modeled by the external plume model, so that total concentrations could include the local point source impacts (plume model) plus the regional contributions from all other sources (CAMx RTRAC).

10.2 Description of RTCMC

Like RTRAC, the purpose of RTCMC is to add tracer species to a CAMx “core model” simulation and have the tracers undergo chemical changes that depend, in part, upon the evolution of CAMx core model species. The RTCMC approach differs from the original RTRAC approach by allowing arbitrarily complex chemical reaction schemes, but it is exactly like RTRAC in every other respect. The current implementation of RTCMC is for gas-phase reactions, i.e., gas-phase tracers reacting with each other and/or gas-phase host model species. The core model’s photochemical mechanisms remain intact and separate from the reactive tracer chemistry.

10.2.1 RTCMC Gas-Phase Chemistry

The RTCMC allows users to input, in a text-based format, a set of chemical reactions (mechanism) for certain target species to be treated by the CAMx Reactive Tracer Probing Tool. RTCMC is an extension of the original RTRAC algorithm that reads (and solves) a completely independent, user-defined chemical mechanism for reactive tracers that can utilize concentrations of any photochemical species from the core model mechanism. Upon startup, RTCMC compiles information on the chemical mechanism and configures the reactive tracer chemistry solver. During the model simulation, the RTCMC chemistry solver receives ambient pollutant information from the core photochemical mechanism and uses this to calculate the evolution of RTRAC species.

The format of the RTCMC input file is essentially the same as the “IMC” input file format of the SCICHEM Lagrangian puff model (EPRI, 2000). An example IMC format file is shown in Figure 10-3. There are four sections in an IMC file that are identified by a keyword at the start of each section, as follows:

```

#Control
  rate_species_units = 'ppm'
  rate_time_units = 'min'
  solver = 'dlsode'
  Jacobian = 'numeric'
#Name, Type, Ambient,      ATol,    Dep, Wet Scav,      MW, Spec Map
O3      A      1.0  1.0E-12  0.0    0.0    0.0
OH      A      1.0  1.0E-12  0.0    0.0    0.0
ATRAC   F      1.0  1.0E-12  0.010  0.0    0.0
BTRAC   F      1.0  1.0E-12  0.001  0.0    0.0
CTRAC   F      1.0  1.0E-12  0.020  0.0    0.0
DTRAC   F      1.0  1.0E-12  0.001  0.0    0.0
ETRAC   F      1.0  1.0E-12  0.030  0.0    0.0
FTRAC   F      1.0  1.0E-12  -0.001 0.0    0.0 NO2
#Table
  0          0.          15.          30.          45.          60.          75.
  80.          86.          87.          88.
  1 4.1590E-04 4.0600E-04 3.7540E-04 3.27E-04 2.6040E-04 9.4990E-05
2.9930E-05 4.8590E-06 8.3030E-08 1.0000E-09
#Equations
  1 [ATRAC]                -> (2.0) [BTRAC] ; 0 0.000E-00
  2 (1.5) [CTRAC] + [OH]  -> (0.5) [DTRAC] ; 1 4.2000E+04
  3 [ETRAC] + [O3]        -> [FTRAC] ; 1 1.8000E-02

```

Figure 10-3. Example free-format RTCMC IMC chemistry input file.

#Control	Configuration information identified by keywords
#Species	Names of chemical species and associated data
#Table	Photolysis rate data for any photolytic reactions
#Equations	Chemical reactions and thermal rate constants

The IMC file uses space-delimited free-form text format. Leading white space at the start of any line will be ignored. CAMx reads the IMC file as *case insensitive*.

The hash symbol (#) before each section keyword marks the start of a section and should be reserved for this purpose. The four sections should appear in the order shown above. The only section that may be unnecessary in some cases (i.e., if there are no photolytic reactions) is the #Table section and guidance on handling this case is provided below.

10.2.1.1 The Control Section

According to the SCICHEM documentation, the #Control section of the IMC file must always have at least three lines, as follows:

```

#CONTROL
&CONTROL
&END

```

The first line is the keyword identifying the control section. The second and third lines are additional keywords denoting the start and end of the control section. Note, however, that CAMx ignores the &CONTROL and &END lines.

One or more control options may be specified using keywords, inserted one per line, ahead of the closing &END line, like this:

```
#CONTROL
  &CONTROL
    Keyword = 'option'
    Keyword = 'option'
  &END
```

The keywords used by CAMx and SCICHEM are listed in Table 10-1 and are case insensitive. Not all keywords are used by both models, and CAMx will ignore any non-recognized keyword. A “=” symbol must separate each keyword and option. The option must be enclosed within single quotes. In practice, only the first six letters of each keyword and the first three letters of each option are considered and you may abbreviate accordingly (i.e., `keyword = 'opt'`).

Table 10-1. Keywords, options and default values for the Control section of the IMC file.

Keyword	Used by SCICHEM	Used by CAMx	Options Allowed by CAMx
Ambient_file	•		n/a
Species_units	•		n/a
Emission_units	•		n/a
Rate_species_units	•	•	molecules/cm ³ (<i>default</i>) ppm
Rate_time_units	•	•	seconds (<i>default</i>) minutes hours
Solver		•	DLSODE (<i>default</i>) SLSODE Rosenbrock
Rtol	•	•	Real number (<i>default</i> = 1.0E-5)
Atol		•	Real number (<i>default</i> = 1.0E-18)
Jacobian		•	Numeric (<i>default</i>) Algebraic

All CAMx recognized keywords have a default option that will be used if the keyword is omitted, meaning that the CAMx RTCMC may be run without specifying any keywords provided that all other input data (e.g., rate constants) are consistent with the defaults. The allowed keyword options in Table 10-1 are discussed below:

Rate_species_units

The concentration units for thermal rate constant expressions.

Rate_time_units

The time units for photolysis and thermal rate constant expressions.

Solver

The name of the numerical integrator to be used as the chemistry solver. SLSODE and DLSODE are, respectively, the single and double precision versions of the Livermore Solver for Ordinary Differential Equations (Hindmarsh 1983). The Rosenbrock solver is the double precision RODAS solver (Hairer and Wanner, 1991).

Rtol

The relative error tolerance (convergence criterion) employed for all chemical species by the chemistry solver.

Atol

The absolute error tolerance (convergence criterion) employed for all chemical species by the chemistry solver. CAMx does not use species-specific Atol values that may appear in the species section, as discussed below.

Jacobian

The chemistry solvers employ a Jacobian matrix of first-order derivatives of each chemical species with respect to all species. The Jacobian matrix is constructed automatically by the RTCMC. This option controls whether the Jacobian is constructed algebraically or numerically. Both options may be used with the double precision solvers and numeric may be more efficient. The algebraic option is strongly recommended for the single precision SLSODE solver (because single precision may be inadequate for constructing a numeric Jacobian by finite difference).

10.2.1.1.1 Concentration Units

CAMx does not use the Species_units or Emission_units keywords and will ignore them if they are present. CAMx will output RTCMC species average concentrations in ppm units. Emissions of RTCMC species must be provided in moles/hour.

10.2.1.1.2 Setting Error Tolerances

All three RTCMC chemistry solvers use the Rtol and Atol parameters specified in the control section to manage errors in predicted concentrations. CAMx does not use the species-specific Atol values that may appear in the species section because it is difficult to select reliable Atol values for each species. The error (*err*) in the predicted concentration (*con*) for species *i* should be roughly less than:

$$err(i) = rtol \times con(i) + atol$$

The combined Rtol and Atol determine accuracy. Setting Atol to zero will result in pure relative error control. Relative error control has the advantage of being easily understood (the errors should be smaller than X percent) but suffers the disadvantage of excessive

computational resources that may be expended to manage errors in species concentrations that are essentially zero. Note that RTCMC sets a concentration floor of 1.0E-16 ppm.

The default settings for `Rtol` and `Atol` listed in Table 10-1 should be generally applicable because they are conservative and effectively result in pure relative error control. We recommend against setting `Rtol` greater than 0.001. Appropriate settings for `Atol` depend upon the magnitude of concentration predictions and the need for accurate predictions in high vs. low concentration areas (e.g., plume centerline vs. out of plume).

Do not request infeasible accuracy from single precision SLSODE by setting `Rtol` and `Atol` smaller than about 1.0E-7.

10.2.1.2 The Species Section

The species section of the IMC file lists chemical species and associated data. All chemical species referred to in the equation section must appear in the species section. Extra species may appear in the species section, but including numerous extra species may cause a run-time error by exceeding the memory available for storing species information (if this happens, delete some of the unused species from the species section).

The first line is the keyword identifying the species section. The following information must be provided for each listed species:

Name

Species names may be up to 8 characters and must start with a letter. They are case insensitive. Accurate names are important because other CAMx input data (e.g., emissions, boundary conditions) will be matched to RTRAC species by name.

Type

There are four permissible species types identified by first letter: Ambient (A), Fast (F), Slow (S), and Equilibrium (E). Setting the species type is discussed in more detail below.

Ambient

The ambient value is not used by CAMx, but is used by SCICHEM. Provide a real number (e.g., 0.0).

Atol

Species specific error tolerances are not used by CAMx, but are used by SCICHEM. Provide a real number (e.g., 0.0).

Dep

The species deposition velocity in m/s. This deposition velocity will be used for all land surface types, which is a simplification compared to the CAMx dry deposition scheme. Provide a real number (e.g., 0.0).

Wet Scav

The wet scavenging coefficient is not used by CAMx. For SCICHEM, this is a washout ratio. CAMx does not use the washout ratio because this approach is incompatible with the CAMx wet deposition algorithms. Provide a real number (e.g., 0.0).

MW

The molecular weight is not needed by CAMx. Provide a real number (e.g., 1.0).

Spec Map

The core model species name from which to use internally-calculated dry deposition velocity for the RTCMC species. This is triggered by a negative "Dep" value in the same record. Provide a 10-character string. In the example below, RTCMC tracer O3A will use deposition velocities calculated by CAMx for the core model species O3:

```
#Name, Type, Ambient, ATol, Dep, Wet Scav, MW, Spec Map
O3A      F      1.0  1.000E-08  -3.00E-03  0.0  48.0  O3
```

10.2.1.2.1 Choosing the Species Type

The `Type` for each RTCMC species should be set according to: (a) whether the species concentration should be obtained from the core model or modeled using the RTCMC; and (b) the most accurate and efficient numerical method for performing chemistry within RTCMC.

All species to be obtained from the core model (e.g., O₃, OH, NO, NO₂, H₂O, M, O₂) must be set to type `Ambient`. This rule will be enforced by CAMx and, for example, the species O3 must be set to type `A`, because it is part of all the core chemical mechanisms.

Species that are solved by the RTCMC may be type `F`, `S` or `E`. The recommended default type is `F` (fast) in which case chemistry will be performed using the selected chemistry solver (e.g., DLSODE). Species that undergo slow chemical change (lifetime of hours or longer) may be set to type `S` (slow) with potential gain in efficiency but some loss in accuracy. Species that undergo extremely rapid chemical change (lifetime smaller than a second) may be set to type `E` (equilibrium) and solved using a steady-state approximation with some gain in efficiency but some loss in accuracy. The Rosenbrock solver does not work well with species types `S` or `E`. Equilibrium species may be used effectively with the single precision SLSODE solver to avoid the need for double precision. You should use types `S` or `E` with caution and evaluate both computational speed and concentration accuracy by comparing against results with using type `F`.

10.2.1.3 The Table Section

The table section of the IMC file provides photolysis rates for any photolytic reactions in the RTCMC mechanism. It must contain at least two lines:

```
#Table
0 zenith1, zenith2, zenith3, ...
```

The first line is the keyword identifying the table section. The second line must begin with 0 (zero) followed by a list of space-delimited zenith angles (in degrees) starting with zero degrees and ascending to the largest angle. If the largest zenith angle specified is less than 90 degrees a value of 90 degrees is implicitly added to the list. By default, up to 15 zenith angles are allowed (this may be changed as described under adjustable parameters, below). If the final zenith angle is not 90 degrees, no more than 14 angles should be listed to allow the 15th angle to be implicitly set to 90 degrees.

If the reaction mechanism has no photolytic reactions, include just the first two lines (keyword followed by zenith angles) in the table section. If the reaction mechanism includes photolytic reactions, list them one reaction per space-delimited line after the zenith angles:

```
reaction_ID, rate1, rate2, rate3, ...
```

The `reaction_ID` must be the integer identification number of the photolytic reaction followed by the photolysis rate at each zenith angle, from zero to the largest angle. Photolysis reactions are first order and have rate units of reciprocal time to be provided in the `Rate_time_units` specified in the control section of the IMC file. A photolysis rate of zero is implicitly assumed at 90 degrees unless you specify otherwise.

A negative "`reaction_ID`" in the table section causes the photolysis rate to be set to a core model reaction number, which is set in the position of "`rate1`". In the example below, RTCMC reaction #1 is photolytic and rates will be set according to the CAMx core photolysis reaction number 9:

```
#Table
  0   0.  10.  20.  30.  40.  50.  60.  70.  78.  86.
-001  9
```

10.2.1.4 The Equations Section

The equations section of the IMC file lists the chemical reactions and rate constants for the RTCMC reaction mechanism and must contain at least two lines:

```
#Equations
reaction_ID [Reactants] > (Stoichiometry) [Products] ; Rate_Constant
```

The first line is the keyword identifying the equations section and must be followed by at least one reaction line. Reaction lines list reactions and rate constants and are delimited by white space and separators. The `reaction_ID` and the `Reactants` must be separated by white space. The `Reactants` and `Products` must be separated by a right arrow symbol (the right arrow may be preceded by characters, e.g., => or ->). The `Products` and the `Rate_Constant` must be separated by a semi-colon.

The `reaction_ID` must be an integer value that uniquely identifies each reaction. Reaction identifiers need not be in order or continuous.

The name of `Reactants` and `Products` must be enclosed within square brackets, begin with a letter, and not exceed 8 characters in length. All species names used in the equations section must also appear in the species section. Zero to three reactants are allowed. Zero to 20 products are allowed (the maximum is a user adjustable parameter). Reactant and product names may be preceded by a stoichiometric coefficient enclosed within round brackets. If the stoichiometric coefficient is omitted it is assumed to be unity.

Rate constants are specified using SCICHEM conventions and must be in the units specified by the keywords `Rate_species_units` and `Rate_time_units` in the control section (the

defaults are molecules cm^{-3} and seconds, respectively). SCICHEM supports numerous rate constant expression types and CAMx should interpret all of them correctly, although not all have been thoroughly tested. Table 10-2 defines a sub-set of the SCICHEM rate constant expression types that are recommended for use with CAMx. The format for specifying rate expressions is the integer expression type followed by a list of the numerical values required by that expression type. It is important that rate expressions are defined in units that are consistent with the reaction order, and Table 10-3 defines how the reaction order and rate constant unit dimensions may be determined.

Table 10-2a. Recommended SCICHEM rate constant expression types for use in CAMx.

Expression Type	Description	Expression
0	Photolysis	$k = 0$
1	Constant	$k = k_0$
2	General temperature dependence	$k = AT^{-c} e^{(B/T)}$
3	Troe-type temperature and pressure dependence	$k = \left[\frac{k^0[M]}{1 + k^0[M]/k^\infty} \right] F^G$ $k^0 = AT^B$ $k^\infty = CT^D$ $F = 0.6$ $G = \left\{ 1 + \left[\log(k^0[M]/k^\infty) \right]^2 \right\}^{-1}$
8	Equilibrium with a previously defined reaction (k_{ref})	$k = k_{ref} A e^{(B/T)}$
13	Lindemann - Hinshelwood as used for OH + HNO ₃	$k = k_0 + \frac{k_3[M]}{1 + k_3[M]/k_2}$ $k_0 = A e^{(B/T)}$ $k_2 = C e^{(D/T)}$ $k_3 = E e^{(F/T)}$
7	Simple pressure dependence used for OH + CO	$k = k_0(1 + 0.6P)$

Table 10-2b. Parameters required by SCICHEM rate constant expression types.

Expression Type	Parameters					
	1	2	3	4	5	6
0	O					
1	k_o					
2	A	B	C			
3	A	B	C	D		
8	k_{ref}	A	B			
13	A	B	C	D	E	F
7	k_o					

Table 10-3. Determining the reaction order and consequent unit dimensions for rate constants.

Number of Reactants	Reaction Order	Concentration Unit Dimension	Time Unit Dimension
0	Zero	None	Time ⁻¹
1	First	None	Time ⁻¹
2	Second	Concentration ⁻¹	Time ⁻¹
3	Third	Concentration ⁻²	Time ⁻¹

The CAMx output “diag” file lists diagnostic information on the mechanism and rate constant expressions read by from the IMC file. You should review this diagnostic output to ensure that CAMx correctly read and configured the RTCMC chemistry mechanism.

10.3 Reactive Tracers In IRON PiG

RTRAC/RTCMC calculations for emissions and chemistry have been integrated into the IRON PiG algorithms. There are two ways in which RTRAC tracers may enter a PiG plume: as primary emissions from specifically flagged sources within the RTRAC point source file, or by formation of secondary species from decay of primary plume emissions. There is no entrainment of tracers from the grid to the plume as this is likely to result in negative tracer concentrations, especially if the entrained tracer is a secondary product of a host model species (e.g., secondary formaldehyde). Tracers are assumed to have negligible impact on PiG puff chemistry or oxidant levels. If the tracer concentration in the plume is high enough to enhance or suppress the plume oxidant levels, then the photochemical impacts of the tracer can be accounted for by separately adding the tracer emissions into the host model lumped emissions; e.g., for tracing high concentrations of propene and butene in a plume, one would track the propene/butene concentrations using RTRAC tracers but also add CB-OLE or SAPRC-OLE1 emissions to the plume to account for the oxidant impacts. RTRAC checks to ensure that it is reading its own input point source file. RTRAC and host model point source files must have the same number of sources in the same order; however, the list of species on each file may be different, and the

sources flagged to receive the PiG treatment may vary. A pre-processor program was coded to help prepare consistent RTRAC and host model point source files.

Tracers released from PiG sources decay according to the oxidant and photolytic environment of the plume using user-supplied chemical rate parameters (as described earlier). Oxidant concentrations for the decay calculation are obtained from the CAMx PiG incremental photochemical simulation for each puff at each time step. RTRAC tracers in each puff reactor are updated based on the *total* oxidant concentrations for the reactor, i.e., puff increment plus puff ambient/background. RTRAC enforces a rule that no secondary tracer formation from the decay of host model species are allowed if IRON PiG is active (e.g., no secondary formaldehyde tracer formation is allowed with IRON PiG). Secondary tracer production from primary tracer decay is allowed.

Tracers are transferred from the PiG to the grid using the same approach as for any other host model species (see Section 6). Tracer concentrations at any point are the superposition of the grid concentration plus any collocated PiG puffs.

RTRAC optionally employs surface-layer IRON puff sampling of tracers on a user-defined sampling grid (see Section 6). Sampling grids are entirely passive, and intended to provide a display of the reactive tracer plume concentrations at scales much smaller than typically used for the finest computational grids (i.e., <1 km).

10.4 Running CAMx With Reactive Tracers

10.4.1 CAMx Control File

RTRAC is invoked similarly to the other Probing Tools within the CAMx control file. In the `&CAMx_Control` namelist module, the variable `Probing_Tool` must be set to "RTRAC" or "RTCMC". An additional namelist module called `&RT_Control` must then be provided in the control file to configure the RTRAC portion of the model. The additional namelist module is described below. The order of the variables follows the template available with the source code. Figure 10-5 provides an example of the RTRAC control module.

Description of RTRAC Control in the CAMx Run Control File

<code>&RT_Control</code>	Label for the Probing Tool namelist module that configures the RTRAC option; it must begin in column 2
<code>&</code>	Flag ending a namelist; it must be in column 2
<code>RT_File_Root</code>	Character root output path/filename
<code>RT_Initial_Conditions</code>	Character input master grid RTRAC initial conditions path/filename (optional, ignored if <code>Restart=TRUE</code>)

RT_Boundary_Conditions	Character input master grid RTRAC boundary conditions path/filename (optional)
RT_Master_Restart	Character input master grid RTRAC restart path/filename (ignored if Restart=FALSE)
RT_Nested_Restart	Character input nested grid RTRAC restart path/filename (ignored if Restart=FALSE or Number_of_Grids=1)
RT_Chemistry_Parameters	Character input RTRAC chemistry parameters path/filename, or RTCMC IMC chemistry definition path/filename
RT_Receptor_Definitions	Character input RTRAC receptor definition path/filename (optional)
RT_Point_Sources	Character input RTRAC elevated point source emissions path/filename (optional, ignored if Point_Emissions=FALSE)
RT_Emiss_Grid	Character array (by CAMx grid) input RTRAC gridded emissions path/filename (optional, ignored if Gridded_Emissions=FALSE)
RT_PiG_Sample	Logical sampling grid flag for RTRAC IRON PiG output; sampling grids are defined in the main &CAMx_Control namelist (TRUE=sampling grid output will be generated, FALSE=sampling grid output will not be generated)

```

&RT_Control

  RT_File_Root           = 'CAMx6.test.020614',

  RT_Initial_Conditions = ' ',
  RT_Boundary_Conditions = ' ',
  RT_Master_Restart     = 'CAMx6.test.020613.rt.inst',
  RT_Nested_Restart     = 'CAMx6.test.020613.rt.finst',

  RT_Chemistry_Parameters = 'CAMx6.chemparam.rtrac_test',
  RT_Receptor_Definitions = 'receptor.rtrac.test',
  RT_Point_Sources       = 'pt.rtrac.test',
  RT_Emiss_Grid(1)       = 'emiss.rtrac.36km',
  RT_Emiss_Grid(2)       = 'emiss.rtrac.12km',
  RT_Emiss_Grid(3)       = 'emiss.rtrac.04km',

  RT_PiG_Sample          = .true.,

&

```

Figure 10-4. Example input of RTRAC options and filenames within the CAMx control file.

As with the output for the host model and other Probing Tools, a “root” file name is specified and suffixes are added depending upon the type of output produced. A separate root name for RTRAC (and other Probing Tools) allows the user to direct the output to a completely different path. RTRAC writes several output files that are in Fortran binary format, as described in Section 3. These include the master and nested grid tracer instantaneous concentration files (.rt.inst and .rt.finst), the grid-specific surface tracer average concentration file (.rt.grdnn). These files are written in the same format as for the regular model species described in Section 3.

The “RT_Chemistry_Parameter” namelist variable specifies the path/filename of either the RTRAC chemistry parameters file or the RTCMC IMC chemistry definition file. The choice of which type of file format is read is set according the main “Probing_Tool” variable (i.e., RTRAC or RTCMC).

RTRAC/IRON PiG sampling grids are invoked in the RTRAC namelist by setting a logical flag. If set to TRUE, the user must provide the number of sampling grids and the grid parameters of each in the main &CAMx_Control namelist. Sampling grids are set identically to the way nested grids are specified for the host model, with one exception: there are no vertical levels to define (sampling grids are currently only 2-D surface fields). The same rules that apply for the specification of nested grids holds for the specification of all sampling grids (see Sections 2, 4, and 6). The “mesh factor” sets the resolution or cell size of the sampling grid relative to the master grid. The CAMx diagnostic output file provides information on the location and size of each sampling grid to help ensure proper setup.

10.4.2 User Adjustable Parameters

Once the RTRAC/RTCMC chemistry parameters/definition file is established, the user should be sure that a sufficient allocation of memory is provided for this Probing Tool. This is done by examining the main Probing Tool parameter and common block file in `Includes/camx.prm`. The parameter `MXTRSP` should be set to the total number of species defined in the chemistry parameters file. If sampling grids are to be used, the user should ensure that sufficient memory is available to define the size of sampling grid arrays. This is also set in `Includes/camx.prm`.

User adjustable parameters for RTCMC are set in the CAMx include file `Includes/rtcmcchm.inc`. If an error is encountered at model start up because one of these RTCMC parameter has been exceeded, consult the list of parameters in Table 10-4 and then change the parameter appropriately in the `rtcmcchm.inc` include file. Rebuild the CAMx executable (we recommend performing a "make clean" before making a new CAMx executable) after changing any RTCMC parameter.

Table 10-4. RTCMC parameters default settings in the `Includes/rtcmcchm.inc` include file.

Name	Description	Default
MXRX	maximum number of RTCMC reactions	20
MXPHOT	maximum number of photolysis reactions	10
MXZEN	maximum number of photolysis reaction zenith angles	15
MXRCT	Maximum number of reactants in each reaction	3
MXPRD	maximum number of products in each reaction	20
MXEQM	maximum number of equilibrium species	5
MXSLO	maximum number of slow species	25

11. REFERENCES

- Anthes, R.A. and T.T. Warner. 1978. Development of Hydrodynamic Models Suitable for Air Pollution and Other Mesometeorological Studies. *Mon. Wea. Rev.*, **106**, 1045-1078.
- Ariya, P.A., A. Khalizov and A. Gidas. 2002. Reactions of gaseous mercury with atomic and molecular halogens: kinetics, product studies, and atmospheric implications. *J. Phys. Chem.*, **106**, 7310-7320.
- Astitha M., C. Spyrou, G. Kallos, H. Denier Van der Gon, A. Visschedijk and J. Lelieveld. 2009. Chemical composition change of aerosols along long-range transport paths. 30th NATO/SPS ITM on Air Pollution Modelling and its Applications, May 2009, San Francisco, CA.
- Atkinson, R., W.P. Carter, A.M. Winer. 1983. Effects of temperature and pressure on alkyl nitrate yields in the nitrogen oxide (NO_x) photooxidations of n-pentane and n-heptane. *J. Phys. Chem.*, **87**(11), 2012-2018.
- Atkinson, R.A., D.L. Baulch, R.A. Cox, J.N. Crowley, R.F. Hampson, R.G. Hynes, M.E. Jenkin, J.A. Kerr, M.J. Rossi, J. Troe. 2010. "Evaluated kinetic and photochemical data for atmospheric chemistry - IUPAC subcommittee on gas kinetic data evaluation for atmospheric chemistry." January 3, 2010 web version available at <http://www.iupac-kinetic.ch.cam.ac.uk/index.html>.
- Barlage, M., F. Chen, M. Tewari, K. Ikeda, D. Gochis, J. Dudhia, R. Rasmussen, B. Livneh, M. Ek, K. Mitchell. 2010. Noah land surface model modifications to improve snowpack prediction in the Colorado Rocky Mountains. *J. Geophys. Res.*, **115**, D22101, doi:10.1029/2009JD013470.
- Bertram, T.H., Thornton, J.A. 2009. Toward a general parameterization of N₂O₅ reactivity on aqueous particles: the competing effects of particle liquid water, nitrate and chloride. *Atmos. Chem. Phys.*, **9**, 8351-8363.
- Bott, A. 1989. A Positive Definite Advection Scheme Obtained by Nonlinear Renormalization of the Advective Fluxes. *Mon. Wea. Rev.*, **117**, 1006-1015.
- Brown, S.S., Ryerson, T.B., Wollny, A.G., Brock, C.A., Peltier, R., Sullivan, A.P., Weber, R.J., Dube, W.P., Trainer, M., Meagher, J.F., Fehsenfeld, F.C., Ravishankara, A.R. 2006. Variability in nocturnal nitrogen oxide processing and its role in regional air quality. *Science*, **311**, 67-70.
- Carlton, A.G., B.J. Turpin, K.E. Altieri, S. Seitzinger, A. Reff, H.-J. Lim, B. Ervens. 2007. Atmospheric oxalic acid and SOA production from glyoxal: Results of aqueous photooxidation experiments. *Atmos. Environ.*, **41**, 7588-7602.
- Carpenter, L.J. 2003. Iodine in the marine boundary layer. *Chemical Reviews*, **103**, 4953-4962.
- Carpenter, L.J., S.M. MacDonald, M.D. Shaw, R. Kumar, R.W. Saunders, R. Parthipan, J. Wilson, J.M.C. Plane. 2013. Atmospheric iodine levels influenced by sea surface emissions of inorganic iodine. *Nature Geoscience*, **6**, no. 2: 108-111.

- Carter, W.P.L. 1996. Condensed Atmospheric Photooxidation Mechanisms for Isoprene. *Atmos. Environ.*, **30**, 4275-4290.
- Carter, W.P.L. 2010. Development of the SAPRC-07 chemical mechanism. *Atmos. Environ.*, **44**, 5324-5335.
- Carter, W.P. and G. Heo. 2013. Development of revised SAPRC aromatics mechanisms. *Atmos. Environ.*, **77**, 404-414.
- Chameides, W.L., and D.D. Davis. 1980. Iodine: Its Possible Role in Tropospheric Photochemistry. *J. Geophys. Res.*, **85**, 7383–7398, doi:10.1029/JC085iC12p07383.
- Chance, R., A.R. Baker, L. Carpenter, T.D. Jickells. 2014. The distribution of iodide at the sea surface. *Environmental Science: Processes & Impacts*, **16**, 1841–1859, doi:10.1039/C4EM00139G.
- Chang, J.S., R.A. Brost, I.S.A. Isaksen, S. Madronich, P. Middleton, W.R. Stockwell, and C.J. Walcek. 1987. A Three-dimensional Eulerian Acid Deposition Model: Physical Concepts and Formulation. *J. Geophys. Res.*, **92**, 14,681-14,700.
- Clever, H., S.A. Johnson and E.M. Derrick. 1985. The solubility of mercury and some sparingly soluble mercury salts in water and aqueous solutions. *J. Phys. Chem. Ref. Data*, **14**, 631-680.
- Cohan, D.S., A. Hakami, Y. Hu, and A.G. Russell. 2005. Nonlinear Response of Ozone to Emissions: Source Apportionment and Sensitivity Analysis. *Environ. Sci. Technol.*, **39**, 6739-6748.
- Colella, P., and P.R. Woodward. 1984. The Piecewise Parabolic Method (PPM) for Gas-dynamical Simulations. *J. Comp. Phys.*, **54**, 174-201.
- Del Genio, A.D., M.S. Yao, W. Kovari, K.K.W. Lo. 1996. A prognostic cloud water parameterization for global climate models. *J. Climate*, **9**, 270-304.
- Donahue, N.M., A.L. Robinson, C.O. Stanier, S.N. Pandis. 2006. Coupled partitioning, dilution, and chemical aging of semivolatile organics. *Environ. Sci. Technol.*, **40**, 2635-2643.
- Donahue, N.M., S.A. Epstein, S.N. Pandis, A.L. Robinson. 2011. A two-dimensional volatility basis set: 1. organic-aerosol mixing thermodynamics. *Atmos. Chem. Phys.*, **11**, 3303-3318.
- Donahue, N.M., J.H. Kroll, S.N. Pandis, A.L. Robinson. 2012. A two-dimensional volatility basis set – Part 2: Diagnostics of organic-aerosol evolution. *Atmos. Chem. Phys.*, **12**, 615-634.
- Dunker, A.M. 1980. The response of an atmospheric reaction-transport model to changes in input functions. *Atmos. Environ.*, **14**, 671-679.
- Dunker, A.M. 1981. Efficient calculations of sensitivity coefficients for complex atmospheric models. *Atmos. Environ.* **15**, 1155-1161.
- Dunker A.M., G. Yarwood, J.P. Ortmann, G.M. Wilson. 2002. The decoupled direct method for sensitivity analysis in a three-dimensional air quality model – implementation, accuracy and efficiency. *Environ. Sci. Technol.*, **36**, 2965-2976.

- Edgerton, E.S., B.E. Hartsell and J.J. Jansen. 2001. Atmospheric mercury measurements at a rural and urban site near Atlanta, GA, USA. *6th International Conference on Mercury as a Global Pollutant*, 15-19 October 2001, Minamata, Japan.
- Ek, M.B., K.E. Mitchell, Y. Lin, E. Rogers, P. Grunmann, V. Koren, G. Gayno, J. D. Tarpley. 2003. Implementation of Noah land surface model advances in the National Centers for Environmental Prediction operational mesoscale Eta model. *J. Geophys. Res.*, **108**(D22), 8851, doi:10.1029/2002JD003296.
- Elterman, L. 1968. "UV, Visible, and IR Attenuation for Altitudes to 50 km, 1968." US Air Force Cambridge Research Laboratory Report, AFCRL 68-0153.
- Emery, C., J. Jung, J. Johnson, G. Yarwood, S. Madronich, G. Grell. 2010. Improving the Characterization of Clouds and their Impact on Photolysis Rates within the CAMx Photochemical Grid Model. Prepared for the Texas Commission on Environmental Quality, Austin, TX. Prepared by ENVIRON International Corporation, Novato, CA and the National Center for Atmospheric Research, Boulder, CO (August 27, 2010).
- Emery, C., E. Tai, G. Yarwood, R. Morris. 2011. Investigation into approaches to reduce excessive vertical transport over complex terrain in a regional photochemical grid model. *Atmos. Environ.*, **45**, 7341-7351, doi:10.1016/j.atmosenv.2011.07.052.
- Emery, C., J. Jung, B. Koo, G. Yarwood. 2015. Improvements to CAMx Snow Cover Treatments and Carbon Bond Chemical Mechanism for Winter Ozone. Prepared for the Utah Department of Environmental Quality, Division of Air Quality, Salt Lake City, UT. Prepared by Ramboll Environ, Novato, CA (August 2015).
- Emery, C., Z. Liu, B. Koo, G. Yarwood. 2016. Improved Halogen Chemistry for CAMx Modeling. Prepared for the Texas Commission on Environmental Quality, Austin, TX. Prepared by Ramboll Environ, Novato, CA (May 2016).
- ENVIRON. 2002. Development, Application, and Evaluation of an Advanced Photochemical Air Toxics Modeling System. Prepared for the Coordinating Research Council, Alpharetta, GA, and the U.S. Department of Energy, Office of Heavy Vehicle Technologies (September 27, 2002). Available from www.crao.com.
- EPA. 1990. User's Guide for the Urban Airshed Model-Volume I; User's Manual for UAM(CB-IV). U.S. Environmental Protection Agency, Research Triangle Park, NC, EPA-450/4-90-007a.
- EPA. 1998. User's Guide for the AERMOD Meteorological Preprocessor (Revised Draft). Prepared by the U.S. Environmental Protection Agency, Research Triangle Park, NC (November, 1998).
- EPRI. 2000. SCICHEM Version 1.2: Technical Documentation. Final Report prepared by ARAP/Titan Corporation, Princeton, NJ, for EPRI, Palo Alto, CA. December 2000 (1000713).
- Fahey, K.M. and S.N. Pandis. 2001. Optimizing model performance: variable size resolution in cloud chemistry modeling. *Atmos. Environ.* **35**, 4471-4478.

- Fisher, J.A., Jacob, D.J., Travis, K.R., Kim, P.S., Marais, E.A., Chan Miller, C., Yu, K., Zhu, L., Yantosca, R.M., Sulprizio, M.P., Mao, J., Wennberg, P.O., Crouse, J.D., Teng, A.P., Nguyen, T.B., St. Clair, J.M., Cohen, R.C., Romer, P., Nault, B.A., Wooldridge, P.J., Jimenez, J.L., Campuzano-Jost, P., Day, D.A., Hu, W., Shepson, P.B., Xiong, F., Blake, D.R., Goldstein, A.H., Misztal, P.K., Hanisco, T.F., Wolfe, G.M., Ryerson, T.B., Wisthaler, A., Mikoviny, T. 2016. Organic nitrate chemistry and its implications for nitrogen budgets in an isoprene- and monoterpene-rich atmosphere: constraints from aircraft (SEAC4RS) and ground-based (SOAS) observations in the Southeast US. *Atmos. Chem. Phys.*, **16**, 5969-5991, doi:10.5194/acp-16-5969-2016.
- FLAG. 2000. "Federal Land Managers' Air Quality Related Values Workgroup (FLAG), Phase I Report." Prepared by the US Forest Service, Air Quality Program; National Park Service, Air Resources Division; and US Fish and Wildlife Service, Air Quality Branch (December 2000).
- Gallagher, W.M., K.M. Beswick, J. Duyzer, H. Westrate, T.W. Choularton, J.P. Hummelsho. 1997. Measurements of aerosol fluxes to Speulder forest using a micrometeorological technique. *Atmos. Environ.*, **31**, 359 – 373.
- Ganzeveld, L., D. Helmig, C. W. Fairall, J. Hare, and A. Pozzer. 2009. Atmosphere-ocean ozone exchange: A global modeling study of biogeochemical, atmospheric, and waterside turbulence dependencies. *Global Biogeochem. Cycles*, **23**, GB4021, doi:10.1029/2008GB003301.
- Gardfeldt, K. and M. Johnson. 2003. Is bimolecular reduction of Hg(II) complexes possible in aqueous systems of environmental importance? *J. Phys. Chem.*, **107**, 4478-4482.
- Garland, J. A., and H. Curtis. 1981. Emission of iodine from the sea surface in the presence of ozone. *Journal of Geophysical Research: Oceans* (1978–2012), **86**, no. C4: 3183-3186.
- Gear, C.W. 1971. *Numerical Initial Value Problems in Ordinary Differential Equations*. Prentice-Hall, Englewood Cliffs, NJ.
- Gery, M.W., G.Z. Whitten, J.P. Killus, and M.C. Dodge. 1989. A Photochemical Kinetics Mechanism for Urban and Regional Scale Computer Modeling. *J. Geophys. Res.*, **94**, 925-956.
- Goliff, W.S., W.R. Stockwell, C.V. Lawson. 2013. The regional atmospheric chemistry mechanism, version 2. *Atmos. Environ.*, **68**, 174-185.
- Hairer, E., and G. Wanner. 1991. *Solving ordinary differential equations II Stiff and differential-algebraic problems*. Springer-Verlag, Berlin.
- Hakami, A., M.T. Odman, and A.G. Russell. 2003. High-order, direct sensitivity analysis of multidimensional air quality models. *Environ. Sci. Technol.*, **37**, 2442-2452.
- Hall, B. 1995. The gas-phase oxidation of elemental mercury by ozone. *Water Air Soil Pollut.*, **80**, 301-315.
- Helmig, D., E.K. Lang, L. Bariteau, P. Boylan, C.W. Fairall, L. Ganzeveld, J.E. Hare, J. Hueber, M. Pallandt. 2012. Atmosphere-ocean ozone fluxes during the TexAQS 2006, STRATUS

- 2006, GOMECC 2007, GasEx 2008 and AMMA 2008 Cruises. *J. Geophys. Res.*, **117**, D04305, doi:10.1029/2011JD015955.
- Herman, J.R. and E.A. Celarier. 1997. Earth surface reflectivity climatology at 340-380 nm from TOMS data. *J. Geophys. Res.*, **102**, No. 23.
- Hertel O., R. Berkowics, J. Christensen and O. Hov. 1993. Test of two numerical schemes for use in atmospheric transport-chemistry models. *Atmos. Env.*, **27**, 2591-2611.
- Hildebrandt Ruiz, L.H, and G. Yarwood. 2013. Interactions between organic aerosol and NO_y: Influence on oxidant production. Prepared for the Texas AQRP (Project 12-012), by the University of Texas at Austin, and ENVIRON International Corporation, Novato, CA (http://aqrp.ceer.utexas.edu/projectinfoFY12_13/12-012/12-012%20Final%20Report.pdf).
- Hildebrandt Ruiz, L., Koo, B., Yarwood, G. 2015. Sources of Organic Particulate Matter in Houston: Evidence from DISCOVER-AQ data - Modeling and Experiments. Final Report prepared for the Texas AQRP (Project 14-024), by the University of Texas at Austin, and Ramboll Environ, Novato, CA (http://aqrp.ceer.utexas.edu/projectinfoFY14_15/14-024/14-024%20Final%20Report.pdf).
- Hindmarsh, A.C. 1983. ODEPACK, a Systematized Collection of ODE Solvers. In *Numerical Methods for Scientific Computation*, **55**, R.S. Stepleman, Ed., North-Holland, New York.
- Hodzic, A., B. Aumont, C. Knote, J. Lee-Taylor, S. Madronich, G. Tyndall. 2014. Volatility Dependence of Henry's Law Constants Of Condensable Organics: Application to Estimate Depositional Loss of Secondary Organic Aerosols. *Geophys. Res. Lett.*, **41**, 4795-4804.
- Hodzic, A., P.S. Kasibhatla, D.S. Jo, C.D. Cappa, J.L. Jimenez, S. Madronich, R.J. Park. 2016. Rethinking the global secondary organic aerosol (SOA) budget: stronger production, faster removal, shorter lifetime. *Atmos. Chem. Phys.*, **16**, 7917-7941.
- Holmes, C.D., D.J. Jacob, and X. Yang. 2006. Global lifetime of elemental mercury against oxidation by atomic bromine in the free troposphere. *Geophys. Res. Lett.*, **33**, L20808, doi:10.1029/2006GL027176.
- Huebert, B.J., and C.H. Robert. 1985. The Dry Deposition of Nitric Acid to Grass. *J. Geophys. Res.*, **90**(D1), 2085-2090 (doi:10.1029/JD090iD01p02085).
- Hutzell, W.T., Luecken, D.J., Appel, K.W., Carter, W.P.L. 2012. Interpreting predictions from the SAPRC07 mechanism based on regional and continental simulations. *Atmos. Environ.*, **46**, 417-429.
- Ibusuki, T. and K. Takeuchi. 1987. Sulfur dioxide oxidation by oxygen catalyzed by mixtures of manganese(II) and iron(III) in aqueous solutions at environmental reaction conditions. *Atmos. Environ.*, **21**, 1555-1560.
- IUPAC. 1992. Evaluated Kinetic and Photochemical Data for Atmospheric Chemistry. Supplement IV. IUPAC Subcommittee on Gas Kinetic Data Evaluation for Atmospheric Chemistry (R. Atkinson, D.L. Baulch, R. A. Cox, R. F. Hampson, Jr., J. A. Kerr, and J. Troe). *Journal of Physical and Chemical Reference Data*, **21**, No. 6, 1125-1568.

- IUPAC. 2014a. "Summary of Reactions and Preferred Rate Data, Volume 3 - Inorganic Halogen Species." Available at http://iupac.pole-ether.fr/datasheets/summary/vol3_summary.xml.
- IUPAC. 2014b. "Summary of Reactions and Preferred Rate Data, Volume - Organic Halogen Species." Available at http://iupac.pole-ether.fr/datasheets/summary/vol4_summary.xml.
- IUPAC. 2015. "Task Group on Atmospheric Chemical Kinetic Data Evaluation – Data Sheet NOx33." Available at http://iupac.pole-ether.fr/htdocs/datasheets/pdf/NOx33_N2O5_H2O.pdf.
- Jacob, D.J. 2000. Heterogeneous chemistry and tropospheric ozone. *Atmos. Environ.*, **34**, 2131-2159.
- Jacobs, M.I., Burke, W.J., Elrod, M.J. 2014. Kinetics of the reactions of isoprene-derived hydroxynitrates: gas phase epoxide formation and solution phase hydrolysis. *Atmos. Chem. Phys.*, **14**, 8933-8946, doi:10.5194/acp-14-8933-2014.
- Jacobson, M.Z. 1997. Development and application of a new air pollution modeling system—II. Aerosol module structure and design. *Atmos. Environ.*, **31**, 131-144.
- Jaegle, L., D.J. Jacob, W.H. Brune and P.O. Wennberg. 2001. Chemistry of HO_x radicals in the upper troposphere. *Atmos. Environ.*, **35**, 469-489.
- Jathar, S.H., Gordon, T.D., Hennigan, C.J., Pye, H.O.T., Pouliot, G., Adams, P.J., Donahue, N.M., Robinson, A.L. 2014. Unspeciated organic emissions from combustion sources and their influence on the secondary organic aerosol budget in the United States. *Proc. Natl. Acad. Sci.*, **111**, 10473-10478.
- Jeffries, H. E., and G.S. Tonnesen. 1994. Comparison of two photochemical reaction mechanisms using a mass balance and process analysis. *Atmos. Environ.*, **28**, 2991-3003.
- Kalberer, M., D. Paulson, M. Sax, M. Steinbacher, J. Dommen, A.S.H. Prevot, R. Fisseha, E. Weingartner, V. Frankevich, R. Zenob, and U. Baltensperger. 2004. Identification of polymers as major components of atmospheric organic aerosols. *Science*, **303**, 1659-1662.
- Karamchandani, P., A. Koo, C. Seigneur. 1998. Reduced gas-phase kinetic mechanism for atmospheric plume chemistry. *Environ. Sci. Technol.*, **32**, 1709-1720.
- Knote, C., A. Hodzic, J.L. Jimenez. 2015. The effect of dry and wet deposition of condensable vapors on secondary organic aerosols concentrations over the continental US. *Atmos. Chem. Phys.*, **15**, 1-18.
- Koo, B., A.S. Ansari, and S.N. Pandis. 2003. Integrated Approaches to Modeling the Organic and Inorganic Atmospheric Aerosol Components. *Atmos. Environ.*, **37**, 4757-4768.
- Koo, B., G. Yarwood, D.S. Cohan. 2007a. Incorporation of High-order Decoupled Direct Method (HDDM) Sensitivity Analysis Capability into CAMx. Prepared for the Texas Commission on Environmental Quality, Austin, TX. Prepared by ENVIRON International Corporation, Novato, CA and Rice University, Houston, TX.

- Koo, B., A.M. Dunker, G. Yarwood. 2007b. Implementing the Decoupled Direct Method for Sensitivity Analysis in a Particulate Matter Air Quality Model. *Environ. Sci. Technol.*, **41**, 2847-2854.
- Koo, B., G. Yarwood, D.S. Cohan. 2008. Higher-order Decoupled Direct Method (HDDM) for Ozone Modeling Sensitivity Analyses and Code Refinements. Prepared for the Texas Commission on Environmental Quality, Austin, TX. Prepared by ENVIRON International Corporation, Novato, CA and Rice University, Houston, TX.
- Koo, B., G.M. Wilson, R.E. Morris, A.M. Dunker, G. Yarwood. 2009. Comparison of Source Apportionment and Sensitivity Analysis in a Particulate Matter Air Quality Model. *Environ. Sci. Technol.*, **43**, 6669-6675.
- Koo, B., G. Yarwood and J. Roberts. 2012. An Assessment of Nitryl Chloride Formation Chemistry and its Importance in Ozone Non-Attainment Areas in Texas. Final report for Texas Air Quality Research Program project 10-015. Prepared by ENVIRON International Corporation, Novato, CA and NOAA/ESRL, Boulder, CO. Available at <http://aqrp.ceer.utexas.edu/projectinfo%5C10-015%5C10-015%20Final%20Report.pdf>.
- Koo, B., E. Knipping, G. Yarwood. 2014. 1.5-Dimensional volatility basis set approach for modeling organic aerosol in CAMx and CMAQ. *Atmos. Environ.*, **95**, 158-164.
- Kumar, N., F.W. Lurmann, A.S. Wexler, S. Pandis, and J.H. Seinfeld. 1996. Development and Application of a Three Dimensional Aerosol Model. Presented at the A&WMA Specialty Conference on Computing in Environmental Resource Management, Research Triangle Park, NC, December 2-4, 1996.
- Kumar, N. and A. G. Russell. 1996. Development of a Computationally efficient, Reactive Sub-Grid-Scale Plume Model and the Impact in the Northeastern United States Using Increasing Levels of Chemical Detail. *J. Geophys. Res.*, **101**, 16,737-16,744.
- Lamarque, J.F., L.K. Emmons, P.G. Hess, D.E. Kinnison, S. Tilmes, F. Vitt, C.L. Heald, E.A. Holland, P.H. Lauritzen, J. Neu, J.J. Orlando, P.J. Rasch, G.K. Tyndall. 2012. CAM-chem: description and evaluation of interactive atmospheric chemistry in the Community Earth System Model. *Geosci. Model Dev.*, **5**, 369-411, doi:10.5194/gmd-5-369-2012.
- Landis, M.S. and G. Keeler. 2002. Atmospheric mercury deposition to Lake Michigan during the Lake Michigan Mass Balance Study. *Environ. Sci. Technol.*, **36**, 4518-4524.
- Lane, T.E., N.M. Donahue, S.N. Pandis. 2008. Simulating secondary organic aerosol formation using the volatility basis-set approach in a chemical transport model. *Atmos. Environ.*, **42**, 7439-7451.
- Lee, L., P.J. Wooldridge, J.B. Gilman, C. Warneke, J. de Gouw, R.C. Cohen. 2014. Low temperatures enhance organic nitrate formation: evidence from observations in the 2012 Uintah Basin Winter Ozone Study. *Atmos. Chem. Phys. Disc.*, **14**(11), 17401-17438.
- Lim, Y.B., Y. Tan, B.J. Turpin. 2013. Chemical insights, explicit chemistry, and yields of secondary organic aerosol from OH radical oxidation of methylglyoxal and glyoxal in the aqueous phase. *Atmos. Chem. Phys.*, **13**, 8651-8667.

- Lin, C.J. and S.O. Pehkonen. 1997. Aqueous-free radical chemistry of mercury in the presence of iron oxides and ambient aerosol. *Atmos. Environ.*, **31**, 4125-4137.
- Lin, C.J. and S.O. Pehkonen. 1998. Oxidation of elemental mercury by aqueous chlorine (HOCl/OCl⁻): Implications for tropospheric mercury chemistry. *J. Geophys. Res.*, **103**, 28093-28102.
- Lindberg, S., O.R. Bullock, R. Ebinghaus, D. Engstrom, X. Feng, W. Fitzgerald, N. Pirrone, E. Prestbo, and C. Seigneur. 2007. A synthesis of progress and uncertainties in attributing the sources of mercury in deposition. *Ambio*, **36**, 19-33.
- Lindqvist, O. and H. Rodhe. 1985. Atmospheric mercury - a review. *Tellus*, **37B**, 136-159.
- Livneh, B., Y. Xia, K. E. Mitchell, M.B. Ek. 2010. Noah LSM snow model diagnostics and enhancements. *J. Hydromet.*, **11**, doi:10.1175/2009JHM1174.1.
- Locatelli, J.D. and P.V. Hobbs. 1974. Fall speeds and masses of solid precipitation particles. *J. Geophys. Res.*, **79**(15), 2185-2197.
- Louis, J.F. 1979. A Parametric Model of Vertical Eddy Fluxes in the Atmosphere. *Bound. Lay. Meteor.* **17**, 187-202.
- MacDonald, S.M., J.C. Gómez Martín, R. Chance, S. Warriner, A. Saiz-Lopez, L.J. Carpenter, J.M.C. Plane. 2014. A laboratory characterisation of inorganic iodine emissions from the sea surface: dependence on oceanic variables and parameterization for global modelling. *Atmos. Chem. Phys.*, **14**, 5841-5852, doi:10.5194/acp-14-5841-2014.
- Mahajan, A.S., H. Oetjen, A. Saiz-Lopez, J.D. Lee, G.B. McFiggans, J.M.C. Plane. 2009. Reactive iodine species in a semi-polluted environment. *Geophys. Res. Lett.*, **36**, L16803, doi:10.1029/2009GL038018.
- Mahajan, A.S., J.M.C. Plane, H. Oetjen, L. Mendes, R.W. Saunders, A. Saiz-Lopez, C.E. Jones, L.J. Carpenter, G.B. McFiggans. 2010. Measurement and modelling of tropospheric reactive halogen species over the tropical Atlantic Ocean. *Atmos. Chem. Phys.*, **10**, 4611-4624, 2010 doi:10.5194/acp-10-4611-2010.
- Martin, L.R. and T.W. Good. 1991. Catalyzed oxidation of sulfur dioxide in solution: The ironmanganese synergism. *Atmos. Environ. Part A. General Topics.*, **25**, 2395-2399.
- May, A.A., A.A. Presto, C.J. Hennigan, N.T. Nguyen, T.D. Gordon, A.L. Robinson. 2013a. Gas-particle partitioning of primary organic aerosol emissions: (1) Gasoline vehicle exhaust. *Atmos. Environ.*, **77**, 128-139.
- May, A.A., A.A. Presto, C.J. Hennigan, N.T. Nguyen, T.D. Gordon, A.L. Robinson. 2013b. Gas-Particle Partitioning of Primary Organic Aerosol Emissions: (2) Diesel Vehicles. *Environ. Sci. Technol.*, **47**, 8288-8296.
- May, A.A., E.J.T. Levin, C.J. Hennigan, I. Riipinen, T. Lee, J.L. Collett Jr., J.L. Jimenez, S.M. Kreidenweis, A.L. Robinson. 2013c. Gas-particle partitioning of primary organic aerosol emissions: 3. Biomass burning. *J. Geophys. Res.*, **118**, 11327-11338.
- Moore, R. and Tokarczyk, R. 1993. Volatile Biogenic Halocarbons in the Northwest Atlantic. *Global Biogeochem. Cy.*, **7**, 195-210,

- Moore, R. and Zafiriou, O. 1994. Photochemical production of methyl iodide in seawater. *J. Geophys. Res.*, **99**, 16415–16420, doi:10.1029/94JD00786.
- Morris, R.E., S. Lau, and G. Yarwood. 2003. Development and Application of an Advanced Air Toxics Hybrid Photochemical Grid Modeling System. Presented at 96th Annual Conference and Exhibition of the A&WMA, San Diego, California (June 2003).
- Munthe, J. 1992. The aqueous oxidation of elemental mercury by ozone. *Atmos. Environ., Part A*, **26**, 1461-1468.
- Murphy, B.N., S.N. Pandis. 2009. Simulating the Formation of Semivolatile Primary and Secondary Organic Aerosol in a Regional Chemical Transport Model. *Environ. Sci. Technol.*, **43**, 4722-4728.
- NASA. 1997. Chemical Kinetics and Photochemical Data for Use in Stratospheric Modeling, *JPL Publication 97-4*. Jet Propulsion Laboratory, California Institute of Technology, Pasadena, California. January 15.
- NCAR. 2011. The Tropospheric Visible and Ultraviolet (TUV) Radiation Model web page. National Center for Atmospheric Research, Atmospheric Chemistry Division, Boulder, Colorado, <http://cprm.acd.ucar.edu/Models/TUV/index.shtml>.
- Nenes, A, C. Pilinis, and S.N. Pandis. 1998. ISORROPIA: A New Thermodynamic Model for Multiphase Multicomponent Inorganic Aerosols. *Aquatic Geochemistry*, **4**, 123-152.
- Nenes, A., C. Pilinis, and S.N. Pandis. 1999. Continued Development and Testing of a New Thermodynamic Aerosol Module for Urban and Regional Air Quality Models. *Atmos. Environ.* **33**, 1553-1560.
- Odman, M. T. and Ingram, C. L. 1993. Multiscale Air Quality Simulation Platform (MAQSIP): Source Code Documentation and Validation. Technical report, 83 pp., ENV-96TR002, MCNC–North Carolina Supercomputing Center, Research Triangle Park, North Carolina, 1996.
- Ordóñez, C., J.-F. Lamarque, S. Tilmes, D.E. Kinnison, E.L. Atlas, D.R. Blake, G. Sousa Santos, G. Brasseur, and A. Saiz-Lopez. 2012. Bromine and iodine chemistry in a global chemistry-climate model: description and evaluation of very short-lived oceanic sources. *Atmos. Chem. Phys.*, **12**, 1423-1447, doi:10.5194/acp-12-1423-2012.
- Ortiz-Montalvo, D.L., Y.B. Lim, M.J. Perri, S.P. Seitzinger, B.J. Turpin. 2012. Volatility and Yield of Glycolaldehyde SOA Formed through Aqueous Photochemistry and Droplet Evaporation. *Aerosol Sci. Technol.*, **46**, 1002-1014.
- Pal, B., and P.A. Ariya. 2003. Atmospheric reactions of gaseous mercury with ozone and hydroxyl radical: kinetics and product studies. *J. Phys.*, **107**, 189–192.
- Pal, B. and P.A. Ariya. 2004. Gas-phase HO₂-initiated reactions of elemental mercury: Kinetics, product studies and atmospheric implications. *Environ. Sci. Technol.*, **38**, 5555-5566.
- Pandis, S.N., A.S. Wexler, and J.H. Seinfeld. 1993. Secondary organic aerosol formation and transport, II, Predicting the ambient secondary organic aerosol size distribution. *Atmos. Environ.*, **27A**, 2403-2416.

- Parrella, J. P., D.J. Jacob, Q. Liang, Y. Zhang, L. J. Mickley, B. Miller, M. J. Evans et al. 2012. Tropospheric bromine chemistry: implications for present and pre-industrial ozone and mercury. *Atmos. Chem. Phys.*, **12**, no. 15: 6723-6740.
- Paulot, F., J.D. Crouse, H.G. Kjaergaard, J.H. Kroll, J.H. Seinfeld, P.O. Wennberg. 2009a. Isoprene photooxidation: new insights into the production of acids and organic nitrates. *Atmos. Chem. Phys.*, **9**, 1479-1501.
- Paulot, F., J.D. Crouse, H.G. Kjaergaard, A. Kurten, J.M. St.Clair, J.H. Seinfeld, P.O. Wennberg. 2009b. Unexpected Epoxide Formation in the Gas-Phase Photooxidation of Isoprene. *Science*, **325**, 730-733.
- Peeters, J., Nguyen, T.L., Vereecken, L. 2009. HOx radical regeneration in the oxidation of isoprene. *Phys. Chem. and Chem. Phys.*, **11**, 5935-5939
- Pehkonen, S.O. and C.J. Lin. 1998. Aqueous photochemistry of divalent mercury with organic acids. *J. Air Waste Manage. Assoc.*, **48**, 144-150.
- Perring, A.E., S.E. Pusede, R.C. Cohen. 2013. An observational perspective on the atmospheric impacts of alkyl and multifunctional nitrates on ozone and secondary organic aerosol. *Chemical Reviews*, **113**(8), 5848-5870.
- Pleim, J. 2007. A combined local and nonlocal closure model for the atmospheric boundary layer. Part I: Model description and testing. *J. Appl. Met. and Clim.*, **46**, 1383-1395.
- Prados-Roman, C., C.A. Cuevas, R.P. Fernandez, D.E. Kinnison, J.F. Lamarque, A. Saiz-Lopez. 2015. A negative feedback between anthropogenic ozone pollution and enhanced ocean emissions of iodine. *Atmospheric Chemistry and Physics*, **15**(4), 2215-2224.
- Radhakrishnan, K. and A.C. Hindmarsh. 1993. *Description and Use of LSODE, the Livermore Solver for Ordinary Differential Equations*. NASA reference Publication 1327. Lawrence Livermore National Laboratory, Livermore, CA.
- Ranjan, M., A.A. Presto, A.A. May, A.L. Robinson. 2012. Temperature Dependence of Gas-Particle Partitioning of Primary Organic Aerosol Emissions from a Small Diesel Engine. *Aerosol Sci. Technol.*, **46**, 13-21.
- Raouf, F. and P.A. Ariya. 2003. Reactions of BrO with mercury: kinetic studies. *J. Phys. IV*, **107**, 1119-1121.
- Robinson, A.L., N.M. Donahue, M.K. Shrivastava, E.A. Weitkamp, A.M. Sage, A.P. Grieshop, T.E. Lane, J.R. Pierce, S.N. Pandis. 2007. Rethinking organic aerosols: semivolatile emissions and photochemical aging. *Science*, **315**, 1259-1262.
- Rollins, A.W., Pusede, S., Wooldridge, P., Min, K.-E., Gentner, D.R., Goldstein, A.H., Liu, S., Day, D.A., Russell, L.M., Rubitschun, C.L., Surratt, J.D., Cohen, R.C. 2013. Gas/particle partitioning of total alkyl nitrates observed with TD-LIF in Bakersfield. *J. Geophys. Res. Atmos.*, **118**, 6651-6662, doi:10.1002/jgrd.50522.
- Russell, L.M., S.N. Pandis, and J.H. Seinfeld. 1994. Aerosol production and growth in the marine boundary layer. *J. Geophys. Res.*, **99**, 20989-21003.

- Rutter, A.P., and J.J. Schauer. 2007a. The effect of temperature on the gas-particle partitioning of reactive mercury in atmospheric aerosols. *Atmos. Environ.*, **41**, 8647-8657.
- Rutter, A.P.; Schauer, J.J. 2007b. The impact of aerosol composition on the particle to gas partitioning of reactive mercury. *Environ. Sci. Technol.*, **41**, 3934-3939.
- Ryaboshapko, A., R. Bullock, R. Ebinghaus, I. Ilyin, K. Lohman, J. Munthe, G. Petersen, C. Seigneur and I. Wängberg. 2002. Comparison of mercury chemistry models. *Atmos. Environ.*, **36**, 3881-3898.
- Sander, S.P., R.R. Friedl, D.M. Golden, M.J. Kurylo, R.E. Huie, V.L. Orkin, G.K. Moortgat, P.H. Wine, A.R. Ravishankara, C.E. Kolb, M.J. Molina, B.J. Finlayson-Pitts. 2006. Evaluation number 15: Chemical kinetics and photochemical data for use in atmospheric studies. NASA Panel for Data Evaluation, JPL Publication 06-2, Jet Propulsion Laboratory, California Institute of Technology, Pasadena, California.
- Sanemasa, I. 1975. The solubility of elemental mercury vapor in water. *Bull. Chem. Soc. Jpn.*, **48**, 1795-1798.
- Saunders, S.M., M.E. Jenkin, R.G. Derwent, M.J. Pilling. 2003. Protocol for the development of the Master Chemical Mechanism, MCM v3 (Part A): tropospheric degradation of non-aromatic volatile organic compounds. *Atmospheric Chemistry and Physics*, 3(1), 161-180.
- Sauter, D.P. and P.K. Wang. 1989. An experimental study of the scavenging of aerosol particles by natural snow crystals. *J. Atmos. Sci.*, **46**, 1650-1655.
- Schroeder, W.H. and J. Munthe. 1998. Atmospheric mercury – An overview. *Atmos. Environ.*, **32**, 809-822.
- Scott, B.C. 1978. Parameterization of sulfate removal by precipitation. *J. Appl. Meteor.*, **17**, 1375-1389.
- Sehmel, G.A. 1980. Particle and Gas Deposition, a Review. *Atmos. Environ.*, **14**, 983-1011.
- Seigneur, C., H. Abeck, G. Chia, M. Reinhard, N.S. Bloom, E. Prestbo and P. Saxena. 1998. Mercury adsorption to elemental carbon (soot) particles and atmospheric particulate matter. *Atmos. Environ.*, **32**, 2649-2657.
- Seigneur, C., P. Karamchandani, K. Lohman, K. Vijayaraghavan and R.-L. Shia. 2001a. Multiscale modeling of the atmospheric fate and transport of mercury. *J. Geophys. Res.*, **106**, 27795-27809.
- Seigneur, C., P. Karamchandani, K. Lohman and J. Jansen. 2001b. Modeling of mercury in power plant plumes. *6th International Conference on Mercury as a Global Pollutant*, 15-19 October 2001, Minamata, Japan.
- Seigneur, C., P. Karamchandani, K. Vijayaraghavan, K. Lohman and G. Yelluru. 2003. *Scoping Study for Mercury Deposition in the Upper Midwest*. AER Report CP149-03-01a, prepared for the Midwest Regional Planning Organization, Des Plaines, IL.

- Seigneur, C., K. Vijayaraghavan, K. Lohman and P. Karamchandani. 2004. Modeling the atmospheric fate and transport of mercury over North America. *Fuel Processing Technol.*, **85**, 441-450.
- Seigneur, C. and K. Lohman. 2008. Effect of bromine chemistry on the atmospheric mercury cycle. *J. Geophys. Res.*, **113**, D23309, doi:10.1029/2008JD010262.
- Seinfeld, J.H., and S.N. Pandis. 1998. *Atmospheric Chemistry and Physics, From Air Pollution to Climate Change*. John Wiley and Sons, Inc., NY.
- Sillen, G.L. and A.E. Martell, (Eds.). 1964. Stability constants of metal ion complexes, *Spec. Publ. Chem. Soc.*, **17**, 754.
- Sillman, S. 1995. The Use of NO_y, H₂O₂, and HNO₃ as Indicators for Ozone - NO_x-Hydrocarbon Sensitivity in Urban Locations. *J. Geophys. Res.*, **100**, 14,175-14,188.
- Slinn, S.A. and W.G.N. Slinn. 1980. Predictions for particle deposition on natural waters. *Atmos. Environ.*, **24**, 1013-1016.
- Slinn, W.G.N. 1982. Predictions for particle deposition to vegetative surfaces. *Atmos. Environ.*, **16**, 1785-1794.
- Smagorinsky, J. 1963. General Circulation Experiments with the Primitive Equations: I. The Basic Experiment. *Mon. Wea. Rev.*, **91**, 99-164.
- Smoydzin, L., and R. von Glasow. 2009. Modelling chemistry over the Dead Sea: bromine and ozone chemistry. *Atmospheric Chemistry and Physics*, **9**(14), 5057-5072.
- Sommar, J., K. Gårdfeldt, D. Strömberg and X. Feng. 2001. A kinetic study of the gas-phase reaction between the hydroxyl radical and atomic mercury. *Atmos. Environ.*, **35**, 3049-3054.
- Strader, R., F. Lurmann, and S.N. Pandis. 1999. Evaluation of secondary organic aerosol formation in winter. *Atmos. Environ.*, **33**, 4849-4863.
- Takemura, T., T. Nakajima, O. Dubovik, B.N. Holben, S. Kinne. 2002. Single-scattering albedo and radiative forcing of various aerosol species with a global three-dimensional model. *J. Climate*, **15**(4), 333-352.
- Tanaka, P.L., D. T. Allen, E. C. McDonald-Buller, S. Chang, Y. Kimura, C.B. Mullins, G. Yarwood, and J.D. Neece. 2003. Development of a chlorine mechanism for use in the carbon bond IV chemistry model. *J. Geophys. Res.: Atmos.*, **108**(D4), 1984-2012.
- Tokos, J.J.S., B. Hall, J.A. Calhoun, and E.M. Prestbo. 1998. Homogeneous gas-phase reaction of Hg⁰ with H₂O₂, O₃, CH₃I, and (CH₃)₂S: Implications for atmospheric Hg cycling. *Atmos. Environ.*, **32**, 823-827.
- Tonnesen, G.S. and R.L. Dennis. 2000. Analysis of radical propagation efficiency to assess ozone sensitivity to hydrocarbons and NO_x. Part 1: Local indicators of odd oxygen production sensitivity. *J. Geophys. Res.*, **105**, 9213-9225.
- Turner, D.B., T. Chico, and A. Catalano. 1986. TUPOS: A Multiple Source Gaussian Dispersion Algorithm Using On-Site Turbulence Data. U.S Environmental Protection Agency, Research Triangle Park, North Carolina (EPA-600/8-86/010).

- Turner, D.B. and R.H. Schulze. 2007. *Practical Guide to Atmospheric Dispersion Modeling*. Air and Waste Management Association.
- van Loon, L., E. Mader, and S.L. Scott. 2000. Reduction of the aqueous mercuric ion by sulfite: UV spectrum of HgSO₃ and its intramolecular redox reactions. *J. Phys. Chem.*, **104**, 1621-1626.
- van Loon, L.L., E.A. Mader, and S.L. Scott. 2001. Sulfite stabilization and reduction of the aqueous mercuric ion: kinetic determination of sequential formation constants. *J. Phys. Chem.*, **105**, 3190-3195.
- Vijayaraghavan, K., P. Karamchandani, C. Seigneur, R. Balmori, and S.-Y. Chen. 2008. Plume-in-grid modeling of atmospheric mercury. *J. Geophys. Res.*, **113**, D24305, doi:10.1029/2008JD010580.
- Vogt, R., R. Sander, R. von Glasow, and P.J. Crutzen. 1999. Iodine chemistry and its role in halogen activation and ozone loss in the marine boundary layer: A model study. *J. Atmos. Chem.*, **32**(3), 375-395.
- Voulgarakis, A., N.H. Savage, O. Wild, G.D. Carver, K.C. Clemitshaw, J.A. Pyle. 2009. Upgrading photolysis in the p-TOMCAT CTM: model evaluation and assessment of the role of clouds. *Geo. Mod. Devel.*, **2**, 59-72.
- Wang, Z., J. E. Langstaff, and H.E. Jeffries. 1995. The Application of the Integrated Process Rate Analysis Method for Investigation of Urban Airshed Model (UAM) Sensitivity to Speciation in VOC Emissions Data. Air & Waste Management Association annual meeting, San Antonio, TX.
- Wang, Z., and X. Zeng. 2010. Evaluation of snow albedo in land models for weather and climate studies. *J. Appl. Met Clim.*, **49**, doi: 10.1175/2009JAMC2134.1.
- Wesely, M.L. 1989. Parameterization of Surface Resistances to Gaseous Dry Deposition in Regional-Scale Numerical Models. *Atmos. Environ.*, **23**, 1293-1304.
- Wesely, M.L., and B.B. Hicks. 2000. A review of the current status of knowledge on dry deposition. *Atmos. Environ.*, **34**, 2261.
- Whitten, G., H.P. Deuel, C.S. Burton, and J.L. Haney. 1996. "Overview of the Implementation of an Updated Isoprene Chemistry Mechanism in CB4/UAM-V." (Revised Memorandum to OTAG Participants, July 22).
- Whitten, G.Z., and G. Yarwood. 2008. The Ozone Productivity of n-Propyl Bromide: Part 2—An Exception to the Maximum Incremental Reactivity Scale. *J. Air Waste Manag. Assoc.*, **58**(7), 891-901.
- Whitten, G.Z., G. Heo, Y. Kimura, E. McDonald-Buller, D.T. Allen, W.P.I. Carter, G. Yarwood. 2010. A New Condensed Toluene Mechanism for Carbon Bond: CB05-TU. *Atmos. Environ.*, **44**(40), doi: 10.1016/j.atmosenv.2009.12.029.
- Woody, M.C., Baker, K.R., Hayes, P.L., Jimenez, J.L., Koo, B., Pye, H.O.T. 2016. Understanding sources of organic aerosol during CalNex-2010 using the CMAQ-VBS. *Atmos. Chem. Phys.*, **16**, 4081-4100 (doi:10.5194/acp-16-4081-2016).

- Yamartino, R. 2000. Refinement of Horizontal Diffusion in Photochemical Grid Models. Presented at the American Meteorological Society 11th Joint Conference on the Applications of Air Pollution Meteorology with the Air and Waste Management Association, Long Beach, CA, January 9-13.
- Yang, X., R.A. Cox, N.J. Warwick, J.A. Pyle, G.D. Carver, F.M. O'Connor, and N.H. Savage. 2005. Tropospheric bromine chemistry and its impacts on ozone: A model study. *J. Geophys. Res.: Atmos.*, **110**(D23), DOI: 10.1029/2005JD006244.
- Yarwood, G., R.E. Morris, M.A. Yocke, H. Hogo and T. Chico. 1996a. Development of a Methodology for Source Apportionment of Ozone Concentration Estimates from a Photochemical Grid Model. Presented at the 89th AWMA Annual Meeting, Nashville TN, June 23-28.
- Yarwood, G., T.E. Stoeckenius, G. Wilson, R.E. Morris, and M.A. Yocke. 1996b. Development of a Methodology to Assess Geographic and Temporal Ozone Control Strategies for the South Coast Air Basin. Prepared for South Coast Air Quality Management District, Diamond Bar, CA.
- Yarwood, G., R.E. Morris, G.M. Wilson. 2004. Particulate Matter Source Apportionment Technology (PSAT) in the CAMx Photochemical Grid Model. Proceedings of the 27th NATO/ CCMS International Technical Meeting on Air Pollution Modeling and Application. Springer Verlag (Available from http://camx.com/publ/pdfs/yarwood_itm_paper.pdf).
- Yarwood, G., G.Z. Whitten, and S. Rao. 2005a. Updates to the Carbon Bond 4 Photochemical Mechanism. Prepared for the Lake Michigan Air Directors Consortium, Des Plaines, Illinois.
- Yarwood, G., S. Rao, M. Yocke, and G.Z. Whitten. 2005b. Updates to the Carbon Bond chemical mechanism: CB05. Final Report prepared for US EPA. Available at http://www.camx.com/publ/pdfs/CB05_Final_Report_120805.pdf.
- Yarwood, G., J. Jung, G. Z. Whitten, G. Heo, J. Mellberg and E. Estes. 2010. Updates to the Carbon Bond Mechanism for Version 6 (CB6). Presented at the 9th Annual CMAS Conference, Chapel Hill, October.
- Yarwood, G., H. Gookyoung, W.P.L. Carter, G.Z. Whitten. 2012a. Environmental Chamber Experiments to Evaluate NOx Sinks and Recycling in Atmospheric Chemical Mechanisms. Final Report prepared for the Texas Air Quality Research Program, University of Texas, Austin, Texas (AQRP Project 10-042, February 2012).
- Yarwood, G., J. Jung, U. Nopmongcol, C. Emery. 2012b. Improving CAMx Performance in Simulating Ozone Transport from the Gulf of Mexico. Final Report prepared for the Texas Commission on Environmental Quality, Austin, Texas (September 2012). Prepared by ENVIRON International Corporation, Novato, CA.
- Yarwood, G., T. Sakulyanontvittaya, U. Nopmongcol, B. Koo. 2014. Ozone Depletion by Bromine and Iodine over the Gulf of Mexico. Final Report prepared for the Texas Commission on Environmental Quality, Austin, Texas (November 2014). Prepared by ENVIRON International Corporation, Novato, CA.

- Yarwood, G. and B. Koo. 2015. Improved OSAT, APCA and PSAT Algorithms for CAMx. Final report prepared for the Texas Commission on Environmental Quality, Austin, Texas (August, 2015). Prepared by Ramboll Environ, Novato, CA.
- Yeh, G.K. and P.J. Ziemann. 2014. Alkyl Nitrate Formation from the Reactions of C8–C14 n-Alkanes with OH Radicals in the Presence of NOx: Measured Yields with Essential Corrections for Gas–Wall Partitioning. *J. Phys. Chem.*, **118**(38), 8797-8806.
- Zhang, L., S. Gong, J. Padro, L. Barrie. 2001. A size-segregated particle dry deposition scheme for an atmospheric aerosol module. *Atmos. Environ.*, **35**, 549-560.
- Zhang, L., J. R. Brook, and R. Vet. 2003. A revised parameterization for gaseous dry deposition in air-quality models. *Atmos. Chem. Phys.*, **3**, 2067–2082.
- Zhang, X., S. Kondragunta, C. Schmidt, and F. Kogan. 2008. Near real time monitoring of biomass burning particulate emissions (PM2.5) across contiguous United States using multiple satellite instruments. *Atmospheric Environment*, **42**, 6959-6972.
- Zhang, X., C.D. Cappa, S.H. Jathar, R.C. McVay, J.J. Ensberg, M.J. Kleeman, J.H. Seinfeld. 2014. Influence of vapor wall loss in laboratory chambers on yields of secondary organic aerosol. *P. Natl. Acad. Sci.*, **111**, 5802–5807.
- Zheng, B., Q. Zhang, Y. Zhang, Y., K.B. He, K. Wang, G.J. Zheng, F.K. Duan, Y.L. Ma, T. Kimoto. 2015. Heterogeneous chemistry: a mechanism missing in current models to explain secondary inorganic aerosol formation during the January 2013 haze episode in North China. *Atmos. Chem. Phys.*, **15**, 2031-2049.

Appendix A

CAMx Mechanism 2: CB6r2 Gas-Phase Chemistry

Table A-1. Reactions and rate constant expressions for the CB6r2 mechanism. k_{298} is the rate constant at 298 K and 1 atmosphere using units in molecules/cm³ and 1/s. For photolysis reactions k_{298} shows the photolysis rate at a solar zenith angle of 60° and height of 600 m MSL/AGL. See Table 5-2 for species names. See Section 3.1 on temperature and pressure dependencies.

Number	Reactants and Products	Rate Constant Expression	k_{298}
1	NO ₂ = NO + O	Photolysis	6.30E-3
2	O + O ₂ + M = O ₃ + M	$k = 5.68E-34 (T/300)^{-2.6}$	5.78E-34
3	O ₃ + NO = NO ₂	$k = 1.40E-12 \exp(-1310/T)$	1.73E-14
4	O + NO + M = NO ₂ + M	$k = 1.00E-31 (T/300)^{-1.6}$	1.01E-31
5	O + NO ₂ = NO	$k = 5.50E-12 \exp(188/T)$	1.03E-11
6	O + NO ₂ = NO ₃	Falloff: F=0.6; n=1 $k(0) = 1.30E-31 (T/300)^{-1.5}$ $k(\text{inf}) = 2.30E-11 (T/300)^{0.24}$	2.11E-12
7	O + O ₃ =	$k = 8.00E-12 \exp(-2060/T)$	7.96E-15
8	O ₃ = O	Photolysis	3.33E-4
9	O ₃ = O ₁ D	Photolysis	8.78E-6
10	O ₁ D + M = O + M	$k = 2.23E-11 \exp(115/T)$	3.28E-11
11	O ₁ D + H ₂ O = 2 OH	$k = 2.14E-10$	2.14E-10
12	O ₃ + OH = HO ₂	$k = 1.70E-12 \exp(-940/T)$	7.25E-14
13	O ₃ + HO ₂ = OH	$k = 2.03E-16 (T/300)^{4.57} \exp(693/T)$	2.01E-15
14	OH + O = HO ₂	$k = 2.40E-11 \exp(110/T)$	3.47E-11
15	HO ₂ + O = OH	$k = 2.70E-11 \exp(224/T)$	5.73E-11
16	OH + OH = O	$k = 6.20E-14 (T/298)^{2.6} \exp(945/T)$	1.48E-12
17	OH + OH = H ₂ O ₂	Falloff: F=0.5; n=1.13 $k(0) = 6.90E-31 (T/300)^{-0.8}$ $k(\text{inf}) = 2.60E-11$	5.25E-12
18	OH + HO ₂ =	$k = 4.80E-11 \exp(250/T)$	1.11E-10
19	HO ₂ + HO ₂ = H ₂ O ₂	$k = k_1 + k_2 [M]$ $k_1 = 2.20E-13 \exp(600/T)$ $k_2 = 1.90E-33 \exp(980/T)$	2.90E-12
20	HO ₂ + HO ₂ + H ₂ O = H ₂ O ₂	$k = k_1 + k_2 [M]$ $k_1 = 3.08E-34 \exp(2800/T)$ $k_2 = 2.66E-54 \exp(3180/T)$	6.53E-30
21	H ₂ O ₂ = 2 OH	Photolysis	3.78E-6
22	H ₂ O ₂ + OH = HO ₂	$k = 2.90E-12 \exp(-160/T)$	1.70E-12
23	H ₂ O ₂ + O = OH + HO ₂	$k = 1.40E-12 \exp(-2000/T)$	1.70E-15
24	NO + NO + O ₂ = 2 NO ₂	$k = 3.30E-39 \exp(530/T)$	1.95E-38
25	HO ₂ + NO = OH + NO ₂	$k = 3.45E-12 \exp(270/T)$	8.54E-12
26	NO ₂ + O ₃ = NO ₃	$k = 1.40E-13 \exp(-2470/T)$	3.52E-17
27	NO ₃ = NO ₂ + O	Photolysis	1.56E-1
28	NO ₃ = NO	Photolysis	1.98E-2
29	NO ₃ + NO = 2 NO ₂	$k = 1.80E-11 \exp(110/T)$	2.60E-11
30	NO ₃ + NO ₂ = NO + NO ₂	$k = 4.50E-14 \exp(-1260/T)$	6.56E-16
31	NO ₃ + O = NO ₂	$k = 1.70E-11$	1.70E-11
32	NO ₃ + OH = HO ₂ + NO ₂	$k = 2.00E-11$	2.00E-11

Number	Reactants and Products	Rate Constant Expression	k ₂₉₈
33	NO ₃ + HO ₂ = OH + NO ₂	k = 4.00E-12	4.00E-12
34	NO ₃ + O ₃ = NO ₂	k = 1.00E-17	1.00E-17
35	NO ₃ + NO ₃ = 2 NO ₂	k = 8.50E-13 exp(-2450/T)	2.28E-16
36	NO ₃ + NO ₂ = N ₂ O ₅	Falloff: F=0.35; n=1.33 k(0) = 3.60E-30 (T/300) ^{-4.1} k(inf) = 1.90E-12 (T/300) ^{0.2}	1.24E-12
37	N ₂ O ₅ = NO ₃ + NO ₂	Falloff: F=0.35; n=1.33 k(0) = 1.30E-3 (T/300) ^{-3.5} exp(-11000/T) k(inf) = 9.70E+14 (T/300) ^{0.1} exp(-11080/T)	4.46E-2
38	N ₂ O ₅ = NO ₂ + NO ₃	Photolysis	2.52E-5
39	N ₂ O ₅ + H ₂ O = 2 HNO ₃	k = 1.00E-22	1.00E-22
40	NO + OH = HONO	Falloff: F=0.81; n=0.87 k(0) = 7.40E-31 (T/300) ^{-2.4} k(inf) = 3.30E-11 (T/300) ^{-0.3}	9.77E-12
41	NO + NO ₂ + H ₂ O = 2 HONO	k = 5.00E-40	5.00E-40
42	HONO + HONO = NO + NO ₂	k = 1.00E-20	1.00E-20
43	HONO = NO + OH	Photolysis	1.04E-3
44	HONO + OH = NO ₂	k = 2.50E-12 exp(260/T)	5.98E-12
45	NO ₂ + OH = HNO ₃	Falloff: F=0.6; n=1 k(0) = 1.80E-30 (T/300) ⁻³ k(inf) = 2.80E-11	1.06E-11
46	HNO ₃ + OH = NO ₃	k = k ₁ + k ₃ [M] / (1 + k ₃ [M] / k ₂) k ₁ = 2.40E-14 exp(460/T) k ₂ = 2.70E-17 exp(2199/T) k ₃ = 6.50E-34 exp(1335/T)	1.54E-13
47	HNO ₃ = OH + NO ₂	Photolysis	2.54E-7
48	HO ₂ + NO ₂ = PNA	Falloff: F=0.6; n=1 k(0) = 1.80E-31 (T/300) ^{-3.2} k(inf) = 4.70E-12	1.38E-12
49	PNA = HO ₂ + NO ₂	Falloff: F=0.6; n=1 k(0) = 4.10E-5 exp(-10650/T) k(inf) = 4.80E+15 exp(-11170/T)	8.31E-2
50	PNA = 0.59 HO ₂ + 0.59 NO ₂ + 0.41 OH + 0.41 NO ₃	Photolysis	2.36E-6
51	PNA + OH = NO ₂	k = 3.20E-13 exp(690/T)	3.24E-12
52	SO ₂ + OH = SULF + HO ₂	Falloff: F=0.53; n=1.1 k(0) = 4.50E-31 (T/300) ^{-3.9} k(inf) = 1.30E-12 (T/300) ^{-0.7}	8.12E-13
53	C ₂ O ₃ + NO = NO ₂ + MEO ₂ + RO ₂	k = 7.50E-12 exp(290/T)	1.98E-11
54	C ₂ O ₃ + NO ₂ = PAN	Falloff: F=0.3; n=1.41 k(0) = 2.70E-28 (T/300) ^{-7.1} k(inf) = 1.20E-11 (T/300) ^{-0.9}	9.40E-12
55	PAN = NO ₂ + C ₂ O ₃	Falloff: F=0.3; n=1.41 k(0) = 4.90E-3 exp(-12100/T) k(inf) = 5.40E+16 exp(-13830/T)	2.98E-4
56	PAN = 0.6 NO ₂ + 0.6 C ₂ O ₃ + 0.4 NO ₃ + 0.4 MEO ₂ + 0.4 RO ₂	Photolysis	3.47E-7

Number	Reactants and Products	Rate Constant Expression	k ₂₉₈
57	C2O3 + HO2 = 0.41 PACD + 0.15 AACD + 0.15 O3 + 0.44 MEO2 + 0.44 RO2 + 0.44 OH	k = 5.20E-13 exp(980/T)	1.39E-11
58	C2O3 + RO2 = C2O3	k = 8.90E-13 exp(800/T)	1.30E-11
59	C2O3 + C2O3 = 2 MEO2 + 2 RO2	k = 2.90E-12 exp(500/T)	1.55E-11
60	C2O3 + CXO3 = MEO2 + ALD2 + XO2H + 2 RO2	k = 2.90E-12 exp(500/T)	1.55E-11
61	CXO3 + NO = NO2 + ALD2 + XO2H + RO2	k = 6.70E-12 exp(340/T)	2.10E-11
62	CXO3 + NO2 = PANX	k = k(ref) K k(ref) = k(54) K = 1.00E+0	9.40E-12
63	PANX = NO2 + CXO3	k = k(ref) K k(ref) = k(55) K = 1.00E+0	2.98E-4
64	PANX = 0.6 NO2 + 0.6 CXO3 + 0.4 NO3 + 0.4 ALD2 + 0.4 XO2H + 0.4 RO2	Photolysis	3.47E-7
65	CXO3 + HO2 = 0.41 PACD + 0.15 AACD + 0.15 O3 + 0.44 ALD2 + 0.44 XO2H + 0.44 RO2 + 0.44 OH	k = 5.20E-13 exp(980/T)	1.39E-11
66	CXO3 + RO2 = 0.8 ALD2 + 0.8 XO2H + 0.8 RO2	k = 8.90E-13 exp(800/T)	1.30E-11
67	CXO3 + CXO3 = 2 ALD2 + 2 XO2H + 2 RO2	k = 3.20E-12 exp(500/T)	1.71E-11
68	RO2 + NO = NO	k = 2.40E-12 exp(360/T)	8.03E-12
69	RO2 + HO2 = HO2	k = 4.80E-13 exp(800/T)	7.03E-12
70	RO2 + RO2 =	k = 6.50E-14 exp(500/T)	3.48E-13
71	MEO2 + NO = FORM + HO2 + NO2	k = 2.30E-12 exp(360/T)	7.70E-12
72	MEO2 + HO2 = 0.9 MEPX + 0.1 FORM	k = 3.80E-13 exp(780/T)	5.21E-12
73	MEO2 + C2O3 = FORM + 0.9 HO2 + 0.9 MEO2 + 0.1 AACD + 0.9 RO2	k = 2.00E-12 exp(500/T)	1.07E-11
74	MEO2 + RO2 = 0.685 FORM + 0.315 MEOH + 0.37 HO2 + RO2	k = k(ref) K k(ref) = k(70) K = 1.00E+0	3.48E-13
75	XO2H + NO = NO2 + HO2	k = 2.70E-12 exp(360/T)	9.04E-12
76	XO2H + HO2 = ROOH	k = 6.80E-13 exp(800/T)	9.96E-12
77	XO2H + C2O3 = 0.8 HO2 + 0.8 MEO2 + 0.2 AACD + 0.8 RO2	k = k(ref) K k(ref) = k(58) K = 1.00E+0	1.30E-11
78	XO2H + RO2 = 0.6 HO2 + RO2	k = k(ref) K k(ref) = k(70) K = 1.00E+0	3.48E-13
79	XO2 + NO = NO2	k = k(ref) K k(ref) = k(75) K = 1.00E+0	9.04E-12
80	XO2 + HO2 = ROOH	k = k(ref) K k(ref) = k(76) K = 1.00E+0	9.96E-12
81	XO2 + C2O3 = 0.8 MEO2 + 0.2 AACD + 0.8 RO2	k = k(ref) K k(ref) = k(58) K = 1.00E+0	1.30E-11

Number	Reactants and Products	Rate Constant Expression	k ₂₉₈
82	XO2 + RO2 = RO2	k = k(ref) K k(ref) = k(70) K = 1.00E+0	3.48E-13
83	XO2N + NO = 0.5 NTR1 + 0.5 NTR2	k = k(ref) K k(ref) = k(75) K = 1.00E+0	9.04E-12
84	XO2N + HO2 = ROOH	k = k(ref) K k(ref) = k(76) K = 1.00E+0	9.96E-12
85	XO2N + C2O3 = 0.8 HO2 + 0.8 MEO2 + 0.2 AACD + 0.8 RO2	k = k(ref) K k(ref) = k(58) K = 1.00E+0	1.30E-11
86	XO2N + RO2 = RO2	k = k(ref) K k(ref) = k(70) K = 1.00E+0	3.48E-13
87	MEPX + OH = 0.6 MEO2 + 0.6 RO2 + 0.4 FORM + 0.4 OH	k = 5.30E-12 exp(190/T)	1.00E-11
88	MEPX = MEO2 + RO2 + OH	Photolysis	2.68E-6
89	ROOH + OH = 0.54 XO2H + 0.06 XO2N + 0.6 RO2 + 0.4 OH	k = 5.30E-12 exp(190/T)	1.00E-11
90	ROOH = HO2 + OH	Photolysis	2.68E-6
91	NTR1 + OH = NTR2	k = 2.00E-12	2.00E-12
92	NTR1 = NO2	Photolysis	1.06E-6
93	FACD + OH = HO2	k = 4.50E-13	4.50E-13
94	AACD + OH = MEO2 + RO2	k = 4.00E-14 exp(850/T)	6.93E-13
95	PACD + OH = C2O3	k = 5.30E-12 exp(190/T)	1.00E-11
96	FORM + OH = HO2 + CO	k = 5.40E-12 exp(135/T)	8.49E-12
97	FORM = 2 HO2 + CO	Photolysis	1.78E-5
98	FORM = CO + H2	Photolysis	2.38E-5
99	FORM + O = OH + HO2 + CO	k = 3.40E-11 exp(-1600/T)	1.58E-13
100	FORM + NO3 = HNO3 + HO2 + CO	k = 5.50E-16	5.50E-16
101	FORM + HO2 = HCO3	k = 9.70E-15 exp(625/T)	7.90E-14
102	HCO3 = FORM + HO2	k = 2.40E+12 exp(-7000/T)	1.51E+2
103	HCO3 + NO = FACD + NO2 + HO2	k = 5.60E-12	5.60E-12
104	HCO3 + HO2 = 0.5 MEPX + 0.5 FACD + 0.2 OH + 0.2 HO2	k = 5.60E-15 exp(2300/T)	1.26E-11
105	ALD2 + O = C2O3 + OH	k = 1.80E-11 exp(-1100/T)	4.49E-13
106	ALD2 + OH = C2O3	k = 4.70E-12 exp(345/T)	1.50E-11
107	ALD2 + NO3 = C2O3 + HNO3	k = 1.40E-12 exp(-1860/T)	2.73E-15
108	ALD2 = MEO2 + RO2 + CO + HO2	Photolysis	1.76E-6
109	ALDX + O = CXO3 + OH	k = 1.30E-11 exp(-870/T)	7.02E-13
110	ALDX + OH = CXO3	k = 4.90E-12 exp(405/T)	1.91E-11
111	ALDX + NO3 = CXO3 + HNO3	k = 6.30E-15	6.30E-15
112	ALDX = ALD2 + XO2H + RO2 + CO + HO2	Photolysis	6.96E-6
113	GLYD + OH = 0.2 GLY + 0.2 HO2 + 0.8 C2O3	k = 8.00E-12	8.00E-12
114	GLYD = 0.74 FORM + 0.89 CO + 1.4 HO2 + 0.15 MEOH + 0.19 OH + 0.11 GLY + 0.11 XO2H + 0.11 RO2	Photolysis	1.56E-6
115	GLYD + NO3 = HNO3 + C2O3	k = 1.40E-12 exp(-1860/T)	2.73E-15

Number	Reactants and Products	Rate Constant Expression	k ₂₉₈
116	GLY + OH = 1.8 CO + 0.2 XO ₂ + 0.2 RO ₂ + HO ₂	k = 3.10E-12 exp(340/T)	9.70E-12
117	GLY = 2 HO ₂ + 2 CO	Photolysis	5.50E-5
118	GLY + NO ₃ = HNO ₃ + 1.5 CO + 0.5 XO ₂ + 0.5 RO ₂ + HO ₂	k = 1.40E-12 exp(-1860/T)	2.73E-15
119	MGLY = C ₂ O ₃ + HO ₂ + CO	Photolysis	1.46E-4
120	MGLY + NO ₃ = HNO ₃ + C ₂ O ₃ + XO ₂ + RO ₂	k = 1.40E-12 exp(-1860/T)	2.73E-15
121	MGLY + OH = C ₂ O ₃ + CO	k = 1.90E-12 exp(575/T)	1.31E-11
122	H ₂ + OH = HO ₂	k = 7.70E-12 exp(-2100/T)	6.70E-15
123	CO + OH = HO ₂	k = k ₁ + k ₂ [M] k ₁ = 1.44E-13 k ₂ = 3.43E-33	2.28E-13
124	CH ₄ + OH = MEO ₂ + RO ₂	k = 1.85E-12 exp(-1690/T)	6.37E-15
125	ETHA + OH = 0.991 ALD ₂ + 0.991 XO ₂ H + 0.009 XO ₂ N + RO ₂	k = 6.90E-12 exp(-1000/T)	2.41E-13
126	MEOH + OH = FORM + HO ₂	k = 2.85E-12 exp(-345/T)	8.95E-13
127	ETOH + OH = 0.95 ALD ₂ + 0.9 HO ₂ + 0.1 XO ₂ H + 0.1 RO ₂ + 0.078 FORM + 0.011 GLYD	k = 3.00E-12 exp(20/T)	3.21E-12
128	KET = 0.5 ALD ₂ + 0.5 C ₂ O ₃ + 0.5 XO ₂ H + 0.5 CXO ₃ + 0.5 MEO ₂ + RO ₂ - 2.5 PAR	Photolysis	2.27E-7
129	ACET = 0.38 CO + 1.38 MEO ₂ + 1.38 RO ₂ + 0.62 C ₂ O ₃	Photolysis	2.08E-7
130	ACET + OH = FORM + C ₂ O ₃ + XO ₂ + RO ₂	k = 1.41E-12 exp(-620.6/T)	1.76E-13
131	PRPA + OH = 0.71 ACET + 0.26 ALDX + 0.26 PAR + 0.97 XO ₂ H + 0.03 XO ₂ N + RO ₂	k = 7.60E-12 exp(-585/T)	1.07E-12
132	PAR + OH = 0.11 ALDX + 0.76 ROR + 0.13 XO ₂ N + 0.11 XO ₂ H + 0.76 XO ₂ + RO ₂ - 0.11 PAR	k = 8.10E-13	8.10E-13
133	ROR = 0.2 KET + 0.42 ACET + 0.74 ALD ₂ + 0.37 ALDX + 0.04 XO ₂ N + 0.94 XO ₂ H + 0.98 RO ₂ + 0.02 ROR - 2.7 PAR	k = 5.70E+12 exp(-5780/T)	2.15E+4
134	ROR + O ₂ = KET + HO ₂	k = 1.50E-14 exp(-200/T)	7.67E-15
135	ROR + NO ₂ = NTR1	k = 8.60E-12 exp(400/T)	3.29E-11
136	ETHY + OH = 0.7 GLY + 0.7 OH + 0.3 FACD + 0.3 CO + 0.3 HO ₂	Falloff: F=0.37; n=1.3 k(0) = 5.00E-30 (T/300) ^{-1.5} k(inf) = 1.00E-12	7.52E-13
137	ETH + O = FORM + HO ₂ + CO + 0.7 XO ₂ H + 0.7 RO ₂ + 0.3 OH	k = 1.04E-11 exp(-792/T)	7.29E-13
138	ETH + OH = XO ₂ H + RO ₂ + 1.56 FORM + 0.22 GLYD	Falloff: F=0.48; n=1.15 k(0) = 8.60E-29 (T/300) ^{-3.1} k(inf) = 9.00E-12 (T/300) ^{-0.85}	7.84E-12
139	ETH + O ₃ = FORM + 0.51 CO + 0.16 HO ₂ + 0.16 OH + 0.37 FACD	k = 9.10E-15 exp(-2580/T)	1.58E-18
140	ETH + NO ₃ = 0.5 NO ₂ + 0.5 NTR1 + 0.5 XO ₂ H + 0.5 XO ₂ + RO ₂ + 1.125 FORM	k = 3.30E-12 exp(-2880/T)	2.10E-16
141	OLE + O = 0.2 ALD ₂ + 0.3 ALDX + 0.1 HO ₂ + 0.2 XO ₂ H + 0.2 CO + 0.2 FORM + 0.01 XO ₂ N + 0.21 RO ₂ + 0.2 PAR + 0.1 OH	k = 1.00E-11 exp(-280/T)	3.91E-12

Number	Reactants and Products	Rate Constant Expression	k ₂₉₈
142	OLE + OH = 0.781 FORM + 0.488 ALD2 + 0.488 ALDX + 0.976 XO2H + 0.195 XO2 + 0.024 XO2N + 1.195 RO2 - 0.73 PAR	Falloff: F=0.5; n=1.13 k(0) = 8.00E-27 (T/300) ^{-3.5} k(inf) = 3.00E-11 (T/300) ⁻¹	2.86E-11
143	OLE + O3 = 0.295 ALD2 + 0.555 FORM + 0.27 ALDX + 0.15 XO2H + 0.15 RO2 + 0.334 OH + 0.08 HO2 + 0.378 CO + 0.075 GLY + 0.075 MGLY + 0.09 FACD + 0.13 AACD + 0.04 H2O2 - 0.79 PAR	k = 5.50E-15 exp(-1880/T)	1.00E-17
144	OLE + NO3 = 0.5 NO2 + 0.5 NTR1 + 0.48 XO2 + 0.48 XO2H + 0.04 XO2N + RO2 + 0.5 FORM + 0.25 ALD2 + 0.375 ALDX - 1 PAR	k = 4.60E-13 exp(-1155/T)	9.54E-15
145	IOLE + O = 1.24 ALD2 + 0.66 ALDX + 0.1 XO2H + 0.1 RO2 + 0.1 CO + 0.1 PAR	k = 2.30E-11	2.30E-11
146	IOLE + OH = 1.3 ALD2 + 0.7 ALDX + XO2H + RO2	k = 1.05E-11 exp(519/T)	5.99E-11
147	IOLE + O3 = 0.732 ALD2 + 0.442 ALDX + 0.128 FORM + 0.245 CO + 0.5 OH + 0.3 XO2H + 0.3 RO2 + 0.24 GLY + 0.06 MGLY + 0.29 PAR + 0.08 AACD + 0.08 H2O2	k = 4.70E-15 exp(-1013/T)	1.57E-16
148	IOLE + NO3 = 0.5 NO2 + 0.5 NTR1 + 0.48 XO2 + 0.48 XO2H + 0.04 XO2N + RO2 + 0.5 ALD2 + 0.625 ALDX + PAR	k = 3.70E-13	3.70E-13
149	ISOP + OH = ISO2 + RO2	k = 2.70E-11 exp(390/T)	9.99E-11
150	ISOP + O = 0.75 ISPD + 0.5 FORM + 0.25 XO2 + 0.25 RO2 + 0.25 HO2 + 0.25 CXO3 + 0.25 PAR	k = 3.00E-11	3.00E-11
151	ISO2 + NO = 0.1 INTR + 0.9 NO2 + 0.673 FORM + 0.9 ISPD + 0.818 HO2 + 0.082 XO2H + 0.082 RO2	k = 2.39E-12 exp(365/T)	8.13E-12
152	ISO2 + HO2 = 0.88 ISPX + 0.12 OH + 0.12 HO2 + 0.12 FORM + 0.12 ISPD	k = 7.43E-13 exp(700/T)	7.78E-12
153	ISO2 + C2O3 = 0.598 FORM + 1 ISPD + 0.728 HO2 + 0.072 XO2H + 0.8 MEO2 + 0.2 AACD + 0.872 RO2	k = k(ref) K k(ref) = k(58) K = 1.00E+0	1.30E-11
154	ISO2 + RO2 = 0.598 FORM + 1 ISPD + 0.728 HO2 + 0.072 XO2H + 0.072 RO2	k = k(ref) K k(ref) = k(70) K = 1.00E+0	3.48E-13
155	ISO2 = HO2 + HPLD	k = 3.30E+9 exp(-8300/T)	2.64E-3
156	ISOP + O3 = 0.6 FORM + 0.65 ISPD + 0.15 ALDX + 0.2 CXO3 + 0.35 PAR + 0.266 OH + 0.2 XO2 + 0.2 RO2 + 0.066 HO2 + 0.066 CO	k = 1.03E-14 exp(-1995/T)	1.27E-17
157	ISOP + NO3 = 0.35 NO2 + 0.65 NTR2 + 0.64 XO2H + 0.33 XO2 + 0.03 XO2N + RO2 + 0.35 FORM + 0.35 ISPD	k = 3.03E-12 exp(-448/T)	6.74E-13
158	ISPD + OH = 0.022 XO2N + 0.521 XO2 + 0.115 MGLY + 0.115 MEO2 + 0.269 GLYD + 0.269 C2O3 + 0.457 OPO3 + 0.117 PAR + 0.137 ACET + 0.137 CO + 0.137 HO2 + 0.658 RO2	k = 5.58E-12 exp(511/T)	3.10E-11

Number	Reactants and Products	Rate Constant Expression	k ₂₉₈
159	ISPD + O3 = 0.04 ALD2 + 0.231 FORM + 0.531 MGLY + 0.17 GLY + 0.17 ACET + 0.543 CO + 0.461 OH + 0.15 FACD + 0.398 HO2 + 0.143 C2O3	k = 3.88E-15 exp(-1770/T)	1.02E-17
160	ISPD + NO3 = 0.717 HNO3 + 0.142 NTR2 + 0.142 NO2 + 0.142 XO2 + 0.142 XO2H + 0.113 GLYD + 0.113 MGLY + 0.717 PAR + 0.717 CXO3 + 0.284 RO2	k = 4.10E-12 exp(-1860/T)	7.98E-15
161	ISPD = 0.76 HO2 + 0.34 XO2H + 0.16 XO2 + 0.34 MEO2 + 0.208 C2O3 + 0.26 FORM + 0.24 OLE + 0.24 PAR + 0.17 ACET + 0.128 GLYD + 0.84 RO2	Photolysis	1.60E-5
162	ISPX + OH = 0.904 EPOX + 0.933 OH + 0.067 ISO2 + 0.067 RO2 + 0.029 IOLE + 0.029 ALDX	k = 2.23E-11 exp(372/T)	7.77E-11
163	HPLD = OH + ISPD	Photolysis	4.41E-4
164	HPLD + NO3 = HNO3 + ISPD	k = 6.00E-12 exp(-1860/T)	1.17E-14
165	EPOX + OH = EPX2 + RO2	k = 5.78E-11 exp(-400/T)	1.51E-11
166	EPX2 + HO2 = 0.275 GLYD + 0.275 GLY + 0.275 MGLY + 1.125 OH + 0.825 HO2 + 0.375 FORM + 0.074 FACD + 0.251 CO + 2.175 PAR	k = 7.43E-13 exp(700/T)	7.78E-12
167	EPX2 + NO = 0.275 GLYD + 0.275 GLY + 0.275 MGLY + 0.125 OH + 0.825 HO2 + 0.375 FORM + NO2 + 0.251 CO + 2.175 PAR	k = 2.39E-12 exp(365/T)	8.13E-12
168	EPX2 + C2O3 = 0.22 GLYD + 0.22 GLY + 0.22 MGLY + 0.1 OH + 0.66 HO2 + 0.3 FORM + 0.2 CO + 1.74 PAR + 0.8 MEO2 + 0.2 AACD + 0.8 RO2	k = k(ref) K k(ref) = k(58) K = 1.00E+0	1.30E-11
169	EPX2 + RO2 = 0.275 GLYD + 0.275 GLY + 0.275 MGLY + 0.125 OH + 0.825 HO2 + 0.375 FORM + 0.251 CO + 2.175 PAR + RO2	k = k(ref) K k(ref) = k(70) K = 1.00E+0	3.48E-13
170	INTR + OH = 0.63 XO2 + 0.37 XO2H + RO2 + 0.444 NO2 + 0.185 NO3 + 0.104 INTR + 0.592 FORM + 0.331 GLYD + 0.185 FACD + 2.7 PAR + 0.098 OLE + 0.078 ALDX + 0.266 NTR2	k = 3.10E-11	3.10E-11
171	TERP + O = 0.15 ALDX + 5.12 PAR	k = 3.60E-11	3.60E-11
172	TERP + OH = 0.75 XO2H + 0.5 XO2 + 0.25 XO2N + 1.5 RO2 + 0.28 FORM + 1.66 PAR + 0.47 ALDX	k = 1.50E-11 exp(449/T)	6.77E-11
173	TERP + O3 = 0.57 OH + 0.07 XO2H + 0.69 XO2 + 0.18 XO2N + 0.94 RO2 + 0.24 FORM + 0.001 CO + 7 PAR + 0.21 ALDX + 0.39 CXO3	k = 1.20E-15 exp(-821/T)	7.63E-17
174	TERP + NO3 = 0.47 NO2 + 0.28 XO2H + 0.75 XO2 + 0.25 XO2N + 1.28 RO2 + 0.47 ALDX + 0.53 NTR2	k = 3.70E-12 exp(175/T)	6.66E-12
175	BENZ + OH = 0.53 CRES + 0.352 BZO2 + 0.352 RO2 + 0.118 OPEN + 0.118 OH + 0.53 HO2	k = 2.30E-12 exp(-190/T)	1.22E-12

Number	Reactants and Products	Rate Constant Expression	k ₂₉₈
176	BZO2 + NO = 0.918 NO2 + 0.082 NTR2 + 0.918 GLY + 0.918 OPEN + 0.918 HO2	k = 2.70E-12 exp(360/T)	9.04E-12
177	BZO2 + C2O3 = GLY + OPEN + HO2 + MEO2 + RO2	k = k(ref) K k(ref) = k(58) K = 1.00E+0	1.30E-11
178	BZO2 + HO2 =	k = 1.90E-13 exp(1300/T)	1.49E-11
179	BZO2 + RO2 = GLY + OPEN + HO2 + RO2	k = k(ref) K k(ref) = k(70) K = 1.00E+0	3.48E-13
180	TOL + OH = 0.18 CRES + 0.65 TO2 + 0.72 RO2 + 0.1 OPEN + 0.1 OH + 0.07 XO2H + 0.18 HO2	k = 1.80E-12 exp(340/T)	5.63E-12
181	TO2 + NO = 0.86 NO2 + 0.14 NTR2 + 0.417 GLY + 0.443 MGLY + 0.66 OPEN + 0.2 XOPN + 0.86 HO2	k = 2.70E-12 exp(360/T)	9.04E-12
182	TO2 + C2O3 = 0.48 GLY + 0.52 MGLY + 0.77 OPEN + 0.23 XOPN + HO2 + MEO2 + RO2	k = k(ref) K k(ref) = k(58) K = 1.00E+0	1.30E-11
183	TO2 + HO2 =	k = 1.90E-13 exp(1300/T)	1.49E-11
184	TO2 + RO2 = 0.48 GLY + 0.52 MGLY + 0.77 OPEN + 0.23 XOPN + HO2 + RO2	k = k(ref) K k(ref) = k(70) K = 1.00E+0	3.48E-13
185	XYL + OH = 0.155 CRES + 0.544 XLO2 + 0.602 RO2 + 0.244 XOPN + 0.244 OH + 0.058 XO2H + 0.155 HO2	k = 1.85E-11	1.85E-11
186	XLO2 + NO = 0.86 NO2 + 0.14 NTR2 + 0.221 GLY + 0.675 MGLY + 0.3 OPEN + 0.56 XOPN + 0.86 HO2	k = 2.70E-12 exp(360/T)	9.04E-12
187	XLO2 + HO2 =	k = 1.90E-13 exp(1300/T)	1.49E-11
188	XLO2 + C2O3 = 0.26 GLY + 0.77 MGLY + 0.35 OPEN + 0.65 XOPN + HO2 + MEO2 + RO2	k = k(ref) K k(ref) = k(58) K = 1.00E+0	1.30E-11
189	XLO2 + RO2 = 0.26 GLY + 0.77 MGLY + 0.35 OPEN + 0.65 XOPN + HO2 + RO2	k = k(ref) K k(ref) = k(70) K = 1.00E+0	3.48E-13
190	CRES + OH = 0.025 GLY + 0.025 OPEN + HO2 + 0.2 CRO + 0.732 CAT1 + 0.02 XO2N + 0.02 RO2	k = 1.70E-12 exp(950/T)	4.12E-11
191	CRES + NO3 = 0.3 CRO + HNO3 + 0.48 XO2 + 0.12 XO2H + 0.24 GLY + 0.24 MGLY + 0.48 OPO3 + 0.1 XO2N + 0.7 RO2	k = 1.40E-11	1.40E-11
192	CRO + NO2 = CRON	k = 2.10E-12	2.10E-12
193	CRO + HO2 = CRES	k = 5.50E-12	5.50E-12
194	CRON + OH = NTR2 + 0.5 CRO	k = 1.53E-12	1.53E-12
195	CRON + NO3 = NTR2 + 0.5 CRO + HNO3	k = 3.80E-12	3.80E-12
196	CRON = HONO + HO2 + FORM + OPEN	Photolysis	9.45E-5
197	XOPN = 0.4 GLY + XO2H + 0.7 HO2 + 0.7 CO + 0.3 C2O3	Photolysis	5.04E-4

Number	Reactants and Products	Rate Constant Expression	k ₂₉₈
198	XOPN + OH = MGLY + 0.4 GLY + 2 XO2H + 2 RO2	k = 9.00E-11	9.00E-11
199	XOPN + O3 = 1.2 MGLY + 0.5 OH + 0.6 C2O3 + 0.1 ALD2 + 0.5 CO + 0.3 XO2H + 0.3 RO2	k = 1.08E-16 exp(-500/T)	2.02E-17
200	XOPN + NO3 = 0.5 NO2 + 0.5 NTR2 + 0.45 XO2H + 0.45 XO2 + 0.1 XO2N + RO2 + 0.25 OPEN + 0.25 MGLY	k = 3.00E-12	3.00E-12
201	OPEN = OPO3 + HO2 + CO	Photolysis	5.04E-4
202	OPEN + OH = 0.6 OPO3 + 0.4 XO2H + 0.4 RO2 + 0.4 GLY	k = 4.40E-11	4.40E-11
203	OPEN + O3 = 1.4 GLY + 0.24 MGLY + 0.5 OH + 0.12 C2O3 + 0.08 FORM + 0.02 ALD2 + 1.98 CO + 0.56 HO2	k = 5.40E-17 exp(-500/T)	1.01E-17
204	OPEN + NO3 = OPO3 + HNO3	k = 3.80E-12	3.80E-12
205	CAT1 + OH = 0.14 FORM + 0.2 HO2 + 0.5 CRO	k = 5.00E-11	5.00E-11
206	CAT1 + NO3 = CRO + HNO3	k = 1.70E-10	1.70E-10
207	OPO3 + NO = NO2 + 0.5 GLY + 0.5 CO + 0.8 HO2 + 0.2 CXO3	k = 1.00E-11	1.00E-11
208	OPO3 + NO2 = OPAN	k = k(ref) K k(ref) = k(54) K = 1.00E+0	9.40E-12
209	OPAN = OPO3 + NO2	k = k(ref) K k(ref) = k(55) K = 1.00E+0	2.98E-4
210	OPO3 + HO2 = 0.41 PACD + 0.15 AACD + 0.15 O3 + 0.44 ALDX + 0.44 XO2H + 0.44 RO2 + 0.44 OH	k = k(ref) K k(ref) = k(57) K = 1.00E+0	1.39E-11
211	OPO3 + C2O3 = MEO2 + XO2 + ALDX + 2 RO2	k = k(ref) K k(ref) = k(59) K = 1.00E+0	1.55E-11
212	OPO3 + RO2 = 0.8 XO2H + 0.8 ALDX + 1.8 RO2 + 0.2 AACD	k = k(ref) K k(ref) = k(58) K = 1.00E+0	1.30E-11
213	OPAN + OH = 0.5 NO2 + 0.5 GLY + CO + 0.5 NTR2	k = 3.60E-11	3.60E-11
214	PANX + OH = ALD2 + NO2	k = 3.00E-12	3.00E-12
215	NTR2 = HNO3	k = 2.30E-5	2.30E-5
216	ECH4 + OH = MEO2 + RO2	k = 1.85E-12 exp(-1690/T)	6.37E-15

Appendix B

CAMx Mechanism 3: CB6r2 with Halogen Chemistry

Table B-1. Listing of the CB6r2 halogen mechanism (see Table A-1 for a complete listing of CB6r2). k_{298} is the rate constant at 298 K and 1 atmosphere using units in molecules/cm³ and 1/s. For photolysis reactions k_{298} shows the photolysis rate at a solar zenith angle of 60° and height of 600 m MSL/AGL. See Table B-2 for species names. See Section 3.1 on temperature and pressure dependencies.

Number	Reactants and Products	Rate Constant Expression	k_{298}
1	CL2 = 2 CL	Photolysis	1.56E-3
2	HOCL = CL + OH	Photolysis	1.34E-4
3	CL + O3 = CLO	$k = 2.30E-11 \exp(-200/T)$	1.18E-11
4	CLO + CLO = 0.3 CL2 + 1.4 CL	$k = 1.63E-14$	1.63E-14
5	CLO + NO = CL + NO2	$k = 6.40E-12 \exp(290/T)$	1.69E-11
6	CLO + HO2 = HOCL	$k = 2.70E-12 \exp(220/T)$	5.65E-12
7	CLO + NO2 = CLN3	Falloff: F=0.6; n=1 $k(0) = 1.80E-31 (T/300)^{-3.4}$ $k(\text{inf}) = 1.50E-11 (T/300)^{-1.9}$	2.34E-12
8	CLN3 = CLO + NO2	Falloff: F=0.6; n=1 $k(0) = 4.48E-5 (T/300)^{-1} \exp(-12530/T)$ $k(\text{inf}) = 3.71E+15 (T/300)^{3.5} \exp(-12530/T)$	3.11E-4
9	CLN3 = CLO + NO2	Photolysis	4.97E-6
10	CLN3 = CL + NO3	Photolysis	4.67E-4
11	CLN3 + H2O = HOCL + HNO3	$k = 2.50E-22$	2.50E-22
12	OH + HCL = CL	$k = 6.58E-13 (T/300)^{1.2} \exp(58/T)$	7.93E-13
13	OH + FMCL = CL + CO	$k = 3.67E-11 \exp(-1419/T)$	3.14E-13
14	FMCL = CL + CO + HO2	Photolysis	6.10E-8
15	CLO + MEO2 = CL + FORM + HO2	$k = 4.10E-13 \exp(-800/T)$	2.80E-14
16	CL + CH4 = HCL + MEO2	$k = 6.60E-12 \exp(-1240/T)$	1.03E-13
17	CL + PAR = HCL	$k = 5.00E-11$	5.00E-11
18	CL + ETHA = HCL + 0.991 ALD2 + 0.991 XO2H + 0.009 XO2N + RO2	$k = 8.30E-11 \exp(-100/T)$	5.93E-11
19	CL + PRPA = HCL + ACET + 0.97 XO2H + 0.03 XO2N + RO2	$k = 1.40E-10$	1.40E-10
20	CL + ISOP = FMCL + ISPD + 0.96 XO2H + 0.04 XO2N + RO2	$k = 4.30E-10$	4.30E-10
21	HCL + N2O5 = CLN2 + HNO3	$k = 6.00E-13$	6.00E-13
22	CLN2 = CL + NO2	Photolysis	2.86E-4
23	BR2 = 2 BR	Photolysis	2.79E-2
24	HOBR = BR + OH	Photolysis	1.51E-3
25	BR2 + OH = HOBR + BR	$k = 5.40E-11 \exp(180/T)$	9.88E-11
26	HBR + OH = BR	$k = 5.50E-12 \exp(-200/T)$	2.81E-12
27	BR + O3 = BRO	$k = 1.60E-11 \exp(780/T)$	2.19E-10
28	BR + HO2 = HBR	$k = 4.80E-12 \exp(310/T)$	1.36E-11
29	BR + NO2 = BRN2	Falloff: F=0.6; n=1 $k(0) = 4.20E-31 (T/300)^{-2.4}$ $k(\text{inf}) = 2.70E-11$	4.89E-12
30	BR + NO3 = BRO + NO2	$k = 1.60E-11$	1.60E-11
31	BRO = BR + O	Photolysis	2.05E-2
32	BRO + HO2 = HOBR	$k = 4.50E-12 \exp(460/T)$	2.11E-11

Appendix B: Mechanism 3 – CB6r2 with Halogen Chemistry

Number	Reactants and Products	Rate Constant Expression	k ₂₉₈
33	BRO + OH = BR + HO ₂	k = 1.70E-11 exp(250/T)	3.93E-11
34	BRO + BRO = 2 BR	k = 2.40E-12 exp(40/T)	2.74E-12
35	BRO + BRO = BR ₂	k = 2.80E-14 exp(860/T)	5.02E-13
36	BRO + NO = BR + NO ₂	k = 8.80E-12 exp(260/T)	2.11E-11
37	BRO + NO ₂ = BRN ₃	Falloff: F=0.6; n=1 k(0) = 5.20E-31 (T/300) ^{-3.2} k(inf) = 6.90E-12	2.81E-12
38	BRN ₂ = BR + NO ₂	Photolysis	3.21E-3
39	BRN ₃ = BR + NO ₃	Photolysis	9.76E-4
40	BRN ₃ + H ₂ O = HOBR + HNO ₃	k = 2.50E-22	2.50E-22
41	FMBR + OH = BR + CO	k = 5.00E-12	5.00E-12
42	FMBR = BR + CO + HO ₂	Photolysis	4.15E-6
43	BRO + MEO ₂ = 0.75 HOBR + 0.25 BR + FORM	k = 4.10E-13 exp(-800/T)	2.80E-14
44	BR + FORM = HBR + CO + HO ₂	k = 7.70E-11 exp(-580/T)	1.10E-11
45	BR + ALD ₂ = HBR + C ₂ O ₃	k = 1.80E-11 exp(-460/T)	3.84E-12
46	BR + OLE = FMBR + ALD ₂ + XO ₂ H - 1 PAR + RO ₂	k = 3.60E-12	3.60E-12
47	BR + ISOP = FMBR + ISPD + 0.96 XO ₂ H + 0.04 XO ₂ N + RO ₂	k = 5.00E-12	5.00E-12
48	I ₂ = 2 I	Photolysis	1.30E-1
49	HOI = I + OH	Photolysis	6.36E-2
50	I ₂ + OH = I + HOI	k = 2.10E-10	2.10E-10
51	I ₂ + NO ₃ = I + INO ₃	k = 1.50E-12	1.50E-12
52	HI + OH = I	k = 1.60E-11 exp(440/T)	7.00E-11
53	I + O ₃ = IO	k = 2.10E-11 exp(-830/T)	1.30E-12
54	I + HO ₂ = HI	k = 1.50E-11 exp(-1090/T)	3.87E-13
55	I + NO ₂ = INO ₂	Falloff: F=0.63; n=1 k(0) = 3.00E-31 (T/300) ⁻¹ k(inf) = 6.60E-11	5.24E-12
56	IO = I + O	Photolysis	1.18E-1
57	IO + IO = 0.4 I + 0.4 OIO + 0.6 I ₂ O ₂	k = 5.40E-11 exp(180/T)	9.88E-11
58	IO + HO ₂ = HOI	k = 1.40E-11 exp(540/T)	8.57E-11
59	IO + NO = I + NO ₂	k = 7.15E-12 exp(300/T)	1.96E-11
60	IO + NO ₂ = INO ₃	Falloff: F=0.4; n=1 k(0) = 7.70E-31 (T/300) ⁻⁵ k(inf) = 1.60E-11	3.55E-12
61	HOI + OH = IO	k = 5.00E-12	5.00E-12
62	OIO = I	Photolysis	1.28E-1
63	OIO + OH = HIO ₃	Falloff: F=0.3; n=1 k(0) = 1.50E-27 (T/300) ^{-3.93} k(inf) = 5.50E-10 exp(46/T)	4.72E-10
64	OIO + IO = IXOY	k = 1.00E-10	1.00E-10
65	OIO + OIO = IXOY	k = 1.50E-10	1.50E-10
66	OIO + NO = IO + NO ₂	k = 1.10E-12 exp(542/T)	6.78E-12
67	I ₂ O ₂ = I + OIO	k = 1.00E+1	1.00E+1
68	I ₂ O ₂ + O ₃ = IXOY	k = 1.00E-12	1.00E-12
69	INO ₂ = I + NO ₂	Photolysis	3.21E-3
70	INO ₂ + INO ₂ = I ₂ + 2 NO ₂	k = 4.70E-13 exp(-1670/T)	1.73E-15
71	INO ₃ = I + NO ₃	Photolysis	1.25E-2
72	INO ₃ + H ₂ O = HOI + HNO ₃	k = 2.50E-22	2.50E-22

Appendix B: Mechanism 3 – CB6r2 with Halogen Chemistry

Number	Reactants and Products	Rate Constant Expression	k ₂₉₈
73	CLO + BRO = CL + BR	$k = 4.70E-12 \exp(320/T)$	1.38E-11
74	CLO + IO = CL + I	$k = 4.70E-12 \exp(280/T)$	1.20E-11
75	BRO + IO = BR + I	$k = 1.50E-11 \exp(510/T)$	8.31E-11
76	CH3I = I + MEO2	Photolysis	3.19E-6
77	MI2 = 2 I + FORM	Photolysis	4.69E-3
78	MIB = I + BR + FORM	Photolysis	2.53E-4
79	MIC = I + CL + FORM	Photolysis	7.48E-5
80	MB3 = 3 BR + HO2 + CO	Photolysis	4.64E-7
81	MB3 + OH = 3 BR + CO	$k = 1.35E-12 \exp(-600/T)$	1.80E-13
82	MB2 + OH = 2 BR + HO2 + CO	$k = 2.00E-12 \exp(-840/T)$	1.19E-13
83	MBC + OH = BR + MEO2	$k = 2.35E-12 \exp(-1300/T)$	3.00E-14
84	MBC2 + OH = BR + MEO2	$k = 9.00E-13 \exp(-600/T)$	1.20E-13
85	MB2C + OH = BR + MEO2	$k = 9.00E-13 \exp(-600/T)$	1.20E-13
86	IALK = I + ALDX + XO2H + RO2	Photolysis	5.88E-7
87	SSCL + HNO3 = HCL + SSN3	$k = 1.00E-12$	1.00E-12
88	SSBR + HOBR = BR2	$k = 1.00E-12$	1.00E-12

Table B-2. Chemical species included in CB6r2h.

Species	Description	Constituents						Mol. Wt.	
		C	H	O	N	Cl	Br		I
CL2	Molecular chlorine					2			70.9
CL	Chlorine atom					1			35.5
CLO	Chlorine monoxide			1		1			51.4
HCL	Hydrogen chloride		1			1			36.5
HOCL	Hypochlorous acid		1	1		1			52.4
CLN2	Nitryl chloride: ClNO ₂			2		1			81.4
CLN3	Chlorine nitrate: ClONO ₂			3		1			97.4
FMCL	Formyl chloride: HC(O)Cl	1	1	1		1			64.5
BR2	Molecular bromine						2		159.8
BR	Bromine atom						1		79.9
BRO	Bromine monoxide			1			1		95.9
HBR	Hydrogen bromide		1				1		80.9
HOBR	Hypobromous acid		1	1			1		96.9
BRN2	Nitryl bromide: BrNO ₂			2			1		125.9
BRN3	Bromine nitrate: BrONO ₂			3			1		141.9
FMBR	Formyl bromide: HC(O)Br	1	1	1			1		108.9
I2	Molecular iodine							2	253.8
I	Iodine atom							1	126.9
IO	Iodine monoxide			1				1	142.9
OIO	Iodine dioxide			2				1	158.9
I2O2	Diiodine dioxide			2				2	285.8
IXOY	Condensable iodine oxides (> I ₂ O ₂)			3				2	301.8
HI	Hydrogen iodide		1					1	127.9
HOI	Hypoiodous acid		1	1				1	143.9
HIO3	Iodic acid: HONO ₂		1	3				1	175.9
INO2	Nitryl iodide: INO ₂			2				1	172.9
INO3	Iodine nitrate: IONO ₂			3				1	188.9
CH3I	Iodomethane	1	3					1	141.9
MI2	Diiodomethane: CH ₂ I ₂	1	2					2	267.8
MIB	Bromoiodomethane: CH ₂ BrI	1	2				1	1	220.8
MIC	Chloroiodomethane: CH ₂ ClI	1	2			1		1	176.4
MBC	Chlorobromomethane: CH ₂ ClBr	1	2			1	1		129.4
MB2	Dibromomethane: CH ₂ Br ₂	1	2				2		173.8
MBC2	Dichlorobromomethane: CHCl ₂ Br	1	3			2	1		165.8
MB2C	Chlorodibromomethane: CHClBr ₂	1	3			1	2		210.3
MB3	Bromoform CHBr ₃	1	1				3		252.7
IALK	Alkyl iodides	3	7					1	170.0
SSCL	Pseudo gas-phase species for sea salt chloride	0				1			35.5
SSBR	Pseudo gas-phase species for sea salt bromide	0					1		79.9
SSN3	Pseudo gas-phase species for sea salt nitrate	0		3	1				62.0

Appendix C

CAMx Mechanism 4: CB6r4 Gas-Phase Chemistry

Table C-1. Reactions and rate constant expressions for the CB6r4 mechanism. k_{298} is the rate constant at 298 K and 1 atmosphere using units in molecules/cm³ and 1/s. See Table C-2 for species names. See Section 3.1 on temperature and pressure dependencies. For photolysis reactions k_{298} shows the photolysis rate at a solar zenith angle of 60° and height of 600 m MSL/AGL. See Table C-3 for a listing of photolysis rates by zenith angle.

Number	Reactants and Products	Rate Constant Expression	k_{298}
1	NO ₂ = NO + O	Photolysis	6.30E-3
2	O + O ₂ + M = O ₃ + M	$k = 5.68E-34 (T/300)^{-2.6}$	5.78E-34
3	O ₃ + NO = NO ₂	$k = 1.40E-12 \exp(-1310/T)$	1.73E-14
4	O + NO + M = NO ₂ + M	$k = 1.00E-31 (T/300)^{-1.6}$	1.01E-31
5	O + NO ₂ = NO	$k = 5.50E-12 \exp(188/T)$	1.03E-11
6	O + NO ₂ = NO ₃	Falloff: F=0.6; n=1 $k(O) = 1.30E-31 (T/300)^{-1.5}$ $k(\infty) = 2.30E-11 (T/300)^{0.24}$	2.11E-12
7	O + O ₃ =	$k = 8.00E-12 \exp(-2060/T)$	7.96E-15
8	O ₃ = O	Photolysis	3.33E-4
9	O ₃ = O ₁ D	Photolysis	8.78E-6
10	O ₁ D + M = O + M	$k = 2.23E-11 \exp(115/T)$	3.28E-11
11	O ₁ D + H ₂ O = 2 OH	$k = 2.14E-10$	2.14E-10
12	O ₃ + OH = HO ₂	$k = 1.70E-12 \exp(-940/T)$	7.25E-14
13	O ₃ + HO ₂ = OH	$k = 2.03E-16 (T/300)^{4.57} \exp(693/T)$	2.01E-15
14	OH + O = HO ₂	$k = 2.40E-11 \exp(110/T)$	3.47E-11
15	HO ₂ + O = OH	$k = 2.70E-11 \exp(224/T)$	5.73E-11
16	OH + OH = O	$k = 6.20E-14 (T/298)^{2.6} \exp(945/T)$	1.48E-12
17	OH + OH = H ₂ O ₂	Falloff: F=0.5; n=1.13 $k(O) = 6.90E-31 (T/300)^{-0.8}$ $k(\infty) = 2.60E-11$	5.25E-12
18	OH + HO ₂ =	$k = 4.80E-11 \exp(250/T)$	1.11E-10
19	HO ₂ + HO ₂ = H ₂ O ₂	$k = k_1 + k_2 [M]$ $k_1 = 2.20E-13 \exp(600/T)$ $k_2 = 1.90E-33 \exp(980/T)$	2.90E-12
20	HO ₂ + HO ₂ + H ₂ O = H ₂ O ₂	$k = k_1 + k_2 [M]$ $k_1 = 3.08E-34 \exp(2800/T)$ $k_2 = 2.66E-54 \exp(3180/T)$	6.53E-30
21	H ₂ O ₂ = 2 OH	Photolysis	3.78E-6
22	H ₂ O ₂ + OH = HO ₂	$k = 2.90E-12 \exp(-160/T)$	1.70E-12
23	H ₂ O ₂ + O = OH + HO ₂	$k = 1.40E-12 \exp(-2000/T)$	1.70E-15
24	NO + NO + O ₂ = 2 NO ₂	$k = 3.30E-39 \exp(530/T)$	1.95E-38
25	HO ₂ + NO = OH + NO ₂	$k = 3.45E-12 \exp(270/T)$	8.54E-12
26	NO ₂ + O ₃ = NO ₃	$k = 1.40E-13 \exp(-2470/T)$	3.52E-17
27	NO ₃ = NO ₂ + O	Photolysis	1.56E-1
28	NO ₃ = NO	Photolysis	1.98E-2
29	NO ₃ + NO = 2 NO ₂	$k = 1.80E-11 \exp(110/T)$	2.60E-11
30	NO ₃ + NO ₂ = NO + NO ₂	$k = 4.50E-14 \exp(-1260/T)$	6.56E-16
31	NO ₃ + O = NO ₂	$k = 1.70E-11$	1.70E-11
32	NO ₃ + OH = HO ₂ + NO ₂	$k = 2.00E-11$	2.00E-11
33	NO ₃ + HO ₂ = OH + NO ₂	$k = 4.00E-12$	4.00E-12
34	NO ₃ + O ₃ = NO ₂	$k = 1.00E-17$	1.00E-17

Number	Reactants and Products	Rate Constant Expression	k ₂₉₈
35	NO ₃ + NO ₃ = 2 NO ₂	k = 8.50E-13 exp(-2450/T)	2.28E-16
36	NO ₃ + NO ₂ = N ₂ O ₅	Falloff: F=0.35; n=1.33 k(0) = 3.60E-30 (T/300) ^{-4.1} k(inf) = 1.90E-12 (T/300) ^{0.2}	1.24E-12
37	N ₂ O ₅ = NO ₃ + NO ₂	Falloff: F=0.35; n=1.33 k(0) = 1.30E-3 (T/300) ^{-3.5} exp(-11000/T) k(inf) = 9.70E+14 (T/300) ^{0.1} exp(-11080/T)	4.46E-2
38	N ₂ O ₅ = NO ₂ + NO ₃	Photolysis	2.52E-5
39	N ₂ O ₅ + H ₂ O = 2 HNO ₃	k = 1.00E-22	1.00E-22
40	NO + OH = HONO	Falloff: F=0.81; n=0.87 k(0) = 7.40E-31 (T/300) ^{-2.4} k(inf) = 3.30E-11 (T/300) ^{-0.3}	9.77E-12
41	NO + NO ₂ + H ₂ O = 2 HONO	k = 5.00E-40	5.00E-40
42	HONO + HONO = NO + NO ₂	k = 1.00E-20	1.00E-20
43	HONO = NO + OH	Photolysis	1.04E-3
44	HONO + OH = NO ₂	k = 2.50E-12 exp(260/T)	5.98E-12
45	NO ₂ + OH = HNO ₃	Falloff: F=0.6; n=1 k(0) = 1.80E-30 (T/300) ⁻³ k(inf) = 2.80E-11	1.06E-11
46	HNO ₃ + OH = NO ₃	k = k ₁ + k ₃ [M] / (1 + k ₃ [M] / k ₂) k ₁ = 2.40E-14 exp(460/T) k ₂ = 2.70E-17 exp(2199/T) k ₃ = 6.50E-34 exp(1335/T)	1.54E-13
47	HNO ₃ = OH + NO ₂	Photolysis	2.54E-7
48	HO ₂ + NO ₂ = PNA	Falloff: F=0.6; n=1 k(0) = 1.80E-31 (T/300) ^{-3.2} k(inf) = 4.70E-12	1.38E-12
49	PNA = HO ₂ + NO ₂	Falloff: F=0.6; n=1 k(0) = 4.10E-5 exp(-10650/T) k(inf) = 4.80E+15 exp(-11170/T)	8.31E-2
50	PNA = 0.59 HO ₂ + 0.59 NO ₂ + 0.41 OH + 0.41 NO ₃	Photolysis	2.36E-6
51	PNA + OH = NO ₂	k = 3.20E-13 exp(690/T)	3.24E-12
52	SO ₂ + OH = SULF + HO ₂	Falloff: F=0.53; n=1.1 k(0) = 4.50E-31 (T/300) ^{-3.9} k(inf) = 1.30E-12 (T/300) ^{-0.7}	8.12E-13
53	C ₂ O ₃ + NO = NO ₂ + MEO ₂ + RO ₂	k = 7.50E-12 exp(290/T)	1.98E-11
54	C ₂ O ₃ + NO ₂ = PAN	Falloff: F=0.3; n=1.41 k(0) = 2.70E-28 (T/300) ^{-7.1} k(inf) = 1.20E-11 (T/300) ^{-0.9}	9.40E-12
55	PAN = NO ₂ + C ₂ O ₃	Falloff: F=0.3; n=1.41 k(0) = 4.90E-3 exp(-12100/T) k(inf) = 5.40E+16 exp(-13830/T)	2.98E-4
56	PAN = 0.6 NO ₂ + 0.6 C ₂ O ₃ + 0.4 NO ₃ + 0.4 MEO ₂ + 0.4 RO ₂	Photolysis	3.47E-7
57	C ₂ O ₃ + HO ₂ = 0.41 PACD + 0.15 AACD + 0.15 O ₃ + 0.44 MEO ₂ + 0.44 RO ₂ + 0.44 OH	k = 5.20E-13 exp(980/T)	1.39E-11
58	C ₂ O ₃ + RO ₂ = C ₂ O ₃	k = 8.90E-13 exp(800/T)	1.30E-11
59	C ₂ O ₃ + C ₂ O ₃ = 2 MEO ₂ + 2 RO ₂	k = 2.90E-12 exp(500/T)	1.55E-11
60	C ₂ O ₃ + CXO ₃ = MEO ₂ + ALD ₂ + XO ₂ H + 2 RO ₂	k = 2.90E-12 exp(500/T)	1.55E-11

Number	Reactants and Products	Rate Constant Expression	k ₂₉₈
61	CXO3 + NO = NO2 + ALD2 + XO2H + RO2	k = 6.70E-12 exp(340/T)	2.10E-11
62	CXO3 + NO2 = PANX	k = k(ref) K k(ref) = k(54) K = 1.00E+0	9.40E-12
63	PANX = NO2 + CXO3	k = k(ref) K k(ref) = k(55) K = 1.00E+0	2.98E-4
64	PANX = 0.6 NO2 + 0.6 CXO3 + 0.4 NO3 + 0.4 ALD2 + 0.4 XO2H + 0.4 RO2	Photolysis	3.47E-7
65	CXO3 + HO2 = 0.41 PACD + 0.15 AACD + 0.15 O3 + 0.44 ALD2 + 0.44 XO2H + 0.44 RO2 + 0.44 OH	k = 5.20E-13 exp(980/T)	1.39E-11
66	CXO3 + RO2 = 0.8 ALD2 + 0.8 XO2H + 0.8 RO2	k = 8.90E-13 exp(800/T)	1.30E-11
67	CXO3 + CXO3 = 2 ALD2 + 2 XO2H + 2 RO2	k = 3.20E-12 exp(500/T)	1.71E-11
68	RO2 + NO = NO	k = 2.40E-12 exp(360/T)	8.03E-12
69	RO2 + HO2 = HO2	k = 4.80E-13 exp(800/T)	7.03E-12
70	RO2 + RO2 =	k = 6.50E-14 exp(500/T)	3.48E-13
71	MEO2 + NO = FORM + HO2 + NO2	k = 2.30E-12 exp(360/T)	7.70E-12
72	MEO2 + HO2 = 0.9 MEPX + 0.1 FORM	k = 3.80E-13 exp(780/T)	5.21E-12
73	MEO2 + C2O3 = FORM + 0.9 HO2 + 0.9 MEO2 + 0.1 AACD + 0.9 RO2	k = 2.00E-12 exp(500/T)	1.07E-11
74	MEO2 + RO2 = 0.685 FORM + 0.315 MEOH + 0.37 HO2 + RO2	k = k(ref) K k(ref) = k(70) K = 1.00E+0	3.48E-13
75	XO2H + NO = NO2 + HO2	k = 2.70E-12 exp(360/T)	9.04E-12
76	XO2H + HO2 = ROOH	k = 6.80E-13 exp(800/T)	9.96E-12
77	XO2H + C2O3 = 0.8 HO2 + 0.8 MEO2 + 0.2 AACD + 0.8 RO2	k = k(ref) K k(ref) = k(58) K = 1.00E+0	1.30E-11
78	XO2H + RO2 = 0.6 HO2 + RO2	k = k(ref) K k(ref) = k(70) K = 1.00E+0	3.48E-13
79	XO2 + NO = NO2	k = k(ref) K k(ref) = k(75) K = 1.00E+0	9.04E-12
80	XO2 + HO2 = ROOH	k = k(ref) K k(ref) = k(76) K = 1.00E+0	9.96E-12
81	XO2 + C2O3 = 0.8 MEO2 + 0.2 AACD + 0.8 RO2	k = k(ref) K k(ref) = k(58) K = 1.00E+0	1.30E-11
82	XO2 + RO2 = RO2	k = k(ref) K k(ref) = k(70) K = 1.00E+0	3.48E-13
83	XO2N + NO = 0.5 NTR1 + 0.5 NTR2	k = k(ref) K k(ref) = k(75) K = 1.00E+0	9.04E-12
84	XO2N + HO2 = ROOH	k = k(ref) K k(ref) = k(76) K = 1.00E+0	9.96E-12

Number	Reactants and Products	Rate Constant Expression	k ₂₉₈
85	XO2N + C2O3 = 0.8 HO2 + 0.8 MEO2 + 0.2 AACD + 0.8 RO2	k = k(ref) K k(ref) = k(58) K = 1.00E+0	1.30E-11
86	XO2N + RO2 = RO2	k = k(ref) K k(ref) = k(70) K = 1.00E+0	3.48E-13
87	MEPX + OH = 0.6 MEO2 + 0.6 RO2 + 0.4 FORM + 0.4 OH	k = 5.30E-12 exp(190/T)	1.00E-11
88	MEPX = MEO2 + RO2 + OH	Photolysis	2.68E-6
89	ROOH + OH = 0.54 XO2H + 0.06 XO2N + 0.6 RO2 + 0.4 OH	k = 5.30E-12 exp(190/T)	1.00E-11
90	ROOH = HO2 + OH	Photolysis	2.68E-6
91	NTR1 + OH = NTR2	k = 2.00E-12	2.00E-12
92	NTR1 = NO2	Photolysis	1.06E-6
93	FACD + OH = HO2	k = 4.50E-13	4.50E-13
94	AACD + OH = MEO2 + RO2	k = 4.00E-14 exp(850/T)	6.93E-13
95	PACD + OH = C2O3	k = 5.30E-12 exp(190/T)	1.00E-11
96	FORM + OH = HO2 + CO	k = 5.40E-12 exp(135/T)	8.49E-12
97	FORM = 2 HO2 + CO	Photolysis	1.78E-5
98	FORM = CO + H2	Photolysis	2.38E-5
99	FORM + NO3 = HNO3 + HO2 + CO	k = 5.50E-16	5.50E-16
100	FORM + HO2 = HCO3	k = 9.70E-15 exp(625/T)	7.90E-14
101	HCO3 = FORM + HO2	k = 2.40E+12 exp(-7000/T)	1.51E+2
102	HCO3 + NO = FACD + NO2 + HO2	k = 5.60E-12	5.60E-12
103	HCO3 + HO2 = 0.5 MEPX + 0.5 FACD + 0.2 OH + 0.2 HO2	k = 5.60E-15 exp(2300/T)	1.26E-11
104	ALD2 + OH = C2O3	k = 4.70E-12 exp(345/T)	1.50E-11
105	ALD2 + NO3 = C2O3 + HNO3	k = 1.40E-12 exp(-1860/T)	2.73E-15
106	ALD2 = MEO2 + RO2 + CO + HO2	Photolysis	1.76E-6
107	ALDX + OH = CXO3	k = 4.90E-12 exp(405/T)	1.91E-11
108	ALDX + NO3 = CXO3 + HNO3	k = 6.30E-15	6.30E-15
109	ALDX = ALD2 + XO2H + RO2 + CO + HO2	Photolysis	6.96E-6
110	GLYD + OH = 0.2 GLY + 0.2 HO2 + 0.8 C2O3	k = 8.00E-12	8.00E-12
111	GLYD = 0.74 FORM + 0.89 CO + 1.4 HO2 + 0.15 MEOH + 0.19 OH + 0.11 GLY + 0.11 XO2H + 0.11 RO2	Photolysis	1.56E-6
112	GLYD + NO3 = HNO3 + C2O3	k = 1.40E-12 exp(-1860/T)	2.73E-15
113	GLY + OH = 1.8 CO + 0.2 XO2 + 0.2 RO2 + HO2	k = 3.10E-12 exp(340/T)	9.70E-12
114	GLY = 2 HO2 + 2 CO	Photolysis	5.50E-5
115	GLY + NO3 = HNO3 + 1.5 CO + 0.5 XO2 + 0.5 RO2 + HO2	k = 1.40E-12 exp(-1860/T)	2.73E-15
116	MGLY = C2O3 + HO2 + CO	Photolysis	1.46E-4
117	MGLY + NO3 = HNO3 + C2O3 + XO2 + RO2	k = 1.40E-12 exp(-1860/T)	2.73E-15
118	MGLY + OH = C2O3 + CO	k = 1.90E-12 exp(575/T)	1.31E-11
119	H2 + OH = HO2	k = 7.70E-12 exp(-2100/T)	6.70E-15
120	CO + OH = HO2	k = k1 + k2 [M] k1 = 1.44E-13 k2 = 3.43E-33	2.28E-13
121	CH4 + OH = MEO2 + RO2	k = 1.85E-12 exp(-1690/T)	6.37E-15
122	ETHA + OH = 0.991 ALD2 + 0.991 XO2H + 0.009 XO2N + RO2	k = 6.90E-12 exp(-1000/T)	2.41E-13

Number	Reactants and Products	Rate Constant Expression	k ₂₉₈
123	MEOH + OH = FORM + HO2	k = 2.85E-12 exp(-345/T)	8.95E-13
124	ETOH + OH = 0.95 ALD2 + 0.9 HO2 + 0.1 XO2H + 0.1 RO2 + 0.078 FORM + 0.011 GLYD	k = 3.00E-12 exp(20/T)	3.21E-12
125	KET = 0.5 ALD2 + 0.5 C2O3 + 0.5 XO2H + 0.5 CXO3 + 0.5 MEO2 + RO2 - 2.5 PAR	Photolysis	2.27E-7
126	ACET = 0.38 CO + 1.38 MEO2 + 1.38 RO2 + 0.62 C2O3	Photolysis	2.08E-7
127	ACET + OH = FORM + C2O3 + XO2 + RO2	k = 1.41E-12 exp(-620.6/T)	1.76E-13
128	PRPA + OH = XPRP	k = 7.60E-12 exp(-585/T)	1.07E-12
129	PAR + OH = XPAR	k = 8.10E-13	8.10E-13
130	ROR = 0.2 KET + 0.42 ACET + 0.74 ALD2 + 0.37 ALDX + 0.04 XO2N + 0.94 XO2H + 0.98 RO2 + 0.02 ROR - 2.7 PAR	k = 5.70E+12 exp(-5780/T)	2.15E+4
131	ROR + O2 = KET + HO2	k = 1.50E-14 exp(-200/T)	7.67E-15
132	ROR + NO2 = NTR1	k = 8.60E-12 exp(400/T)	3.29E-11
133	ETHY + OH = 0.7 GLY + 0.7 OH + 0.3 FACD + 0.3 CO + 0.3 HO2	Falloff: F=0.37; n=1.3 k(0) = 5.00E-30 (T/300) ^{-1.5} k(inf) = 1.00E-12	7.52E-13
134	ETH + OH = XO2H + RO2 + 1.56 FORM + 0.22 GLYD	Falloff: F=0.48; n=1.15 k(0) = 8.60E-29 (T/300) ^{-3.1} k(inf) = 9.00E-12 (T/300) ^{-0.85}	7.84E-12
135	ETH + O3 = FORM + 0.51 CO + 0.16 HO2 + 0.16 OH + 0.37 FACD	k = 9.10E-15 exp(-2580/T)	1.58E-18
136	ETH + NO3 = 0.5 NO2 + 0.5 NTR1 + 0.5 XO2H + 0.5 XO2 + RO2 + 1.125 FORM	k = 3.30E-12 exp(-2880/T)	2.10E-16
137	OLE + OH = 0.781 FORM + 0.488 ALD2 + 0.488 ALDX + 0.976 XO2H + 0.195 XO2 + 0.024 XO2N + 1.195 RO2 - 0.73 PAR	Falloff: F=0.5; n=1.13 k(0) = 8.00E-27 (T/300) ^{-3.5} k(inf) = 3.00E-11 (T/300) ⁻¹	2.86E-11
138	OLE + O3 = 0.295 ALD2 + 0.555 FORM + 0.27 ALDX + 0.15 XO2H + 0.15 RO2 + 0.334 OH + 0.08 HO2 + 0.378 CO + 0.075 GLY + 0.075 MGLY + 0.09 FACD + 0.13 AACD + 0.04 H2O2 - 0.79 PAR	k = 5.50E-15 exp(-1880/T)	1.00E-17
139	OLE + NO3 = 0.5 NO2 + 0.5 NTR1 + 0.48 XO2 + 0.48 XO2H + 0.04 XO2N + RO2 + 0.5 FORM + 0.25 ALD2 + 0.375 ALDX - 1 PAR	k = 4.60E-13 exp(-1155/T)	9.54E-15
140	IOLE + OH = 1.3 ALD2 + 0.7 ALDX + XO2H + RO2	k = 1.05E-11 exp(519/T)	5.99E-11
141	IOLE + O3 = 0.732 ALD2 + 0.442 ALDX + 0.128 FORM + 0.245 CO + 0.5 OH + 0.3 XO2H + 0.3 RO2 + 0.24 GLY + 0.06 MGLY + 0.29 PAR + 0.08 AACD + 0.08 H2O2	k = 4.70E-15 exp(-1013/T)	1.57E-16
142	IOLE + NO3 = 0.5 NO2 + 0.5 NTR1 + 0.48 XO2 + 0.48 XO2H + 0.04 XO2N + RO2 + 0.5 ALD2 + 0.625 ALDX + PAR	k = 3.70E-13	3.70E-13
143	ISOP + OH = ISO2 + RO2	k = 2.70E-11 exp(390/T)	9.99E-11
144	ISO2 + NO = 0.1 INTR + 0.9 NO2 + 0.673 FORM + 0.9 ISPD + 0.818 HO2 + 0.082 XO2H + 0.082 RO2	k = 2.39E-12 exp(365/T)	8.13E-12
145	ISO2 + HO2 = 0.88 ISPX + 0.12 OH + 0.12 HO2 + 0.12 FORM + 0.12 ISPD	k = 7.43E-13 exp(700/T)	7.78E-12

Number	Reactants and Products	Rate Constant Expression	k ₂₉₈
146	ISO2 + C2O3 = 0.598 FORM + 1 ISPD + 0.728 HO2 + 0.072 XO2H + 0.8 MEO2 + 0.2 AACD + 0.872 RO2	k = k(ref) K k(ref) = k(58) K = 1.00E+0	1.30E-11
147	ISO2 + RO2 = 0.598 FORM + 1 ISPD + 0.728 HO2 + 0.072 XO2H + 1.072 RO2	k = k(ref) K k(ref) = k(70) K = 1.00E+0	3.48E-13
148	ISO2 = HO2 + HPLD	k = 3.30E+9 exp(-8300/T)	2.64E-3
149	ISOP + O3 = 0.6 FORM + 0.65 ISPD + 0.15 ALDX + 0.2 CXO3 + 0.35 PAR + 0.266 OH + 0.2 XO2 + 0.2 RO2 + 0.066 HO2 + 0.066 CO	k = 1.03E-14 exp(-1995/T)	1.27E-17
150	ISOP + NO3 = 0.35 NO2 + 0.65 NTR2 + 0.64 XO2H + 0.33 XO2 + 0.03 XO2N + RO2 + 0.35 FORM + 0.35 ISPD	k = 3.03E-12 exp(-448/T)	6.74E-13
151	ISPD + OH = 0.022 XO2N + 0.521 XO2 + 0.115 MGLY + 0.115 MEO2 + 0.269 GLYD + 0.269 C2O3 + 0.457 OPO3 + 0.117 PAR + 0.137 ACET + 0.137 CO + 0.137 HO2 + 0.658 RO2	k = 5.58E-12 exp(511/T)	3.10E-11
152	ISPD + O3 = 0.04 ALD2 + 0.231 FORM + 0.531 MGLY + 0.17 GLY + 0.17 ACET + 0.543 CO + 0.461 OH + 0.15 FACD + 0.398 HO2 + 0.143 C2O3	k = 3.88E-15 exp(-1770/T)	1.02E-17
153	ISPD + NO3 = 0.717 HNO3 + 0.142 NTR2 + 0.142 NO2 + 0.142 XO2 + 0.142 XO2H + 0.113 GLYD + 0.113 MGLY + 0.717 PAR + 0.717 CXO3 + 0.284 RO2	k = 4.10E-12 exp(-1860/T)	7.98E-15
154	ISPD = 0.76 HO2 + 0.34 XO2H + 0.16 XO2 + 0.34 MEO2 + 0.208 C2O3 + 0.26 FORM + 0.24 OLE + 0.24 PAR + 0.17 ACET + 0.128 GLYD + 0.84 RO2	Photolysis	1.60E-5
155	ISPX + OH = 0.904 EPOX + 0.933 OH + 0.067 ISO2 + 0.067 RO2 + 0.029 IOLE + 0.029 ALDX	k = 2.23E-11 exp(372/T)	7.77E-11
156	HPLD = OH + ISPD	Photolysis	4.41E-4
157	HPLD + NO3 = HNO3 + ISPD	k = 6.00E-12 exp(-1860/T)	1.17E-14
158	EPOX + OH = EPX2 + RO2	k = 5.78E-11 exp(-400/T)	1.51E-11
159	EPX2 + HO2 = 0.275 GLYD + 0.275 GLY + 0.275 MGLY + 1.125 OH + 0.825 HO2 + 0.375 FORM + 0.074 FACD + 0.251 CO + 2.175 PAR	k = 7.43E-13 exp(700/T)	7.78E-12
160	EPX2 + NO = 0.275 GLYD + 0.275 GLY + 0.275 MGLY + 0.125 OH + 0.825 HO2 + 0.375 FORM + NO2 + 0.251 CO + 2.175 PAR	k = 2.39E-12 exp(365/T)	8.13E-12
161	EPX2 + C2O3 = 0.22 GLYD + 0.22 GLY + 0.22 MGLY + 0.1 OH + 0.66 HO2 + 0.3 FORM + 0.2 CO + 1.74 PAR + 0.8 MEO2 + 0.2 AACD + 0.8 RO2	k = k(ref) K k(ref) = k(58) K = 1.00E+0	1.30E-11
162	EPX2 + RO2 = 0.275 GLYD + 0.275 GLY + 0.275 MGLY + 0.125 OH + 0.825 HO2 + 0.375 FORM + 0.251 CO + 2.175 PAR + RO2	k = k(ref) K k(ref) = k(70) K = 1.00E+0	3.48E-13

Number	Reactants and Products	Rate Constant Expression	k ₂₉₈
163	INTR + OH = 0.63 XO2 + 0.37 XO2H + RO2 + 0.444 NO2 + 0.185 NO3 + 0.104 INTR + 0.592 FORM + 0.331 GLYD + 0.185 FACD + 2.7 PAR + 0.098 OLE + 0.078 ALDX + 0.266 NTR2	k = 3.10E-11	3.10E-11
164	TERP + OH = 0.75 XO2H + 0.5 XO2 + 0.25 XO2N + 1.5 RO2 + 0.28 FORM + 1.66 PAR + 0.47 ALDX	k = 1.50E-11 exp(449/T)	6.77E-11
165	TERP + O3 = 0.57 OH + 0.07 XO2H + 0.69 XO2 + 0.18 XO2N + 0.94 RO2 + 0.24 FORM + 0.001 CO + 7 PAR + 0.21 ALDX + 0.39 CXO3	k = 1.20E-15 exp(-821/T)	7.63E-17
166	TERP + NO3 = 0.47 NO2 + 0.28 XO2H + 0.75 XO2 + 0.25 XO2N + 1.28 RO2 + 0.47 ALDX + 0.53 NTR2	k = 3.70E-12 exp(175/T)	6.66E-12
167	BENZ + OH = 0.53 CRES + 0.352 BZO2 + 0.352 RO2 + 0.118 OPEN + 0.118 OH + 0.53 HO2	k = 2.30E-12 exp(-190/T)	1.22E-12
168	BZO2 + NO = 0.918 NO2 + 0.082 NTR2 + 0.918 GLY + 0.918 OPEN + 0.918 HO2	k = 2.70E-12 exp(360/T)	9.04E-12
169	BZO2 + C2O3 = GLY + OPEN + HO2 + MEO2 + RO2	k = k(ref) K k(ref) = k(58) K = 1.00E+0	1.30E-11
170	BZO2 + HO2 =	k = 1.90E-13 exp(1300/T)	1.49E-11
171	BZO2 + RO2 = GLY + OPEN + HO2 + RO2	k = k(ref) K k(ref) = k(70) K = 1.00E+0	3.48E-13
172	TOL + OH = 0.18 CRES + 0.65 TO2 + 0.72 RO2 + 0.1 OPEN + 0.1 OH + 0.07 XO2H + 0.18 HO2	k = 1.80E-12 exp(340/T)	5.63E-12
173	TO2 + NO = 0.86 NO2 + 0.14 NTR2 + 0.417 GLY + 0.443 MGLY + 0.66 OPEN + 0.2 XOPN + 0.86 HO2	k = 2.70E-12 exp(360/T)	9.04E-12
174	TO2 + C2O3 = 0.48 GLY + 0.52 MGLY + 0.77 OPEN + 0.23 XOPN + HO2 + MEO2 + RO2	k = k(ref) K k(ref) = k(58) K = 1.00E+0	1.30E-11
175	TO2 + HO2 =	k = 1.90E-13 exp(1300/T)	1.49E-11
176	TO2 + RO2 = 0.48 GLY + 0.52 MGLY + 0.77 OPEN + 0.23 XOPN + HO2 + RO2	k = k(ref) K k(ref) = k(70) K = 1.00E+0	3.48E-13
177	XYL + OH = 0.155 CRES + 0.544 XLO2 + 0.602 RO2 + 0.244 XOPN + 0.244 OH + 0.058 XO2H + 0.155 HO2	k = 1.85E-11	1.85E-11
178	XLO2 + NO = 0.86 NO2 + 0.14 NTR2 + 0.221 GLY + 0.675 MGLY + 0.3 OPEN + 0.56 XOPN + 0.86 HO2	k = 2.70E-12 exp(360/T)	9.04E-12
179	XLO2 + HO2 =	k = 1.90E-13 exp(1300/T)	1.49E-11
180	XLO2 + C2O3 = 0.26 GLY + 0.77 MGLY + 0.35 OPEN + 0.65 XOPN + HO2 + MEO2 + RO2	k = k(ref) K k(ref) = k(58) K = 1.00E+0	1.30E-11

Number	Reactants and Products	Rate Constant Expression	k ₂₉₈
181	XLO2 + RO2 = 0.26 GLY + 0.77 MGLY + 0.35 OPEN + 0.65 XOPN + HO2 + RO2	k = k(ref) K k(ref) = k(70) K = 1.00E+0	3.48E-13
182	CRES + OH = 0.025 GLY + 0.025 OPEN + HO2 + 0.2 CRO + 0.732 CAT1 + 0.02 XO2N + 0.02 RO2	k = 1.70E-12 exp(950/T)	4.12E-11
183	CRES + NO3 = 0.3 CRO + HNO3 + 0.48 XO2 + 0.12 XO2H + 0.24 GLY + 0.24 MGLY + 0.48 OPO3 + 0.1 XO2N + 0.7 RO2	k = 1.40E-11	1.40E-11
184	CRO + NO2 = CRON	k = 2.10E-12	2.10E-12
185	CRO + HO2 = CRES	k = 5.50E-12	5.50E-12
186	CRON + OH = NTR2 + 0.5 CRO	k = 1.53E-12	1.53E-12
187	CRON + NO3 = NTR2 + 0.5 CRO + HNO3	k = 3.80E-12	3.80E-12
188	CRON = HONO + HO2 + FORM + OPEN	Photolysis	9.45E-5
189	XOPN = 0.4 GLY + XO2H + 0.7 HO2 + 0.7 CO + 0.3 C2O3	Photolysis	5.04E-4
190	XOPN + OH = MGLY + 0.4 GLY + 2 XO2H + 2 RO2	k = 9.00E-11	9.00E-11
191	XOPN + O3 = 1.2 MGLY + 0.5 OH + 0.6 C2O3 + 0.1 ALD2 + 0.5 CO + 0.3 XO2H + 0.3 RO2	k = 1.08E-16 exp(-500/T)	2.02E-17
192	XOPN + NO3 = 0.5 NO2 + 0.5 NTR2 + 0.45 XO2H + 0.45 XO2 + 0.1 XO2N + RO2 + 0.25 OPEN + 0.25 MGLY	k = 3.00E-12	3.00E-12
193	OPEN = OPO3 + HO2 + CO	Photolysis	5.04E-4
194	OPEN + OH = 0.6 OPO3 + 0.4 XO2H + 0.4 RO2 + 0.4 GLY	k = 4.40E-11	4.40E-11
195	OPEN + O3 = 1.4 GLY + 0.24 MGLY + 0.5 OH + 0.12 C2O3 + 0.08 FORM + 0.02 ALD2 + 1.98 CO + 0.56 HO2	k = 5.40E-17 exp(-500/T)	1.01E-17
196	OPEN + NO3 = OPO3 + HNO3	k = 3.80E-12	3.80E-12
197	CAT1 + OH = 0.14 FORM + 0.2 HO2 + 0.5 CRO	k = 5.00E-11	5.00E-11
198	CAT1 + NO3 = CRO + HNO3	k = 1.70E-10	1.70E-10
199	OPO3 + NO = NO2 + 0.5 GLY + 0.5 CO + 0.8 HO2 + 0.2 CXO3	k = 1.00E-11	1.00E-11
200	OPO3 + NO2 = OPAN	k = k(ref) K k(ref) = k(54) K = 1.00E+0	9.40E-12
201	OPAN = OPO3 + NO2	k = k(ref) K k(ref) = k(55) K = 1.00E+0	2.98E-4
202	OPO3 + HO2 = 0.41 PACD + 0.15 AACD + 0.15 O3 + 0.44 ALDX + 0.44 XO2H + 0.44 RO2 + 0.44 OH	k = k(ref) K k(ref) = k(57) K = 1.00E+0	1.39E-11
203	OPO3 + C2O3 = MEO2 + XO2 + ALDX + 2 RO2	k = k(ref) K k(ref) = k(59) K = 1.00E+0	1.55E-11
204	OPO3 + RO2 = 0.8 XO2H + 0.8 ALDX + 1.8 RO2 + 0.2 AACD	k = k(ref) K k(ref) = k(58) K = 1.00E+0	1.30E-11
205	OPAN + OH = 0.5 NO2 + 0.5 GLY + CO + 0.5 NTR2	k = 3.60E-11	3.60E-11

Number	Reactants and Products	Rate Constant Expression	k ₂₉₈
206	PANX + OH = ALD2 + NO2	k = 3.00E-12	3.00E-12
207	NTR2 = HNO3	k = 2.30E-5	2.30E-5
208	ECH4 + OH = MEO2 + RO2	k = 1.85E-12 exp(-1690/T)	6.37E-15
209	I2 = 2 I	Photolysis	1.44E-1
210	HOI = I + OH	Photolysis	6.36E-2
211	I + O3 = IO	k = 2.10E-11 exp(-830/T)	1.30E-12
212	IO = I + O	Photolysis	1.18E-1
213	IO + IO = 0.4 I + 0.4 OIO + 0.6 I2O2	k = 5.40E-11 exp(180/T)	9.88E-11
214	IO + HO2 = HOI	k = 1.40E-11 exp(540/T)	8.57E-11
215	IO + NO = I + NO2	k = 7.15E-12 exp(300/T)	1.96E-11
216	IO + NO2 = INO3	Falloff: F=0.4; n=1 k(0) = 7.70E-31 (T/300)^-5 k(inf) = 1.60E-11	3.55E-12
217	OIO = I	Photolysis	1.41E-1
218	OIO + OH = HIO3	Falloff: F=0.3; n=1 k(0) = 1.50E-27 (T/300)^-3.93 k(inf) = 5.50E-10 exp(46/T)	4.72E-10
219	OIO + IO = IXOY	k = 1.00E-10	1.00E-10
220	OIO + NO = IO + NO2	k = 1.10E-12 exp(542/T)	6.78E-12
221	I2O2 = I + OIO	k = 1.00E+1	1.00E+1
222	I2O2 + O3 = IXOY	k = 1.00E-12	1.00E-12
223	INO3 = I + NO3	Photolysis	1.25E-2
224	INO3 + H2O = HOI + HNO3	k = 2.50E-22	2.50E-22
225	XPRP = XO2N + RO2	Falloff: F=0.41; n=1 k(0) = 2.37E-21 k(inf) = 4.30E-1 (T/298)^-8	3.09E-2
226	XPRP = 0.732 ACET + 0.268 ALDX + 0.268 PAR + XO2H + RO2	k = 1.00E+0	1.00E+0
227	XPAR = XO2N + RO2	Falloff: F=0.41; n=1 k(0) = 4.81E-20 k(inf) = 4.30E-1 (T/298)^-8	1.49E-1
228	XPAR = 0.126 ALDX + 0.874 ROR + 0.126 XO2H + 0.874 XO2 + RO2 - 0.126 PAR	k = 1.00E+0	1.00E+0
229	INTR = HNO3	k = 1.40E-4	1.40E-4

Table C-2. CB6r4 species names and descriptions.

Species	Description	Carbon #	C	H	O	N	I	MW
BZO2	Peroxy radical from OH addition to benzene	6	6	7	5			159.06
C2O3	Acetylperoxy radical	2	2	3	3			75.01
CRO	Alkoxy radical from cresol	7	7	7	1			107.11
CXO3	C3 and higher acylperoxy radicals	3	3	5	3			89.04
EPX2	Peroxy radical from EPOX reaction with OH	5	5	9	5			149.06
HCO3	Adduct from HO2 plus formaldehyde	1	1	3	3			63.00
HO2	Hydroperoxy radical			1	2			32.99
ISO2	Peroxy radical from OH addition to isoprene	5	5	9	3			117.08
MEO2	Methylperoxy radical	1	1	3	2			47.01
O	Oxygen atom in the O3(P) electronic state				1			15.99
O1D	Oxygen atom in the O1(D) electronic state				1			15.99
OH	Hydroxyl radical			1	1			17.00
OPO3	Peroxyacyl radical from OPEN	4	4	3	4			115.02
RO2	Operator to approximate total peroxy radical concentration		4	7	2			87.07
ROR	Secondary alkoxy radical	1	4	7	1			71.08
TO2	Peroxy radical from OH addition to TOL	7	7	9	5			173.08
XLO2	Peroxy radical from OH addition to XYL	8	8	11	5			187.11
XO2	NO to NO2 conversion from alkylperoxy (RO2) radical		4	7	2			87.07
XO2H	NO to NO2 conversion (XO2) accompanied by HO2 production		4	7	2			87.07
XO2N	NO to organic nitrate conversion from alkylperoxy (RO2) radical		4	7	2			87.07
I	Iodine atom						1	126.90
IO	Iodine monoxide				1		1	142.89
OIO	Iodine dioxide				2		1	158.88
XPRP	Operator for organic nitrates from PRPA	3	3	7	2	1		89.06
XPAR	Operator for organic nitrates from PAR	1	5	11	2	1		117.11
AACD	Acetic acid	2	2	4	2			60.03
ACET	Acetone	3	3	6	1			58.06
ALD2	Acetaldehyde	2	2	4	1			44.04
ALDX	Propionaldehyde and higher aldehydes	3	3	6	1			58.06
BENZ	Benzene	6	6	6				78.10
CAT1	Methyl-catechols	7	7	8	2			124.11
CO	Carbon monoxide	1	1		1			28.00
CRES	Cresols	7	7	8	1			108.12
CRON	Nitro-cresols	7	7	7	3	1		153.09
EPOX	Epoxide formed from ISPX reaction with OH	5	5	10	3			118.09
ETH	Ethene	2	2	4				28.05
ETHA	Ethane	2	2	6				30.06
ETHY	Ethyne	2	2	2				26.03
ETOH	Ethanol	2	2	6	1			46.05
FACD	Formic acid	1	1	2	2			46.00
FORM	Formaldehyde	1	1	2	1			30.01
GLY	Glyoxal	2	2	2	2			58.01
GLYD	Glycolaldehyde	2	2	4	2			60.03
H2O2	Hydrogen peroxide			2	2			33.99
HNO3	Nitric acid			1	3	1		62.98
HONO	Nitrous acid			1	2	1		46.99

Species	Description	Carbon #	C	H	O	N	I	MW
HPLD	hydroperoxyaldehyde	5	5	8	3			116.08
INTR	Organic nitrates from ISO ₂ reaction with NO	5	5	9	4	1		147.07
IOL	Internal olefin carbon bond (R-C=C-R)	4	4	8				56.10
ISOP	Isoprene	5	5	8				68.11
ISPD	Isoprene product (lumped methacrolein, methyl vinyl ketone, etc.)	4	4	6	1			70.07
ISPX	Hydroperoxides from ISO ₂ reaction with HO ₂	5	5	10	3			118.09
KET	Ketone carbon bond (C=O)	4	4	8	1			72.09
MEOH	Methanol	1	1	4	1			32.03
MEPX	Methylhydroperoxide	1	1	4	2			48.02
MGLY	Methylglyoxal	3	3	4	2			72.04
N ₂ O ₅	Dinitrogen pentoxide				5	2		107.95
NO	Nitric oxide				1	1		29.99
NO ₂	Nitrogen dioxide				2	1		45.98
NO ₃	Nitrate radical				3	1		61.97
NTR1	Simple organic nitrates		4	9	3	1		119.07
NTR2	Multi-functional organic nitrates		4	9	4	1		135.06
O ₃	Ozone				3			47.97
OLE	Terminal olefin carbon bond (R-C=C)	3	3	6				42.07
OPAN	Peroxyacyl nitrate (PAN compound) from OPO ₃	4	4	3	6	1		161.00
OPEN	Aromatic ring opening product (unsaturated dicarbonyl)	4	4	4	2			84.05
PACD	Peroxyacetic and higher peroxyacetic acids	2	2	4	3			76.02
PAN	Peroxyacetyl Nitrate	2	2	3	5	1		120.99
PANX	C ₃ and higher peroxyacyl nitrate	3	3	5	5	1		135.02
PAR	Paraffin carbon bond (C-C)	1	5	12				72.13
PNA	Peroxyacetic acid			1	4	1		78.97
PRPA	Propane	3	3	8				44.09
ROOH	Higher organic peroxide		4	10	2			90.09
SO ₂	Sulfur dioxide				2			64.04
SULF	Sulfuric acid (gaseous)			2	4			98.03
TERP	Monoterpenes	10	10	16				136.21
TOL	Toluene and other monoalkyl aromatics	7	7	8				92.13
XOPN	Aromatic ring opening product (unsaturated dicarbonyl)	5	5	6	2			98.07
XYL	Xylene and other polyalkyl aromatics	8	8	10				106.15
ECH ₄	Emitted methane (to enable tracking separate from CH ₄)	1	1	4				16.04
I ₂	Molecular iodine						2	253.80
I ₂ O ₂	Diiodine dioxide				2		2	285.78
IXOY	Condensable iodine oxides				3		2	301.77
HOI	Hypoiodous acid			1	1		1	143.90
HIO ₃	Iodic acid			1	3		1	175.88
INO ₃	Iodine nitrate				3	1	1	188.87

Table C-3. CB6r4 primary (unshaded) and secondary (shaded) photolysis rates (1/s) by solar zenith angle at 600 m MSL/AGL.

Reaction ID	Solar zenith angle (degree)									
	0	10	20	30	40	50	60	70	78	86
1	1.01E-02	9.99E-03	9.77E-03	9.38E-03	8.75E-03	7.77E-03	6.30E-03	4.15E-03	2.09E-03	5.12E-04
8	4.26E-04	4.24E-04	4.19E-04	4.10E-04	3.94E-04	3.71E-04	3.33E-04	2.69E-04	1.79E-04	4.27E-05
9	4.55E-05	4.41E-05	3.99E-05	3.35E-05	2.54E-05	1.67E-05	8.78E-06	3.17E-06	9.20E-07	1.52E-07
21	8.79E-06	8.66E-06	8.26E-06	7.60E-06	6.64E-06	5.35E-06	3.78E-06	2.05E-06	8.81E-07	2.03E-07
27	1.88E-01	1.88E-01	1.86E-01	1.84E-01	1.79E-01	1.71E-01	1.56E-01	1.26E-01	8.22E-02	1.79E-02
28	2.32E-02	2.32E-02	2.31E-02	2.28E-02	2.23E-02	2.14E-02	1.98E-02	1.64E-02	1.12E-02	2.63E-03
38	5.54E-05	5.46E-05	5.23E-05	4.84E-05	4.26E-05	3.48E-05	2.52E-05	1.42E-05	6.30E-06	1.48E-06
43	1.74E-03	1.73E-03	1.68E-03	1.61E-03	1.49E-03	1.31E-03	1.04E-03	6.69E-04	3.29E-04	8.35E-05
47	8.47E-07	8.28E-07	7.70E-07	6.80E-07	5.57E-07	4.09E-07	2.54E-07	1.16E-07	4.20E-08	7.98E-09
50	7.02E-06	6.88E-06	6.46E-06	5.78E-06	4.84E-06	3.66E-06	2.36E-06	1.12E-06	4.16E-07	7.73E-08
56	9.53E-07	9.36E-07	8.81E-07	7.94E-07	6.72E-07	5.19E-07	3.47E-07	1.75E-07	7.05E-08	1.52E-08
88	6.02E-06	5.94E-06	5.68E-06	5.25E-06	4.61E-06	3.75E-06	2.68E-06	1.49E-06	6.52E-07	1.53E-07
92	3.29E-06	3.22E-06	3.01E-06	2.68E-06	2.22E-06	1.66E-06	1.06E-06	4.98E-07	1.85E-07	3.60E-08
97	4.35E-05	4.28E-05	4.08E-05	3.74E-05	3.24E-05	2.58E-05	1.78E-05	9.29E-06	3.78E-06	7.90E-07
98	4.85E-05	4.80E-05	4.62E-05	4.32E-05	3.87E-05	3.23E-05	2.38E-05	1.37E-05	6.19E-06	1.51E-06
106	6.51E-06	6.36E-06	5.89E-06	5.16E-06	4.16E-06	2.98E-06	1.76E-06	7.29E-07	2.30E-07	3.57E-08
109	2.20E-05	2.15E-05	2.01E-05	1.79E-05	1.48E-05	1.11E-05	6.96E-06	3.20E-06	1.15E-06	2.10E-07
111	6.13E-06	5.98E-06	5.51E-06	4.78E-06	3.81E-06	2.69E-06	1.56E-06	6.43E-07	2.06E-07	3.39E-08
114	9.13E-05	9.06E-05	8.84E-05	8.45E-05	7.82E-05	6.87E-05	5.50E-05	3.58E-05	1.78E-05	4.29E-06
116	2.36E-04	2.35E-04	2.29E-04	2.19E-04	2.04E-04	1.80E-04	1.46E-04	9.67E-05	4.92E-05	1.16E-05
125	1.16E-06	1.12E-06	1.02E-06	8.55E-07	6.50E-07	4.28E-07	2.27E-07	8.20E-08	2.34E-08	3.59E-09
126	1.02E-06	9.94E-07	9.02E-07	7.62E-07	5.83E-07	3.88E-07	2.08E-07	7.70E-08	2.25E-08	3.51E-09
154	2.96E-05	2.93E-05	2.84E-05	2.69E-05	2.45E-05	2.09E-05	1.60E-05	9.75E-06	4.60E-06	1.16E-06
64	9.53E-07	9.36E-07	8.81E-07	7.94E-07	6.72E-07	5.19E-07	3.47E-07	1.75E-07	7.05E-08	1.52E-08
90	6.02E-06	5.94E-06	5.68E-06	5.25E-06	4.61E-06	3.75E-06	2.68E-06	1.49E-06	6.52E-07	1.53E-07
156	7.04E-04	6.99E-04	6.84E-04	6.57E-04	6.12E-04	5.44E-04	4.41E-04	2.91E-04	1.46E-04	3.58E-05
188	1.51E-04	1.50E-04	1.47E-04	1.41E-04	1.31E-04	1.17E-04	9.45E-05	6.23E-05	3.13E-05	7.68E-06
189	8.04E-04	7.99E-04	7.82E-04	7.51E-04	7.00E-04	6.21E-04	5.04E-04	3.32E-04	1.67E-04	4.09E-05
193	8.04E-04	7.99E-04	7.82E-04	7.51E-04	7.00E-04	6.21E-04	5.04E-04	3.32E-04	1.67E-04	4.09E-05
209	1.73E-01	1.73E-01	1.72E-01	1.69E-01	1.65E-01	1.57E-01	1.44E-01	1.16E-01	7.58E-02	1.65E-02
210	1.02E-01	1.01E-01	9.87E-02	9.48E-02	8.84E-02	7.84E-02	6.36E-02	4.19E-02	2.11E-02	5.17E-03
212	1.88E-01	1.87E-01	1.83E-01	1.75E-01	1.64E-01	1.45E-01	1.18E-01	7.77E-02	3.91E-02	9.57E-03
217	1.71E-01	1.70E-01	1.69E-01	1.67E-01	1.62E-01	1.55E-01	1.41E-01	1.15E-01	7.46E-02	1.63E-02
223	2.54E-02	2.51E-02	2.42E-02	2.26E-02	2.02E-02	1.69E-02	1.25E-02	7.17E-03	3.23E-03	7.88E-04

Appendix D

CAMx Mechanism 5: SAPRC07TC Gas-Phase Chemistry

Table D-1. Reactions and rate constants for the SAPRC07TC mechanism. k_{300} is the rate constant at 300 K and 1 atmosphere using units in molecules/cm³ and 1/s. See Table D-2 for species names. See Section 3.1 on temperature and pressure dependencies.

Number	Reactants and Products	Rate Constant Expression	k_{300}
1	NO ₂ = NO + O ₃ P	Photolysis	6.37E-3
2	O ₃ P + O ₂ + M = O ₃	$k = 5.68E-34 (T/300)^{-2.6}$	5.68E-34
3	O ₃ P + O ₃ =	$k = 8.00E-12 \exp(-2060/T)$	8.34E-15
4	O ₃ P + NO = NO ₂	Falloff: F=0.6; n=1 $k(0) = 9.00E-32 (T/300)^{-1.5}$ $k(\text{inf}) = 3.00E-11$	1.64E-12
5	O ₃ P + NO ₂ = NO	$k = 5.50E-12 \exp(188/T)$	1.03E-11
6	O ₃ P + NO ₂ = NO ₃	Falloff: F=0.6; n=1 $k(0) = 2.50E-31 (T/300)^{-1.8}$ $k(\text{inf}) = 2.20E-11 (T/300)^{-0.7}$	3.24E-12
7	O ₃ + NO = NO ₂	$k = 3.00E-12 \exp(-1500/T)$	2.02E-14
8	O ₃ + NO ₂ = NO ₃	$k = 1.40E-13 \exp(-2470/T)$	3.72E-17
9	NO + NO ₃ = 2. NO ₂	$k = 1.80E-11 \exp(110/T)$	2.60E-11
10	NO + NO + O ₂ = 2. NO ₂	$k = 3.30E-39 \exp(530/T)$	1.93E-38
11	NO ₂ + NO ₃ = N ₂ O ₅	Falloff: F=0.35; n=1.33 $k(0) = 3.60E-30 (T/300)^{-4.1}$ $k(\text{inf}) = 1.90E-12 (T/300)^{0.2}$	1.24E-12
12	N ₂ O ₅ = NO ₂ + NO ₃	Falloff: F=0.35; n=1.33 $k(0) = 1.30E-3 (T/300)^{-3.5} \exp(-11000/T)$ $k(\text{inf}) = 9.70E+14 (T/300)^{0.1} \exp(-11080/T)$	5.69E-2
13	N ₂ O ₅ + H ₂ O = 2. HNO ₃	$k = 1.00E-22$	1.00E-22
14	N ₂ O ₅ + H ₂ O + H ₂ O = 2. HNO ₃	$k = 0.00E+0$	0.00E+0
15	NO ₂ + NO ₃ = NO + NO ₂	$k = 4.50E-14 \exp(-1260/T)$	6.75E-16
16	NO ₃ = NO	Photolysis	1.98E-2
17	NO ₃ = NO ₂ + O ₃ P	Photolysis	1.56E-1
18	O ₃ = O ₁ D	Photolysis	9.47E-6
19	O ₃ = O ₃ P	Photolysis	3.40E-4
20	O ₁ D + H ₂ O = 2. OH	$k = 1.63E-10 \exp(60/T)$	1.99E-10
21	O ₁ D + M = O ₃ P	$k = 2.38E-11 \exp(96/T)$	3.28E-11
22	OH + NO = HONO	Falloff: F=0.6; n=1 $k(0) = 7.00E-31 (T/300)^{-2.6}$ $k(\text{inf}) = 3.60E-11 (T/300)^{-0.1}$	7.31E-12
23	HONO = OH + NO	Photolysis	9.88E-4
24	OH + HONO = NO ₂	$k = 2.50E-12 \exp(260/T)$	5.95E-12
25	OH + NO ₂ = HNO ₃	Falloff: F=0.6; n=1 $k(0) = 1.80E-30 (T/300)^{-3}$ $k(\text{inf}) = 2.80E-11$	1.05E-11
26	OH + NO ₃ = HO ₂ + NO ₂	$k = 2.00E-11$	2.00E-11
27	OH + HNO ₃ = NO ₃	$k = k_1 + k_3 [M] / (1 + k_3 [M] / k_2)$ $k_1 = 2.40E-14 \exp(460/T)$ $k_2 = 2.70E-17 \exp(2199/T)$ $k_3 = 6.50E-34 \exp(1335/T)$	1.51E-13
28	HNO ₃ = OH + NO ₂	Photolysis	2.55E-7

Number	Reactants and Products	Rate Constant Expression	k ₃₀₀
29	OH + CO = HO2 + CO2	k = k1 + k2 [M] k1 = 1.44E-13 k2 = 3.43E-33	2.28E-13
30	OH + O3 = HO2	k = 1.70E-12 exp(-940/T)	7.41E-14
31	HO2 + NO = OH + NO2	k = 3.60E-12 exp(270/T)	8.85E-12
32	HO2 + NO2 = PNA	Falloff: F=0.6; n=1 k(0) = 2.00E-31 (T/300) ^{-3.4} k(inf) = 2.90E-12 (T/300) ^{-1.1}	1.12E-12
33	PNA = HO2 + NO2	Falloff: F=0.6; n=1 k(0) = 3.72E-5 (T/300) ^{-2.4} exp(-10650/T) k(inf) = 5.42E+15 (T/300) ^{-2.3} exp(-11170/T)	1.07E-1
34	PNA = 0.61 HO2 + 0.61 NO2 + 0.39 OH + 0.39 NO3	Photolysis	3.17E-6
35	PNA + OH = NO2	k = 1.30E-12 exp(380/T)	4.61E-12
36	HO2 + O3 = OH	k = 2.03E-16 (T/300) ^{4.57} exp(693/T)	2.05E-15
37	HO2 + HO2 = H2O2	k = k1 + k2 [M] k1 = 2.20E-13 exp(600/T) k2 = 1.90E-33 exp(980/T)	2.84E-12
38	HO2 + HO2 + H2O = H2O2	k = k1 + k2 [M] k1 = 3.08E-34 exp(2800/T) k2 = 2.66E-54 exp(3180/T)	6.09E-30
39	NO3 + HO2 = 0.8 OH + 0.8 NO2 + 0.2 HNO3	k = 4.00E-12	4.00E-12
40	NO3 + NO3 = 2. NO2	k = 8.50E-13 exp(-2450/T)	2.41E-16
41	H2O2 = 2. OH	Photolysis	3.78E-6
42	H2O2 + OH = HO2	k = 1.80E-12	1.80E-12
43	OH + HO2 =	k = 4.80E-11 exp(250/T)	1.10E-10
44	OH + SO2 = HO2 + SULF	Falloff: F=0.6; n=1 k(0) = 3.30E-31 (T/300) ^{-4.3} k(inf) = 1.60E-12	9.49E-13
45	OH + H2 = HO2	k = 7.70E-12 exp(-2100/T)	7.02E-15
46	MEO2 + NO = NO2 + HCHO + HO2	k = 2.30E-12 exp(360/T)	7.64E-12
47	MEO2 + HO2 = COOH	k = 3.46E-13 (T/300) ^{0.36} exp(780/T)	4.66E-12
48	MEO2 + HO2 = HCHO	k = 3.34E-14 (T/300) ^{-3.53} exp(780/T)	4.50E-13
49	MEO2 + NO3 = HCHO + HO2 + NO2	k = 1.30E-12	1.30E-12
50	MEO2 + MEO2 = MEOH + HCHO	k = 6.39E-14 (T/300) ^{-1.8} exp(365/T)	2.16E-13
51	MEO2 + MEO2 = 2. HCHO + 2. HO2	k = 7.40E-13 exp(-520/T)	1.31E-13
52	RO2C + NO = NO2	k = 2.60E-12 exp(380/T)	9.23E-12
53	RO2C + HO2 =	k = 3.80E-13 exp(900/T)	7.63E-12
54	RO2C + NO3 = NO2	k = 2.30E-12	2.30E-12
55	RO2C + MEO2 = 0.5 HO2 + 0.75 HCHO + 0.25 MEOH	k = 2.00E-13	2.00E-13
56	RO2C + RO2C =	k = 3.50E-14	3.50E-14
57	RO2X + NO = XN	k = k(52)	9.23E-12
58	RO2X + HO2 =	k = k(53)	7.63E-12
59	RO2X + NO3 = NO2	k = k(54)	2.30E-12
60	RO2X + MEO2 = 0.5 HO2 + 0.75 HCHO + 0.25 MEOH	k = k(55)	2.00E-13
61	RO2X + RO2C =	k = k(56)	3.50E-14
62	RO2X + RO2X =	k = k(56)	3.50E-14

Number	Reactants and Products	Rate Constant Expression	k ₃₀₀
63	MCO3 + NO2 = PAN	Falloff: F=0.3; n=1.41 k(0) = 2.70E-28 (T/300) ^{-7.1} k(inf) = 1.21E-11 (T/300) ^{-0.9}	9.38E-12
64	PAN = MCO3 + NO2	Falloff: F=0.3; n=1.41 k(0) = 4.90E-3 exp(-12100/T) k(inf) = 4.00E+16 exp(-13600/T)	6.27E-4
65	PAN = 0.6 MCO3 + 0.6 NO2 + 0.4 MEO2 + 0.4 CO2 + 0.4 NO3	Photolysis	3.50E-7
66	MCO3 + NO = MEO2 + CO2 + NO2	k = 7.50E-12 exp(290/T)	1.97E-11
67	MCO3 + HO2 = 0.7 CO3H + 0.3 AACD + 0.3 O3	k = 5.20E-13 exp(980/T)	1.36E-11
68	MCO3 + NO3 = MEO2 + CO2 + NO2	k = k(54)	2.30E-12
69	MCO3 + MEO2 = 0.1 AACD + HCHO + 0.9 HO2 + 0.9 MEO2 + 0.9 CO2	k = 2.00E-12 exp(500/T)	1.06E-11
70	MCO3 + RO2C = MEO2 + CO2	k = 4.40E-13 exp(1070/T)	1.56E-11
71	MCO3 + RO2X = MEO2 + CO2	k = k(70)	1.56E-11
72	MCO3 + MCO3 = 2. MEO2 + 2. CO2	k = 2.90E-12 exp(500/T)	1.54E-11
73	RCO3 + NO2 = PAN2	k = 1.21E-11 (T/300) ^{-1.07}	1.21E-11
74	PAN2 = RCO3 + NO2	k = 8.30E+16 exp(-13940/T)	5.48E-4
75	PAN2 = 0.6 RCO3 + 0.6 NO2 + 0.4 RO2C + 0.4 XHO2 + 0.4 YRPX + 0.4 XCCH + 0.4 CO2 + 0.4 NO3	Photolysis	3.50E-7
76	RCO3 + NO = NO2 + RO2C + XHO2 + YRPX + XCCH + CO2	k = 6.70E-12 exp(340/T)	2.08E-11
77	RCO3 + HO2 = 0.75 RO3H + 0.25 PACD + 0.25 O3	k = k(67)	1.36E-11
78	RCO3 + NO3 = NO2 + RO2C + XHO2 + YRPX + XCCH + CO2	k = k(54)	2.30E-12
79	RCO3 + MEO2 = HCHO + HO2 + RO2C + XHO2 + XCCH + YRPX + CO2	k = k(69)	1.06E-11
80	RCO3 + RO2C = RO2C + XHO2 + XCCH + YRPX + CO2	k = k(70)	1.56E-11
81	RCO3 + RO2X = RO2C + XHO2 + XCCH + YRPX + CO2	k = k(70)	1.56E-11
82	RCO3 + MCO3 = 2. CO2 + MEO2 + RO2C + XHO2 + YRPX + XCCH	k = k(72)	1.54E-11
83	RCO3 + RCO3 = 2. RO2C + 2. XHO2 + 2. XCCH + 2. YRPX + 2. CO2	k = k(72)	1.54E-11
84	BZC3 + NO2 = PBZN	k = 1.37E-11	1.37E-11
85	PBZN = BZC3 + NO2	k = 7.90E+16 exp(-14000/T)	4.27E-4
86	PBZN = 0.6 BZC3 + 0.6 NO2 + 0.4 CO2 + 0.4 BZO + 0.4 RO2C + 0.4 NO3	Photolysis	3.50E-7
87	BZC3 + NO = NO2 + CO2 + BZO + RO2C	k = k(76)	2.08E-11
88	BZC3 + HO2 = 0.75 RO3H + 0.25 PACD + 0.25 O3 + 4. XC	k = k(67)	1.36E-11
89	BZC3 + NO3 = NO2 + CO2 + BZO + RO2C	k = k(54)	2.30E-12
90	BZC3 + MEO2 = HCHO + HO2 + RO2C + BZO + CO2	k = k(69)	1.06E-11
91	BZC3 + RO2C = RO2C + BZO + CO2	k = k(70)	1.56E-11
92	BZC3 + RO2X = RO2C + BZO + CO2	k = k(70)	1.56E-11
93	BZC3 + MCO3 = 2. CO2 + MEO2 + BZO + RO2C	k = k(72)	1.54E-11

Number	Reactants and Products	Rate Constant Expression	k ₃₀₀
94	BZC3 + RCO3 = 2. CO2 + 2. RO2C + XHO2 + YRPX + XCCH + BZO	k = k(72)	1.54E-11
95	BZC3 + BZC3 = 2. BZO + 2. RO2C + 2. CO2	k = k(72)	1.54E-11
96	MAC3 + NO2 = MPAN	k = k(73)	1.21E-11
97	MPAN = MAC3 + NO2	k = 1.60E+16 exp(-13486/T)	4.80E-4
98	MPAN = 0.6 MAC3 + 0.6 NO2 + 0.4 CO2 + 0.4 HCHO + 0.4 MCO3 + 0.4 NO3	Photolysis	3.50E-7
99	MAC3 + NO = NO2 + CO2 + HCHO + MCO3	k = k(76)	2.08E-11
100	MAC3 + HO2 = 0.75 RO3H + 0.25 PACD + 0.25 O3 + XC	k = k(67)	1.36E-11
101	MAC3 + NO3 = NO2 + CO2 + HCHO + MCO3	k = k(54)	2.30E-12
102	MAC3 + MEO2 = 2. HCHO + HO2 + CO2 + MCO3	k = k(69)	1.06E-11
103	MAC3 + RO2C = CO2 + HCHO + MCO3	k = k(70)	1.56E-11
104	MAC3 + RO2X = CO2 + HCHO + MCO3	k = k(70)	1.56E-11
105	MAC3 + MCO3 = 2. CO2 + MEO2 + HCHO + MCO3	k = k(72)	1.54E-11
106	MAC3 + RCO3 = HCHO + MCO3 + RO2C + XHO2 + YRPX + XCCH + 2. CO2	k = k(72)	1.54E-11
107	MAC3 + BZC3 = HCHO + MCO3 + BZO + RO2C + 2. CO2	k = k(72)	1.54E-11
108	MAC3 + MAC3 = 2. HCHO + 2. MCO3 + 2. CO2	k = k(72)	1.54E-11
109	TBUO + NO2 = RNO3 - 2. XC	k = 2.40E-11	2.40E-11
110	TBUO = ACET + MEO2	k = 7.50E+14 exp(-8152/T)	1.19E+3
111	BZO + NO2 = NPHE	k = 2.30E-11 exp(150/T)	3.79E-11
112	BZO + HO2 = CRES - 1. XC	k = k(53)	7.63E-12
113	BZO = CRES + RO2C + XHO2 - 1. XC	k = 1.00E-3	1.00E-3
114	XHO2 + NO = NO + HO2	k = k(52)	9.23E-12
115	XHO2 + HO2 = HO2	k = k(53)	7.63E-12
116	XHO2 + NO3 = NO3 + HO2	k = k(54)	2.30E-12
117	XHO2 + MEO2 = MEO2 + 0.5 HO2	k = k(55)	2.00E-13
118	XHO2 + RO2C = RO2C + 0.5 HO2	k = k(56)	3.50E-14
119	XHO2 + RO2X = RO2X + 0.5 HO2	k = k(56)	3.50E-14
120	XHO2 + MCO3 = MCO3 + HO2	k = k(70)	1.56E-11
121	XHO2 + RCO3 = RCO3 + HO2	k = k(70)	1.56E-11
122	XHO2 + BZC3 = BZC3 + HO2	k = k(70)	1.56E-11
123	XHO2 + MAC3 = MAC3 + HO2	k = k(70)	1.56E-11
124	XOH + NO = NO + OH	k = k(52)	9.23E-12
125	XOH + HO2 = HO2	k = k(53)	7.63E-12
126	XOH + NO3 = NO3 + OH	k = k(54)	2.30E-12
127	XOH + MEO2 = MEO2 + 0.5 OH	k = k(55)	2.00E-13
128	XOH + RO2C = RO2C + 0.5 OH	k = k(56)	3.50E-14
129	XOH + RO2X = RO2X + 0.5 OH	k = k(56)	3.50E-14
130	XOH + MCO3 = MCO3 + OH	k = k(70)	1.56E-11
131	XOH + RCO3 = RCO3 + OH	k = k(70)	1.56E-11
132	XOH + BZC3 = BZC3 + OH	k = k(70)	1.56E-11
133	XOH + MAC3 = MAC3 + OH	k = k(70)	1.56E-11
134	XNO2 + NO = NO + NO2	k = k(52)	9.23E-12
135	XNO2 + HO2 = HO2 + XN	k = k(53)	7.63E-12
136	XNO2 + NO3 = NO3 + NO2	k = k(54)	2.30E-12
137	XNO2 + MEO2 = MEO2 + 0.5 NO2 + 0.5 XN	k = k(55)	2.00E-13

Number	Reactants and Products	Rate Constant Expression	k ₃₀₀
138	XNO2 + RO2C = RO2C + 0.5 NO2 + 0.5 XN	k = k(56)	3.50E-14
139	XNO2 + RO2X = RO2X + 0.5 NO2 + 0.5 XN	k = k(56)	3.50E-14
140	XNO2 + MCO3 = MCO3 + NO2	k = k(70)	1.56E-11
141	XNO2 + RCO3 = RCO3 + NO2	k = k(70)	1.56E-11
142	XNO2 + BZC3 = BZC3 + NO2	k = k(70)	1.56E-11
143	XNO2 + MAC3 = MAC3 + NO2	k = k(70)	1.56E-11
144	XMEO + NO = NO + MEO2	k = k(52)	9.23E-12
145	XMEO + HO2 = HO2 + XC	k = k(53)	7.63E-12
146	XMEO + NO3 = NO3 + MEO2	k = k(54)	2.30E-12
147	XMEO + MEO2 = 1.5 MEO2 + 0.5 XC	k = k(55)	2.00E-13
148	XMEO + RO2C = RO2C + 0.5 MEO2 + 0.5 XC	k = k(56)	3.50E-14
149	XMEO + RO2X = RO2X + 0.5 MEO2 + 0.5 XC	k = k(56)	3.50E-14
150	XMEO + MCO3 = MCO3 + MEO2	k = k(70)	1.56E-11
151	XMEO + RCO3 = RCO3 + MEO2	k = k(70)	1.56E-11
152	XMEO + BZC3 = BZC3 + MEO2	k = k(70)	1.56E-11
153	XMEO + MAC3 = MAC3 + MEO2	k = k(70)	1.56E-11
154	XMC3 + NO = NO + MCO3	k = k(52)	9.23E-12
155	XMC3 + HO2 = HO2 + 2. XC	k = k(53)	7.63E-12
156	XMC3 + NO3 = NO3 + MCO3	k = k(54)	2.30E-12
157	XMC3 + MEO2 = MEO2 + 0.5 MCO3 + XC	k = k(55)	2.00E-13
158	XMC3 + RO2C = RO2C + 0.5 MCO3 + XC	k = k(56)	3.50E-14
159	XMC3 + RO2X = RO2X + 0.5 MCO3 + XC	k = k(56)	3.50E-14
160	XMC3 + MCO3 = 2. MCO3	k = k(70)	1.56E-11
161	XMC3 + RCO3 = RCO3 + MCO3	k = k(70)	1.56E-11
162	XMC3 + BZC3 = BZC3 + MCO3	k = k(70)	1.56E-11
163	XMC3 + MAC3 = MAC3 + MCO3	k = k(70)	1.56E-11
164	XRC3 + NO = NO + RCO3	k = k(52)	9.23E-12
165	XRC3 + HO2 = HO2 + 3. XC	k = k(53)	7.63E-12
166	XRC3 + NO3 = NO3 + RCO3	k = k(54)	2.30E-12
167	XRC3 + MEO2 = MEO2 + 0.5 RCO3 + 1.5 XC	k = k(55)	2.00E-13
168	XRC3 + RO2C = RO2C + 0.5 RCO3 + 1.5 XC	k = k(56)	3.50E-14
169	XRC3 + RO2X = RO2X + 0.5 RCO3 + 1.5 XC	k = k(56)	3.50E-14
170	XRC3 + MCO3 = MCO3 + RCO3	k = k(70)	1.56E-11
171	XRC3 + RCO3 = 2. RCO3	k = k(70)	1.56E-11
172	XRC3 + BZC3 = BZC3 + RCO3	k = k(70)	1.56E-11
173	XRC3 + MAC3 = MAC3 + RCO3	k = k(70)	1.56E-11
174	XMA3 + NO = NO + MAC3	k = k(52)	9.23E-12
175	XMA3 + HO2 = HO2 + 4. XC	k = k(53)	7.63E-12
176	XMA3 + NO3 = NO3 + MAC3	k = k(54)	2.30E-12
177	XMA3 + MEO2 = MEO2 + 0.5 MAC3 + 2. XC	k = k(55)	2.00E-13
178	XMA3 + RO2C = RO2C + 0.5 MAC3 + 2. XC	k = k(56)	3.50E-14
179	XMA3 + RO2X = RO2X + 0.5 MAC3 + 2. XC	k = k(56)	3.50E-14
180	XMA3 + MCO3 = MCO3 + MAC3	k = k(70)	1.56E-11
181	XMA3 + RCO3 = RCO3 + MAC3	k = k(70)	1.56E-11
182	XMA3 + BZC3 = BZC3 + MAC3	k = k(70)	1.56E-11
183	XMA3 + MAC3 = 2. MAC3	k = k(70)	1.56E-11
184	XTBU + NO = NO + TBUO	k = k(52)	9.23E-12
185	XTBU + HO2 = HO2 + 4. XC	k = k(53)	7.63E-12
186	XTBU + NO3 = NO3 + TBUO	k = k(54)	2.30E-12
187	XTBU + MEO2 = MEO2 + 0.5 TBUO + 2. XC	k = k(55)	2.00E-13
188	XTBU + RO2C = RO2C + 0.5 TBUO + 2. XC	k = k(56)	3.50E-14

Number	Reactants and Products	Rate Constant Expression	k ₃₀₀
189	XTBU + RO2X = RO2X + 0.5 TBUO + 2. XC	k = k(56)	3.50E-14
190	XTBU + MCO3 = MCO3 + TBUO	k = k(70)	1.56E-11
191	XTBU + RCO3 = RCO3 + TBUO	k = k(70)	1.56E-11
192	XTBU + BZC3 = BZC3 + TBUO	k = k(70)	1.56E-11
193	XTBU + MAC3 = MAC3 + TBUO	k = k(70)	1.56E-11
194	XCO + NO = NO + CO	k = k(52)	9.23E-12
195	XCO + HO2 = HO2 + XC	k = k(53)	7.63E-12
196	XCO + NO3 = NO3 + CO	k = k(54)	2.30E-12
197	XCO + MEO2 = MEO2 + 0.5 CO + 0.5 XC	k = k(55)	2.00E-13
198	XCO + RO2C = RO2C + 0.5 CO + 0.5 XC	k = k(56)	3.50E-14
199	XCO + RO2X = RO2X + 0.5 CO + 0.5 XC	k = k(56)	3.50E-14
200	XCO + MCO3 = MCO3 + CO	k = k(70)	1.56E-11
201	XCO + RCO3 = RCO3 + CO	k = k(70)	1.56E-11
202	XCO + BZC3 = BZC3 + CO	k = k(70)	1.56E-11
203	XCO + MAC3 = MAC3 + CO	k = k(70)	1.56E-11
204	HCHO = 2. HO2 + CO	Photolysis	1.78E-5
205	HCHO = CO	Photolysis	2.38E-5
206	HCHO + OH = HO2 + CO	k = 5.40E-12 exp(135/T)	8.47E-12
207	HCHO + NO3 = HNO3 + HO2 + CO	k = 2.00E-12 exp(-2431/T)	6.05E-16
208	CCHO + OH = MCO3	k = 4.40E-12 exp(365/T)	1.49E-11
209	CCHO = CO + HO2 + MEO2	Photolysis	1.77E-6
210	CCHO + NO3 = HNO3 + MCO3	k = 1.40E-12 exp(-1860/T)	2.84E-15
211	RCHO + OH = 0.965 RCO3 + 0.035 RO2C + 0.035 XHO2 + 0.035 XCO + 0.035 XCCH + 0.035 YRPX	k = 5.10E-12 exp(405/T)	1.97E-11
212	RCHO = RO2C + XHO2 + YRPX + XCCH + CO + HO2	Photolysis	6.95E-6
213	RCHO + NO3 = HNO3 + RCO3	k = 1.40E-12 exp(-1601/T)	6.74E-15
214	ACET + OH = RO2C + XMC3 + XHCH + YRPX	k = 4.56E-14 (T/300)^3.65 exp(429/T)	1.91E-13
215	ACET = 0.62 MCO3 + 1.38 MEO2 + 0.38 CO	Photolysis	1.04E-7
216	MEK + OH = 0.967 RO2C + 0.039 RO2X + 0.039 ZRN3 + 0.376 XHO2 + 0.51 XMC3 + 0.074 XRC3 + 0.088 XHCH + 0.504 XCCH + 0.376 XRCH + YRPX + 0.3 XC	k = 1.30E-12 (T/300)^2 exp(-25/T)	1.20E-12
217	MEK = MCO3 + RO2C + XHO2 + XCCH + YRPX	Photolysis	8.13E-7
218	MEOH + OH = HCHO + HO2	k = 2.85E-12 exp(-345/T)	9.02E-13
219	FACD + OH = HO2 + CO2	k = 4.50E-13	4.50E-13
220	AACD + OH = 0.509 MEO2 + 0.491 RO2C + 0.509 CO2 + 0.491 XHO2 + 0.491 XMGL + 0.491 YRPX - 0.491 XC	k = 4.20E-14 exp(855/T)	7.26E-13
221	PACD + OH = RO2C + XHO2 + 0.143 CO2 + 0.142 XCCH + 0.4 XRCH + 0.457 XBAC + YRPX - 0.455 XC	k = 1.20E-12	1.20E-12
222	COOH + OH = 0.3 HCHO + 0.3 OH + 0.7 MEO2	k = 3.80E-12 exp(200/T)	7.40E-12
223	COOH = HCHO + HO2 + OH	Photolysis	2.72E-6
224	ROOH + OH = 0.744 OH + 0.251 RO2C + 0.004 RO2X + 0.004 ZRN3 + 0.744 RCHO + 0.239 XHO2 + 0.012 XOH + 0.012 XHCH + 0.012 XCCH + 0.205 XRCH + 0.034 XPD2 + 0.256 YRPX - 0.115 XC	k = 2.50E-11	2.50E-11
225	ROOH = RCHO + HO2 + OH	Photolysis	2.72E-6

Number	Reactants and Products	Rate Constant Expression	k ₃₀₀
226	R6PX + OH = 0.84 OH + 0.222 RO2C + 0.029 RO2X + 0.029 ZRN3 + 0.84 PRD2 + 0.09 XHO2 + 0.041 XOH + 0.02 XCCH + 0.075 XRCH + 0.084 XPD2 + 0.16 YRPX + 0.02 XC	k = 5.60E-11	5.60E-11
227	R6PX = OH + 0.142 HO2 + 0.782 RO2C + 0.077 RO2X + 0.077 ZRN3 + 0.085 RCHO + 0.142 PRD2 + 0.782 XHO2 + 0.026 XCCH + 0.058 XRCH + 0.698 XPD2 + 0.858 Y6PX + 0.017 XC	Photolysis	2.72E-6
228	RAPX + OH = 0.139 OH + 0.148 HO2 + 0.589 RO2C + 0.124 RO2X + 0.124 ZRN3 + 0.074 PRD2 + 0.147 MGLY + 0.139 IPRD + 0.565 XHO2 + 0.024 XOH + 0.448 XRCH + 0.026 XGLY + 0.03 XMEK + 0.252 XMGL + 0.073 XAF1 + 0.073 XAF2 + 0.713 Y6PX + 2.674 XC	k = 1.41E-10	1.41E-10
229	RAPX = OH + HO2 + 0.5 GLY + 0.5 MGLY + 0.5 AFG1 + 0.5 AFG2 + 0.5 XC	Photolysis	2.72E-6
230	GLY = 2. CO + 2. HO2	Photolysis	7.88E-5
231	GLY = HCHO + CO	Photolysis	2.23E-5
232	GLY + OH = 0.63 HO2 + 1.26 CO + 0.37 RCO3 - 0.37 XC	k = 1.10E-11	1.10E-11
233	GLY + NO3 = HNO3 + 0.63 HO2 + 1.26 CO + 0.37 RCO3 - 0.37 XC	k = 2.80E-12 exp(-2376/T)	1.02E-15
234	MGLY = HO2 + CO + MCO3	Photolysis	1.39E-4
235	MGLY + OH = CO + MCO3	k = 1.50E-11	1.50E-11
236	MGLY + NO3 = HNO3 + CO + MCO3	k = 1.40E-12 exp(-1895/T)	2.53E-15
237	BACL = 2. MCO3	Photolysis	2.45E-4
238	CRES + OH = 0.2 BZO + 0.8 RO2C + 0.8 XHO2 + 0.8 Y6PX + 0.25 XMGL + 5.05 XC	k = 1.70E-12 exp(950/T)	4.03E-11
239	CRES + NO3 = HNO3 + BZO + XC	k = 1.40E-11	1.40E-11
240	NPHE + OH = BZO + XN	k = 3.50E-12	3.50E-12
241	NPHE = HONO + 6. XC	Photolysis	9.55E-6
242	NPHE = 6. XC + XN	Photolysis	9.55E-5
243	BALD + OH = BZC3	k = 1.20E-11	1.20E-11
244	BALD = 7. XC	Photolysis	2.48E-5
245	BALD + NO3 = HNO3 + BZC3	k = 1.34E-12 exp(-1860/T)	2.72E-15
246	AFG1 + OH = 0.217 MAC3 + 0.723 RO2C + 0.06 RO2X + 0.06 ZRN3 + 0.521 XHO2 + 0.201 XMC3 + 0.334 XCO + 0.407 XRCH + 0.129 XMEK + 0.107 XGLY + 0.267 XMGL + 0.783 Y6PX + 0.284 XC	k = 7.40E-11	7.40E-11
247	AFG1 + O3 = 0.826 OH + 0.522 HO2 + 0.652 RO2C + 0.522 CO + 0.174 CO2 + 0.432 GLY + 0.568 MGLY + 0.652 XRC3 + 0.652 XHCH + 0.652 Y6PX - 0.872 XC	k = 9.66E-18	9.66E-18
248	AFG1 = 1.023 HO2 + 0.173 MEO2 + 0.305 MCO3 + 0.5 MAC3 + 0.695 CO + 0.195 GLY + 0.305 MGLY + 0.217 XC	Photolysis	3.07E-3
249	AFG2 + OH = 0.217 MAC3 + 0.723 RO2C + 0.06 RO2X + 0.06 ZRN3 + 0.521 XHO2 + 0.201 XMC3 + 0.334 XCO + 0.407 XRCH + 0.129 XMEK + 0.107 XGLY + 0.267 XMGL + 0.783 Y6PX + 0.284 XC	k = 7.40E-11	7.40E-11

Number	Reactants and Products	Rate Constant Expression	k ₃₀₀
250	AFG2 + O3 = 0.826 OH + 0.522 HO2 + 0.652 RO2C + 0.522 CO + 0.174 CO2 + 0.432 GLY + 0.568 MGLY + 0.652 XRC3 + 0.652 XHCH + 0.652 Y6PX - 0.872 XC	k = 9.66E-18	9.66E-18
251	AFG2 = PRD2 - 1. XC	Photolysis	3.07E-3
252	AFG3 + OH = 0.206 MAC3 + 0.733 RO2C + 0.117 RO2X + 0.117 ZRN3 + 0.561 XHO2 + 0.117 XMC3 + 0.114 XCO + 0.274 XGLY + 0.153 XMGL + 0.019 XBAC + 0.195 XAF1 + 0.195 XAF2 + 0.231 XIPR + 0.794 Y6PX + 0.938 XC	k = 9.35E-11	9.35E-11
253	AFG3 + O3 = 0.471 OH + 0.554 HO2 + 0.013 MCO3 + 0.258 RO2C + 0.007 RO2X + 0.007 ZRN3 + 0.58 CO + 0.19 CO2 + 0.366 GLY + 0.184 MGLY + 0.35 AFG1 + 0.35 AFG2 + 0.139 AFG3 + 0.003 MACR + 0.004 MVK + 0.003 IPRD + 0.095 XHO2 + 0.163 XRC3 + 0.163 XHCH + 0.095 XMGL + 0.264 Y6PX - 0.575 XC	k = 1.43E-17	1.43E-17
254	MACR + OH = 0.5 MAC3 + 0.5 RO2C + 0.5 XHO2 + 0.416 XCO + 0.084 XHCH + 0.416 XMEK + 0.084 XMGL + 0.5 YRPX - 0.416 XC	k = 8.00E-12 exp(380/T)	2.84E-11
255	MACR + O3 = 0.208 OH + 0.108 HO2 + 0.1 RO2C + 0.45 CO + 0.117 CO2 + 0.1 HCHO + 0.9 MGLY + 0.333 FACD + 0.1 XRC3 + 0.1 XHCH + 0.1 YRPX - 0.1 XC	k = 1.40E-15 exp(-2100/T)	1.28E-18
256	MACR + NO3 = 0.5 MAC3 + 0.5 RO2C + 0.5 HNO3 + 0.5 XHO2 + 0.5 XCO + 0.5 YRPX + 1.5 XC + 0.5 XN	k = 1.50E-12 exp(-1815/T)	3.54E-15
257	MACR + O3P = RCHO + XC	k = 6.34E-12	6.34E-12
258	MACR = 0.33 OH + 0.67 HO2 + 0.34 MCO3 + 0.33 MAC3 + 0.33 RO2C + 0.67 CO + 0.34 HCHO + 0.33 XMC3 + 0.33 XHCH + 0.33 YRPX	Photolysis	1.39E-6
259	MVK + OH = 0.975 RO2C + 0.025 RO2X + 0.025 ZRN3 + 0.3 XHO2 + 0.675 XMC3 + 0.3 XHCH + 0.675 XGLD + 0.3 XMGL + YRPX - 0.05 XC	k = 2.60E-12 exp(610/T)	1.99E-11
260	MVK + O3 = 0.164 OH + 0.064 HO2 + 0.05 RO2C + 0.05 XHO2 + 0.475 CO + 0.124 CO2 + 0.05 HCHO + 0.95 MGLY + 0.351 FACD + 0.05 XRC3 + 0.05 XHCH + 0.05 YRPX - 0.05 XC	k = 8.50E-16 exp(-1520/T)	5.36E-18
261	MVK + O3P = 0.45 RCHO + 0.55 MEK + 0.45 XC	k = 4.32E-12	4.32E-12
262	MVK = 0.4 MEO2 + 0.6 CO + 0.6 PRD2 + 0.4 MAC3 - 2.2 XC	Photolysis	5.25E-7
263	IPRD + OH = 0.289 MAC3 + 0.67 RO2C + 0.67 XHO2 + 0.041 RO2X + 0.041 ZRN3 + 0.336 XCO + 0.055 XHCH + 0.129 XGLD + 0.013 XRCH + 0.15 XMEK + 0.332 XPD2 + 0.15 XGLY + 0.174 XMGL - 0.504 XC + 0.711 Y6PX	k = 6.19E-11	6.19E-11
264	IPRD + O3 = 0.285 OH + 0.4 HO2 + 0.048 RO2C + 0.048 XRC3 + 0.498 CO + 0.14 CO2 + 0.124 HCHO + 0.21 MEK + 0.023 GLY + 0.742 MGLY + 0.1 FACD + 0.372 PACD + 0.047 XGLD + 0.001 XHCH + 0.048 Y6PX - 0.329 XC	k = 4.18E-18	4.18E-18

Number	Reactants and Products	Rate Constant Expression	k ₃₀₀
265	IPRD + NO ₃ = 0.15 MAC ₃ + 0.15 HNO ₃ + 0.799 RO ₂ C + 0.799 XHO ₂ + 0.051 RO ₂ X + 0.051 ZRN ₃ + 0.572 XCO + 0.227 XHCH + 0.218 XRCH + 0.008 XMGL + 0.572 XRN ₃ + 0.85 Y6PX + 0.278 XN - 0.815 XC	k = 1.00E-13	1.00E-13
266	IPRD = 1.233 HO ₂ + 0.467 MCO ₃ + 0.3 RCO ₃ + 1.233 CO + 0.3 HCHO + 0.467 GLYD + 0.233 MEK - 0.233 XC	Photolysis	1.39E-6
267	PRD ₂ + OH = 0.472 HO ₂ + 0.379 XHO ₂ + 0.029 XMC ₃ + 0.049 XRC ₃ + 0.473 RO ₂ C + 0.071 RO ₂ X + 0.071 ZRN ₃ + 0.002 HCHO + 0.211 XHCH + 0.001 CCHO + 0.083 XCCH + 0.143 RCHO + 0.402 XRCH + 0.115 XMEK + 0.329 PRD ₂ + 0.007 XPD ₂ + 0.528 Y6PX + 0.877 XC	k = 1.55E-11	1.55E-11
268	PRD ₂ = 0.913 XHO ₂ + 0.4 MCO ₃ + 0.6 RCO ₃ + 1.59 RO ₂ C + 0.087 RO ₂ X + 0.087 ZRN ₃ + 0.303 XHCH + 0.163 XCCH + 0.78 XRCH + Y6PX - 0.091 XC	Photolysis	2.26E-8
269	RNO ₃ + OH = 0.189 HO ₂ + 0.305 XHO ₂ + 0.019 NO ₂ + 0.313 XNO ₂ + 0.976 RO ₂ C + 0.175 RO ₂ X + 0.175 ZRN ₃ + 0.011 XHCH + 0.429 XCCH + 0.001 RCHO + 0.036 XRCH + 0.004 XACE + 0.01 MEK + 0.17 XMEK + 0.008 PRD ₂ + 0.031 XPD ₂ + 0.189 RNO ₃ + 0.305 XRN ₃ + 0.157 YRPX + 0.636 Y6PX + 0.174 XN + 0.04 XC	k = 7.20E-12	7.20E-12
270	RNO ₃ = 0.344 HO ₂ + 0.554 XHO ₂ + NO ₂ + 0.721 RO ₂ C + 0.102 RO ₂ X + 0.102 ZRN ₃ + 0.074 HCHO + 0.061 XHCH + 0.214 CCHO + 0.23 XCCH + 0.074 RCHO + 0.063 XRCH + 0.008 XACE + 0.124 MEK + 0.083 XMEK + 0.19 PRD ₂ + 0.261 XPD ₂ + 0.066 YRPX + 0.591 Y6PX + 0.396 XC	Photolysis	1.20E-6
271	GLYD + OH = MCO ₃	k = k(208)	1.49E-11
272	GLYD = CO + 2. HO ₂ + HCHO	Photolysis	2.75E-6
273	GLYD + NO ₃ = HNO ₃ + MCO ₃	k = k(210)	2.84E-15
274	ACRO + OH = 0.25 XHO ₂ + 0.75 MAC ₃ + 0.25 RO ₂ C + 0.167 XCO + 0.083 XHCH + 0.167 XCCH + 0.083 XGLY + 0.25 YRPX - 0.75 XC	k = 1.99E-11	1.99E-11
275	ACRO + O ₃ = 0.83 HO ₂ + 0.33 OH + 1.005 CO + 0.31 CO ₂ + 0.5 HCHO + 0.185 FACD + 0.5 GLY	k = 1.40E-15 exp(-2528/T)	3.07E-19
276	ACRO + NO ₃ = 0.031 XHO ₂ + 0.967 MAC ₃ + 0.031 RO ₂ C + 0.002 RO ₂ X + 0.002 ZRN ₃ + 0.967 HNO ₃ + 0.031 XCO + 0.031 XRN ₃ + 0.033 YRPX + 0.002 XN - 1.097 XC	k = 1.18E-15	1.18E-15
277	ACRO + O ₃ P = RCHO	k = 2.37E-12	2.37E-12
278	ACRO = 1.066 HO ₂ + 0.178 OH + 0.234 MEO ₂ + 0.33 MAC ₃ + 1.188 CO + 0.102 CO ₂ + 0.34 HCHO + 0.05 AACD - 0.284 XC	Photolysis	1.28E-6
279	CO ₃ H + OH = 0.98 MCO ₃ + 0.02 RO ₂ C + 0.02 CO ₂ + 0.02 XOH + 0.02 XHCH + 0.02 YRPX	k = 5.28E-12	5.28E-12
280	CO ₃ H = MEO ₂ + CO ₂ + OH	Photolysis	3.60E-7

Number	Reactants and Products	Rate Constant Expression	k ₃₀₀
281	RO3H + OH = 0.806 RCO3 + 0.194 RO2C + 0.194 YRPX + 0.11 CO2 + 0.11 XOH + 0.11 XCCH + 0.084 XHO2 + 0.084 XRCH	k = 6.42E-12	6.42E-12
282	RO3H = XHO2 + XCCH + YRPX + CO2 + OH	Photolysis	3.60E-7
283	XHCH + NO = NO + HCHO	k = k(52)	9.23E-12
284	XHCH + HO2 = HO2 + XC	k = k(53)	7.63E-12
285	XHCH + NO3 = NO3 + HCHO	k = k(54)	2.30E-12
286	XHCH + MEO2 = MEO2 + 0.5 HCHO + 0.5 XC	k = k(55)	2.00E-13
287	XHCH + RO2C = RO2C + 0.5 HCHO + 0.5 XC	k = k(56)	3.50E-14
288	XHCH + RO2X = RO2X + 0.5 HCHO + 0.5 XC	k = k(56)	3.50E-14
289	XHCH + MCO3 = MCO3 + HCHO	k = k(70)	1.56E-11
290	XHCH + RCO3 = RCO3 + HCHO	k = k(70)	1.56E-11
291	XHCH + BZC3 = BZC3 + HCHO	k = k(70)	1.56E-11
292	XHCH + MAC3 = MAC3 + HCHO	k = k(70)	1.56E-11
293	XCCH + NO = NO + CCHO	k = k(52)	9.23E-12
294	XCCH + HO2 = HO2 + 2. XC	k = k(53)	7.63E-12
295	XCCH + NO3 = NO3 + CCHO	k = k(54)	2.30E-12
296	XCCH + MEO2 = MEO2 + 0.5 CCHO + XC	k = k(55)	2.00E-13
297	XCCH + RO2C = RO2C + 0.5 CCHO + XC	k = k(56)	3.50E-14
298	XCCH + RO2X = RO2X + 0.5 CCHO + XC	k = k(56)	3.50E-14
299	XCCH + MCO3 = MCO3 + CCHO	k = k(70)	1.56E-11
300	XCCH + RCO3 = RCO3 + CCHO	k = k(70)	1.56E-11
301	XCCH + BZC3 = BZC3 + CCHO	k = k(70)	1.56E-11
302	XCCH + MAC3 = MAC3 + CCHO	k = k(70)	1.56E-11
303	XRCH + NO = NO + RCHO	k = k(52)	9.23E-12
304	XRCH + HO2 = HO2 + 3. XC	k = k(53)	7.63E-12
305	XRCH + NO3 = NO3 + RCHO	k = k(54)	2.30E-12
306	XRCH + MEO2 = MEO2 + 0.5 RCHO + 1.5 XC	k = k(55)	2.00E-13
307	XRCH + RO2C = RO2C + 0.5 RCHO + 1.5 XC	k = k(56)	3.50E-14
308	XRCH + RO2X = RO2X + 0.5 RCHO + 1.5 XC	k = k(56)	3.50E-14
309	XRCH + MCO3 = MCO3 + RCHO	k = k(70)	1.56E-11
310	XRCH + RCO3 = RCO3 + RCHO	k = k(70)	1.56E-11
311	XRCH + BZC3 = BZC3 + RCHO	k = k(70)	1.56E-11
312	XRCH + MAC3 = MAC3 + RCHO	k = k(70)	1.56E-11
313	XACE + NO = NO + ACET	k = k(52)	9.23E-12
314	XACE + HO2 = HO2 + 3. XC	k = k(53)	7.63E-12
315	XACE + NO3 = NO3 + ACET	k = k(54)	2.30E-12
316	XACE + MEO2 = MEO2 + 0.5 ACET + 1.5 XC	k = k(55)	2.00E-13
317	XACE + RO2C = RO2C + 0.5 ACET + 1.5 XC	k = k(56)	3.50E-14
318	XACE + RO2X = RO2X + 0.5 ACET + 1.5 XC	k = k(56)	3.50E-14
319	XACE + MCO3 = MCO3 + ACET	k = k(70)	1.56E-11
320	XACE + RCO3 = RCO3 + ACET	k = k(70)	1.56E-11
321	XACE + BZC3 = BZC3 + ACET	k = k(70)	1.56E-11
322	XACE + MAC3 = MAC3 + ACET	k = k(70)	1.56E-11
323	XMEK + NO = NO + MEK	k = k(52)	9.23E-12
324	XMEK + HO2 = HO2 + 4. XC	k = k(53)	7.63E-12
325	XMEK + NO3 = NO3 + MEK	k = k(54)	2.30E-12
326	XMEK + MEO2 = MEO2 + 0.5 MEK + 2. XC	k = k(55)	2.00E-13
327	XMEK + RO2C = RO2C + 0.5 MEK + 2. XC	k = k(56)	3.50E-14
328	XMEK + RO2X = RO2X + 0.5 MEK + 2. XC	k = k(56)	3.50E-14
329	XMEK + MCO3 = MCO3 + MEK	k = k(70)	1.56E-11

Number	Reactants and Products	Rate Constant Expression	k ₃₀₀
330	XMEK + RCO3 = RCO3 + MEK	k = k(70)	1.56E-11
331	XMEK + BZC3 = BZC3 + MEK	k = k(70)	1.56E-11
332	XMEK + MAC3 = MAC3 + MEK	k = k(70)	1.56E-11
333	XPD2 + NO = NO + PRD2	k = k(52)	9.23E-12
334	XPD2 + HO2 = HO2 + 6. XC	k = k(53)	7.63E-12
335	XPD2 + NO3 = NO3 + PRD2	k = k(54)	2.30E-12
336	XPD2 + MEO2 = MEO2 + 0.5 PRD2 + 3. XC	k = k(55)	2.00E-13
337	XPD2 + RO2C = RO2C + 0.5 PRD2 + 3. XC	k = k(56)	3.50E-14
338	XPD2 + RO2X = RO2X + 0.5 PRD2 + 3. XC	k = k(56)	3.50E-14
339	XPD2 + MCO3 = MCO3 + PRD2	k = k(70)	1.56E-11
340	XPD2 + RCO3 = RCO3 + PRD2	k = k(70)	1.56E-11
341	XPD2 + BZC3 = BZC3 + PRD2	k = k(70)	1.56E-11
342	XPD2 + MAC3 = MAC3 + PRD2	k = k(70)	1.56E-11
343	XGLY + NO = NO + GLY	k = k(52)	9.23E-12
344	XGLY + HO2 = HO2 + 2. XC	k = k(53)	7.63E-12
345	XGLY + NO3 = NO3 + GLY	k = k(54)	2.30E-12
346	XGLY + MEO2 = MEO2 + 0.5 GLY + XC	k = k(55)	2.00E-13
347	XGLY + RO2C = RO2C + 0.5 GLY + XC	k = k(56)	3.50E-14
348	XGLY + RO2X = RO2X + 0.5 GLY + XC	k = k(56)	3.50E-14
349	XGLY + MCO3 = MCO3 + GLY	k = k(70)	1.56E-11
350	XGLY + RCO3 = RCO3 + GLY	k = k(70)	1.56E-11
351	XGLY + BZC3 = BZC3 + GLY	k = k(70)	1.56E-11
352	XGLY + MAC3 = MAC3 + GLY	k = k(70)	1.56E-11
353	XMGL + NO = NO + MGLY	k = k(52)	9.23E-12
354	XMGL + HO2 = HO2 + 3. XC	k = k(53)	7.63E-12
355	XMGL + NO3 = NO3 + MGLY	k = k(54)	2.30E-12
356	XMGL + MEO2 = MEO2 + 0.5 MGLY + 1.5 XC	k = k(55)	2.00E-13
357	XMGL + RO2C = RO2C + 0.5 MGLY + 1.5 XC	k = k(56)	3.50E-14
358	XMGL + RO2X = RO2X + 0.5 MGLY + 1.5 XC	k = k(56)	3.50E-14
359	XMGL + MCO3 = MCO3 + MGLY	k = k(70)	1.56E-11
360	XMGL + RCO3 = RCO3 + MGLY	k = k(70)	1.56E-11
361	XMGL + BZC3 = BZC3 + MGLY	k = k(70)	1.56E-11
362	XMGL + MAC3 = MAC3 + MGLY	k = k(70)	1.56E-11
363	XBAC + NO = NO + BA CL	k = k(52)	9.23E-12
364	XBAC + HO2 = HO2 + 4. XC	k = k(53)	7.63E-12
365	XBAC + NO3 = NO3 + BA CL	k = k(54)	2.30E-12
366	XBAC + MEO2 = MEO2 + 0.5 BA CL + 2. XC	k = k(55)	2.00E-13
367	XBAC + RO2C = RO2C + 0.5 BA CL + 2. XC	k = k(56)	3.50E-14
368	XBAC + RO2X = RO2X + 0.5 BA CL + 2. XC	k = k(56)	3.50E-14
369	XBAC + MCO3 = MCO3 + BA CL	k = k(70)	1.56E-11
370	XBAC + RCO3 = RCO3 + BA CL	k = k(70)	1.56E-11
371	XBAC + BZC3 = BZC3 + BA CL	k = k(70)	1.56E-11
372	XBAC + MAC3 = MAC3 + BA CL	k = k(70)	1.56E-11
373	XBAL + NO = NO + BALD	k = k(52)	9.23E-12
374	XBAL + HO2 = HO2 + 7. XC	k = k(53)	7.63E-12
375	XBAL + NO3 = NO3 + BALD	k = k(54)	2.30E-12
376	XBAL + MEO2 = MEO2 + 0.5 BALD + 3.5 XC	k = k(55)	2.00E-13
377	XBAL + RO2C = RO2C + 0.5 BALD + 3.5 XC	k = k(56)	3.50E-14
378	XBAL + RO2X = RO2X + 0.5 BALD + 3.5 XC	k = k(56)	3.50E-14
379	XBAL + MCO3 = MCO3 + BALD	k = k(70)	1.56E-11
380	XBAL + RCO3 = RCO3 + BALD	k = k(70)	1.56E-11

Number	Reactants and Products	Rate Constant Expression	k ₃₀₀
381	$\text{XBAL} + \text{BZC3} = \text{BZC3} + \text{BALD}$	$k = k(70)$	1.56E-11
382	$\text{XBAL} + \text{MAC3} = \text{MAC3} + \text{BALD}$	$k = k(70)$	1.56E-11
383	$\text{XAF1} + \text{NO} = \text{NO} + \text{AFG1}$	$k = k(52)$	9.23E-12
384	$\text{XAF1} + \text{HO2} = \text{HO2} + 5. \text{XC}$	$k = k(53)$	7.63E-12
385	$\text{XAF1} + \text{NO3} = \text{NO3} + \text{AFG1}$	$k = k(54)$	2.30E-12
386	$\text{XAF1} + \text{MEO2} = \text{MEO2} + 0.5 \text{AFG1} + 2.5 \text{XC}$	$k = k(55)$	2.00E-13
387	$\text{XAF1} + \text{RO2C} = \text{RO2C} + 0.5 \text{AFG1} + 2.5 \text{XC}$	$k = k(56)$	3.50E-14
388	$\text{XAF1} + \text{RO2X} = \text{RO2X} + 0.5 \text{AFG1} + 2.5 \text{XC}$	$k = k(56)$	3.50E-14
389	$\text{XAF1} + \text{MCO3} = \text{MCO3} + \text{AFG1}$	$k = k(70)$	1.56E-11
390	$\text{XAF1} + \text{RCO3} = \text{RCO3} + \text{AFG1}$	$k = k(70)$	1.56E-11
391	$\text{XAF1} + \text{BZC3} = \text{BZC3} + \text{AFG1}$	$k = k(70)$	1.56E-11
392	$\text{XAF1} + \text{MAC3} = \text{MAC3} + \text{AFG1}$	$k = k(70)$	1.56E-11
393	$\text{XAF2} + \text{NO} = \text{NO} + \text{AFG2}$	$k = k(52)$	9.23E-12
394	$\text{XAF2} + \text{HO2} = \text{HO2} + 5. \text{XC}$	$k = k(53)$	7.63E-12
395	$\text{XAF2} + \text{NO3} = \text{NO3} + \text{AFG2}$	$k = k(54)$	2.30E-12
396	$\text{XAF2} + \text{MEO2} = \text{MEO2} + 0.5 \text{AFG2} + 2.5 \text{XC}$	$k = k(55)$	2.00E-13
397	$\text{XAF2} + \text{RO2C} = \text{RO2C} + 0.5 \text{AFG2} + 2.5 \text{XC}$	$k = k(56)$	3.50E-14
398	$\text{XAF2} + \text{RO2X} = \text{RO2X} + 0.5 \text{AFG2} + 2.5 \text{XC}$	$k = k(56)$	3.50E-14
399	$\text{XAF2} + \text{MCO3} = \text{MCO3} + \text{AFG2}$	$k = k(70)$	1.56E-11
400	$\text{XAF2} + \text{RCO3} = \text{RCO3} + \text{AFG2}$	$k = k(70)$	1.56E-11
401	$\text{XAF2} + \text{BZC3} = \text{BZC3} + \text{AFG2}$	$k = k(70)$	1.56E-11
402	$\text{XAF2} + \text{MAC3} = \text{MAC3} + \text{AFG2}$	$k = k(70)$	1.56E-11
403	$\text{XAF3} + \text{NO} = \text{NO} + \text{AFG3}$	$k = k(52)$	9.23E-12
404	$\text{XAF3} + \text{HO2} = \text{HO2} + 7. \text{XC}$	$k = k(53)$	7.63E-12
405	$\text{XAF3} + \text{NO3} = \text{NO3} + \text{AFG3}$	$k = k(54)$	2.30E-12
406	$\text{XAF3} + \text{MEO2} = \text{MEO2} + 0.5 \text{AFG3} + 3.5 \text{XC}$	$k = k(55)$	2.00E-13
407	$\text{XAF3} + \text{RO2C} = \text{RO2C} + 0.5 \text{AFG3} + 3.5 \text{XC}$	$k = k(56)$	3.50E-14
408	$\text{XAF3} + \text{RO2X} = \text{RO2X} + 0.5 \text{AFG3} + 3.5 \text{XC}$	$k = k(56)$	3.50E-14
409	$\text{XAF3} + \text{MCO3} = \text{MCO3} + \text{AFG3}$	$k = k(70)$	1.56E-11
410	$\text{XAF3} + \text{RCO3} = \text{RCO3} + \text{AFG3}$	$k = k(70)$	1.56E-11
411	$\text{XAF3} + \text{BZC3} = \text{BZC3} + \text{AFG3}$	$k = k(70)$	1.56E-11
412	$\text{XAF3} + \text{MAC3} = \text{MAC3} + \text{AFG3}$	$k = k(70)$	1.56E-11
413	$\text{XMAC} + \text{NO} = \text{NO} + \text{MACR}$	$k = k(52)$	9.23E-12
414	$\text{XMAC} + \text{HO2} = \text{HO2} + 4. \text{XC}$	$k = k(53)$	7.63E-12
415	$\text{XMAC} + \text{NO3} = \text{NO3} + \text{MACR}$	$k = k(54)$	2.30E-12
416	$\text{XMAC} + \text{MEO2} = \text{MEO2} + 0.5 \text{MACR} + 2. \text{XC}$	$k = k(55)$	2.00E-13
417	$\text{XMAC} + \text{RO2C} = \text{RO2C} + 0.5 \text{MACR} + 2. \text{XC}$	$k = k(56)$	3.50E-14
418	$\text{XMAC} + \text{RO2X} = \text{RO2X} + 0.5 \text{MACR} + 2. \text{XC}$	$k = k(56)$	3.50E-14
419	$\text{XMAC} + \text{MCO3} = \text{MCO3} + \text{MACR}$	$k = k(70)$	1.56E-11
420	$\text{XMAC} + \text{RCO3} = \text{RCO3} + \text{MACR}$	$k = k(70)$	1.56E-11
421	$\text{XMAC} + \text{BZC3} = \text{BZC3} + \text{MACR}$	$k = k(70)$	1.56E-11
422	$\text{XMAC} + \text{MAC3} = \text{MAC3} + \text{MACR}$	$k = k(70)$	1.56E-11
423	$\text{XMVK} + \text{NO} = \text{NO} + \text{MVK}$	$k = k(52)$	9.23E-12
424	$\text{XMVK} + \text{HO2} = \text{HO2} + 4. \text{XC}$	$k = k(53)$	7.63E-12
425	$\text{XMVK} + \text{NO3} = \text{NO3} + \text{MVK}$	$k = k(54)$	2.30E-12
426	$\text{XMVK} + \text{MEO2} = \text{MEO2} + 0.5 \text{MVK} + 2. \text{XC}$	$k = k(55)$	2.00E-13
427	$\text{XMVK} + \text{RO2C} = \text{RO2C} + 0.5 \text{MVK} + 2. \text{XC}$	$k = k(56)$	3.50E-14
428	$\text{XMVK} + \text{RO2X} = \text{RO2X} + 0.5 \text{MVK} + 2. \text{XC}$	$k = k(56)$	3.50E-14
429	$\text{XMVK} + \text{MCO3} = \text{MCO3} + \text{MVK}$	$k = k(70)$	1.56E-11
430	$\text{XMVK} + \text{RCO3} = \text{RCO3} + \text{MVK}$	$k = k(70)$	1.56E-11
431	$\text{XMVK} + \text{BZC3} = \text{BZC3} + \text{MVK}$	$k = k(70)$	1.56E-11

Number	Reactants and Products	Rate Constant Expression	k ₃₀₀
432	XMVK + MAC3 = MAC3 + MVK	k = k(70)	1.56E-11
433	XIPR + NO = NO + IPRD	k = k(52)	9.23E-12
434	XIPR + HO2 = HO2 + 5. XC	k = k(53)	7.63E-12
435	XIPR + NO3 = NO3 + IPRD	k = k(54)	2.30E-12
436	XIPR + MEO2 = MEO2 + 0.5 IPRD + 2.5 XC	k = k(55)	2.00E-13
437	XIPR + RO2C = RO2C + 0.5 IPRD + 2.5 XC	k = k(56)	3.50E-14
438	XIPR + RO2X = RO2X + 0.5 IPRD + 2.5 XC	k = k(56)	3.50E-14
439	XIPR + MCO3 = MCO3 + IPRD	k = k(70)	1.56E-11
440	XIPR + RCO3 = RCO3 + IPRD	k = k(70)	1.56E-11
441	XIPR + BZC3 = BZC3 + IPRD	k = k(70)	1.56E-11
442	XIPR + MAC3 = MAC3 + IPRD	k = k(70)	1.56E-11
443	XRN3 + NO = NO + RNO3	k = k(52)	9.23E-12
444	XRN3 + HO2 = HO2 + 6. XC + XN	k = k(53)	7.63E-12
445	XRN3 + NO3 = NO3 + RNO3	k = k(54)	2.30E-12
446	XRN3 + MEO2 = MEO2 + 0.5 RNO3 + 0.5 XN + 3. XC	k = k(55)	2.00E-13
447	XRN3 + RO2C = RO2C + 0.5 RNO3 + 0.5 XN + 3. XC	k = k(56)	3.50E-14
448	XRN3 + RO2X = RO2X + 0.5 RNO3 + 0.5 XN + 3. XC	k = k(56)	3.50E-14
449	XRN3 + MCO3 = MCO3 + RNO3	k = k(70)	1.56E-11
450	XRN3 + RCO3 = RCO3 + RNO3	k = k(70)	1.56E-11
451	XRN3 + BZC3 = BZC3 + RNO3	k = k(70)	1.56E-11
452	XRN3 + MAC3 = MAC3 + RNO3	k = k(70)	1.56E-11
453	YRPX + NO = NO	k = k(52)	9.23E-12
454	YRPX + HO2 = HO2 + ROOH - 3. XC	k = k(53)	7.63E-12
455	YRPX + NO3 = NO3	k = k(54)	2.30E-12
456	YRPX + MEO2 = MEO2 + 0.5 MEK - 2. XC	k = k(55)	2.00E-13
457	YRPX + RO2C = RO2C + 0.5 MEK - 2. XC	k = k(56)	3.50E-14
458	YRPX + RO2X = RO2X + 0.5 MEK - 2. XC	k = k(56)	3.50E-14
459	YRPX + MCO3 = MCO3	k = k(70)	1.56E-11
460	YRPX + RCO3 = RCO3	k = k(70)	1.56E-11
461	YRPX + BZC3 = BZC3	k = k(70)	1.56E-11
462	YRPX + MAC3 = MAC3	k = k(70)	1.56E-11
463	Y6PX + NO = NO	k = k(52)	9.23E-12
464	Y6PX + HO2 = HO2 + R6PX - 6. XC	k = k(53)	7.63E-12
465	Y6PX + NO3 = NO3	k = k(54)	2.30E-12
466	Y6PX + MEO2 = MEO2 + 0.5 PRD2 - 3. XC	k = k(55)	2.00E-13
467	Y6PX + RO2C = RO2C + 0.5 PRD2 - 3. XC	k = k(56)	3.50E-14
468	Y6PX + RO2X = RO2X + 0.5 PRD2 - 3. XC	k = k(56)	3.50E-14
469	Y6PX + MCO3 = MCO3	k = k(70)	1.56E-11
470	Y6PX + RCO3 = RCO3	k = k(70)	1.56E-11
471	Y6PX + BZC3 = BZC3	k = k(70)	1.56E-11
472	Y6PX + MAC3 = MAC3	k = k(70)	1.56E-11
473	YAPX + NO = NO	k = k(52)	9.23E-12
474	YAPX + HO2 = HO2 + RAPX - 8. XC	k = k(53)	7.63E-12
475	YAPX + NO3 = NO3	k = k(54)	2.30E-12
476	YAPX + MEO2 = MEO2 + 0.5 PRD2 - 3. XC	k = k(55)	2.00E-13
477	YAPX + RO2C = RO2C + 0.5 PRD2 - 3. XC	k = k(56)	3.50E-14
478	YAPX + RO2X = RO2X + 0.5 PRD2 - 3. XC	k = k(56)	3.50E-14
479	YAPX + MCO3 = MCO3	k = k(70)	1.56E-11

Number	Reactants and Products	Rate Constant Expression	k ₃₀₀
480	YAPX + RCO3 = RCO3	k = k(70)	1.56E-11
481	YAPX + BZC3 = BZC3	k = k(70)	1.56E-11
482	YAPX + MAC3 = MAC3	k = k(70)	1.56E-11
483	ZRN3 + NO = NO + RNO3 - 1. XN	k = k(52)	9.23E-12
484	ZRN3 + HO2 = HO2 + 6. XC	k = k(53)	7.63E-12
485	ZRN3 + NO3 = NO3 + PRD2 + HO2	k = k(54)	2.30E-12
486	ZRN3 + MEO2 = MEO2 + 0.5 PRD2 + 0.5 HO2 + 3. XC	k = k(55)	2.00E-13
487	ZRN3 + RO2C = RO2C + 0.5 PRD2 + 0.5 HO2 + 3. XC	k = k(56)	3.50E-14
488	ZRN3 + RO2X = RO2X + 0.5 PRD2 + 0.5 HO2 + 3. XC	k = k(56)	3.50E-14
489	ZRN3 + MCO3 = MCO3 + PRD2 + HO2	k = k(70)	1.56E-11
490	ZRN3 + RCO3 = RCO3 + PRD2 + HO2	k = k(70)	1.56E-11
491	ZRN3 + BZC3 = BZC3 + PRD2 + HO2	k = k(70)	1.56E-11
492	ZRN3 + MAC3 = MAC3 + PRD2 + HO2	k = k(70)	1.56E-11
493	XGLD + NO = NO + GLYD	k = k(52)	9.23E-12
494	XGLD + HO2 = HO2 + 2. XC	k = k(53)	7.63E-12
495	XGLD + NO3 = NO3 + GLYD	k = k(54)	2.30E-12
496	XGLD + MEO2 = MEO2 + 0.5 GLYD + XC	k = k(55)	2.00E-13
497	XGLD + RO2C = RO2C + 0.5 GLYD + XC	k = k(56)	3.50E-14
498	XGLD + RO2X = RO2X + 0.5 GLYD + XC	k = k(56)	3.50E-14
499	XGLD + MCO3 = MCO3 + GLYD	k = k(70)	1.56E-11
500	XGLD + RCO3 = RCO3 + GLYD	k = k(70)	1.56E-11
501	XGLD + BZC3 = BZC3 + GLYD	k = k(70)	1.56E-11
502	XGLD + MAC3 = MAC3 + GLYD	k = k(70)	1.56E-11
503	XACR + NO = NO + ACRO	k = k(52)	9.23E-12
504	XACR + HO2 = HO2 + 3. XC	k = k(53)	7.63E-12
505	XACR + NO3 = NO3 + ACRO	k = k(54)	2.30E-12
506	XACR + MEO2 = MEO2 + 0.5 ACRO + 1.5 XC	k = k(55)	2.00E-13
507	XACR + RO2C = RO2C + 0.5 ACRO + 1.5 XC	k = k(56)	3.50E-14
508	XACR + RO2X = RO2X + 0.5 ACRO + 1.5 XC	k = k(56)	3.50E-14
509	XACR + MCO3 = MCO3 + ACRO	k = k(70)	1.56E-11
510	XACR + RCO3 = RCO3 + ACRO	k = k(70)	1.56E-11
511	XACR + BZC3 = BZC3 + ACRO	k = k(70)	1.56E-11
512	XACR + MAC3 = MAC3 + ACRO	k = k(70)	1.56E-11
513	CH4 + OH = MEO2	k = 1.85E-12 exp(-1690/T)	6.62E-15
514	ETHE + OH = XHO2 + RO2C + 1.61 XHCH + 0.195 XGLD + YRPX	Falloff: F=0.6; n=1 k(0) = 1.00E-28 (T/300)^-4.5 k(inf) = 8.80E-12 (T/300)^-0.85	8.15E-12
515	ETHE + O3 = 0.16 HO2 + 0.16 OH + 0.51 CO + 0.12 CO2 + HCHO + 0.37 FACD	k = 9.14E-15 exp(-2580/T)	1.68E-18
516	ETHE + NO3 = XHO2 + RO2C + XRCH + YRPX + XN - 1. XC	k = 3.30E-12 (T/300)^2 exp(-2880/T)	2.24E-16
517	ETHE + O3P = 0.8 HO2 + 0.29 XHO2 + 0.51 MEO2 + 0.29 RO2C + 0.51 CO + 0.278 XCO + 0.278 XHCH + 0.1 CCHO + 0.012 XGLY + 0.29 YRPX + 0.2 XC	k = 1.07E-11 exp(-800/T)	7.43E-13
518	PRPE + OH = 0.984 XHO2 + 0.984 RO2C + 0.016 RO2X + 0.016 ZRN3 + 0.984 XHCH + 0.984 XCCH + YRPX - 0.048 XC	k = 4.85E-12 exp(504/T)	2.60E-11

Number	Reactants and Products	Rate Constant Expression	k ₃₀₀
519	PRPE + O3 = 0.165 HO2 + 0.35 OH + 0.355 MEO2 + 0.525 CO + 0.215 CO2 + 0.5 HCHO + 0.5 CCHO + 0.185 FACD + 0.075 AACD + 0.07 XC	k = 5.51E-15 exp(-1878/T)	1.05E-17
520	PRPE + NO3 = 0.949 XHO2 + 0.949 RO2C + 0.051 RO2X + 0.051 ZRN3 + YRPX + XN + 2.694 XC	k = 4.59E-13 exp(-1156/T)	9.73E-15
521	PRPE + O3P = 0.45 RCHO + 0.55 MEK - 0.55 XC	k = 1.02E-11 exp(-280/T)	4.01E-12
522	BD13 + OH = 0.951 XHO2 + 1.189 RO2C + 0.049 RO2X + 0.049 ZRN3 + 0.708 XHCH + 0.48 XACR + 0.471 XIPR + YRPX - 0.797 XC	k = 1.48E-11 exp(448/T)	6.59E-11
523	BD13 + O3 = 0.08 HO2 + 0.08 OH + 0.255 CO + 0.185 CO2 + 0.5 HCHO + 0.185 FACD + 0.5 ACRO + 0.375 MVK + 0.125 PRD2 - 0.875 XC	k = 1.34E-14 exp(-2283/T)	6.64E-18
524	BD13 + NO3 = 0.815 XHO2 + 0.12 XNO2 + 1.055 RO2C + 0.065 RO2X + 0.065 ZRN3 + 0.115 XHCH + 0.46 XMVK + 0.12 XIPR + 0.355 XRN3 + YRPX + 0.525 XN - 1.075 XC	k = 1.00E-13	1.00E-13
525	BD13 + O3P = 0.25 HO2 + 0.117 XHO2 + 0.118 XMA3 + 0.235 RO2C + 0.015 RO2X + 0.015 ZRN3 + 0.115 XCO + 0.115 XACR + 0.001 XAF1 + 0.001 XAF2 + 0.75 PRD2 + 0.25 YRPX - 1.532 XC	k = 2.26E-11 exp(-40/T)	1.98E-11
526	ISOP + OH = 0.907 XHO2 + 0.986 RO2C + 0.093 RO2X + 0.093 ZRN3 + 0.624 XHCH + 0.23 XMAC + 0.32 XMVK + 0.357 XIPR + Y6PX - 0.167 XC	k = 2.54E-11 exp(410/T)	9.96E-11
527	ISOP + O3 = 0.066 HO2 + 0.266 OH + 0.192 XMA3 + 0.192 RO2C + 0.008 RO2X + 0.008 ZRN3 + 0.275 CO + 0.122 CO2 + 0.4 HCHO + 0.192 XHCH + 0.204 FACD + 0.39 MACR + 0.16 MVK + 0.15 IPRD + 0.1 PRD2 + 0.2 Y6PX - 0.559 XC	k = 7.86E-15 exp(-1912/T)	1.34E-17
528	ISOP + NO3 = 0.749 XHO2 + 0.187 XNO2 + 0.936 RO2C + 0.064 RO2X + 0.064 ZRN3 + 0.936 XIPR + Y6PX + 0.813 XN - 0.064 XC	k = 3.03E-12 exp(-448/T)	6.81E-13
529	ISOP + O3P = 0.25 MEO2 + 0.24 XMA3 + 0.24 RO2C + 0.01 RO2X + 0.01 ZRN3 + 0.24 XHCH + 0.75 PRD2 + 0.25 Y6PX - 1.01 XC	k = 3.50E-11	3.50E-11
530	APIN + OH = 0.799 XHO2 + 0.004 XRC3 + 1.042 RO2C + 0.197 RO2X + 0.197 ZRN3 + 0.002 XCO + 0.022 XHCH + 0.776 XRCH + 0.034 XACE + 0.02 XMGL + 0.023 XBAC + Y6PX + 6.2 XC	k = 1.21E-11 exp(436/T)	5.18E-11
531	APIN + O3 = 0.009 HO2 + 0.102 XHO2 + 0.728 OH + 0.001 XMC3 + 0.297 XRC3 + 1.511 RO2C + 0.337 RO2X + 0.337 ZRN3 + 0.029 CO + 0.051 XCO + 0.017 CO2 + 0.344 XHCH + 0.24 XRCH + 0.345 XACE + 0.008 MEK + 0.002 XGLY + 0.081 XBAC + 0.255 PRD2 + 0.737 Y6PX + 2.999 XC	k = 5.00E-16 exp(-530/T)	8.55E-17

Number	Reactants and Products	Rate Constant Expression	k ₃₀₀
532	APIN + NO3 = 0.056 XHO2 + 0.643 XNO2 + 0.007 XRC3 + 1.05 RO2C + 0.293 RO2X + 0.293 ZRN3 + 0.005 XCO + 0.007 XHCH + 0.684 XRCH + 0.069 XACE + 0.002 XMGL + 0.056 XRN3 + Y6PX + 0.301 XN + 5.608 XC	k = 1.19E-12 exp(490/T)	6.09E-12
533	APIN + O3P = PRD2 + 4. XC	k = 3.20E-11	3.20E-11
534	ACYE + OH = 0.3 HO2 + 0.7 OH + 0.3 CO + 0.3 FACD + 0.7 GLY	Falloff: F=0.6; n=1 k(0) = 5.50E-30 (T/300)^-2 k(inf) = 8.30E-13	7.56E-13
535	ACYE + O3 = 1.5 HO2 + 0.5 OH + 1.5 CO + 0.5 CO2	k = 1.00E-14 exp(-4100/T)	1.16E-20
536	BENZ + OH = 0.57 HO2 + 0.29 XHO2 + 0.116 OH + 0.29 RO2C + 0.024 RO2X + 0.024 ZRN3 + 0.29 XGLY + 0.57 CRES + 0.029 XAF1 + 0.261 XAF2 + 0.116 AFG3 + 0.314 YAPX - 0.976 XC	k = 2.33E-12 exp(-193/T)	1.22E-12
537	TOLU + OH = 0.181 HO2 + 0.454 XHO2 + 0.312 OH + 0.454 RO2C + 0.054 RO2X + 0.054 ZRN3 + 0.238 XGLY + 0.151 XMGL + 0.181 CRES + 0.065 XBAL + 0.195 XAF1 + 0.195 XAF2 + 0.312 AFG3 + 0.073 Y6PX + 0.435 YAPX - 0.109 XC	k = 1.81E-12 exp(338/T)	5.58E-12
538	MXYL + OH = 0.159 HO2 + 0.52 XHO2 + 0.239 OH + 0.52 RO2C + 0.082 RO2X + 0.082 ZRN3 + 0.1 XGLY + 0.38 XMGL + 0.159 CRES + 0.041 XBAL + 0.336 XAF1 + 0.144 XAF2 + 0.239 AFG3 + 0.047 Y6PX + 0.555 YAPX + 0.695 XC	k = 2.31E-11	2.31E-11
539	OXYL + OH = 0.161 HO2 + 0.554 XHO2 + 0.198 OH + 0.554 RO2C + 0.087 RO2X + 0.087 ZRN3 + 0.084 XGLY + 0.238 XMGL + 0.185 XBAC + 0.161 CRES + 0.047 XBAL + 0.253 XAF1 + 0.253 XAF2 + 0.198 AFG3 + 0.055 Y6PX + 0.586 YAPX + 0.484 XC	k = 1.36E-11	1.36E-11
540	PXYL + OH = 0.159 HO2 + 0.487 XHO2 + 0.278 OH + 0.487 RO2C + 0.076 RO2X + 0.076 ZRN3 + 0.286 XGLY + 0.112 XMGL + 0.159 CRES + 0.088 XBAL + 0.045 XAF1 + 0.067 XAF2 + 0.278 AFG3 + 0.286 XAF3 + 0.102 Y6PX + 0.461 YAPX + 0.399 XC	k = 1.43E-11	1.43E-11
541	B124 + OH = 0.022 HO2 + 0.627 XHO2 + 0.23 OH + 0.627 RO2C + 0.121 RO2X + 0.121 ZRN3 + 0.074 XGLY + 0.405 XMGL + 0.112 XBAC + 0.022 CRES + 0.036 XBAL + 0.088 XAF1 + 0.352 XAF2 + 0.23 AFG3 + 0.151 XAF3 + 0.043 Y6PX + 0.705 YAPX + 1.19 XC	k = 3.25E-11	3.25E-11
542	ETOH + OH = 0.95 HO2 + 0.05 XHO2 + 0.05 RO2C + 0.081 XHCH + 0.95 CCHO + 0.01 XGLD + 0.05 YRPX - 0.001 XC	k = 5.49E-13 (T/300)^2 exp(530/T)	3.21E-12
543	ALK1 + OH = XHO2 + RO2C + XCCH + YRPX	k = 1.34E-12 (T/300)^2 exp(-499/T)	2.54E-13
544	ALK2 + OH = 0.965 XHO2 + 0.965 RO2C + 0.035 RO2X + 0.035 ZRN3 + 0.261 XRCH + 0.704 XACE + YRPX - 0.105 XC	k = 1.49E-12 (T/300)^2 exp(-87/T)	1.11E-12

Number	Reactants and Products	Rate Constant Expression	k ₃₀₀
545	ALK3 + OH = 0.695 XHO2 + 0.236 XTBU + 1.253 RO2C + 0.07 RO2X + 0.07 ZRN3 + 0.026 XHCH + 0.445 XCCH + 0.122 XRCH + 0.024 XACE + 0.332 XMEK + 0.983 YRPX + 0.017 Y6PX - 0.046 XC	k = 1.51E-12 exp(126/T)	2.30E-12
546	ALK4 + OH = 0.83 XHO2 + 0.01 XMEO + 0.011 XMC3 + 1.763 RO2C + 0.149 RO2X + 0.149 ZRN3 + 0.002 XCO + 0.029 XHCH + 0.438 XCCH + 0.236 XRCH + 0.426 XACE + 0.106 XMEK + 0.146 XPD2 + Y6PX - 0.119 XC	k = 3.75E-12 exp(44/T)	4.34E-12
547	ALK5 + OH = 0.647 XHO2 + 1.605 RO2C + 0.353 RO2X + 0.353 ZRN3 + 0.04 XHCH + 0.106 XCCH + 0.209 XRCH + 0.071 XACE + 0.086 XMEK + 0.407 XPD2 + Y6PX + 2.004 XC	k = 2.70E-12 exp(374/T)	9.39E-12
548	OLE1 + OH = 0.871 XHO2 + 0.001 XMEO + 1.202 RO2C + 0.128 RO2X + 0.128 ZRN3 + 0.582 XHCH + 0.01 XCCH + 0.007 XGLD + 0.666 XRCH + 0.007 XACE + 0.036 XACR + 0.001 XMAC + 0.012 XMKV + 0.009 XIPR + 0.168 XPD2 + 0.169 YRPX + 0.831 Y6PX + 0.383 XC	k = 6.72E-12 exp(501/T)	3.57E-11
549	OLE1 + O3 = 0.095 HO2 + 0.057 XHO2 + 0.128 OH + 0.09 RO2C + 0.005 RO2X + 0.005 ZRN3 + 0.303 CO + 0.088 CO2 + 0.5 HCHO + 0.011 XCCH + 0.5 RCHO + 0.044 XRCH + 0.003 XACE + 0.009 MEK + 0.185 FACD + 0.159 PACD + 0.268 PRD2 + 0.011 YRPX + 0.052 Y6PX + 0.11 XC	k = 3.19E-15 exp(-1701/T)	1.10E-17
550	OLE1 + NO3 = 0.772 XHO2 + 1.463 RO2C + 0.228 RO2X + 0.228 ZRN3 + 0.013 XCCH + 0.003 XRCH + 0.034 XACE + 0.774 XRN3 + 0.169 YRPX + 0.831 Y6PX + 0.226 XN - 1.149 XC	k = 5.37E-13 exp(-1047/T)	1.64E-14
551	OLE1 + O3P = 0.45 RCHO + 0.39 MEK + 0.16 PRD2 + 1.13 XC	k = 1.61E-11 exp(-326/T)	5.43E-12
552	OLE2 + OH = 0.912 XHO2 + 0.953 RO2C + 0.088 RO2X + 0.088 ZRN3 + 0.179 XHCH + 0.835 XCCH + 0.51 XRCH + 0.144 XACE + 0.08 XMEK + 0.002 XMKV + 0.012 XIPR + 0.023 XPD2 + 0.319 YRPX + 0.681 Y6PX + 0.135 XC	k = 1.26E-11 exp(488/T)	6.41E-11
553	OLE2 + O3 = 0.094 HO2 + 0.041 XHO2 + 0.443 OH + 0.307 MEO2 + 0.156 XMC3 + 0.008 XRC3 + 0.212 RO2C + 0.003 RO2X + 0.003 ZRN3 + 0.299 CO + 0.161 CO2 + 0.131 HCHO + 0.114 XHCH + 0.453 CCHO + 0.071 XCCH + 0.333 RCHO + 0.019 XRCH + 0.051 ACET + 0.033 MEK + 0.001 XMEK + 0.024 FACD + 0.065 AACD + 0.235 PACD + 0.037 PRD2 + 0.073 YRPX + 0.136 Y6PX + 0.16 XC	k = 8.59E-15 exp(-1255/T)	1.31E-16

Number	Reactants and Products	Rate Constant Expression	k ₃₀₀
554	OLE2 + NO3 = 0.4 XHO2 + 0.426 XNO2 + 0.035 XMEO + 1.193 RO2C + 0.14 RO2X + 0.14 ZRN3 + 0.072 XHCH + 0.579 XCCH + 0.163 XRCH + 0.116 XACE + 0.002 XMEK + 0.32 XRN3 + 0.319 YRPX + 0.681 Y6PX + 0.254 XN + 0.13 XC	k = 2.31E-13 exp(382/T)	8.25E-13
555	OLE2 + O3P = 0.079 RCHO + 0.751 MEK + 0.17 PRD2 + 0.739 XC	k = 1.43E-11 exp(111/T)	2.07E-11
556	ARO1 + OH = 0.123 HO2 + 0.566 XHO2 + 0.202 OH + 0.566 RO2C + 0.11 RO2X + 0.11 ZRN3 + 0.158 XGLY + 0.1 XMGL + 0.123 CRES + 0.072 XAF1 + 0.185 XAF2 + 0.202 AFG3 + 0.309 XPD2 + 0.369 Y6PX + 0.31 XC	k = 7.84E-12	7.84E-12
557	ARO2 + OH = 0.077 HO2 + 0.617 XHO2 + 0.178 OH + 0.617 RO2C + 0.128 RO2X + 0.128 ZRN3 + 0.088 XGLY + 0.312 XMGL + 0.134 XBAC + 0.077 CRES + 0.026 XBAL + 0.221 XAF1 + 0.247 XAF2 + 0.178 AFG3 + 0.068 XAF3 + 0.057 XPD2 + 0.101 Y6PX + 1.459 XC	k = 3.09E-11	3.09E-11
558	TERP + OH = 0.734 XHO2 + 0.064 XRC3 + 1.211 RO2C + 0.201 RO2X + 0.201 ZRN3 + 0.001 XCO + 0.411 XHCH + 0.385 XRCH + 0.037 XACE + 0.007 XMEK + 0.003 XMGL + 0.009 XBAC + 0.003 XMVK + 0.002 XIPR + 0.409 XPD2 + Y6PX + 4.375 XC	k = 2.27E-11 exp(435/T)	9.68E-11
559	TERP + O3 = 0.078 HO2 + 0.046 XHO2 + 0.499 OH + 0.202 XMC3 + 0.059 XRC3 + 0.49 RO2C + 0.121 RO2X + 0.121 ZRN3 + 0.249 CO + 0.063 CO2 + 0.127 HCHO + 0.033 XHCH + 0.208 XRCH + 0.057 XACE + 0.002 MEK + 0.172 FACD + 0.068 PACD + 0.003 XMGL + 0.039 XBAC + 0.002 XMAC + 0.001 XIPR + 0.502 PRD2 + 0.428 Y6PX + 3.852 XC	k = 8.28E-16 exp(-785/T)	6.05E-17
560	TERP + NO3 = 0.227 XHO2 + 0.287 XNO2 + 0.026 XRC3 + 1.786 RO2C + 0.46 RO2X + 0.46 ZRN3 + 0.012 XCO + 0.023 XHCH + 0.002 XGLD + 0.403 XRCH + 0.239 XACE + 0.005 XMAC + 0.001 XMVK + 0.004 XIPR + 0.228 XRN3 + Y6PX + 0.485 XN + 3.785 XC	k = 1.33E-12 exp(490/T)	6.81E-12
561	TERP + O3P = 0.237 RCHO + 0.763 PRD2 + 4.711 XC	k = 4.02E-11	4.02E-11
562	SESQ + OH = 0.734 XHO2 + 0.064 XRC3 + 1.211 RO2C + 0.201 RO2X + 0.201 ZRN3 + 0.001 XCO + 0.411 XHCH + 0.385 XRCH + 0.037 XACE + 0.007 XMEK + 0.003 XMGL + 0.009 XBAC + 0.003 XMVK + 0.002 XIPR + 0.409 XPD2 + Y6PX + 9.375 XC	k = k(558)	9.68E-11

Number	Reactants and Products	Rate Constant Expression	k ₃₀₀
563	SESQ + O3 = 0.078 HO2 + 0.046 XHO2 + 0.499 OH + 0.202 XMC3 + 0.059 XRC3 + 0.49 RO2C + 0.121 RO2X + 0.121 ZRN3 + 0.249 CO + 0.063 CO2 + 0.127 HCHO + 0.033 XHCH + 0.208 XRCH + 0.057 XACE + 0.002 MEK + 0.172 FACD + 0.068 PACD + 0.003 XMGL + 0.039 XBAC + 0.002 XMAC + 0.001 XIPR + 0.502 PRD2 + 0.428 Y6PX + 8.852 XC	k = k(559)	6.05E-17
564	SESQ + NO3 = 0.227 XHO2 + 0.287 XNO2 + 0.026 XRC3 + 1.786 RO2C + 0.46 RO2X + 0.46 ZRN3 + 0.012 XCO + 0.023 XHCH + 0.002 XCCH + 0.403 XRCH + 0.239 XACE + 0.005 XMAC + 0.001 XMVK + 0.004 XIPR + 0.228 XRN3 + Y6PX + 0.485 XN + 8.785 XC	k = k(560)	6.81E-12
565	SESQ + O3P = 0.237 RCHO + 0.763 PRD2 + 9.711 XC	k = k(561)	4.02E-11

Table D-2. Explicit species in the SAPRC07TC mechanism.

Species Name	Description
BD13	1,3-butadiene
AACD	Acetic acid
ACET	Acetone
ACRO	Acrolein
ACYE	Acetylene
AFG1	Lumped photoreactive monounsaturated dicarbonyl aromatic fragmentation products that photolyze to form radicals
AFG2	Lumped photoreactive monounsaturated dicarbonyl aromatic fragmentation products that photolyze to form non-radical products
AFG3	Lumped diunsaturated dicarbonyl aromatic fragmentation product.
ALK1	Alkanes and other non-aromatic compounds that react only with OH, and have k_{OH} between 2 and $5E2 \text{ ppm}^{-1} \text{ min}^{-1}$. (Primarily ethane)
ALK2	Alkanes and other non-aromatic compounds that react only with OH, and have k_{OH} between $5E2$ and $2.5E3 \text{ ppm}^{-1} \text{ min}^{-1}$. (Primarily propane and acetylene)
ALK3	Alkanes and other non-aromatic compounds that react only with OH, and have k_{OH} between $2.5E3$ and $5E3 \text{ ppm}^{-1} \text{ min}^{-1}$.
ALK4	Alkanes and other non-aromatic compounds that react only with OH, and have k_{OH} between $5E3$ and $1E4 \text{ ppm}^{-1} \text{ min}^{-1}$.
ALK5	Alkanes and other non-aromatic compounds that react only with OH, and have k_{OH} greater than $1E4 \text{ ppm}^{-1} \text{ min}^{-1}$.
APIN	α -pinene
ARO1	Aromatics with $k_{OH} < 2E4 \text{ ppm}^{-1} \text{ min}^{-1}$.
ARO2	Aromatics with $k_{OH} > 2E4 \text{ ppm}^{-1} \text{ min}^{-1}$.
B124	1,2,4-trimethyl benzene
BACL	Biacetyl
BALD	Aromatic aldehydes (e.g., benzaldehyde)
BENZ	Benzene
BZC3	Peroxyacyl radical formed from Aromatic Aldehydes
BZO	Phenoxy Radicals
CCHO	Acetaldehyde
CO3H	Peroxyacetic acid
CH4	Methane
CO	Carbon Monoxide
CO2	Carbon Dioxide
COOH	Methyl Hydroperoxide
CRES	Phenols and Cresols
ETHE	Ethene
ETOH	Ethanol
FACD	Formic Acid
GLY	Glyoxal
H2	Hydrogen
H2O	Water
HCHO	Formaldehyde
HNO3	Nitric Acid
PNA	Peroxynitric Acid

Species Name	Description
HO2	Hydroperoxide Radicals
H2O2	Hydrogen Peroxide
GLYD	Glycolaldehyde
HONO	Nitrous Acid
IPRD	Lumped isoprene product species
ISOP	Isoprene
M	Atmospheric pressure
MAC3	Peroxyacyl radicals formed from methacrolein and other acroleins.
MACR	Methacrolein
MPAN	PAN analogue formed from Methacrolein
MCO3	Acetyl Peroxy Radicals
MEK	Ketones and other non-aldehyde oxygenated products which react with OH radicals faster than 5E-13 but slower than 5E-12 cm ³ molec ⁻² sec ⁻¹ . (Based on mechanism for methyl ethyl ketone).
MEO2	Methyl Peroxy Radicals
MEOH	Methanol
MGLY	Methyl Glyoxal
MVK	Methyl Vinyl Ketone
MXYL	m-xylene
N2O5	Nitrogen Pentoxide
NO	Nitric Oxide
NO2	Nitrogen Dioxide
NO3	Nitrate Radical
NPHE	Nitrophenols
O1D	Excited Oxygen Atoms
O2	Oxygen
O3	Ozone
O3P	Ground State Oxygen Atoms
OH	Hydroxyl Radicals
OLE1	Alkenes (other than ethene) with $k_{OH} < 7E4 \text{ ppm}^{-1} \text{ min}^{-1}$.
OLE2	Alkenes with $k_{OH} > 7E4 \text{ ppm}^{-1} \text{ min}^{-1}$.
OXYL	o-xylene
PACD	Propanoic acid
PAN	Peroxy Acetyl Nitrate
PAN2	PPN and other higher alkyl PAN analogues
PBZN	PAN analogues formed from Aromatic Aldehydes
PRD2	Ketones and other non-aldehyde oxygenated products which react with OH radicals faster than 5E-12 cm ³ molec ⁻² sec ⁻¹
PRPE	Propene
PXYL	p-xylene
R6PX	Lumped organic hydroperoxides with 5 or more carbons (other than those formed following OH addition to aromatic rings, which is represented separately). Mechanism based on that estimated for 3-hexyl hydroperoxide.
RAPX	Organic hydroperoxides formed following OH addition to aromatic rings, which is represented separately because of their probable role in SOA formation. Mechanism based on two isomers expected to be formed in the m-xylene system.

Species Name	Description
RCHO	Lumped C3+ Aldehydes (mechanism based on propionaldehyde)
RCO3	Peroxy Propionyl and higher peroxy acyl Radicals
RO3H	Higher organic peroxy acids (mechanism based on peroxypropionic acid).
RNO3	Lumped Organic Nitrates
RO2C	Peroxy Radical Operator representing NO to NO2 and NO3 to NO2 conversions, and the effects of peroxy radical reactions on acyl peroxy and other peroxy radicals.
RO2X	Peroxy Radical Operator representing NO consumption (used in conjunction with organic nitrate formation), and the effects of peroxy radical reactions on NO3, acyl peroxy radicals, and other peroxy radicals.
ROOH	Lumped organic hydroperoxides with 2-4 carbons. Mechanism based on that estimated for n-propyl hydroperoxide.
SESQ	Sesquiterpenes
SO2	Sulfur Dioxide
SULF	Sulfates (SO3 or H2SO4)
TBUO	t-Butoxy Radicals
TERP	Terpenes
TOLU	Toluene
XACE	As for xHO2
XACR	As for xHO2
XAF1	As for xHO2
XAF2	As for xHO2
XAF3	As for xHO2
XBAC	As for xHO2
XBAL	As for xHO2
XC	Lost Carbon or carbon in unreactive products
XCCH	As for xHO2
XCO	As for xHO2
XGLY	As for xHO2
XHCH	As for xHO2
XHO2	Formation of HO2 from alkoxy radicals formed in peroxy radical reactions with NO and NO3 (100% yields) and RO2 (50% yields)
XGLD	As for xHO2
XIPR	As for xHO2
XMA3	As for xHO2
XMAC	As for xHO2
XMC3	As for xHO2
XMEK	As for xHO2
XMEO	As for xHO2
XMGL	As for xHO2
XMVK	As for xHO2
XN	Lost Nitrogen or nitrogen in unreactive products
XNO2	As for xHO2
XOH	As for xHO2
XPD2	As for xHO2
XRCH	As for xHO2

Species Name	Description
XRC3	As for xHO2
XRN3	As for xHO2
XTBU	As for xHO2
Y6PX	As for ROOH, but for R6PX
YAPX	As for ROOH, but for RAPX
YRPX	Formation of ROOH following RO2 + HO2 reactions
ZRN3	Formation of RNO3 in the RO2 + NO, reaction.